EVAPORITE AND CLASTIC CYCLE SEQUENCES OF THE PARADOX FORMATION WITH IMPLICATIONS TO THE TIMING AND FORMATION OF THE UNCOMPAHGRE UPLIFT, NORTHERN PARADOX BASIN, UTAH

by

Walter Curtis Arbuckle

A thesis submitted to the Faculty and the Board of Trustees of the Colorado School of Mines in partial fulfillment of the requirements for the degree of Master of Science (Geology).

Golden, Colorado

Date 11/10/2008

Signed: Walter Curtis Arbuckle
Walter Curtis Arbuckle

Signed: Bruce D. Trudgill
Dr. Bruce Trudgill
Thesis Advisor

Golden, Colorado

Date 11/10/08

Signed: John D. Humphrey
Dr. John D. Humphrey
Department Head
Department of Geology and
Geological Engineering

ABSTRACT

The Paradox Basin, located in southwestern Colorado and southeastern Utah, is defined by the regional extent of the Middle Pennsylvanian (Desmoinesian) Paradox Formation. The northern part of the basin is characterized by diapiric salt walls that parallel the northwest-southeast Ancestral Rocky Mountain Uncompahgre Uplift.

Evaporites within the Paradox Formation are characterized by at least 29 well-defined cycles comprised of siliciclastic (interbeds) and evaporite (halite plus additional evaporites) facies. Each individual idealized cycle is composed of a successive layered sequence of (in depositional order) anhydrite, silty dolomite, black shale, silty dolomite, anhydrite and halite. These well defined cycles are identified in the northern half of the basin that is considered to be the oldest and the deepest section of the basin. The cyclicity of the Paradox Formation, and thus the evaporite cycles, are driven by a combination of important processes including tectonics, subsidence, climate and glacio-eustatic sea-level fluctuations. However, stratigraphic rock relationships, palynomorph data, and regional correlations suggest that Gondwanaland glaciations caused the eustatic sea-level fluctuations and were the primary control on Paradox evaporite/carbonate cyclicity.

The relationship between the Paradox Basin and the Uncompahgre Uplift is not completely understood. Many authors have suggested different evolutionary scenarios all linking the timing and formation of the uplift with the development of the basin. To determine the applicability of each model and establish a new evolutionary scenario for the Paradox Basin and Uncompahgre Uplift, age estimates, subsidence modeling and isopach thickness maps (of each individual cycle) were all analyzed.

Age estimates for individual cycles, as well as the entire Paradox Formation, were calculated using sedimentation rates for each specific lithology within a cycle. The purpose of these calculations was to establish a depositional time table for each cycle and the total age of the Paradox Formation. The estimates suggest that each individual cycle was roughly deposited as a fourth order sequence, having a 100,000 – 500,000 year duration; potentially linking the Paradox cyclicity to Milankovitch-forced processes. Age

estimates for the entire formation are far more subjective, but were calculated to range from 1.8 million years to over 4.5 million years, therefore fitting within the Desmoinesian time period of about 309.4 – 305.5 Ma.

Subsidence modeling in the northern part of the basin highlights a four million year period (309 – 305 Ma) of major, rapid subsidence. The start of this rapid subsidence coincides with the beginning of the Desmoinesian and thus indicates that the Paradox Formation was being deposited in a tectonically subsiding basin. The modeling also recognizes the Uncompahgre Uplift as the main driving force of basin subsidence linking the basin and uplift tectonically.

Isopach thickness maps of individual evaporite cycles, and their associated age estimates, also suggest the basin was tectonically subsiding during the Desmoinesian and even before Pennsylvanian time. Evidence derived from the isopach maps indicates there could have been salt flow as early as the end of the Desmoinesian. This implies there was sediment loading of the Cutler Formation (deposited from arkosic material shed off the Uncompahgre Uplift) onto the underlying salt, indicating at least part of the Uncompahgre was a positive feature (above local sea-level) by the end of the Desmoinesian.

Finally, with the evidence presented it is reasonable to conclude that during the initial stages of salt deposition (Paradox Formation) the Paradox and Eagle basins were connected. However, soon thereafter the Uncompahgre started to uplift and become an influencing factor affecting depositional patterns, even though it was not a strongly positive feature until Middle to Late Desmoinesian time. By the end of the Pennsylvanian and into Permian time, the Uncompahgre reached a significant elevation as indicated by the sediment loading of the erosion derived Cutler Formation. It is unlikely by this time that the two basins were still extensively connected through any major passageways and were most likely isolated from each other completely.

TABLE OF CONTENTS

LIST OF FIGURES

LIST OF TABLES

ACKNOWLEDGMENTS

I would like to begin by thanking my advisor, Dr. Bruce Trudgill, who provided the guidance, encouragement, understanding, entertainment and patience needed for me to finally complete this thesis. I would also like to thank Dr. Piret Plink-Björklund and Dr. John Curtis for taking the time to be a part of my committee. Your suggestions and support throughout my work were greatly appreciated.

Special thanks to Walter K. Arbuckle, Elliott Riggs, Travis Brown, Don Rasmussen, and Gary Nydegger all who took the time to talk with me on various occasions during the completion of this project. I greatly appreciate your thoughts and insight.

The core samples used in this project were borrowed courtesy of the USGS Core Research Center, Denver, Colorado. Sample analyses were performed by the Advanced Mineralogy Research Center, Colorado School of Mines, Golden, Colorado and is accompanied with a huge thank you for all of their hard work.

The majority of my graduate work was funded by Gasconade Oil Company and without their continued support the continuation of my education would not have been made possible. The final year of my graduate studies was also sponsored by the Utah Geological Survey.

For the past eight years, while I have pursued my bachelors and masters degrees, the Geology and Geological Engineering Department at the Colorado School of Mines has become a second home to me. I would like to offer an overall general thanks to all the great professors and staff I have been fortunate enough to have known during my time here.

In addition, I would also like to acknowledge the many friends I have made throughout my time here at CSM and the ones I have kept in touch with outside of this institution. Your continued support, entertainment and encouragement of my procrastination have left me with countless stories and memories along with hope of a continued friendship in the years to come.

Lastly, but most importantly, I am extremely grateful to my family for all the support, words of wisdom, confidence and guidance throughout this project. You have always been there to give me a helping hand and a loving hug when I needed it the most, and I extent to you a very sincere and heartfelt thank you! This thesis is dedicated to them.

CHAPTER 1

INTRODUCTION

The Paradox Basin, located in southwestern Colorado and southeastern Utah, is characterized by the regional extent of Pennsylvanian-age evaporitic strata (Figure 1.1). The northern part of the basin is recognized by diapiric salt walls that trend northwest-southeast, paralleling the Ancestral Rocky Mountain Uncompahgre Uplift located along the northeastern margin of the basin.

Evaporite successions in the Paradox Formation are of the Pennsylvanian Hermosa Group and comprise at least 29 well defined cycles containing siliciclastic, as well as evaporitic facies (Figure 1.2). Each cycle typically consists of (in depositional order) anhydrite, silty dolomite, black shale, silty dolomite, anhydrite, and halite (Hite and Buckner, 1981). The cycles are a result of relative and eustatic sea-level fluctuations combined with local tectonics, climate, sediment supply and rapid subsidence.

The relationship of the Paradox Basin and the Uncompahgre Uplift is not fully understood. Many previous authors have modeled and suggested several different evolutionary scenarios involving the timing and formation of the uplift in comparison to the basin without much collaboration or resolution. Therefore, a better understanding of the structural and stratigraphic associations between the Uncompahgre and the Paradox Basin is necessary, and is the main aim of this thesis.

1.1 Purpose of Study and Research Objectives

This study is intended to map and correlate the evaporite facies within the Pennsylvanian Paradox Formation throughout the northern Paradox Basin. This includes correlating individual evaporite cycles and their respective clastic zones. The resulting associations are used to better understand the cyclicity of the Paradox Formation and its

relationship to the structural development and evolution of the Ancestral Rocky Mountain Uncompahgre Uplift. This adds an additional and unique interpretation of the complex and poorly understood partnership between the Paradox Basin and the Uncompahgre Uplift.

Specifically, the research objectives for this study are:

- Create subsurface isopach maps of at least 29 individual evaporite cycles of the Paradox Formation.
- Correlate cycles and cycle boundaries of the 29 evaporite cycles across the study area.
- Calculate depositional age estimates used to determine duration, length and total age of each cycle.
- Characterize and understand the clastic material within the evaporite cycles and distinguish the provenance of such materials.
- Compare the Paradox evaporite cycles to other Pennsylvanian cyclothems in an attempt to classify the Paradox cycles as glacio-eustatic influenced.
- Use subsidence models to quantify and understand the relative timing and cause(s) of basin formation.
- Analyze cycle thickness comparisons in relationship with the positioning of the Uncompahgre Uplift. Such comparisons will help understand the timing and evolution of the uplift.

1.2 Research Contributions

- A compilation of 29 isopach thickness maps of the Paradox Formation evaporite cycles that illustrate the changes and fluctuations in cyclicity and depositional history for each individual cycle.
- Cyclicity and sedimentation evidence supporting the control of glacio-eustatic processes on the cyclicity of the Paradox Formation evaporites.

- Comparison between stratigraphic rock relationships and palynomorph data highlighting the similarities between third- and fourth-order cycle changes.
- Detailed mineralogical analysis of transgressive and regressive dolomites within two consecutive evaporite cycles.
- A subsidence model highlighting the major subsidence events that occurred during Late Pennsylvanian through Early Permian time.
- A new interpretation for the timing and formation of the Uncompahgre Uplift and its relationship to the formation of the northern Paradox Basin.

1.3 Study Area

The area of interest for this study includes the north and northwestern section of the Paradox Basin located in southeastern Utah, United States (Figure 1.1). The Paradox Basin lies within the Colorado Plateau and is characterized by the beautiful Arches and Canyonlands National Parks (Figure 1.3).

The study area extends eastward to the Uncompahgre Uplift and stretches westward across the Green River into Emery County, Utah. The northern boundary is roughly limited to the extent of the Paradox Formation evaporite salt facies. The southern boundary is marked by the border between Grand and San Juan counties. This area is often termed the Paradox 'fold and fault belt' encompassing many of the salt walls and salt related structures including the Salt Valley, Moab Valley, Cane Creek, Onion Creek, Cache Valley and Fisher Valley anticlines.

The outcropping geologic formations in the area are exclusively of Permian, Triassic, Jurassic and Cretaceous ages, except for some poorly exposed areas along river valleys and salt anticlines where older rock units can be identified.

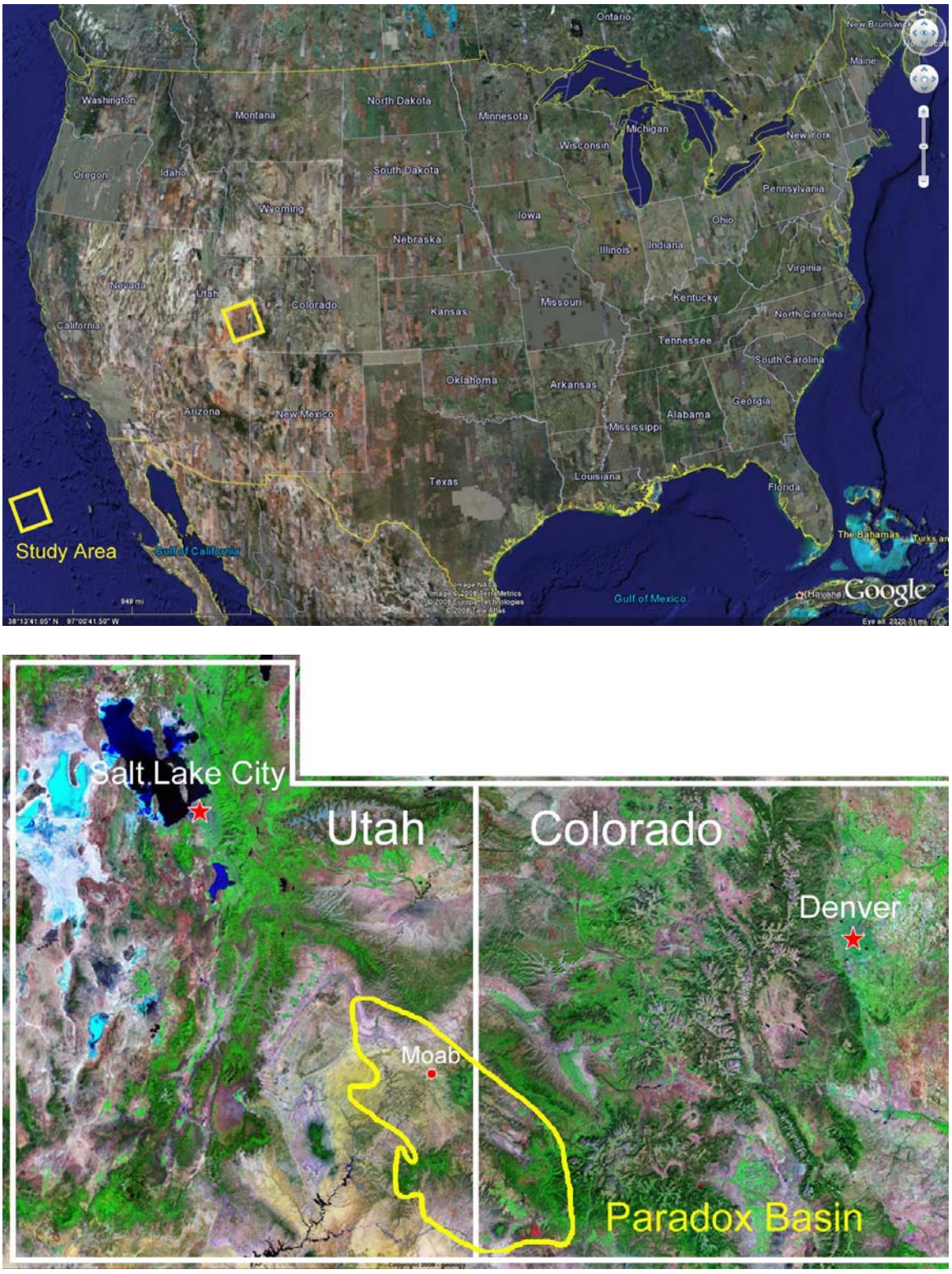

Figure 1.1: Index maps showing the relative location of the Paradox Basin (modified from Google Earth, 2007; Geology, 2008).

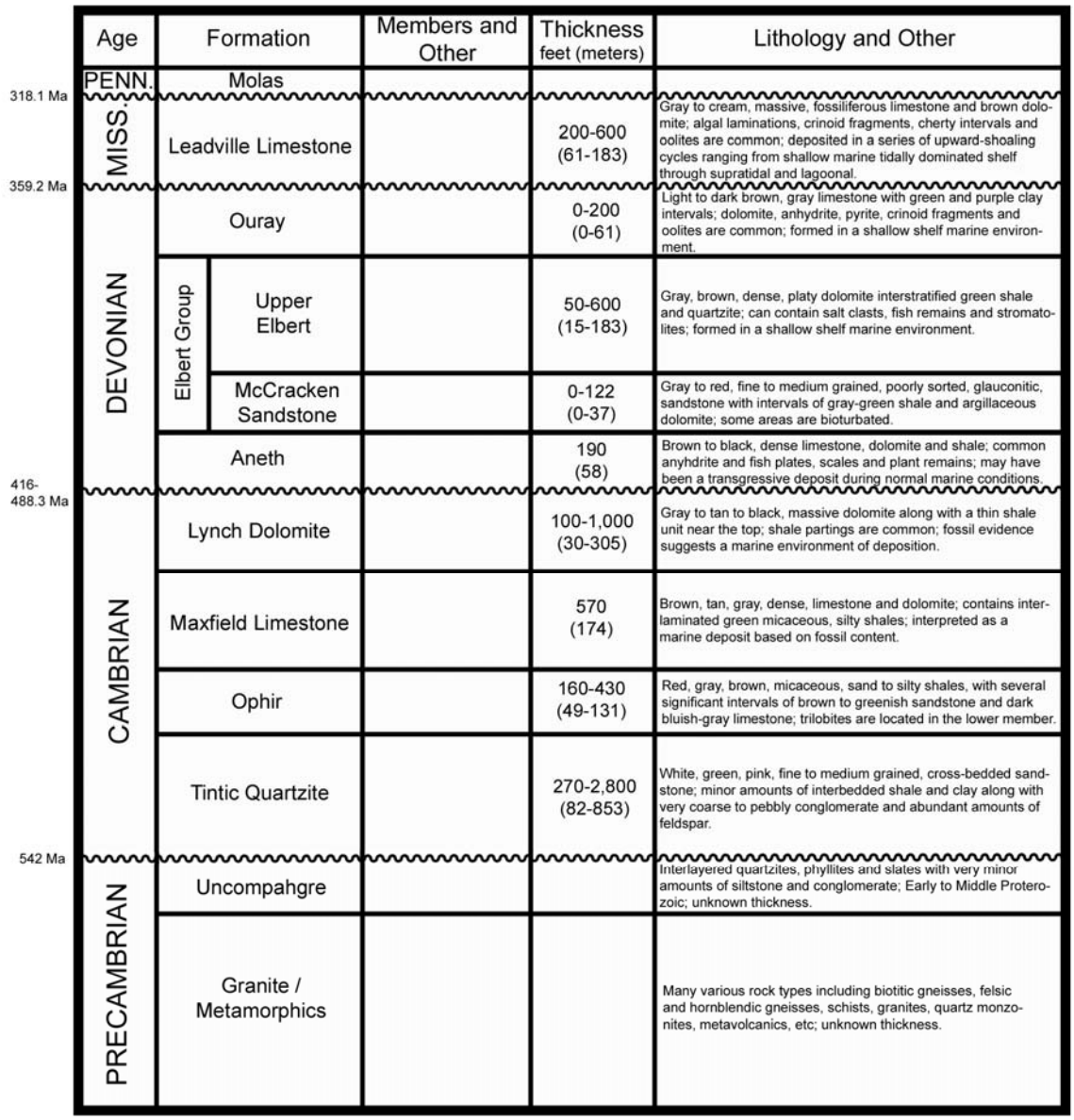

Figure 1.2a: Generalized column illustrating the stratigraphic units in the northern Paradox Basin (compiled from Stokes, 1948; Bradish and Clair, 1956; Wright *et al*., 1962; Molenaar, 1981; Kamola and Chan, 1988; Currie, 1998; Trudgill *et al*., 2004; Draut, 2005). Continued on the next two pages.

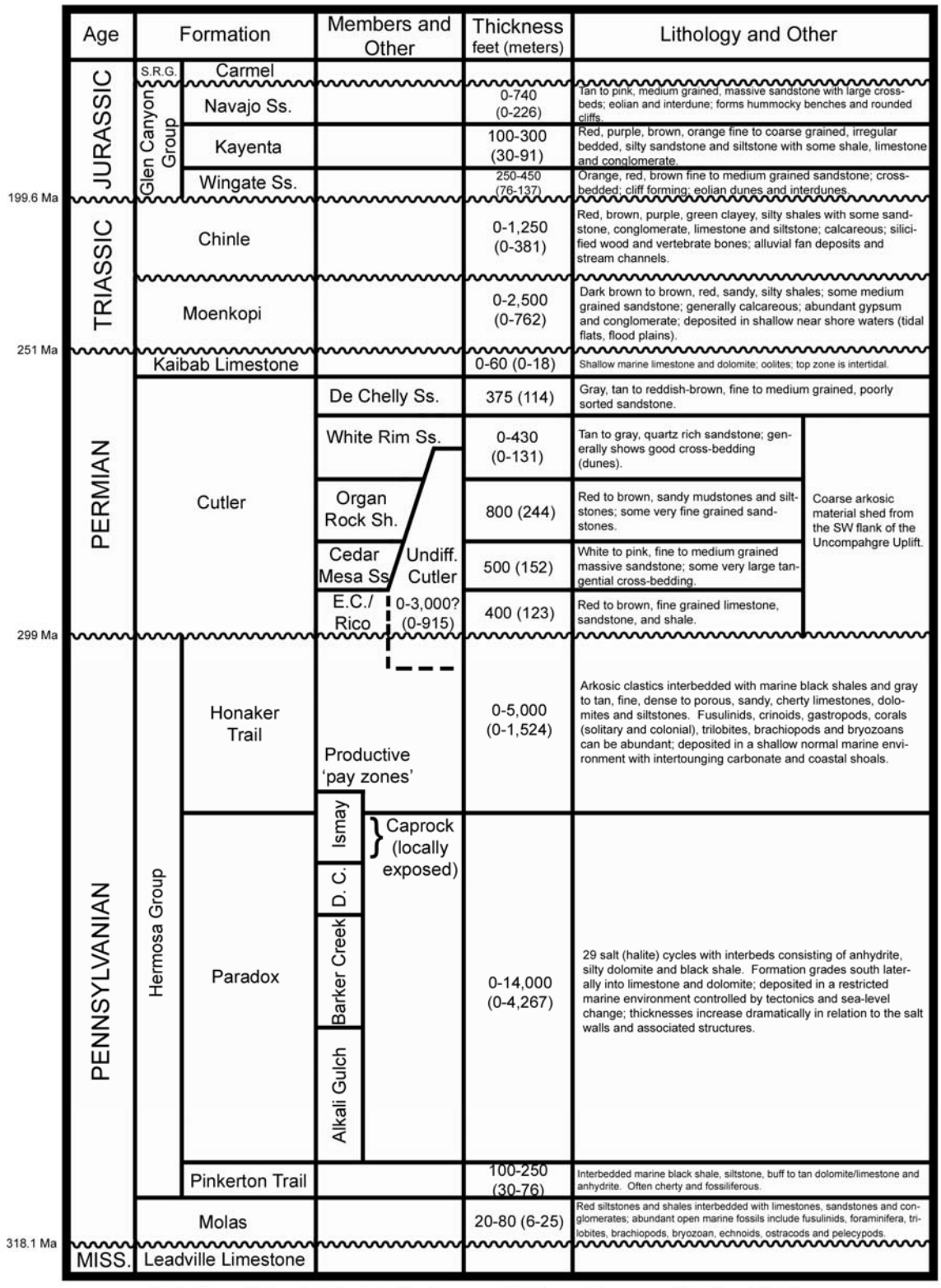

Note: No vertical scale intended. Quaternary and Tertiary rocks are ommitted from this diagram.

Figure 1.2b: Continued.

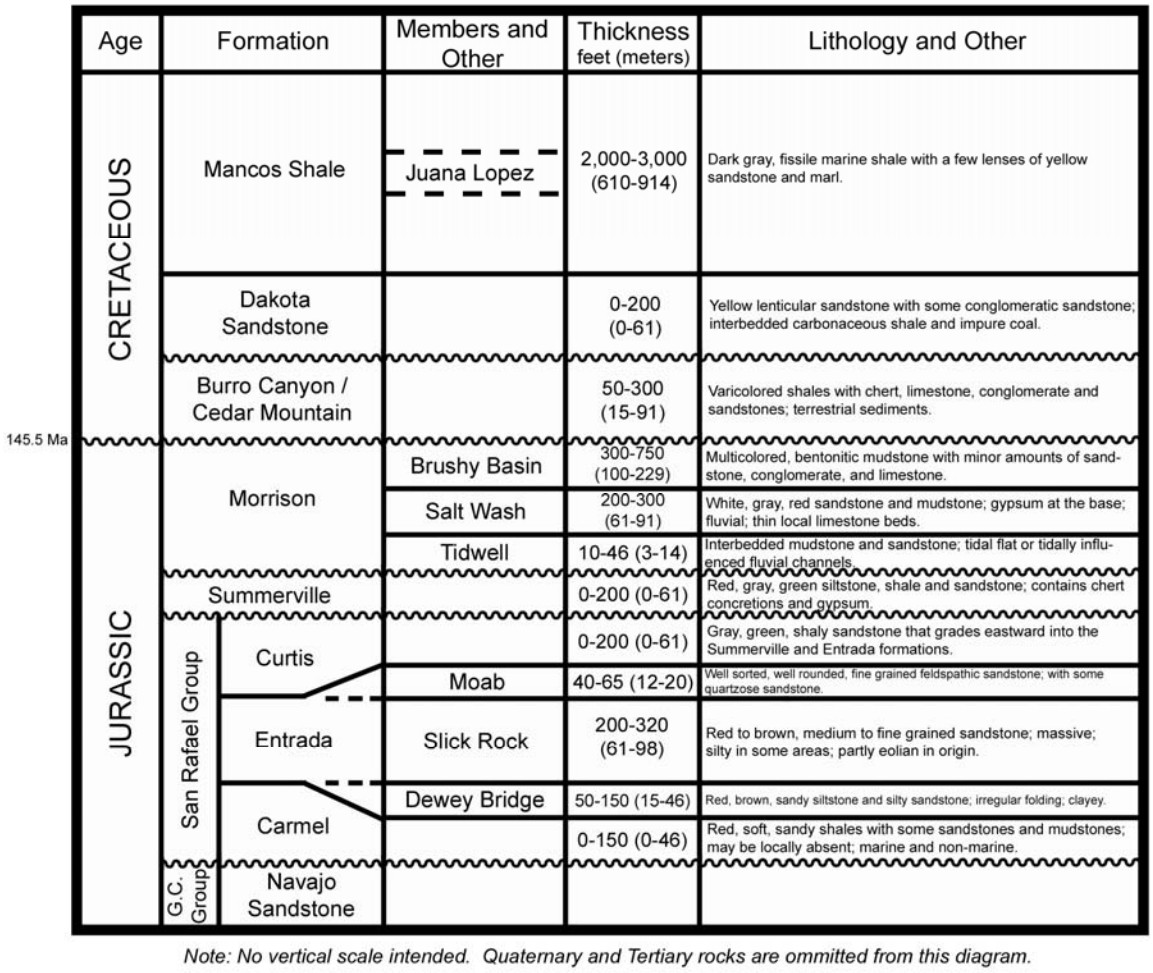

Figure 1.2c: Continued.

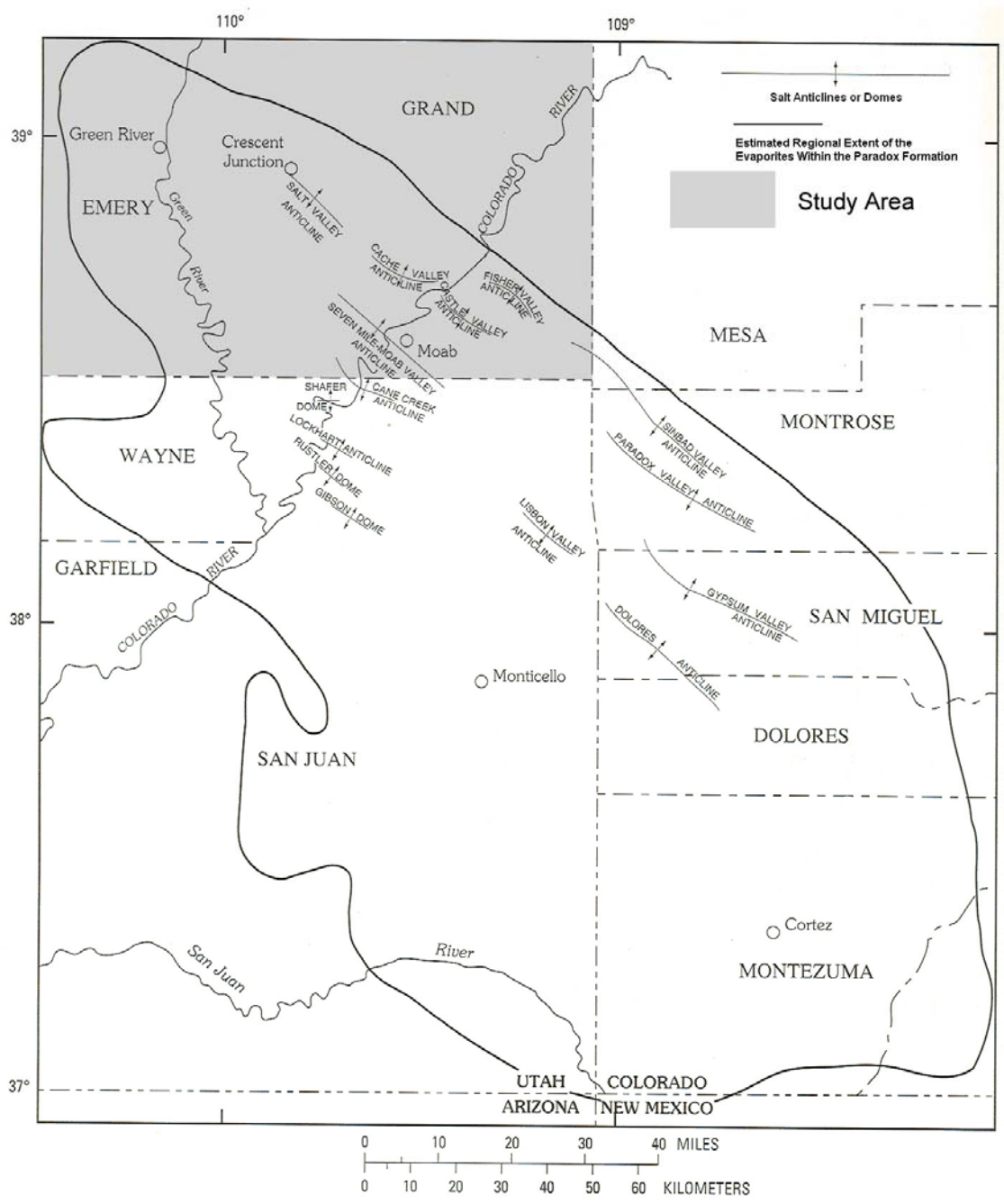

Figure 1.3: Map detailing the outline of the study area for this project within the Paradox Basin, Utah (modified from Raup and Hite, 1992).

1.4 Previous Studies

There has been a significant amount of work throughout the Paradox Basin, but in comparison only a small amount on the evolution of the Paradox Formation and associated evaporite cycles. Several of the most relevant studies to this paper are listed below:

- Early work by Prommel and Crum (1926) attempted to explain the origin of the salt domes and anticlines based on the theory of sub-surface faulting and post-Cretaceous fault lines.
- Harrison (1927) discusses the development of the salt domes, plugs and anticlines. It takes a brief look at the hydrocarbon potential of these features.
- Wengerd and Strickland (1954) studied the stratigraphy of the Pennsylvanian formations and tied in paleogeological and microfossil data.
- Jones (1958) worked to support the idea of how the salt anticlines formed. He suggested they were initiated by compressional forces attributed to sediment loading from the Cutler Formation. He also looked at the mechanical strength of the salt within the anticlines.
- Hite (1960) first attempted to correlate the evaporite sequences across the basin. He used well data and identified several key marker beds that were easily recognized in many of the well logs. His end result was a well log correlation diagram stretching from the northwest down to the southeast portion of the basin.
- Elston and Shoemaker (1960) studied the structural history of the Uncompahgre Front using the stratigraphy of the Paradox Basin.
- Wengerd (1960) studied the Pennsylvanian stratigraphy of the basin including discussion on lithological changes and the relationship with the Uncompahgre Uplift.
- Hite and Buckner (1981) defined several of the evaporite cycles breaking them down into individual facies and attempted to correlate specific cycles over short distances. They also looked at mechanisms that caused the evaporitic cyclicity and discussed origins and sources for the clastic facies.

- Baars and Stevenson (1982) worked with the tectonic evolution of the Paradox Basin and how it corresponded to the formation of the Pennsylvanian evaporite facies.
- Doelling (1983) looked at thickness relationships within not only the Pennsylvanian rocks, but other overlying strata and how they relate to the structure and evolution of the salt valley anticlines.
- Stevenson and Baars (1986) supported the idea of the Paradox Basin being a pull-apart basin and emphasized the impact of regional and local lineaments. These lineaments were associated with basement, right-lateral, wrench faulting.
- Raup and Hite (1992) evaluated several cores taken from wells drilled near the Cane Creek Anticline and Shafer Dome. The study looked at identifying, defining and categorizing several of the evaporite cycles.
- Weber *et al.,* (1995) completed a publication on sequence stratigraphic and reservoir delineation for rock units deposited during Middle Pennsylvanian time. Their work looked specifically at third- and fourth-order cyclicity observed in the Paradox and lower Honaker Trail formations in the central and southern portions of the basin.
- Nuccio and Condon (1996) studied the thermal history and stratigraphy of the basin which included Pennsylvanian strata and a discussion on the Ismay, Desert Creek and Cane Creek cycles/intervals.
- Trudgill *et al*. (2004) demonstrated the basin has a complex relationship between crustal shortening, salt tectonics, and differential sediment loading. This led to the conclusion that salt tectonics were very influential on the structural and stratigraphic development of the basin.

CHAPTER 2

BASIN GEOLOGY

The Paradox Basin is part of the present day Colorado Plateau and is roughly an oval shaped area located in southwestern Colorado and southeastern Utah. The basin can be defined by the regional geographic extent of the Paradox Formation (mostly evaporites) which trends northwest-southeast with an approximate length of around 190 miles (306 km) and a width of about 80 miles (129 km) (Figure 2.1) (Condon, 1995; Doelling, 1983).

2.1 Regional Geologic Setting

The Paradox Basin lies adjacent to the southwestern edge of the Uncompahgre Uplift and is bounded to the east by the San Juan Dome (Figure 2.1). The southeastern edge of the basin is bordered by a lineament named the Hogback monocline and the San Juan Basin (Stevenson and Baars, 1986). The south and southwestern sides are generally structurally uncontrolled as the edge follows the Four Corners Lineament and crosses the Monument Upwrap where it almost reaches the Henry Mountains (Figure 2.1). The basin then extends northwest to the San Rafael Swell and associated lineament. Finally the northern boundary of the basin extends just south of the Uinta Basin, but is influenced by several structural features including the Uncompahgre Uplift (Figure 2.1) (Stevenson and Baars, 1986; Condon, 1995).

The formation of the Paradox Basin is highly controversial. One of the main theories includes the idea of a pure pull-apart basin based on strike-slip motion and associated extension and rotation from Pennsylvanian basement faulting. Another concept models the basin as a flexural depression in the crust directly associated with the rise of the Uncompahgre Uplift. Definite conclusions on basin formation are difficult

because of the structural complexity near the uplift. Salt tectonics has also hampered the ability to reconstruct the basin evolution during the critical Pennsylvanian period.

2.2 Structural Geology

The Paradox Basin is very structurally complex. Basin evolution was the result of a combination of the Uncompahgre Uplift evolution, salt evacuation and an underlying complicated basement framework.

2.2.1 Basement Framework

The Paradox Basin marks the location where two fault zone systems intersected each other during Precambrian time (Figure 2.2). The northwest-southeast-trending series of faults is called the Olympic-Wichita Lineament and stretches from Vancouver, British Columbia down through the present day Arbuckle Mountains in southern Oklahoma. It exhibits a right-lateral strike-slip displacement (Baars and Stevenson, 1981). The Colorado Lineament is a northeast-southwest trending fault system with an apparent left-lateral movement. It extends from the Grand Canyon, Arizona, northeast to Lake Superior. It is thought these two lineaments could have formed from compressional forces acting from the north, or more reasonably, a right-lateral wrenching stress limited to the western half of the United States (Figure 2.2). The timing of both lineaments is estimated to be around 1,700 million years ago based on cross-cutting relationships in the San Juan Mountains and southeastern Wyoming (Warner, 1978; 1980; Baars and Stevenson, 1981). Baars and Stevenson (1981) evaluated the strain associated with the basin (Figure 2.2) and suggested the resulting features would include north-south normal faults and east-west thrusting and folding.

Smaller, more localized lineaments (related to the regional scale systems discussed above) dominate basement faulting in the Paradox Basin (Figure 2.3). The Four Corners Lineament is a northwest-southeast trending fault system that helped

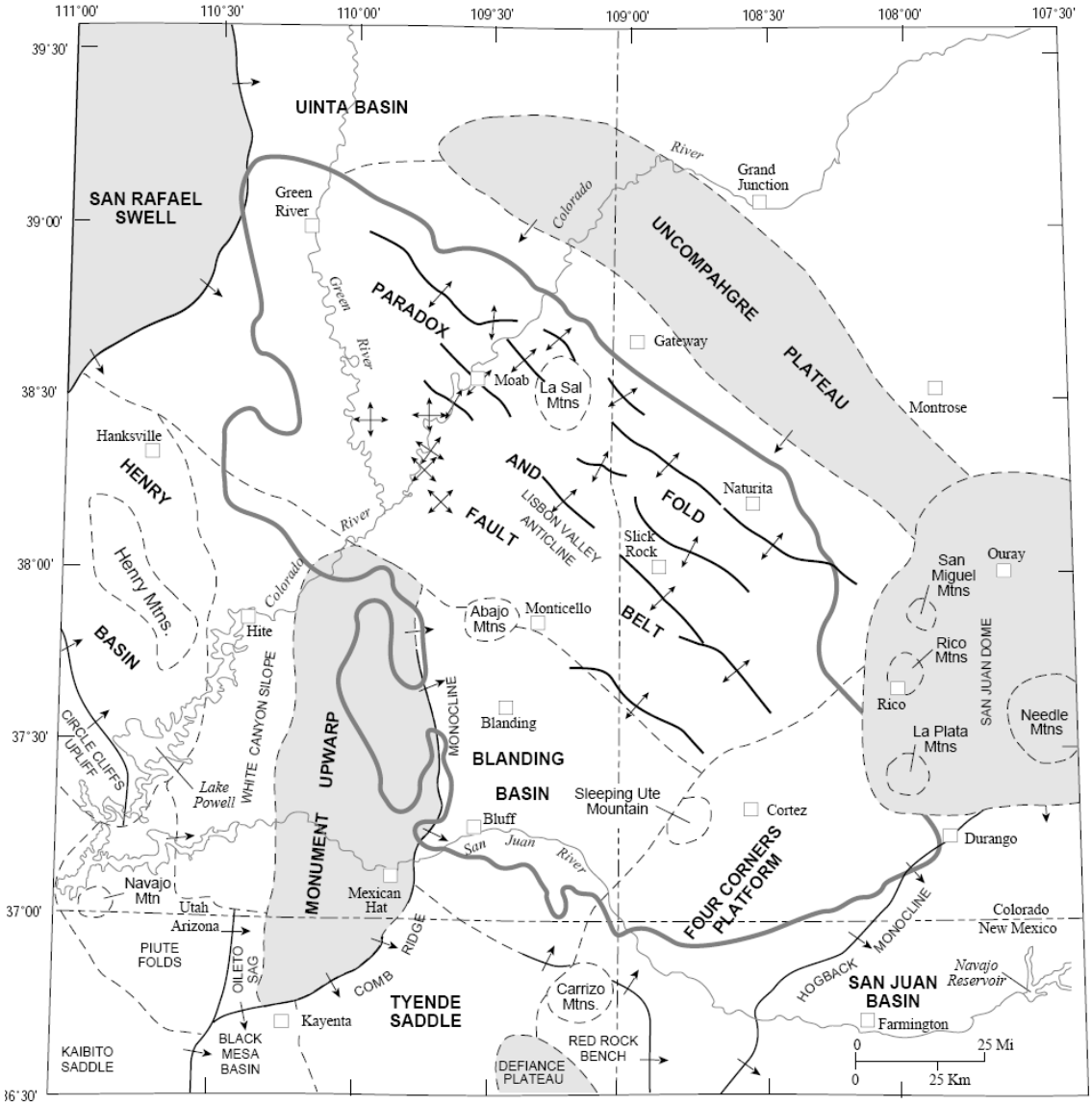

Figure 2.1: Map illustrating the structural features and highlands in and around the Paradox Basin. The La Sal, Abajo, Sleeping Ute and La Plata mountains are igneous intrusive centers all of Tertiary age. The solid gray outline marks the maximum extent of salt within the Paradox Basin (after Nuccio and Condon, 1996).

control several depositional environments within the basin (Stevenson and Baars, 1986). It is interesting to note all salt and anhydrite deposition within the basin is limited to the area northeast of this lineament. Normal marine conditions existed to the west and southwest of the Four Corners Lineament (Stevenson and Baars, 1986).

The Nequoia and Abajo arches also trend to the northwest-southeast (Figure 2.3). These positive features played an important role in the position of salt cycle deposition and related salt structures acting almost like a hinge. The arches were prominent in early Desmoinesian time as evident by thinning of the Paradox salt onto and around these structures (Stevenson and Baars, 1986). To the northeast, salt thicknesses increase dramatically and salt anticlines/synclines become more prevalent. To the southwest, the salt cycles thin and become more carbonaceous (Stevenson and Baars, 1986).

The Cataract Lineament is a northeast-southwest trending basement fault system and is a segment of the Colorado Lineament (Figure 2.3). It stretches from just west of Lake Powell, Utah into western Colorado closely following the Colorado River conduit. The Cataract Lineament marks a weakness in the basement identified by aeromagnetic and gravity data. The lineament displays left-lateral movement indicated by sharp fault splays off the northwest trending local lineaments (Stevenson and Baars, 1986). It is important to note that both the Onion Creek/Fisher Valley and Moab Valley salt anticlines terminate against the Cataract Lineament. The southeastern end of the Salt Valley Anticline illustrates left-lateral fault drag and gravity data suggest a displacement of around 4 miles (6 – 7 km) (Stevenson and Baars, 1986).

The San Rafael Lineament also trends northeast-southwest and helps define the northern edge of the Paradox Basin. It marks the southeastern edge of the steeply dipping San Rafael Swell (the Emery Uplift in Paleozoic time). Pennsylvanian rocks (including the Paradox Formation and its associated salt cycles) thin as they near the uplift and thus the lineament (Stevenson and Baars, 1986).

The Nequoia Arch, Cataract Lineament, Uncompahgre Uplift and the San Rafael Lineament create a roughly rectangular section in the northeast part of the Paradox Basin that was subjected to significant subsidence (Figure 2.3). This area marks the deepest part of the basin and is also home to the oldest of the salt cycles.

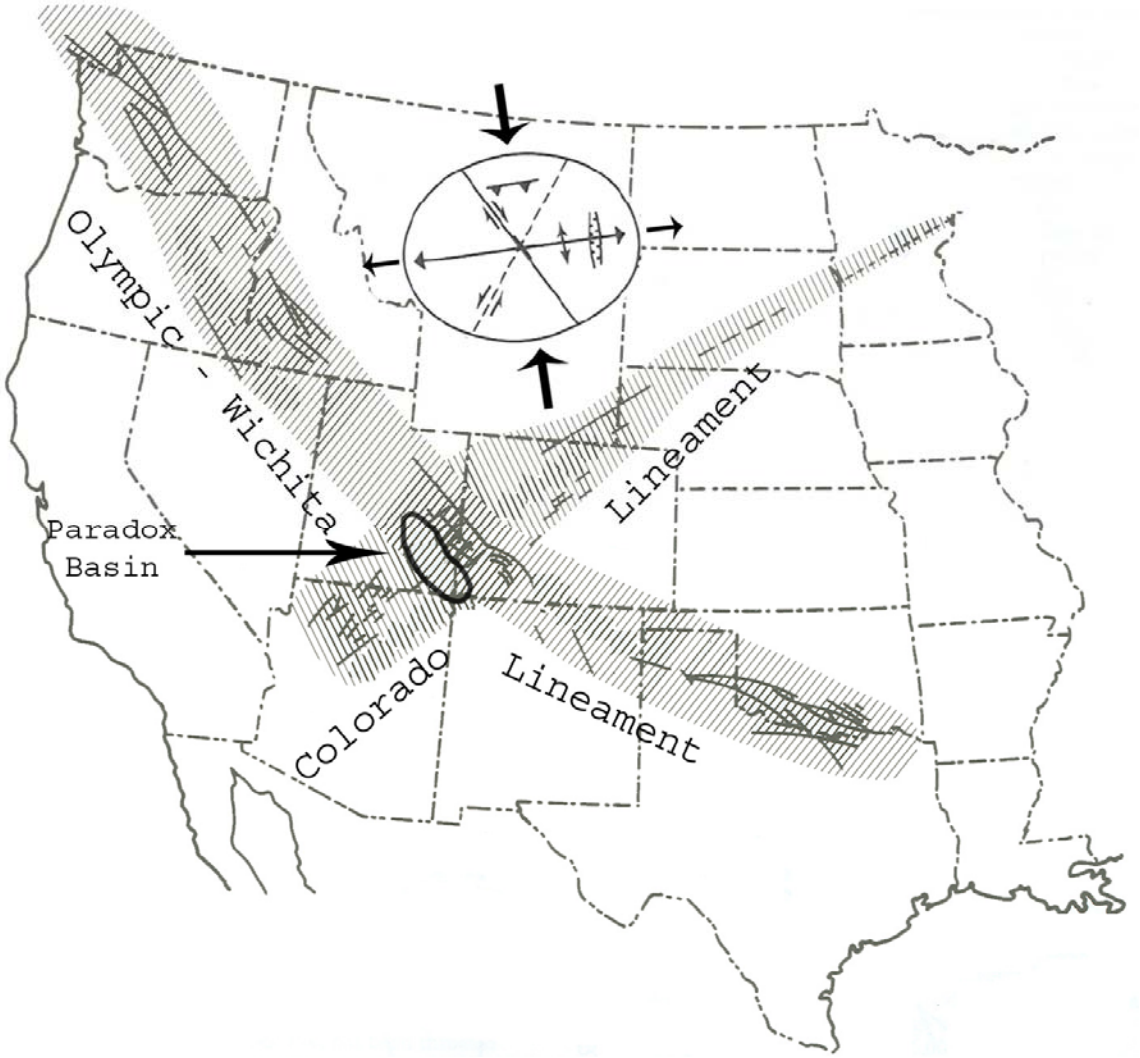

Figure 2.2: The Paradox Basin is part of an intersection between two regional lineaments, the Olympic – Wichita and the Colorado lineaments. The Olympic – Wichita lineament displays right-lateral movement and the Colorado Lineament shows left-lateral movement. It is thought these two lineaments formed from compressional forces acting from the north involving a right-lateral wrenching stress limited to the western half of the United States. A stress-strain ellipsoid indicates maximum compressive stress from the north and south during the Proterozoic. The arrows within the ellipsoid represent strike-slip offset (modified from Stevenson and Baars, 1986).

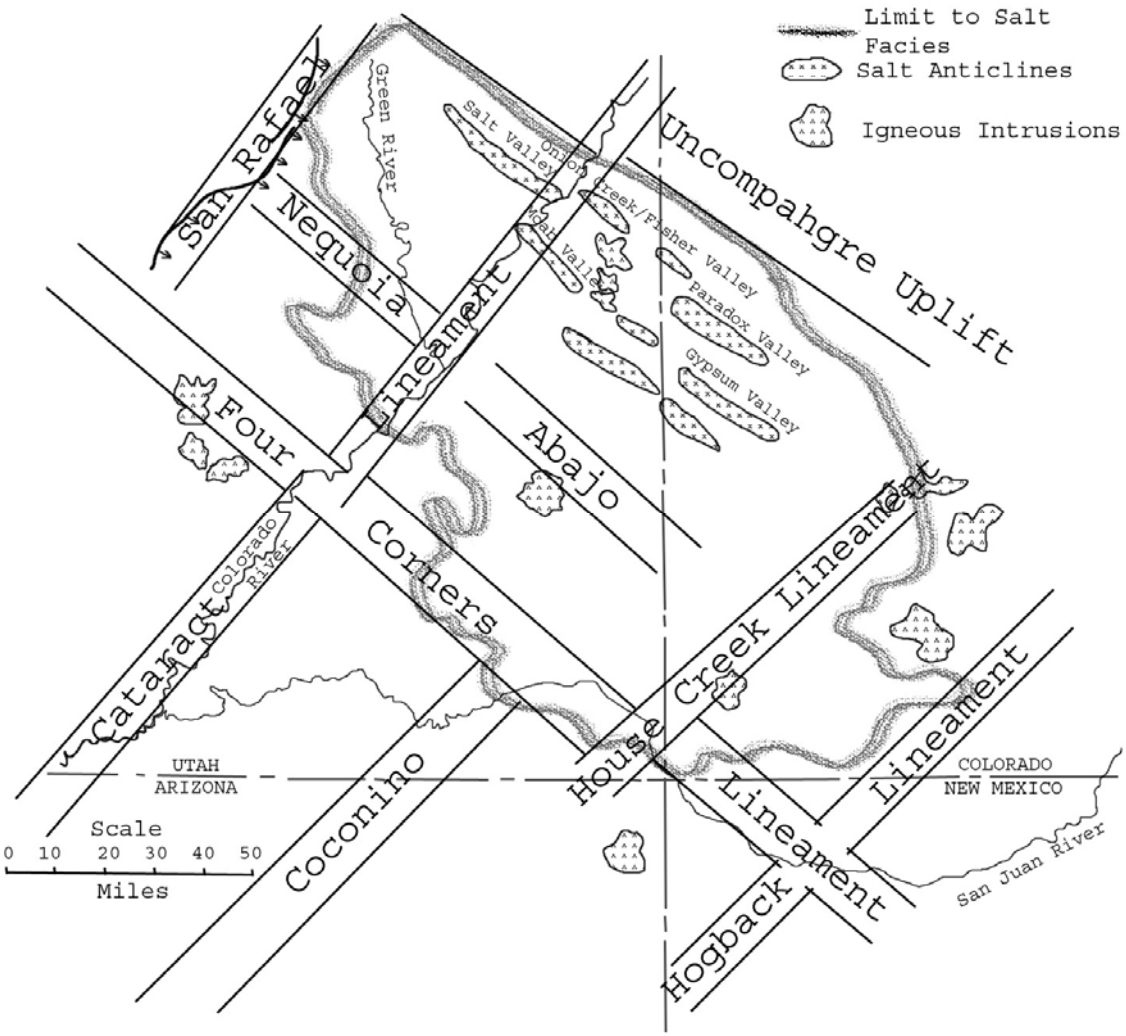

Figure 2.3: Diagram showing the major local fault lineaments of the Paradox Basin. Several of them including the Four Corners Lineament, Hogback Lineament and the San Rafael Lineament represent some of the bounding edges related to the basin (modified from Stevenson and Baars, 1986).

Evidence suggests minor fault and lineament rejuvenations occurred during the Cambrian, Devonian and Mississippian times (Baars and Stevenson, 1981). Although minor, there was a significant amount of movement to influence depositional patterns and create lateral facies changes. An example of this is with the offshore sandbars of the Devonian McCracken Sandstone member of the Elbert Formation and the bioherm mounds located within the Mississippian Leadville Limestone (Baars and Stevenson, 1981).

By Atokan time (Middle Pennsylvanian) and even more so into the Desmoinesian (Middle Pennsylvanian), extensional basement, wrench, normal faulting again started to rejuvenate structural blocks only this time on a larger more pronounced scale (Baars and Stevenson, 1981).

2.2.2 The Ancestral Rocky Mountains and the Uncompahgre Uplift

The Ancestral Rocky Mountains (ARM) are a series of Pennsylvanian uplifts and associated basins in what is now the south and western United States. The timing and orientation of the ARM is thought to be a response to an intraplate orogenic event called the Ouachita – Marathon Orogeny (Kluth, 1986). These two events are closely related and are both the result of a continent to continent collision suturing the southern margin of North America with South America-Africa (Figure 2.4). Suturing and uplifting started during the late Mississippian and continued through early Pennsylvanian time but slowed into the Permian (Figures 2.5, 2.6, 2.7) (Raup and Hite, 1992; Kluth, 1986). Many of the ARM uplifts are separated by basins or troughs corresponding to the adjacent uplifts. Located in the middle of the Colorado Plateau, the Paradox Basin is one of these depressions. It lies adjacent to the southwestern flank of the ARM Uncompahgre Uplift (Figure 2.1).

The Uncompahgre Uplift trends northwest-southeast and is along the northwest flank of the Transcontinental Arch (Figure 2.4) (Maughan and Perry, 1986). It is roughly 30 miles (48 km) wide and 100 miles (160 km) long and extends from near Ridgeway, Colorado to the Cisco Dome, Utah (Figure 2.1) (Cater, 1970). Uplift of the

Uncompahgre began as early as Atokan time but may have been restricted to the very southeastern extent of the uplift (more involving the San Luis Uplift). However by Late Desmoinesian time, massive amounts of coarse arkosic material were being shed from the uplift in the northwestern half of the basin (Baars and Stevenson, 1981). This massive uplifting event and erosional pattern continued into the Permian.

The southwestern edge of the uplift is defined by the Ridgeway thrust fault or fault system. Near Gateway, Colorado this fault system displays nearly 26,000 feet (7,900 m) of offset between the deepest part of the Paradox Basin and the Uncompahgre Uplift (Stevenson and Baars, 1986). Several deep wells (encountering Mississippian strata and older) have been drilled in the very northeast part of the basin. The No. 1 McCormick Federal "C" well, located northwest of Cisco, Utah, drilled to a total depth of 19,302 feet (5,883 m) (Figure 2.8). After 3,600 feet (1,097 m) of Mesozoic strata the well continued to drill through about 14,000 feet (4,267 m) of granitic basement before penetrating through the Uncompahgre fault zone followed by 1,702 feet (59 m) of Paleozoic rocks (Frahme and Vaughn, 1983). The high angle thrust fault has a dip of around 50° – 55° to the northeast and displays over 14,000 feet (4,267 m) of offset (White and Jacobson, 1983). The underlying Paleozoic rocks are thought to be overturned and consist of the Devonian Elbert and Ouray formations along with the Pennsylvanian Paradox Formation. Figure 2.9 is an interpreted northeast-southwest trending seismic line roughly through the well. Figure 2.10 is a generalized cross-section across the same line.

Very little is know about the northwestern termination of the Uncompahgre Uplift. Near Cisco Dome, it plunges sharply into the subsurface. The area is also characterized by weaker magnetic and gravity values when compared to other areas of the uplift (Stevenson and Baars, 1986). Well data suggests the uplift turns slightly westward starting near Cisco Dome. However, this has yet to be proven based on the lack of reliable wells that have penetrated crystalline rock.

2.2.3 Laramide Tectonics

The Laramide Orogeny began near the end of the Cretaceous, about 70 million years ago, and concluded in the Eocene (Tweto, 1980c; Epis *et al.*, 1980). For the most part, the Colorado Plateau resisted much of the compressional forces associated with this orogeny. There was however enhancement of pre-existing features and structures but only on a minor scale when compared to other structures generated by the same orogenic events.

The Paradox Basin itself was not significantly influenced by the Laramide Orogeny. Most of the major structures we see today were generated by salt tectonics and are Late Paleozoic in age. They showed very little, if any, deformation caused by Laramide compression (Baars and Stevenson, 1981). Tweto (1980b) noted the combination of the Uncompahgre and San Luis highlands may have been rejuvenated during the Laramide, but this probably relates more to the southern and eastern sections of the San Luis Uplift.

2.2.4 Basin Formation

There have been numerous theories as to how and why the Paradox Basin formed. In the past it has been referred to as a tectonic depression but this failed to consider timing and tectonics. Stevenson and Baars (1986) believe the basin formed due to pull-apart tectonics. East-west extension in the Middle Pennsylvanian along pre-existing basement lineaments and a wrench fault system created a bend in the Uncompahgre – San Luis uplift(s). This bend released an area of strike-slip offset (Figure 2.11) resulting in extension and thus creating basin wide subsidence. The greatest amount of basin subsidence occurred closer to the major controlling faults (Figure 2.12).

Kluth (1986) interpreted the development of the Paradox Basin and Uncompahgre Uplift to be associated with the collision of North America and South America-Africa resulting in the Ouachita – Marathon Orogeny. This suturing event formed a series of intracratonic block uplifts (ARM) and related basins like the Uncompahgre Uplift and

Figure 2.4: Map of western North America illustrating several Paleozoic and Mesozoic tectonic features. The deformation in this region during Pennsylvanian time has been interpreted to be a result of a continent to continent collision between the southwestern part of North America and northern part of South America-Africa (Kluth, 1986; image modified from Blakey, 2007).

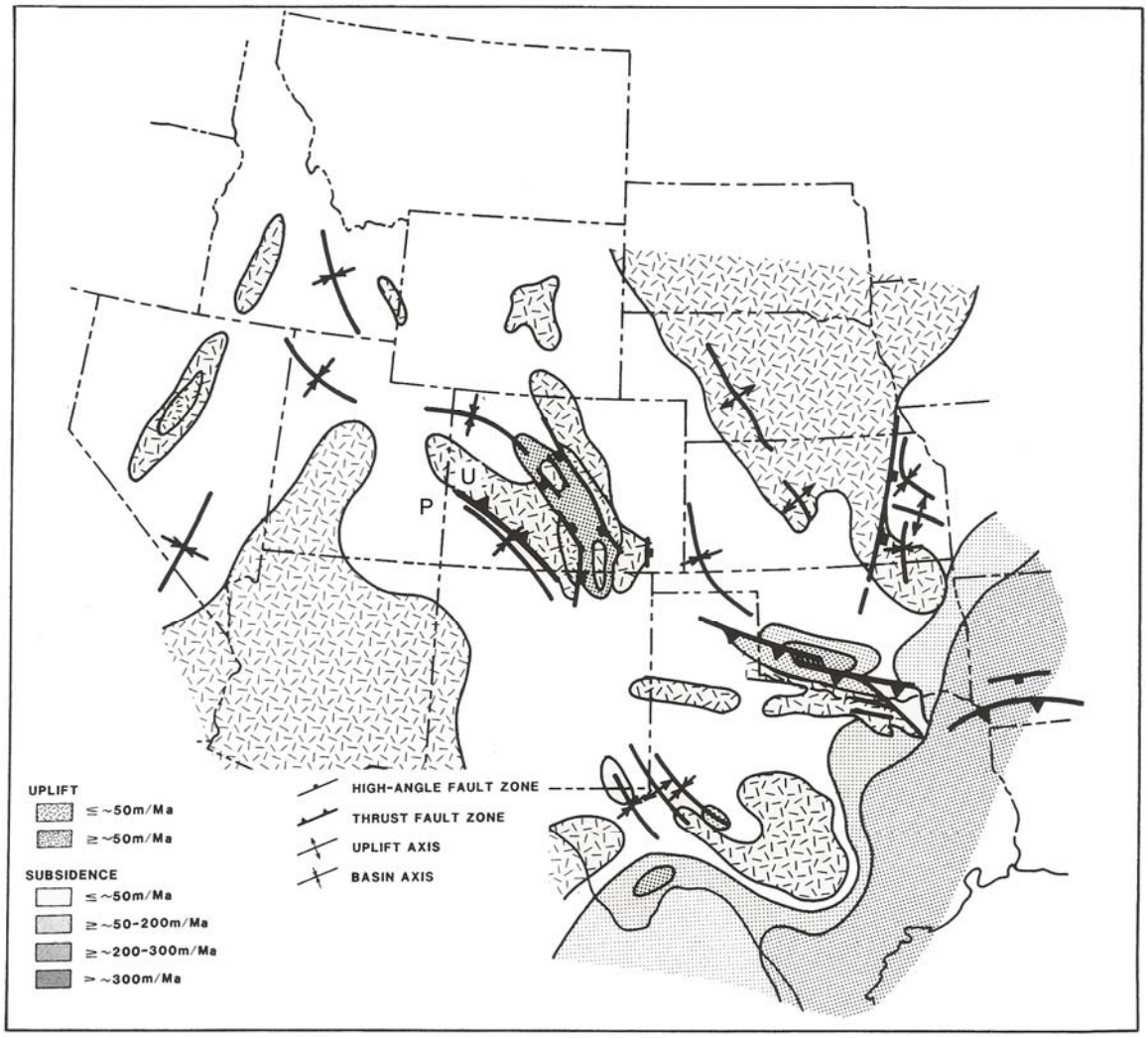

Figure 2.5: Tectonic features of the Ancestral Rocky Mountains during Atokan time. Notice the uplifts and basins forming together in the central Colorado area. Abbreviations: P, Paradox Basin; U, Uncompahgre Uplift (modified from Kluth, 1986).

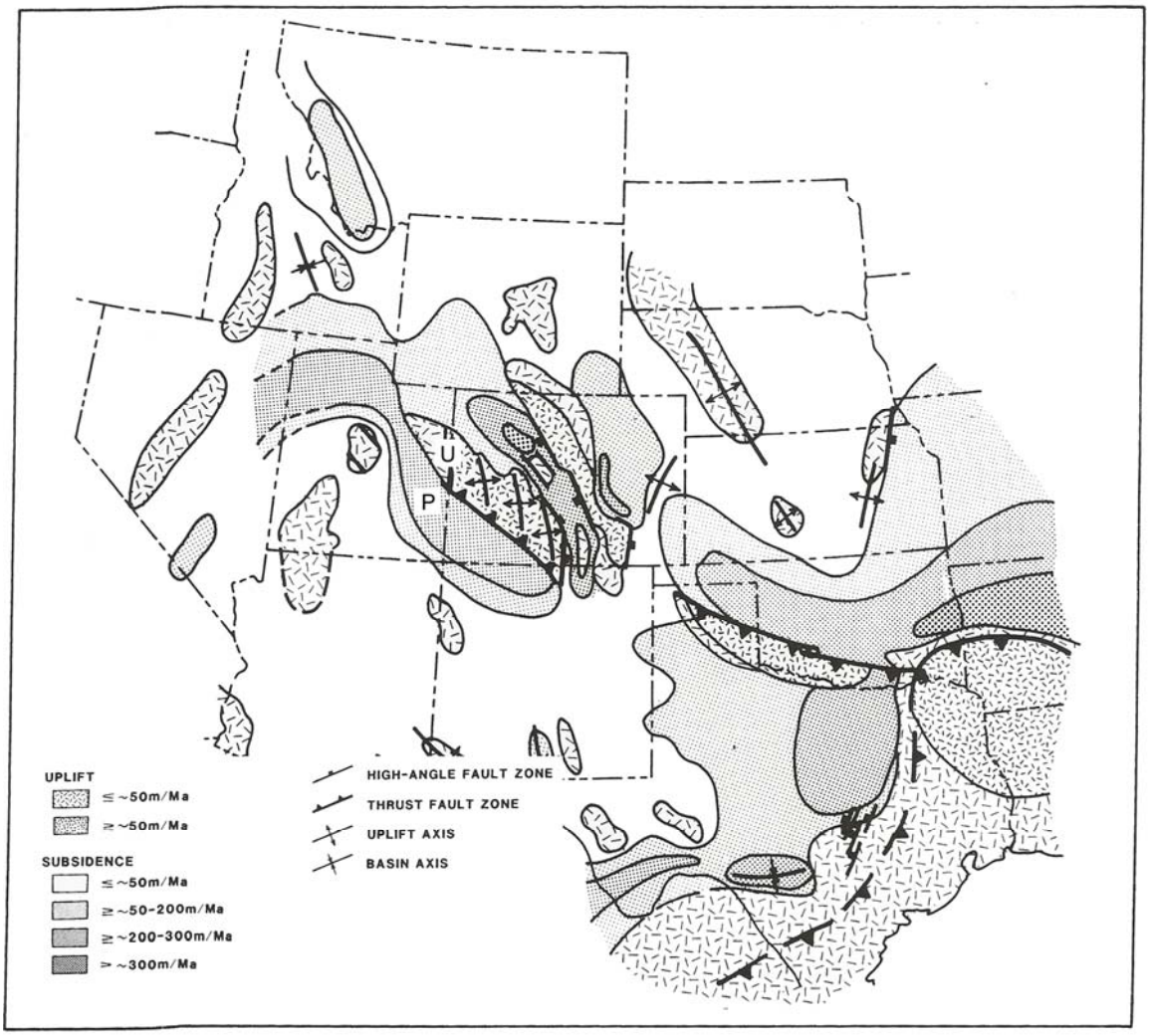

Figure 2.6: Tectonic features of the Ancestral Rocky Mountains during Desmoinesian time. The Paradox Basin is now rapidly subsiding adjacent to the thrusting and uplift of the Uncompahgre highlands. Abbreviations: P, Paradox Basin; U, Uncompahgre Uplift (modified from Kluth, 1986).

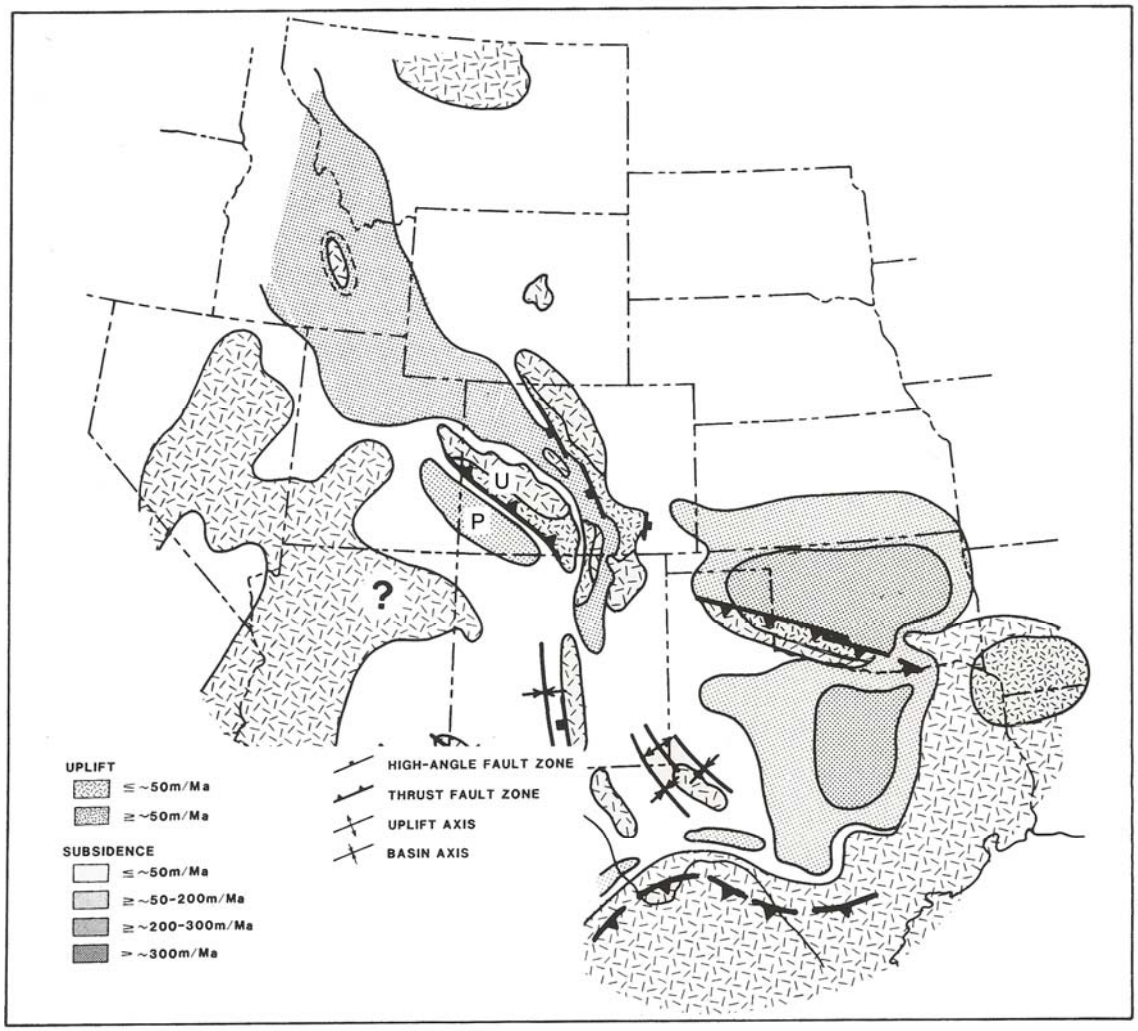

Figure 2.7: Tectonic features of the Ancestral Rocky Mountains during Missourian time. Deformation caused by the Ancestral Rocky Mountains is starting to decrease, but there is still subsidence in the Paradox Basin only on a much smaller regional scale. Abbreviations: P, Paradox Basin; U, Uncompahgre Uplift (modified from Kluth, 1986).

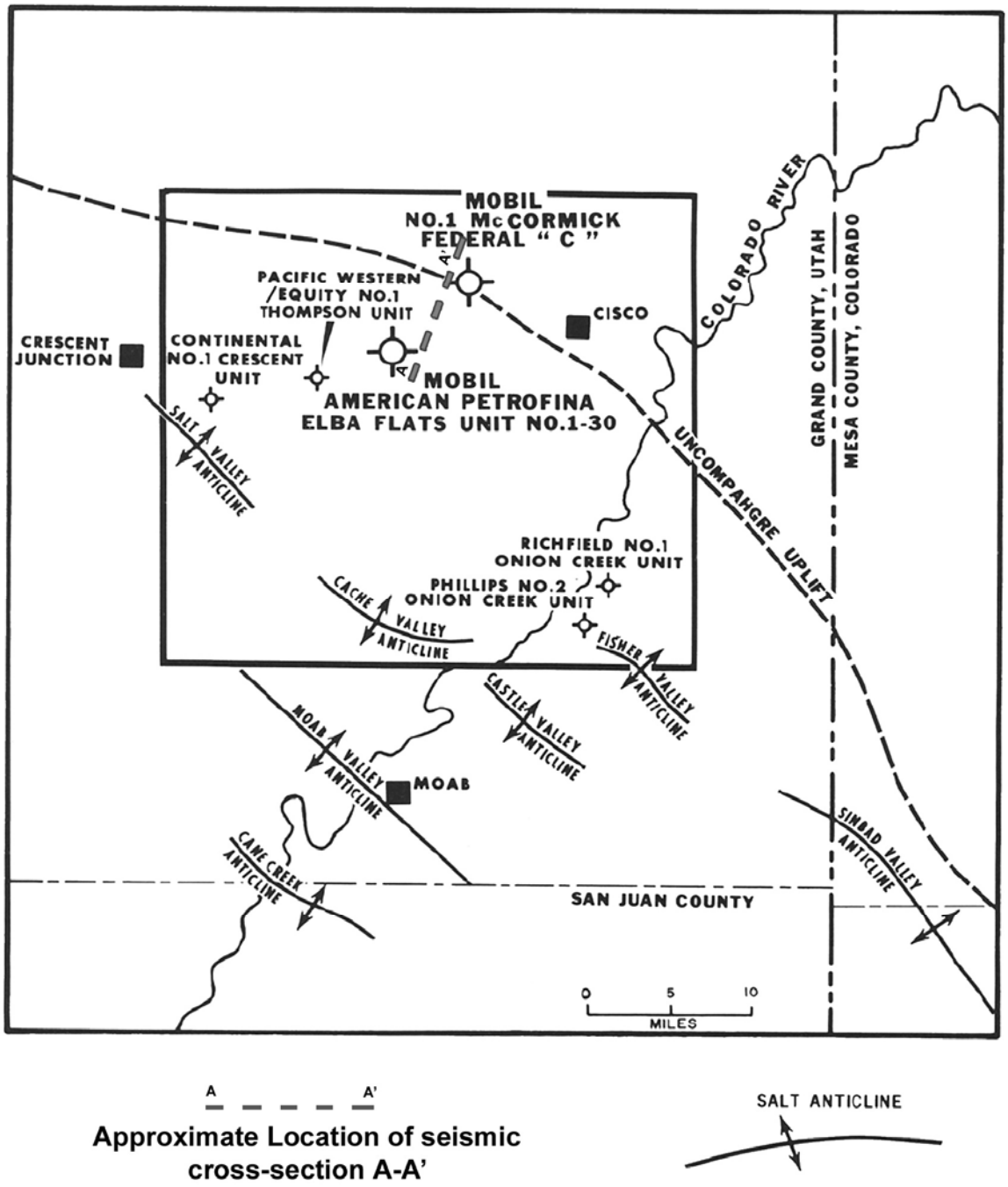

Figure 2.8: Index map of the northern Paradox Basin showing important well locations and the location of seismic line A-A' (modified after Frahme and Vaughn, 1983).

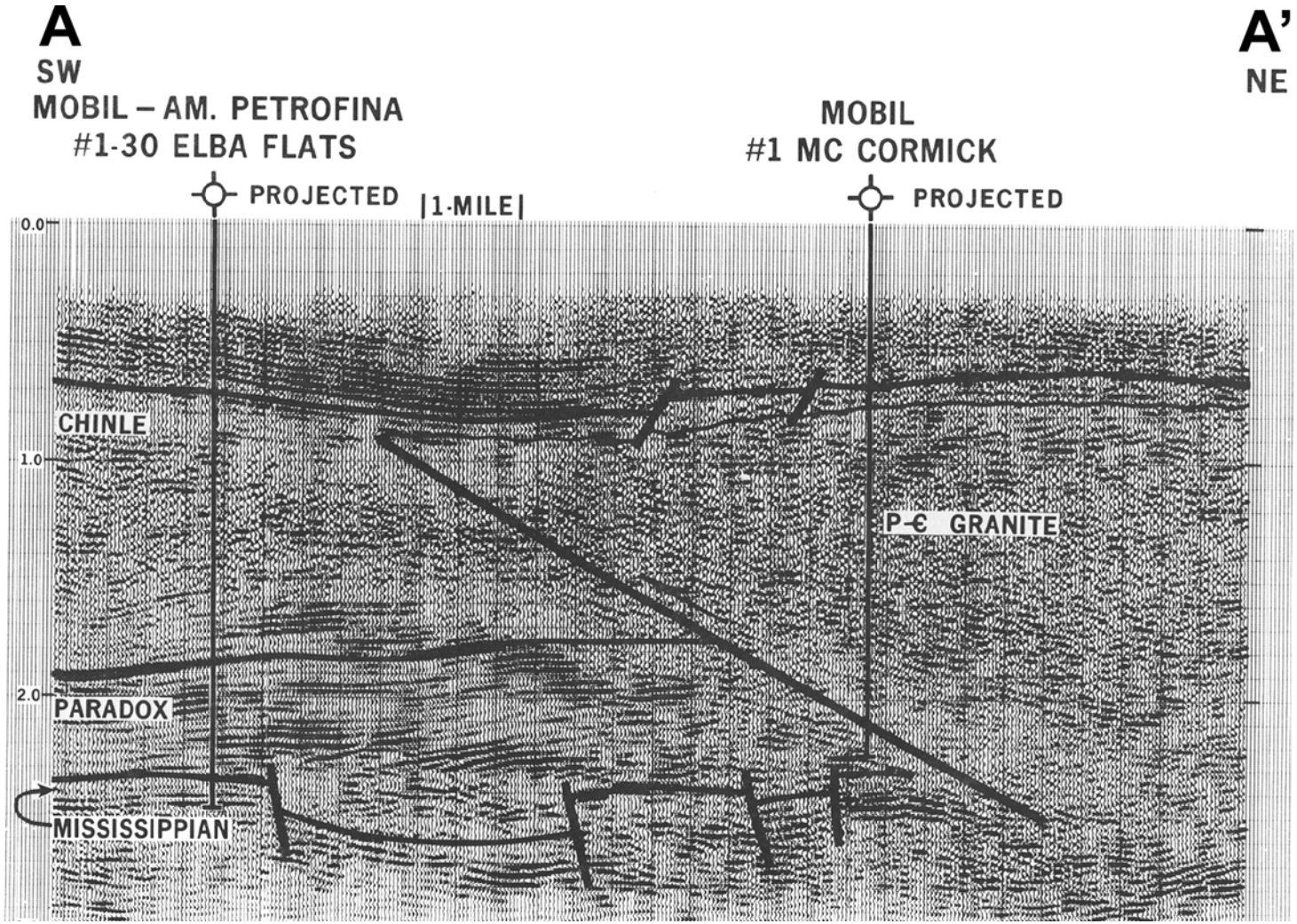

Figure 2.9: Seismic line A-A' showing the position of the Uncompahgre fault zone over what is interpreted as Paleozoic rocks (modified after Frahme and Vaughn, 1983).

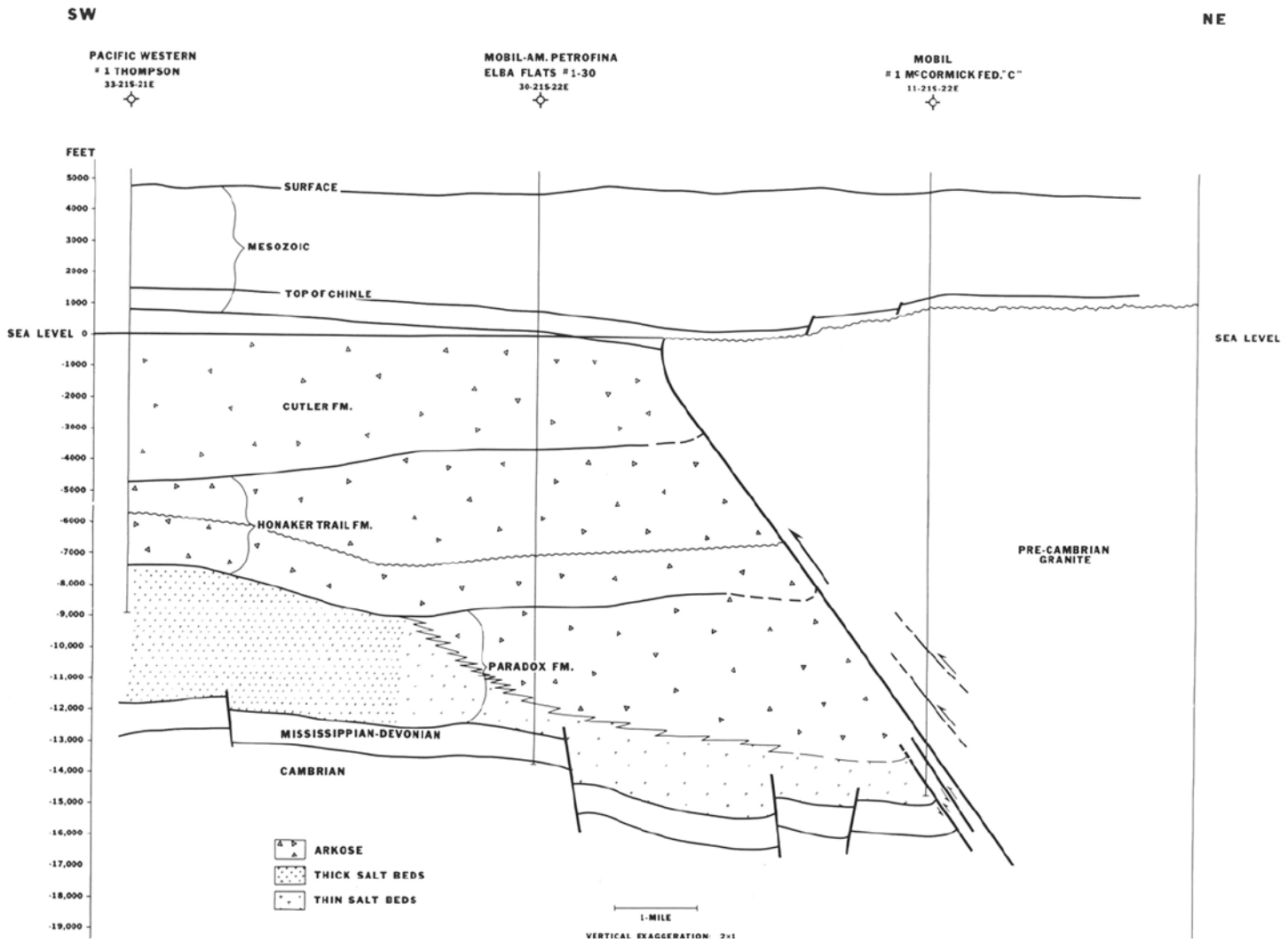

Figure 2.10: Generalized cross-section of the northern Paradox Basin including the fault system of the Uncompahgre Front. The cross-section is roughly along the same line as seismic line A-A' seen in Figure 2.9 (after Frahme and Vaughn, 1983).

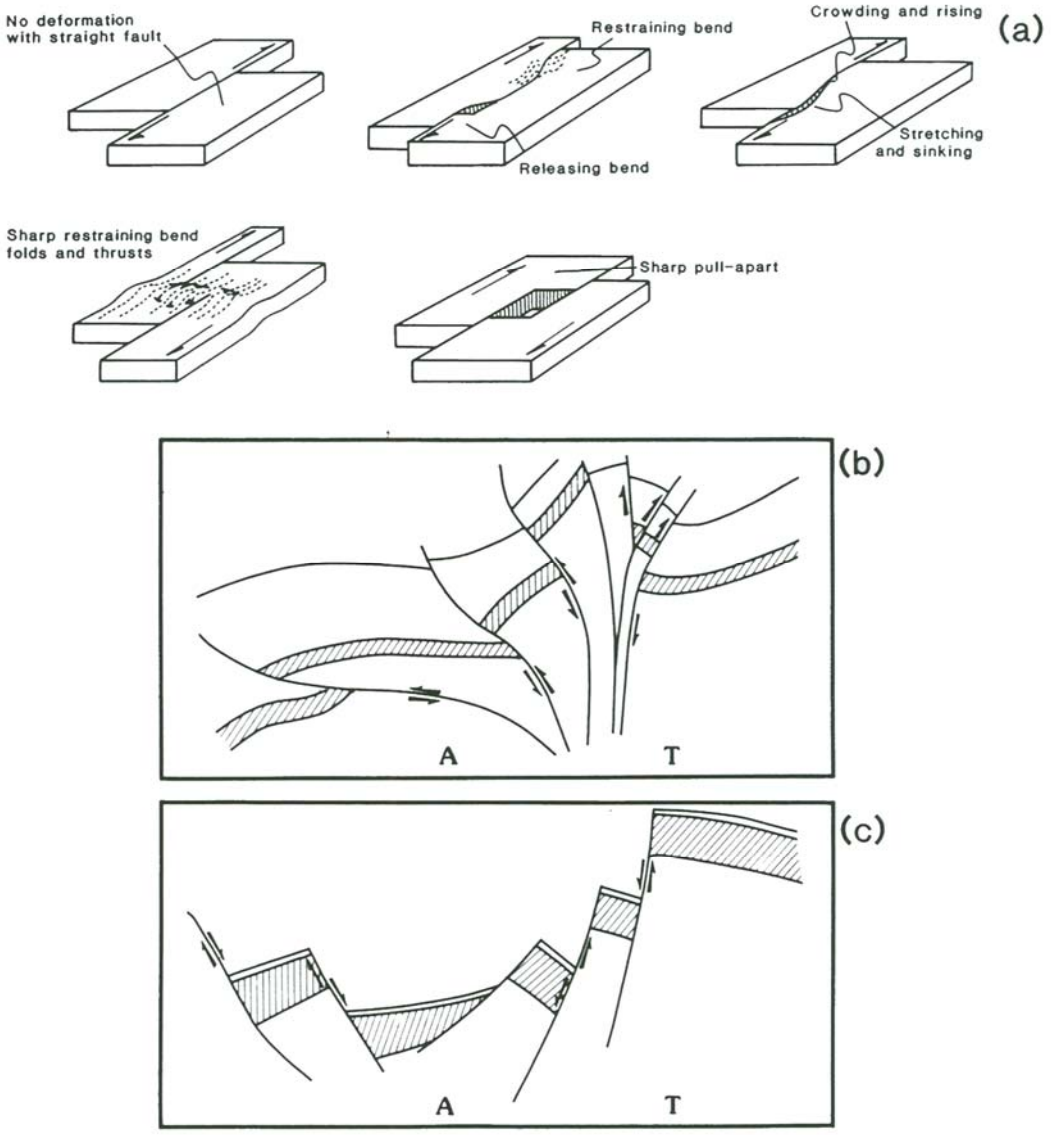

Figure 2.11: (a) Block diagrams illustrating the types of strike-slip fault patterns that might be seen in an extensional environment like Stevenson and Baars (1986) suggested for the Paradox Basin. (b) Cross-sectional diagram of a restraining bend where steeply dipping thrusts or flower structures might be projected. (c) Cross-sectional diagram of a releasing bend where tension and extensional forces create down-faulting or rift type settings (after Stevenson and Baars, 1986).

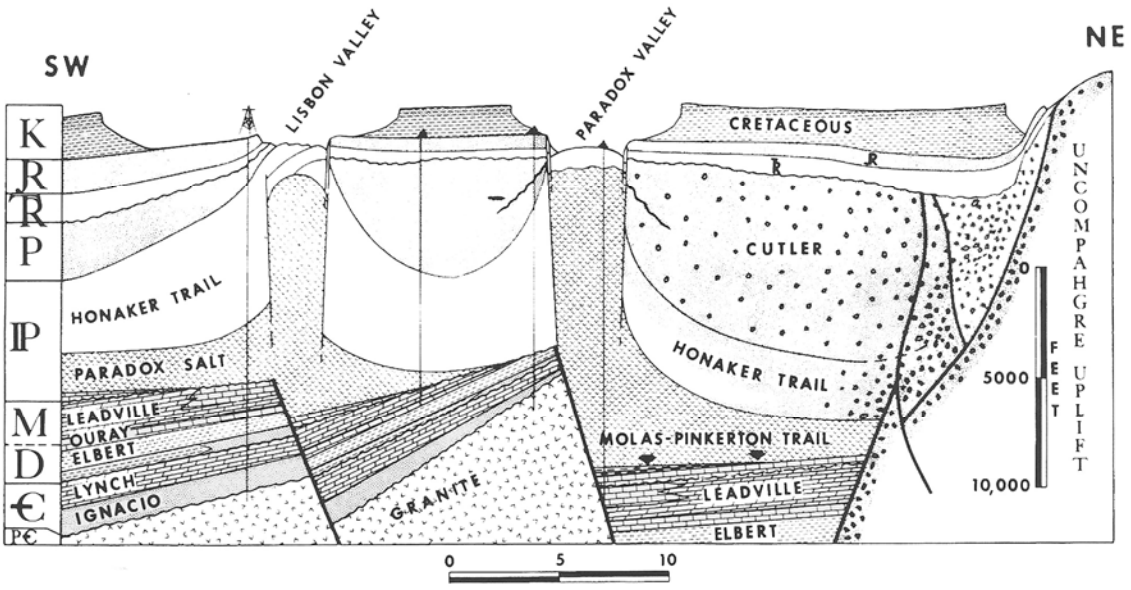

Figure: 2.12: Schematic cross-section across the central-eastern Paradox Basin showing extensional basement faults creating a pull-apart trough. The Uncompahgre fault system is shown here as a braided network of wrench faults, which are locally high-angle reverse faults. The figure also displays the Lisbon and Paradox valley diapiric salt structures formed during Desmoinesian time (modified from Stevenson and Baars, 1986).

Paradox Basin. The margins between uplift and basin generally display significant vertical movement along faulted structural boundaries.

Further investigating by Kluth and DuChene (2006) postulated the idea that the Paradox and Eagle Valley (central western Colorado, Figure 2.13) basins were connected before the rise of the Uncompahgre Uplift. They discussed how sediment loading from the Permian Cutler Formation caused the evaporites of the Pennsylvanian Paradox Formation to evacuate and form diapiric walls. These salt structures grew by down-building of adjacent depocenters. Therefore, the development of the Paradox Basin itself was not connected to the formation of the Uncompahgre Uplift. Similar conclusions were made by Fetzner (1960). He used tectonic evidence and clastic ratio maps of the Hermosa Group to suggest the Uncompahgre Uplift wasn't a positive feature in the northern Paradox Basin during the time of salt (Paradox Formation) deposition. This would have allowed the Paradox and Eagle basins to be connected and/or considered one greater basin. Only after salt deposition did the Uncompahgre Uplift become positive in the northern part of the basin and have a significant influence on deposition of the Honaker Trail and Culter formations.

Barbeau (2003) interpreted the Paradox Basin as an intraforeland flexural basin. He suggested the Paradox Basin formed due to flexural subsidence associated with the ARM Uncompahgre Uplift based on the subsidence history, shape, structural relationships and facies architecture of the basin. His model uses the idea of a foredeep zone that formed adjacent to the uplift as a response from the crustal flexure of the Uncompahgre thrust (Figure 2.14). As a result of this flexure, Barbeau (2003) also suggested a positive crustal rebound structure called a forebulge. This bulge is thought to be associated with the carbonate shelf that rims the south and southwestern edges of the basin. He also compared the Paradox Basin and other flexural-isolated foreland basins, with pull-apart basins. Using an aspect ratio measurement combining basin length and width (Length / Width) Barbeau (2003) showed that the Paradox Basin would generally be considered a flexural-isolated foreland basin and not related to the previous formation theory involving pull-apart tectonics (Figure 2.15).

Neff (1960) tries to make the comparison between salt structures in the Persian Gulf area with those of the Paradox Basin. He notes the similarities in folding and

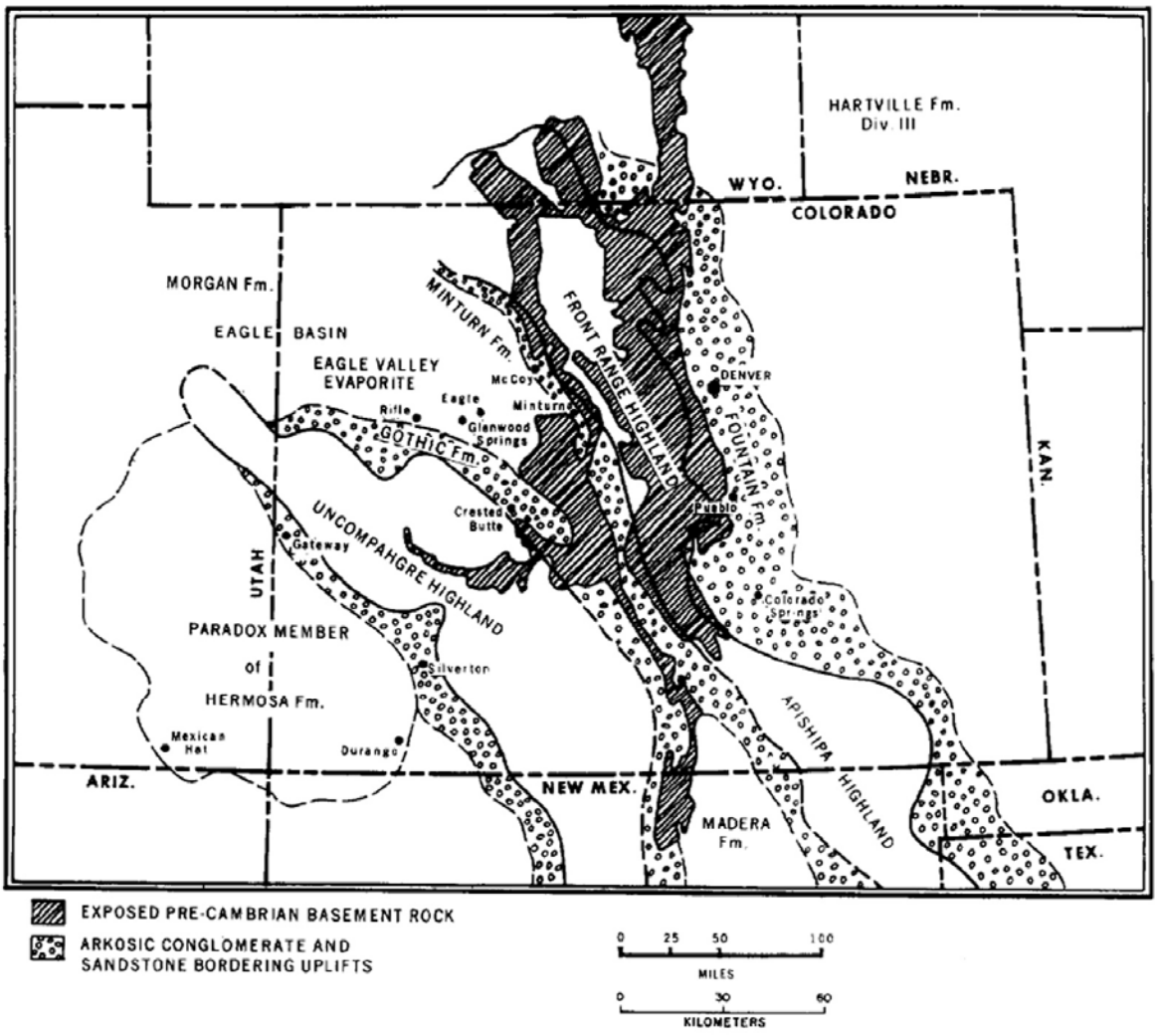

Figure 2.13: Map showing the location of the Eagle Basin and the Eagle Valley evaporites (after Tillman, 1971).

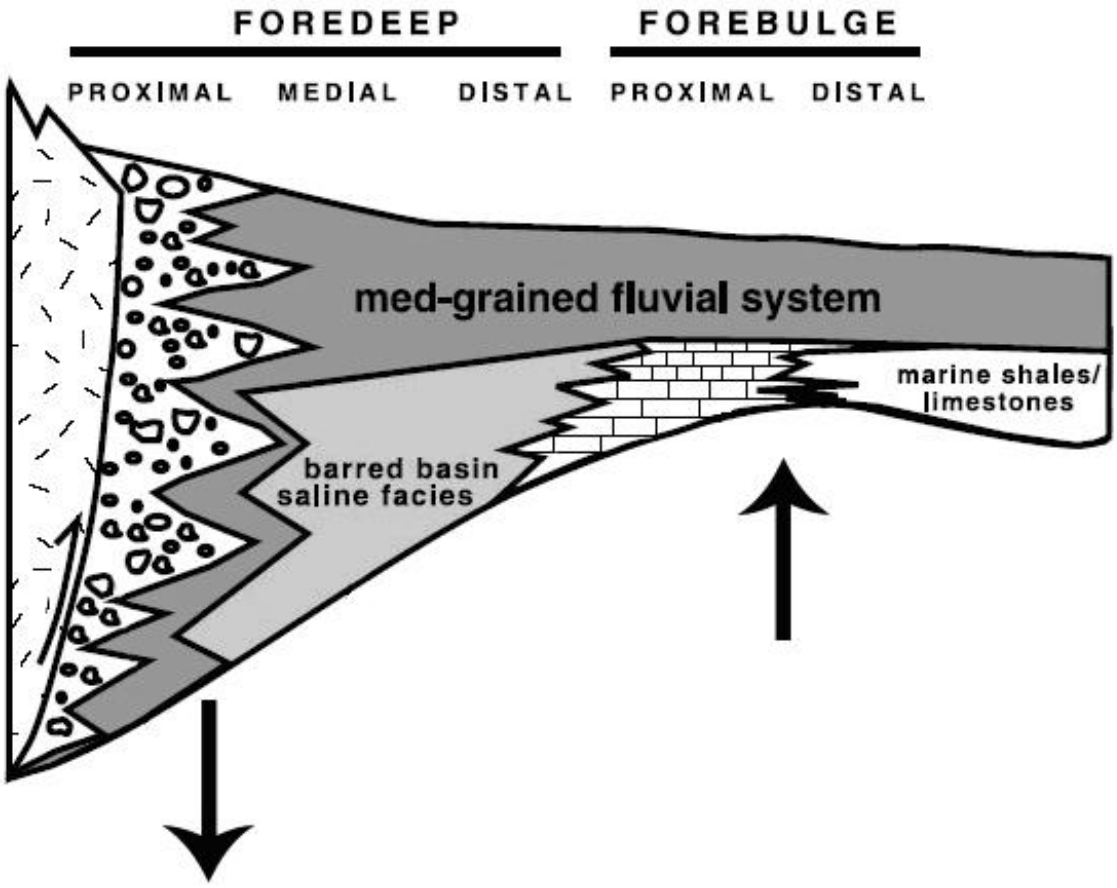

Figure 2.14: D. L. Barbeau's flexural model of the Paradox Basin includes the idea of having a foredeep and forebulge as part of a crustal rebound, or flex, from the protruding Ancestral Rocky Mountain Uncompahgre Uplift. The illustrative cross-section runs roughly from Gateway, Colorado (left) to Blanding and Bluff, Utah (middle) to Kayenta, Arizona (right). The black arrows show relative flex direction of the crust (modified from Barbeau, 2003).

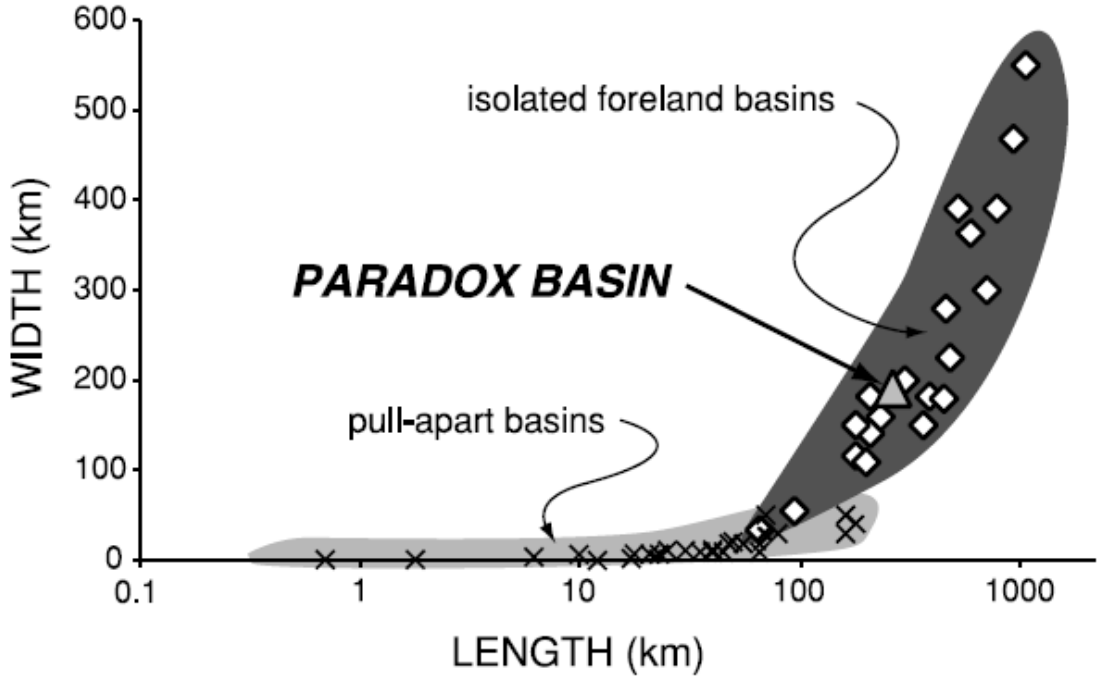

Figure 2.15: Graph of length and width dimensions of several isolated foreland and pull-apart basins found throughout the world. The Paradox Basin plots (length of 265 km; width of 190 km; aspect ratio of 1.39) within the flexural basin range giving rise to the idea that the basin is not structurally related to pull-apart tectonics and associated more with a crustal flex model (after Barbeau, 2003).

formation due to compression. However, the magnitude and length of compressional forces vary between areas. In the Paradox Basin compressonal stresses seemed to be greater in enormity, but transpired over short time intervals. This rapid change in stress promoted rock fracturing, as opposed to folding, which is commonly found around the Persian Gulf.

2.2.5 Salt Structures and Geometries

The northern Paradox Basin is home to a variety of salt structures ranging from complex faulted diapirs and exposed salt walls to buried salt pillows (Figure 2.16). The area is commonly referred to as the "Paradox fold and fault belt" (Kelley, 1955; 1958) and overlies the deepest section of the basin. Here depositional salt thicknesses range between 5,000 feet (1,500 m) and 8,000 feet (2,400 m) (Baars and Stevenson, 1981).

Salt structure geometries vary across the basin from northeast to southwest. The most striking features are the prominent salt walls or collapsed anticlines commonly referred to as "salt valleys". The Salt Valley Anticline, Onion Creek diapir/Fisher Valley salt structure and the Sinbad Valley Anticline are all located close to the Uncompahgre Uplift. Moving further to the southwest are the smaller Castle Valley and Moab/Spanish Valley anticlines. It is important to note all of these structures trend northwest-southeast and strike parallel to the uplift. Southwest of Moab, Utah and beyond the major salt walls are several buried salt structures that tend to be broader and less structurally complex. The Cane Creek Anticline is an example of such a feature that is underlain by a salt pillow that gently strained the overlying strata to create the associated anticline (Trudgill *et al.*, 2004). Many of the larger salt structures are controlled by major northwest-southeast striking basement faults positioned on the southwest boundary of the structures (Shoemaker *et al*., 1958; Joesting *et al.*, 1966; Cater and Elston, 1963). These faults proved to be important factor in salt tectonics because they provided a lateral barrier and a vertical pathway for salt flowage (Baars, 1966).

As salt accumulated in the deeper parts of the basin, alluvial fans consisting of thick arkosic material (undifferentiated Cutler Formation) were being shed off the

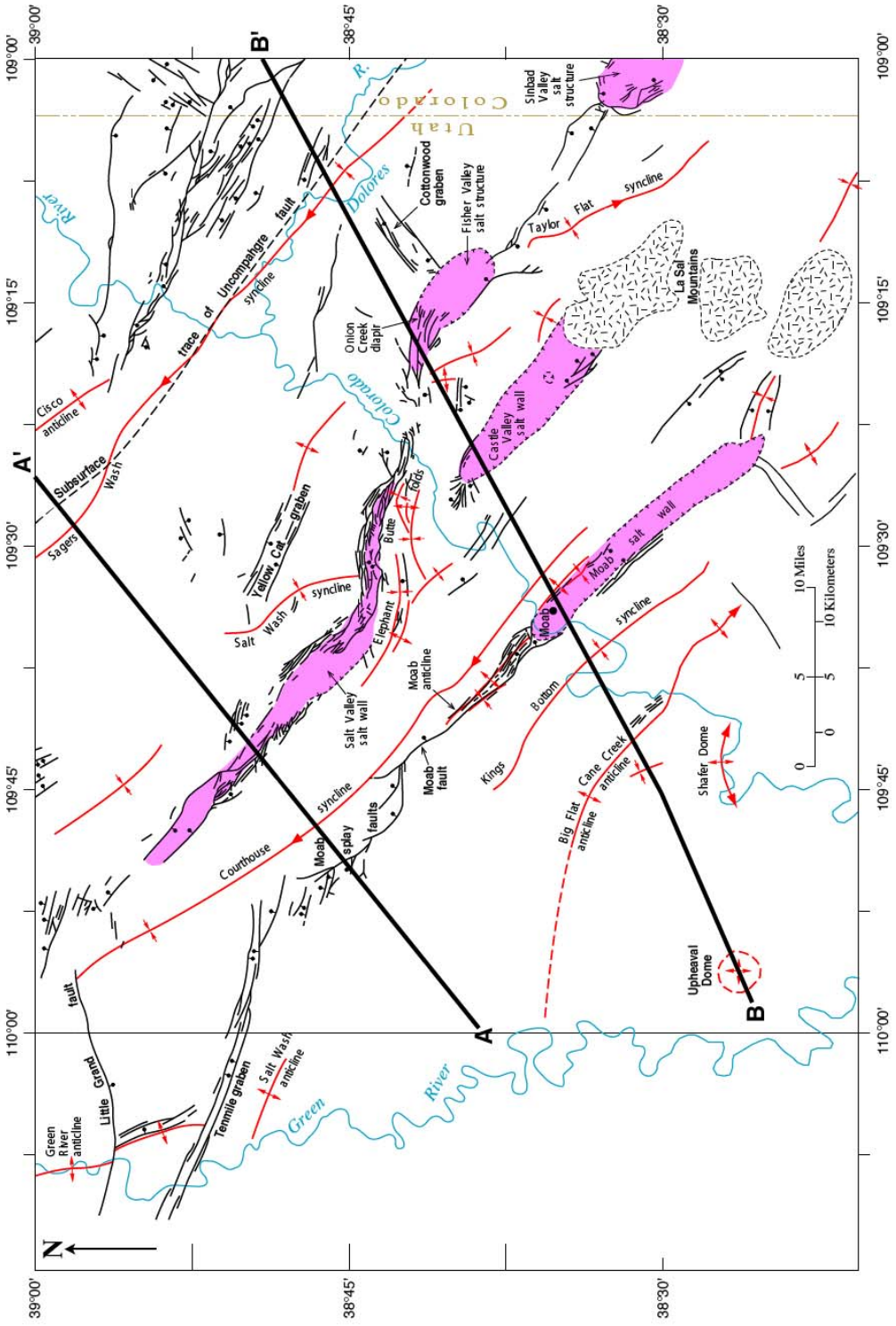

Figure 2.16: Structural features of the northern Paradox Basin. Near surface salt structures are highlighted in pink (after Doelling, 2001; Trudgill *et al.*, 2004). Cross-section A-A' and B-B' (illustrated here) are not displayed in this document.

Uncompahgre Uplift (Baars and Stevenson, 1982). Differential sediment loading from the Cutler onto the underlying salt caused rapid salt movement away from the load of the deposited arkosic material. Jones (1959) calculated a shear strength, using geologic conditions, of less the 30 kg/cm^2 would cause salt to flow. This would be equivalent to about 1,000 feet (300 m) or less of overlying sediments.

Salt movement was at its peak in Late Pennsylvanian and Early Permian times where it flowed southwestward into the salt walls and structures we see today. The uplift of the Uncompahgre plateau ended in the Permian and it was at least partially buried by sediments by the Late Triassic (Chinle Formation). Salt flowage slowed and stopped by Triassic time because the available salt had been depleted and welded out in many places (Baars and Stevenson, 1981).

2.3 Basin Stratigraphy

The Paradox Basin is comprised of a thick sequence of sedimentary rocks that overlie a complex series of Proterozoic Precambrian basement rocks. Cambrian through Jurassic strata overlie basement rocks throughout most of the basin (Figures 1.2 and 2.17) with the exception of several Tertiary igneous intrusive cores that are scattered throughout the basin. There are also several prominent Cretaceous units that are economically significant not only to the Paradox Basin, but also to several surrounding basins. Most of the Tertiary strata within the basin have completely been eroded away (Nuccio and Condon, 1996).

2.3.1 Precambrian Rocks

Precambrian basement rocks underlie almost all sedimentary strata in the Paradox Basin. These early Proterozoic rocks are identified as metamorphic gneisses and schists (Nuccio and Condon, 1996). Analogous outcrops can be seen in the Grand Canyon, the Uinta Mountains and in the Wasatch Mountains to the west and northwest. These

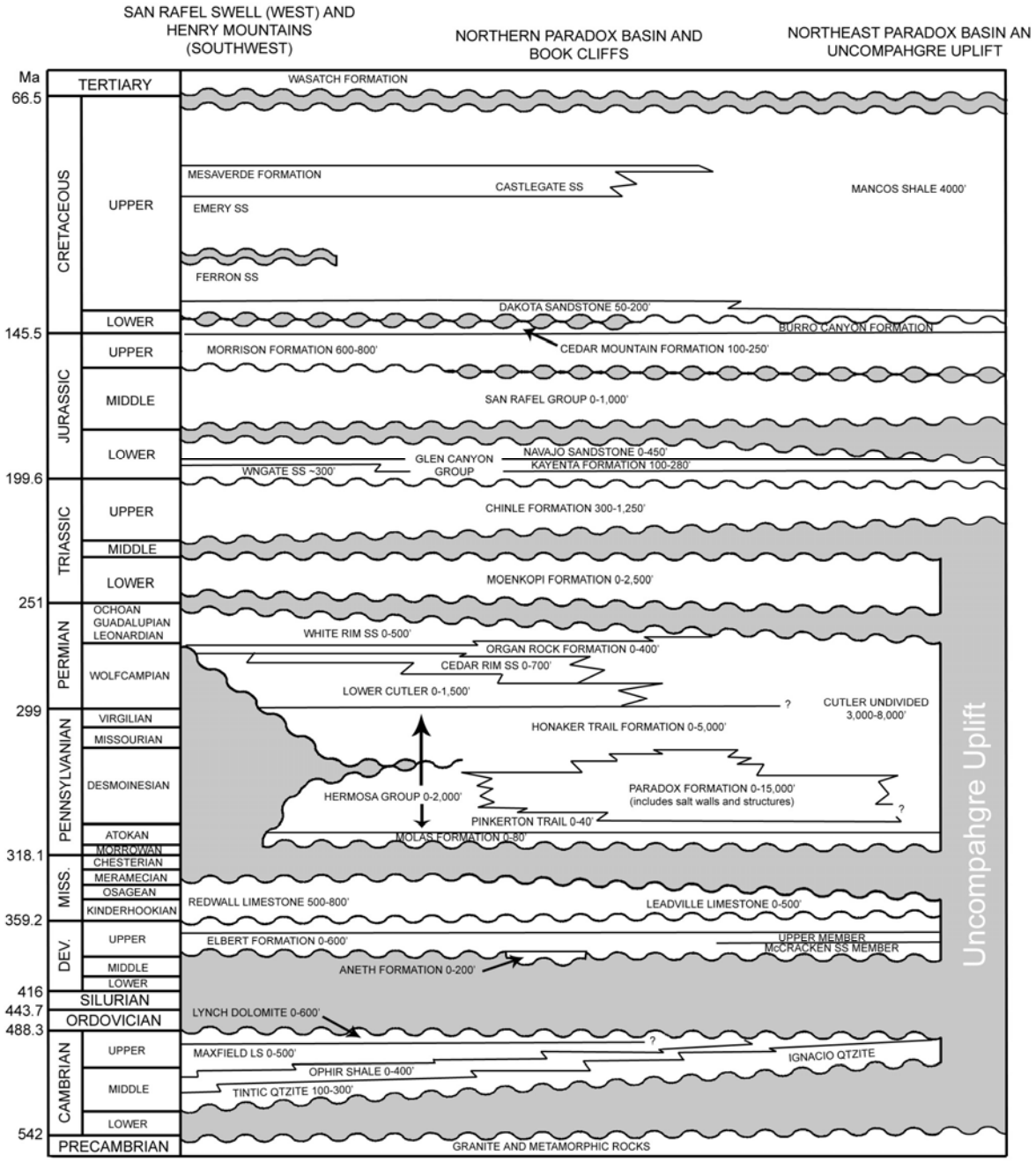

Figure 2.17: Correlation chart for Precambrian through Tertiary rocks of the Paradox Basin. Note the change from east to west involving the Uncompahgre Uplift and the overlying strata. Evidence from wells drilled adjacent to the Uncompahgre display the termination of Cambrian through Lower Triassic rocks against the uplift. Compiled from Molenaar (1981), Baars (1987) and Nuccio and Condon (1996).

outcrops are too diverse to correlate locally and are too far away from the Paradox Basin to accurately characterize the subsurface Precambrian lithologies (Condon, 1995). Only a few wells have penetrated the underlying Precambrian rocks within the basin and therefore provide very few clues.

The Uncompahgre Uplift is predominantly composed of crystalline granites and gneisses with varying amounts of micaceous shists and pegmatites. A younger granitic rock, within the Uncompahgre sequence, as been dated to be at least 1,300 million years old placing these rocks within a comparable age relationship with the rest of the Precambrian in and around the Paradox Basin (Elston *et al*., 1962).

Uncompahgre Formation (Early to Middle Proterozoic)

The Uncompahgre Formation is an Early to Middle Proterozoic sedimentary unit located mainly in the southeastern part of the basin near the Needle Mountains (Figure 1.2) (Tweto, 1980a; Nuccio and Condon, 1996). The formation consists of interlayered quartzites, phyllites and slates with very minor amounts of siltstone and conglomerate (Barker, 1969; Tweto, 1987).

2.3.2 Cambrian Rocks

Overlying the Precambrian Rocks in most of the basin are Cambrian rocks (Figure 1.2). The Lower and Middle Cambrian Tintic Quartzite and its equivalent formations in Colorado (Upper Cambrian Ignacio Quartzite) and Arizona (Middle Cambrian Tapeats Sandstone), mark the first sedimentary unit deposited unconformably on Precambrian rocks. The Middle Cambrian Ophir Formation in central Utah (known as the Bright Angel Shale within the Grand Canyon) conformably overlies the Tintic Quartzite followed by the Middle Cambrian Maxfield Limestone and Upper Cambrian Lynch Dolomite (Condon, 1995).

Lynch Dolomite (Upper Cambrian)

The Lynch Dolomite is the first widely deposited Cambrian unit found within the northern Paradox Basin (Figure 1.2). However this information is unreliable due to a lack of wells reaching such depths. The Lynch Dolomite is described as a series of tan to cream limestones and dolomites interbedded with thin beds of shale and sandstone. Algal material and brachiopods suggest a stable marine shelf environment of deposition (Condon, 1995; Nuccio and Condon, 1996). Frahme and Vaughn (1983) report penetration of Cambrian rocks equivalent to the Maxfield Limestone or the Lynch Dolomite in the Mobil – American Petrofina Elba Flats Unit No. 1-30 well (T 21S, R 22E, sec. 30) at a depth of 18,311 feet (5,580 m).

2.3.3 Ordovician and Silurian Rocks

Rocks of Ordovician and Silurian age are not documented in the Paradox Basin. Thin units may have been deposited but post-Cambrian erosion has removed any such recognizable formations or lithologies.

2.3.4 Devonian Rocks

Much like the Ordovician and Silurian, Early and Middle Devonian rocks are not recognized in the Paradox Basin (Figure 1.2). However several formations were deposited during the Upper Devonian including the Aneth Formation, Elbert Formation and the Ouray Limestone. The Aneth Formation (Frasnian in age) is described as a very fossiliferous dark-gray to dark-brown dolomite and shale. It is consistently only found in the southern third of the basin (Condon, 1995).

Elbert Formation (Frasnian)

The Elbert Formation is divided into the lower McCracken Sandstone member and an upper unnamed member and conformably overlies the Aneth Formation where

present (Figure 1.2). The McCracken Sandstone is distributed throughout most of the basin and is a result of erosion from clastic material shed off highlands in central Colorado (Nuccio and Condon, 1996). It tends to be a white, gray and pink quartzitic sandstone with minor interbedded shale and dolomite (Condon, 1995; Nuccio and Condon, 1996). Thickness ranges from 0 – 122 feet (0 – 37 m).

The upper member of the Elbert Formation is identified throughout the basin. It is primarily a dolomite with red and green shale with some sandstone near the base and was deposited in a shallow shelf marine environment. Thicknesses of the upper member range from zero in the southeast part of the basin to near 600 feet (183 m) in the northwest (Gustafson, 1981).

Ouray Formation (Famennian – Kinderhookian?)

The Ouray Formation is a massive, light- to dark-brown to gray limestone and dolomite with thin shale intervals that conformably overlies the Elbert Formation (Figure 1.2). Oolites, crinoid fragments, brachiopods, pyrite and anhydrite are found in several wells but are inconsistent throughout the basin (Gustafson, 1981; Condon, 1995). Deposition is thought to have occurred in a shallow marine shelf environment much like the Elbert Formation. Thicknesses vary from zero to around 200 feet (61 m) over most of the basin (Condon, 1995). One well in the northeast recorded a thickness of almost 130 feet (40 m) (Frahme and Vaughn, 1983). Most studies agree that contacts with the underlying Elbert Formation and the overlying Leadville Limestone are based upon faunal differences. Devonian vertebrates characterize the Elbert Formation while Devonian invertebrates classify the Ouray. A Mississippian-aged invertebrate marks the boundary with the Leadville (Condon, 1995).

2.3.5 Mississippian Rocks

Leadville Limestone (Kinderhookian – Osagian)

The Leadville Limestone and its equivalent, the Redwall Limestone, is the only unit deposited during Mississippian time (Figures 1.2 and 2.18). It is chiefly composed

of thinly bedded to massive cherty dolomite with increasing amounts of limestone within the upper units (Baars and Stevenson, 1982; Doelling, 1988).

Leadville deposition was a result of a series of sea-level transgressions and regressions initiated from the west during the Antler orogeny (Nuccio and Condon, 1996). The upper section of the Leadville Limestone is characterized by prominent crinoidal biogenic bank deposits. These deposits accumulate most readily in quiet shallow waters (Baars and Stevenson, 1982). However fossils tend to be scarce, probably due to the process of dolomitization (Merrill and Winar, 1958; Frahme and Vaughn, 1983). Leadville carbonates identified in the northeastern part of the basin show a more sandy and silty nature. Frahme and Vaughn (1983) suggest this could represent the initial stages of regional uplift.

Underlying the Leadville is the Devonian Ouray Formation which is also composed of dolomites and limestones. This contact is gradational and often hard to distinguish (Baars and Stevenson, 1982). Overlying the Leadville is the Pennsylvanian Molas Formation. This unconformable contact is heavily karsted and represents a significant period of non-deposition within the basin.

Thicknesses can vary depending on location but range from about 200 – 600 feet (61 – 183 m) thick (Doelling, 1988). Figure 2.19 shows an isopach map of sub-Pennsylvanian rocks.

2.3.6 Pennsylvanian Rocks

Molas Formation (Atokan)

The Molas Formation is only exposed near Molas Lake south of Silverton Colorado, in the San Juan Mountains (Figures 1.2 and 2.20). It is mainly composed of red siltstones and shales interbedded with limestones, sandstones and conglomerates (Merrill and Winar, 1958; Frahme and Vaughn, 1983; Doelling, 1988). Abundant hematite and ferric iron give the formation its red color. Marine fossils present in the upper part of the Molas Formation indicate a middle Atokan age. However, Merrill and

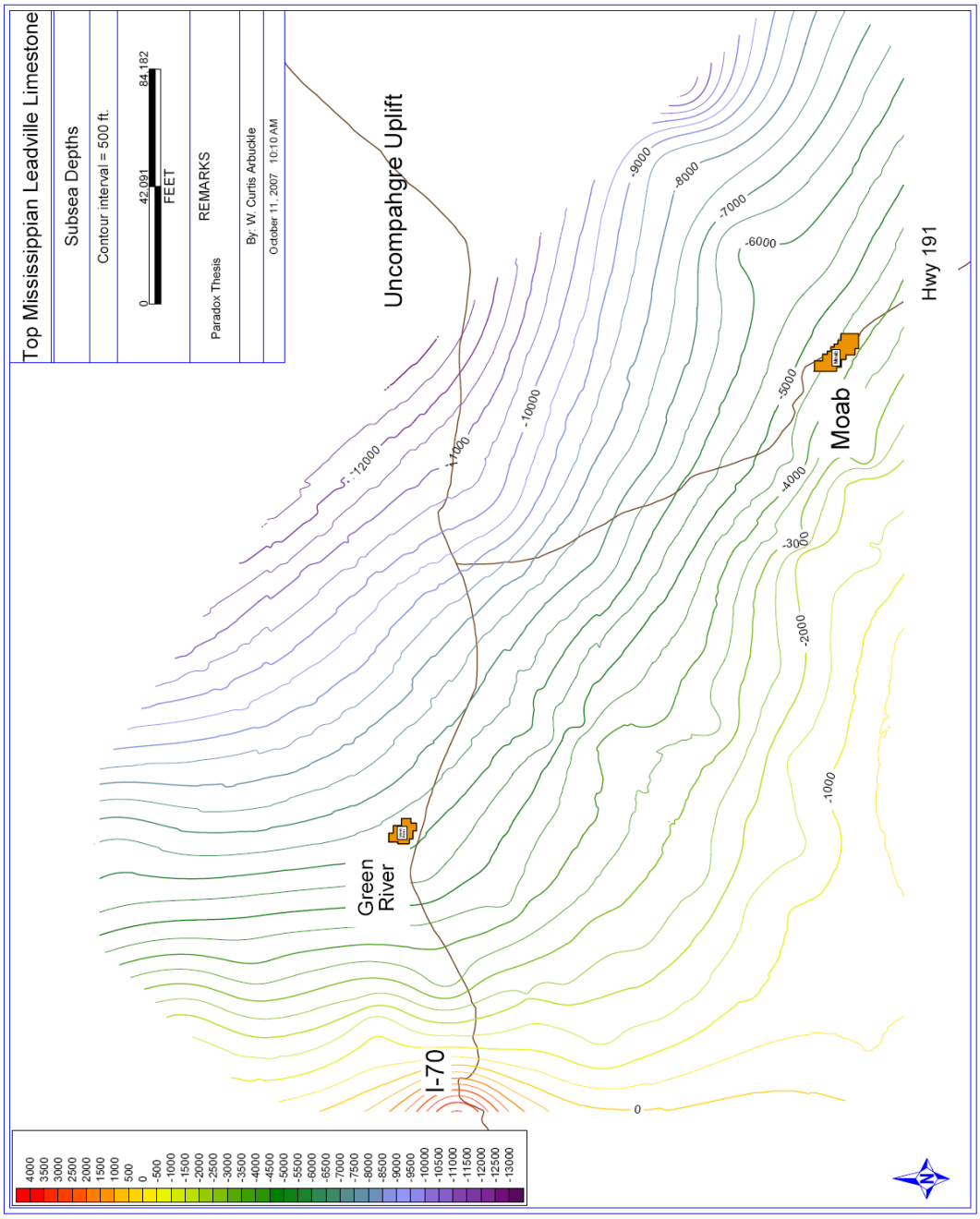

Figure 2.18: Structure contour map of the top of the Mississippian Leadville Limestone. Contour interval = 500 feet (152 m) (subsea depths).

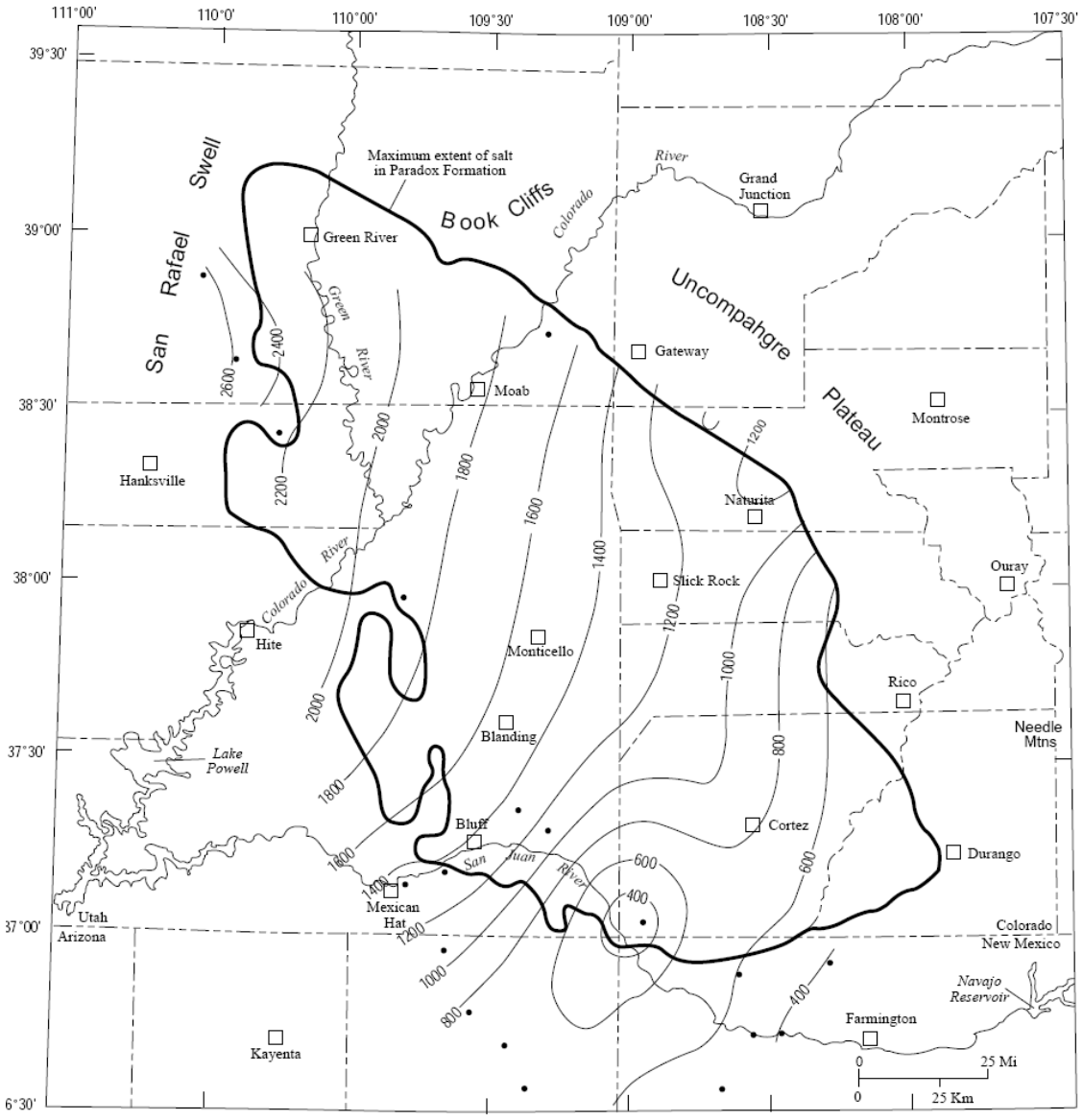

Figure 2.19: Isopach map totaling all stratigraphic units below the Pennsylvanian Molas Formation (after Nuccio and Condon, 1996). Contour interval = 200 feet (61 m).

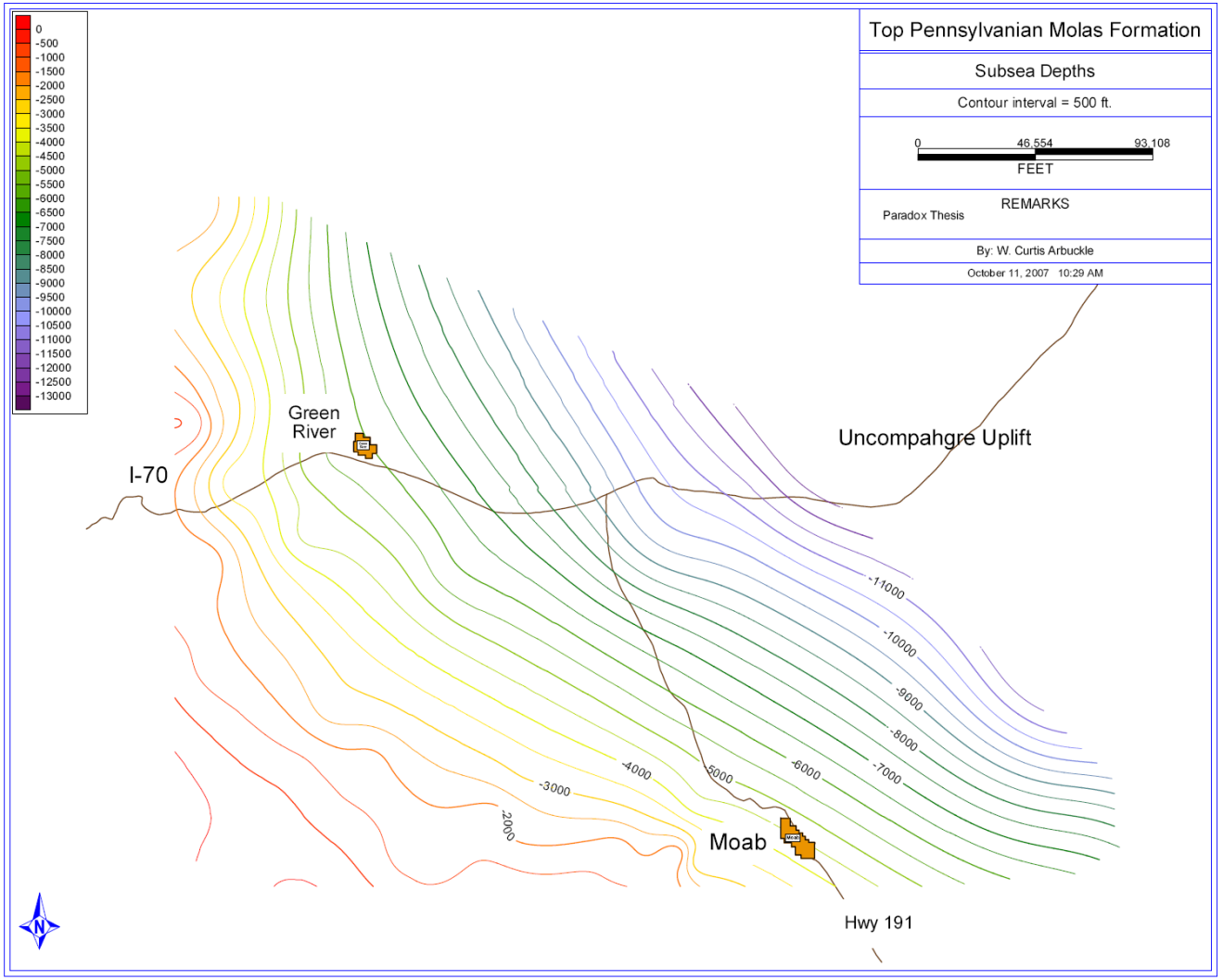

Figure 2.20: Structure contour map of the top of the Pennsylvanian Molas Formation. Contour interval = 500 feet (152 m) (subsea depths).

Winar (1958) suggest an earlier Late Mississippian deposition based on limestone classification within what is deemed the “transition zone” or unit 2 of the Molas.

The oldest of three members, the Coalbank Hill is a regolith deposit and contains rock fragments of chert and limestone derived from the underlying Ouray (Devonian) and Leadville (Mississippian) formations (Merrill and Winar, 1958; Weir and Puffett, 1981). The upper member represents a more marine environment with a red to green shale-sandstone sequence containing several marine fossils including fusulinids, foraminifera, trilobites, brachiopods, bryozoan, echnoids, ostracods and pelecypods (Wengerd and Strickland, 1954; Merrill and Winar, 1958).

The Molas lies unconformably on the karsted surface of the Leadville Formation creating the regolith deposit. The karsting and red shale infill can make it difficult to pick the base of the Molas Formation on some well logs (Condon, 1995). Formation thicknesses range from 20 – 80 feet (6 – 25 m) depending on location.

Hermosa Group (Atokan – Virgilian)

The Hermosa Group is comprised of three formations: from oldest to youngest, the Pinkerton Trail, the Paradox and the Honaker Trail (Figure 1.2). This group consists of both marine and evaporitic sediments in the northern and central parts of the basin. To the south and southwest, abundant carbonate mounds represent the edge of the basin and have historically produced hydrocarbons.

Pinkerton Trail Formation (Atokan – Desmoinesian)

The Pinkerton Trail is the oldest formation of the Hermosa Group (Figures 1.2 and 2.21). It consists of interbedded marine black shales, siltstones, dolomite/limestones and anhydrite (Doelling, 1988; Nuccio and Condon, 1996). It conformably overlies the Molas Formation and marks the transition from normal marine to restricted marine (Herman and Barkell, 1957; Doelling, 1988). The contact between the overlying Paradox Formation is gradational and suggests a transition from a restricted marine carbonate depositing sea (Pinkerton Trail Formation), to a penesaline, evaporitic environment (Paradox Formation) (Wengerd and Strickland, 1954; Herman and Barkell, 1957).

Fusulinids found in both outcrop and well cuttings correlate to an Atokan age (Wengerd and Strickland, 1954).

Thicknesses in the northern half of the basin can range from 100 – 250 feet (30 – 76 m). It tends to thicken in the south and southwest portions of the basin up to as much as 450 feet (137 m) (Hite, 1960; Frahme and Vaughn, 1983; Doelling, 1988). A lack of coarse grained clastics and conglomerates throughout the entire formation implies the Uncompahgre Uplift was absent or exhibited very low relief at the time of deposition (Wengerd and Strickland, 1954).

Paradox Formation (Desmoinesian)

The Paradox Formation is the middle of three formations comprising the Hermosa Group (Figures 1.2 and 2.22). It formed due to the influence of several processes including basin subsidence, eustatic and relative sea-level fluctuations, tectonic pulses and intra-basin depositional cyclicity.

The deepest part of the Paradox Basin lies directly adjacent to the Uncompahgre Uplift and exhibits the thickest section of the Paradox Formation. As the basin slowly subsided, open marine waters were restricted from entering the basin partly because of several uplifts rimming the basin. There were however several sags or sills that still allowed for some circulation including a trough in the south through what is now the San Juan Basin, from the west through the Freemont embayment and from the Oquirrh Basin to the northwest (Figure 2.23) (Wengerd, 1962; Baars and Stevenson, 1982). The San Juan entrance, or Cabezon sag, was bounded to the west by the Zuni and Defiance uplifts and to the east by the southern end of the Uncompahgre Uplift and the Nacimiento Uplift. The Oquirrh entryway was bounded to the south by the Emery Uplift which was a positive structure beneath what is now the San Rafael Swell, and to the east by the northwestern edge of the Uncompahgre Uplift. The Freemont passage was located between the Circle Cliffs and the Emery Uplift (Wengerd, 1962; Baars and Stevenson, 1982). Baars and Stevenson (1982) also suggest several other smaller troughs into the Paradox Basin including one from the southwest across what is now the Black Mesa Basin.

Due to the restriction of open marine waters along the edge of the basin, poor circulation created a stagnant evaporite depositional environment throughout much of Desmoinesian time (Baars and Stevenson, 1982). Because of these conditions, salt deposition began in the deepest area of the basin first, gradually thickening to anywhere from 5,000 to 8,000 feet (1,500 – 2,400 m) (Figures 2.24 and 2.25). Such restricted conditions inhibited most biogenic carbonates from accumulating except in the southern part of the basin where phylloid green algae flourished and created carbonate buildups (Baars and Stevenson, 1982). These mounds presently produce the majority of the oil from within the Paradox Basin.

Hite (1960) identified at least 29 evaporite cycles within the Paradox Formation. However, it is possible deeper parts of the basin could have more cycles, but a lack of good well data and varying amounts of salt tectonics make identification difficult. Several of the upper cycles have been grouped together into zones and named based on the same time equivalent intervals found in the southern end of the basin. These zones include the Ismay, Desert Creek, Barker Creek and Akah (Figure 2.26).

The upper contact with the overlying Honaker Trail Formation is considered to be gradational. It is composed of several hundred feet of anhydrite and carbonates above the last (Hite's (1960) cycle number one) halite and black shale interval/cycle. These anhydrous carbonates are thought to be equivalent to the Ismay and Desert Creek carbonate zones found in the southern part of the basin. However in the northern half of the basin, the Ismay and Desert Creek lithologies are extremely saline when compared to the same intervals in the south. There, the zones are dominated by porous carbonate mounds deposited in normal marine conditions (Brown, 1960).

Honaker Trail Formation (Missourian – Virgilian)

The youngest formation of the Hermosa Group is the Honaker Trail (Figure 1.2). It is generally considered to be a southwest tapering, carbonate-dominated wedge (Barbeau, 2003). It consists of arkosic clastics interbedded with marine black shales, dolomite, limestones and a variety of siltstones. Several of the carbonate packages are rich in fusulinids, crinoids, gastropods, corals (solitary and colonial), trilobites, brachiopods and bryozoans as well as abundant chert nodules (Loope and Kuntz, 1987;

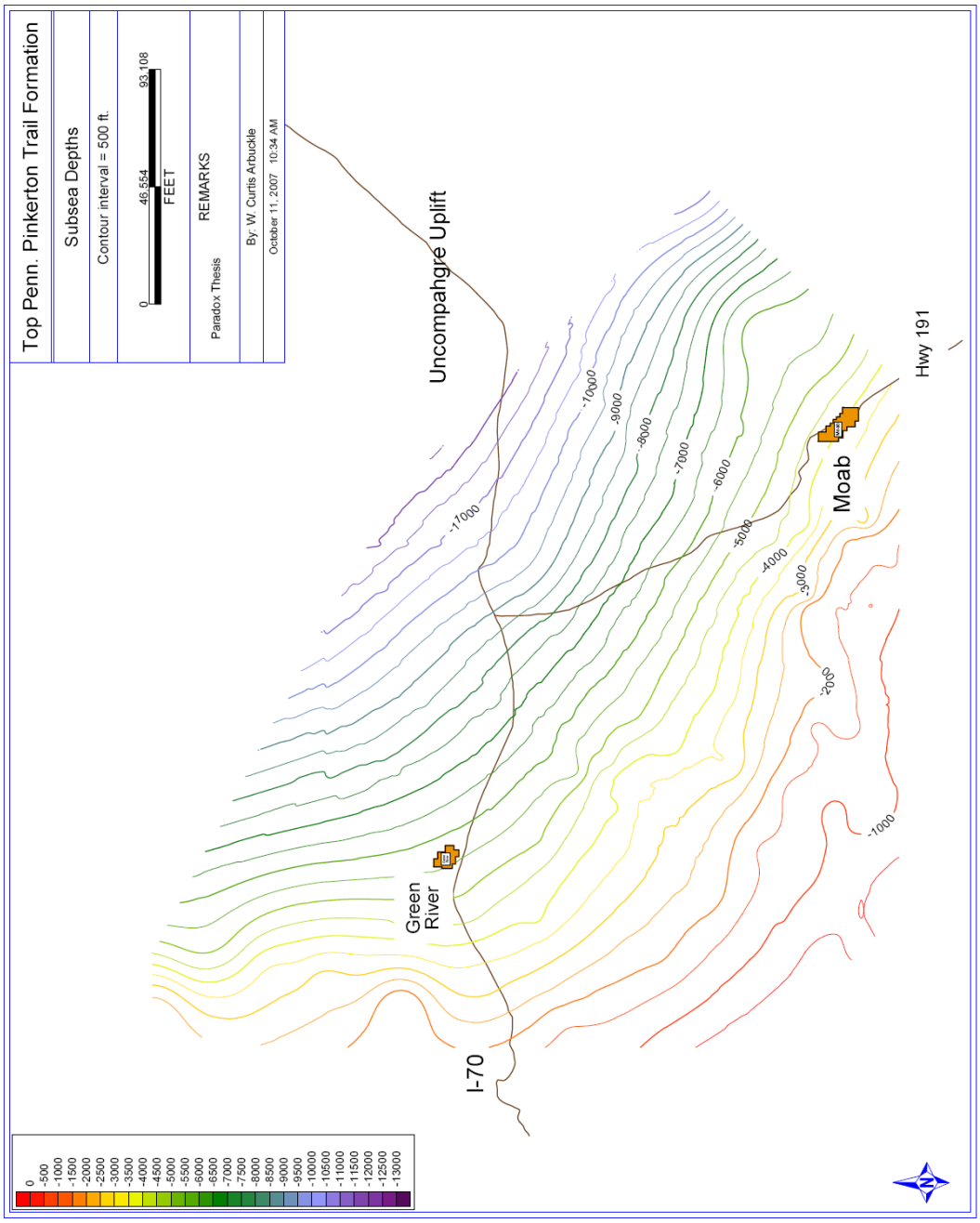

Figure 2.21: Structure contour map of the top of the Pennsylvanian Pinkerton Trail Formation. Contour interval = 500 feet (152 m) (subsea depths).

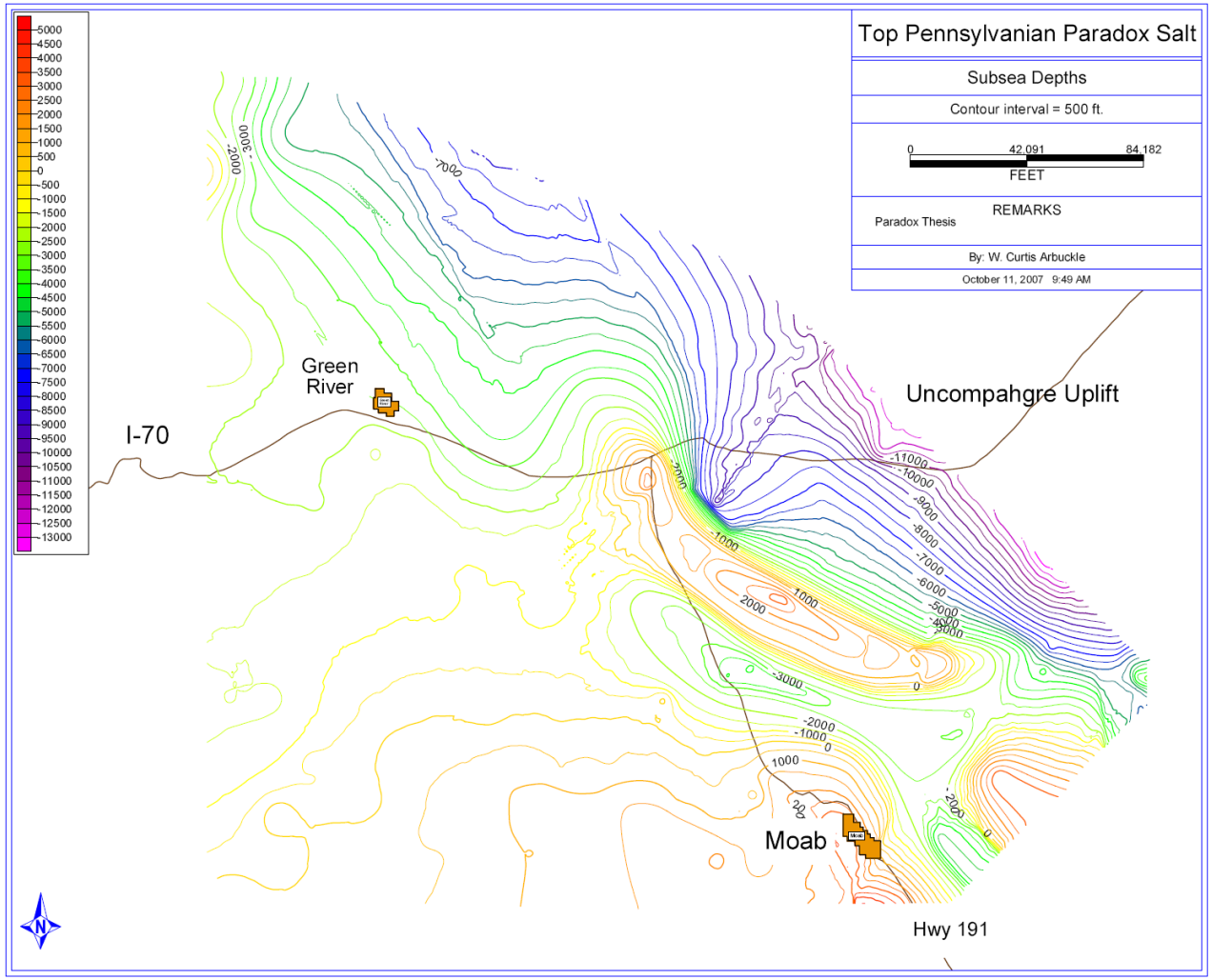

Figure 2.22: Structure contour map of the top of the Pennsylvanian Paradox salt. Note how the structure dips severely from the top of the Salt Valley Anticline northeast towards the Uncompahgre Uplift. Contour interval = 500 feet (152 m) (subsea depths).

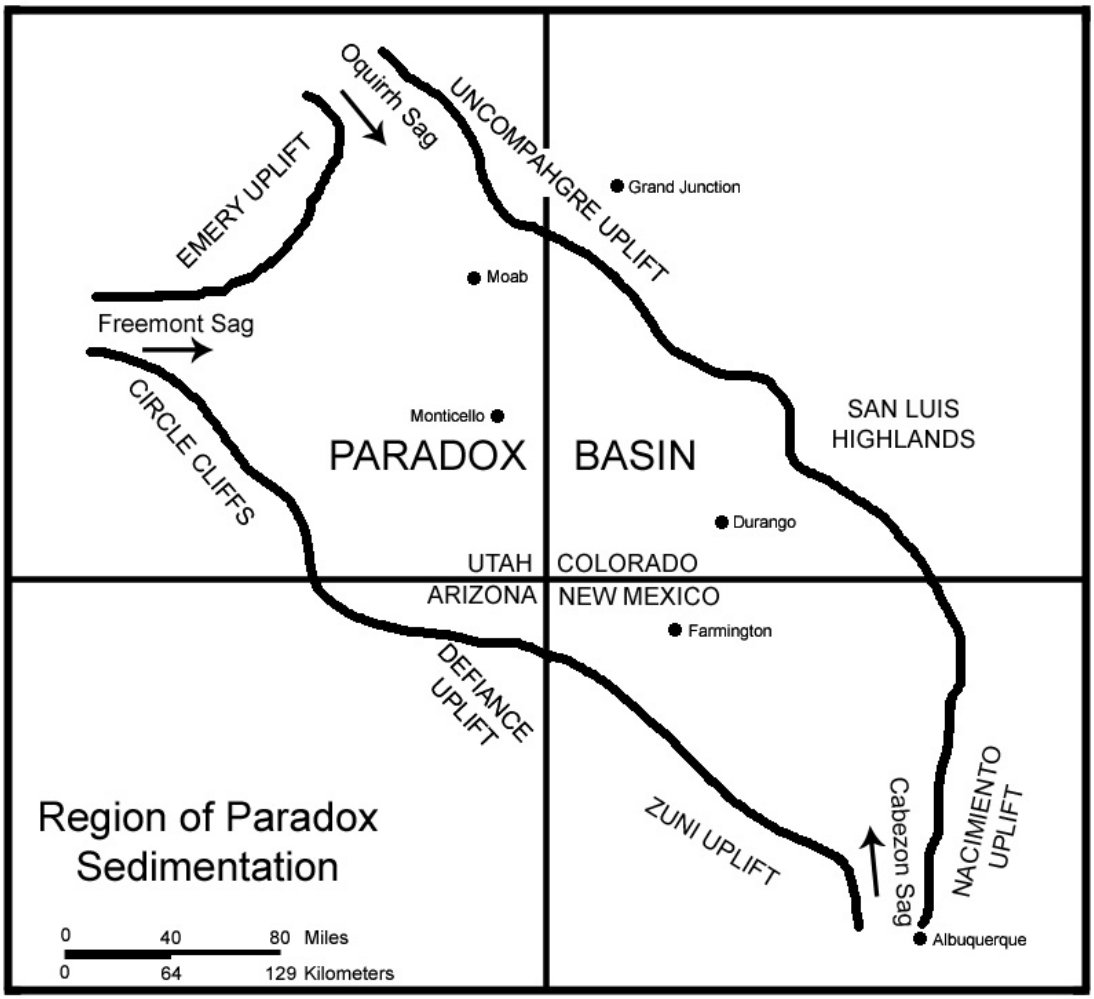

Figure 2.23: Map showing the location of Paradox sedimentation and the three major water entryways into the basin (modified from Wengerd, 1962).

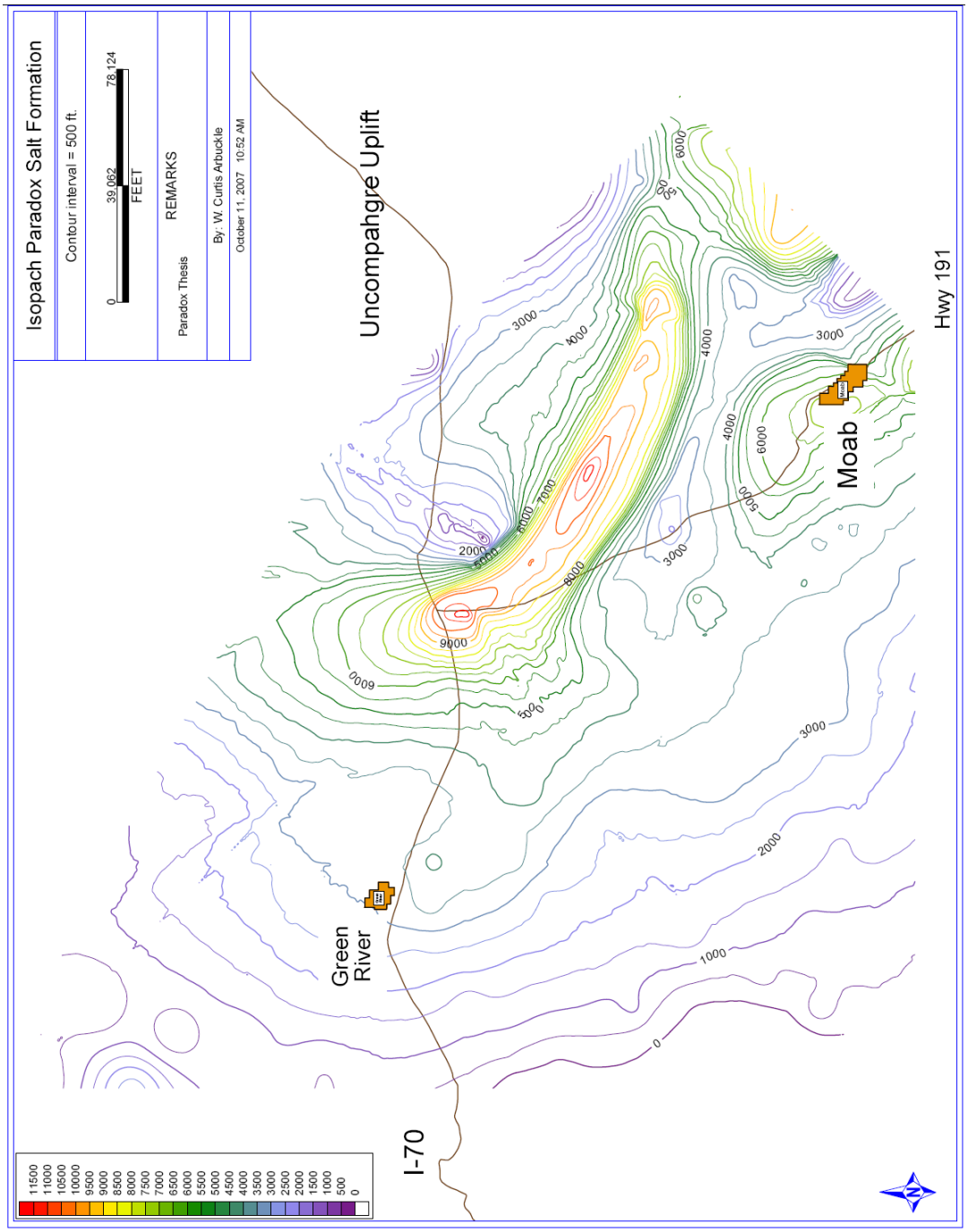

Figure 2.24: Isopach map of the Paradox Salt. Contour interval = 500 feet (152 m).

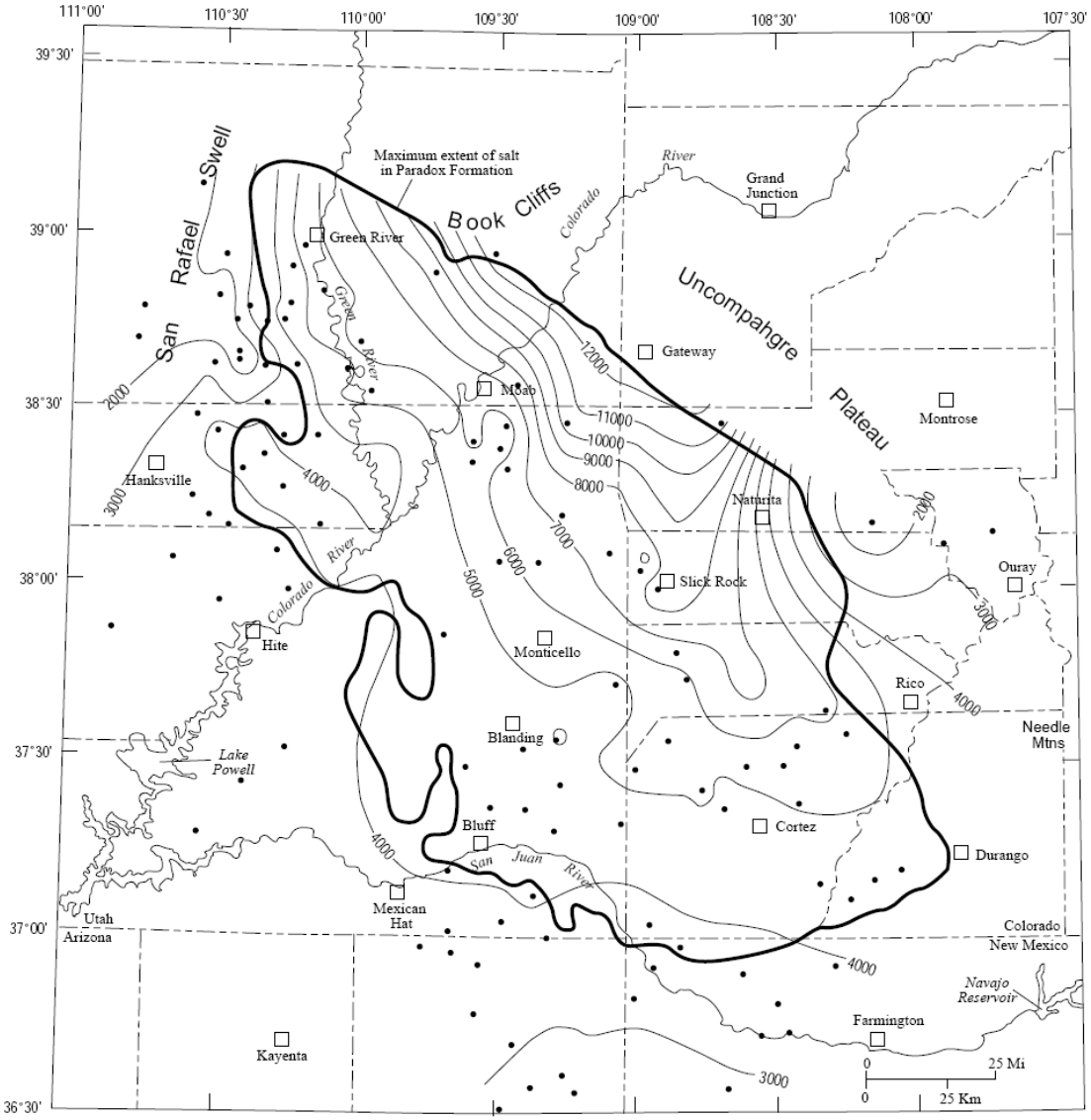

Figure 2.25: Isopach map totaling all of the Pennsylvanian and Permian strata within the Paradox Basin. Note how thicknesses increase in the northeast part of the basin. This is attributed to the clastic influx of coarse arkosic material shed off the Uncompahgre highlands. This area is also the deepest part of the basin (after Nuccio and Condon, 1996). Contour interval = 1,000 feet (328 m).

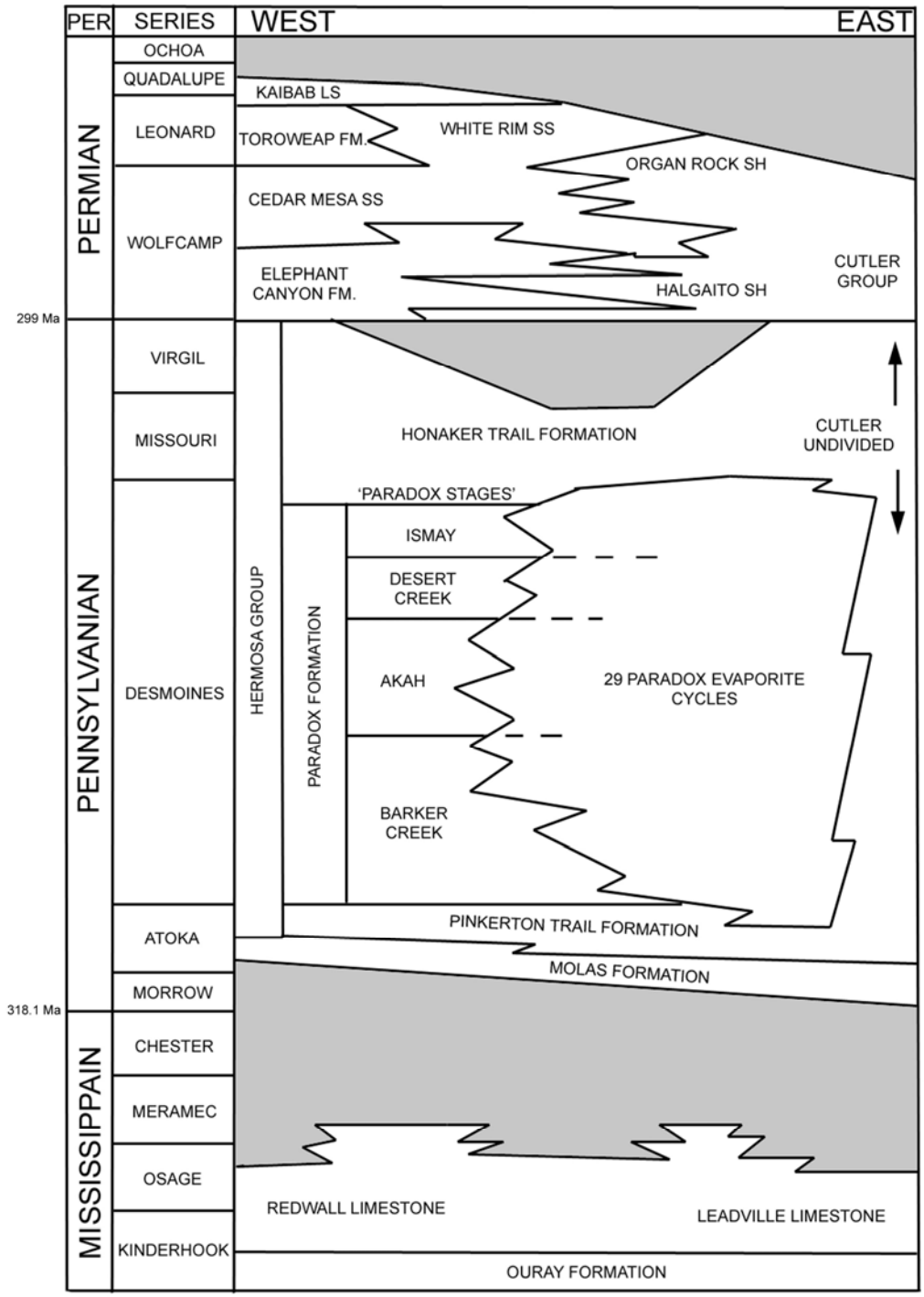

Figure 2.26: Mississippian through Permian correlation chart of the Paradox Basin. Gray areas represent missing time. Here the four main 'Paradox stages', which are based on productive intervals found in the southern edge of the basin, are represented. These stages are bounded and characterized by time-correlative black shale intervals that make correlations between the carbonate cycles in the southern half of the basin with the evaporite cycles located further north (modified from Baars and Stevenson, 1982).

Barbeau, 2003). In the northern part of the basin, cross-stratified quartzose sandstones are also abundant.

The Honaker Trail is characterized by variations in facies and thickness particularly around the salt walls. This suggests at least some salt was already at or very near to the surface during time of deposition (Trudgill *et al*., 2004). The lower contact with the Paradox Formation is gradational and represents the change from a penesaline environment to marine (Hite, 1960). The upper portion of the formation marks the transition from restricted and normal marine to an expansive terrestrial Permian system (Barbeau, 2003). The upper contact with the overlying Permian Cutler Formation is challenging to identify and correlate across the basin due to the complexity of lateral facies changes (Condon, 1997).

Thickness of the Honaker Trail is variable depending on location. Away from salt walls and related anticlines, thicknesses range from around 1,000 to 2,500 feet (305 – 763 m) (Elston and Shoemaker, 1960; Doelling, 1988). Up against the Uncompahgre highlands thicknesses are greatly increased because of the influx of clastic material shed off of the uplift. Nuccio and Condon (1996) note the presence of fluvial and eolian deposits in the northeastern part of the basin adding to the total formation thickness. In the Mobil – American Petrofina Elba Flats Unit No. 1-30 well, the Honaker Trail is 5,008 feet (1,526 m) thick (Frahme and Vaughn, 1983). Onlap and truncation along the flanks of the salt structures is attributed to salt wall and diapir growth driven by sediment loading from the northeast (Trudgill *et al.*, 2004).

2.3.7 Permian Rocks

Cutler Group (Desmoinesian – Leonardian?)

The Cutler Group consists of a heterogeneous sequence of mainly arkosic red-bed conglomerates (Figure 1.2). It also contains lesser amounts of arkosic sandstone, siltstone, mudstone and carbonates in areas away from the Uncompahgre highlands (Wengerd and Strickland, 1954; Baars, 1962; Condon, 1997).

The Cutler Group comprises several formations including, in ascending order: Cutler Formation undivided (also sometimes called the lower Cutler beds and are transitional into the Rico/Elephant Canyon), Cedar Mesa Sandstone, Organ Rock Formation, White Rim Sandstone and the De Chelly Sandstone (Condon, 1997). Closer to the Uncompahgre Uplift most of these formations, except for the Cutler undivided, are absent and were never deposited due to the arkosic influx off the uplift. Towards the center of the basin and to the southwest, these formations were deposited in a very complex and intricate system of eolian, alluvial and marine environments complicated by both lateral and vertical lithology changes (Condon, 1997).

Adjacent to the Uncompahgre Uplift is a narrow zone of coarse arkosic clastics classically called the undivided Cutler Formation. This northwest-southeast trending facies belt is characterized by poorly sorted, fine- to coarse-grained, conglomeratic sandstones. There are interbedded units consisting of shales, siltstones and non-fossiliferous limestones. The limestones are thought to be of lacustrine origin (Baars, 1962). Condon (1997) suggests that deposition of the undivided Cutler began as early as Desmoinesian time as alluvial fans flowing from the southwestern margin of the Uncompahgre Uplift (Figure 2.27). These sediments gradually grade to the west into marine carbonates identified as either the Rico or Elephant Canyon formations which are dated to be Virgilian and Wolfcampian in age (Baars, 1962; Condon, 1997). However the majority of the Cutler Group was deposited during Permian time (Young, 1983).

Where the Elephant Canyon Formation is present the lower contact with the Hermosa Group is gradational and conformable (Condon, 1997). The upper contact of the Cutler Group is unconformable with the overlying Triassic Moenkopi Formation in the northern section of the basin and the Kaibab Limestone in the south and west (Wengerd and Strickland, 1954; Martin, 1981).

Like many of the underlying formations, the Cutler also varies greatly in thickness (Figure 2.25). In the south and west the entire Cutler Group is observed with thicknesses averaging around 2,000 feet (610 m) (Condon, 1997). In the northeastern part of the basin, salt tectonics created drastic thickness variations. Greater thicknesses are seen adjacent to the Uncompahgre Uplift and in between salt related structures ranging from 3,000 to over 8,000 feet (915 – 2,438 m) (Elston and Shoemaker, 1960;

Frahme and Vaughn, 1983; Condon, 1997; Trudgill *et al*., 2004). The Cutler thins or is absent over the crests of many of these salt structures due to erosional processes and/or non-deposition (Doelling, 1988). Differential loading by the undivided Cutler arkosic wedge probably caused salt movement into the local salt related structures (Baars, 1962).

The end of the Cutler Group deposition marks the conclusion of sediment related basin subsidence and significant movement along the Uncompahgre Uplift (Paz Cuellar, 2006).

2.3.8 Triassic Rocks

Moenkopi Formation (Early to Middle Triassic)

Triassic strata unconformably overlie Permian rocks for the majority of the Paradox Basin (Figures 1.2 and 2.28). The basal unit is the Moenkopi Formation and in areas like the Salt Valley Anticline, it overlies and flanks Pennsylvanian strata. The Moenkopi is a low-energy marine deposit marking the first Mesozoic transgression into the basin. Fluvial and tidal facies are found in the eastern portion of the basin and gradually grade into a shallow marine environment to the west (Molenaar, 1981; Condon, 1997). Thicknesses range greatly depending on location due to salt tectonics. In the northeastern portion of the basin, the Moenkopi is anywhere from zero to near 2,500 feet (760 m) thick (Molenaar, 1981; Doelling, 1983). It is important to note the Moenkopi is absent over the Uncompahgre Uplift.

Chinle Formation (Late Triassic)

The Chinle Formation unconformably overlies the Moenkopi formation across the northern Paradox Basin (Figure 1.2). The Chinle can be divided into six members that comprise many depositional environments varying between eolian, fluvial, and lacustrine (Doelling, 1988; Trudgill *et al*., 2004). Much like the Moenkopi, the Chinle varies in thickness from around 300 feet (90 m) to near 1,250 feet (365 m) in the south (Molenaar, 1981). However, unlike the Moenkopi, the Chinle overlies basement rocks on the Uncompahgre Uplift (Doelling, 1983).

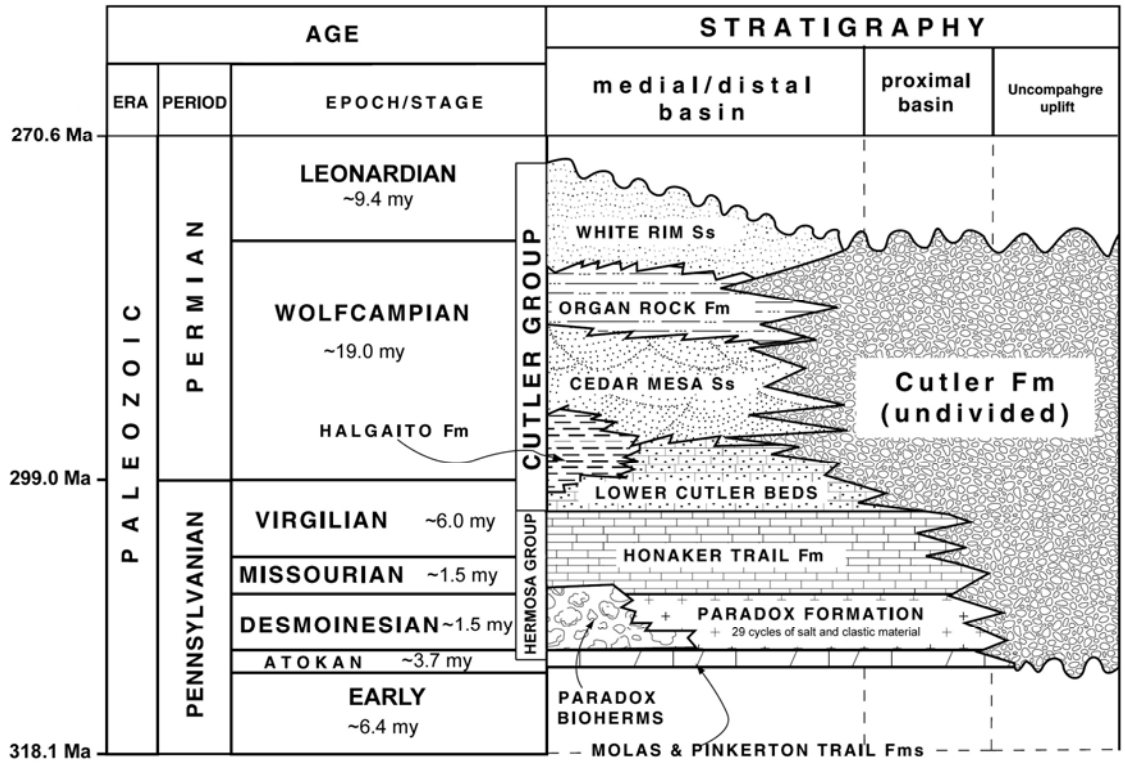

Figure 2.27: Stratigraphic column of Pennsylvanian – Permian time illustrating basin-fill units within the Paradox Basin (after Barbeau, 2003 and Gradstein *et al*., 2004).

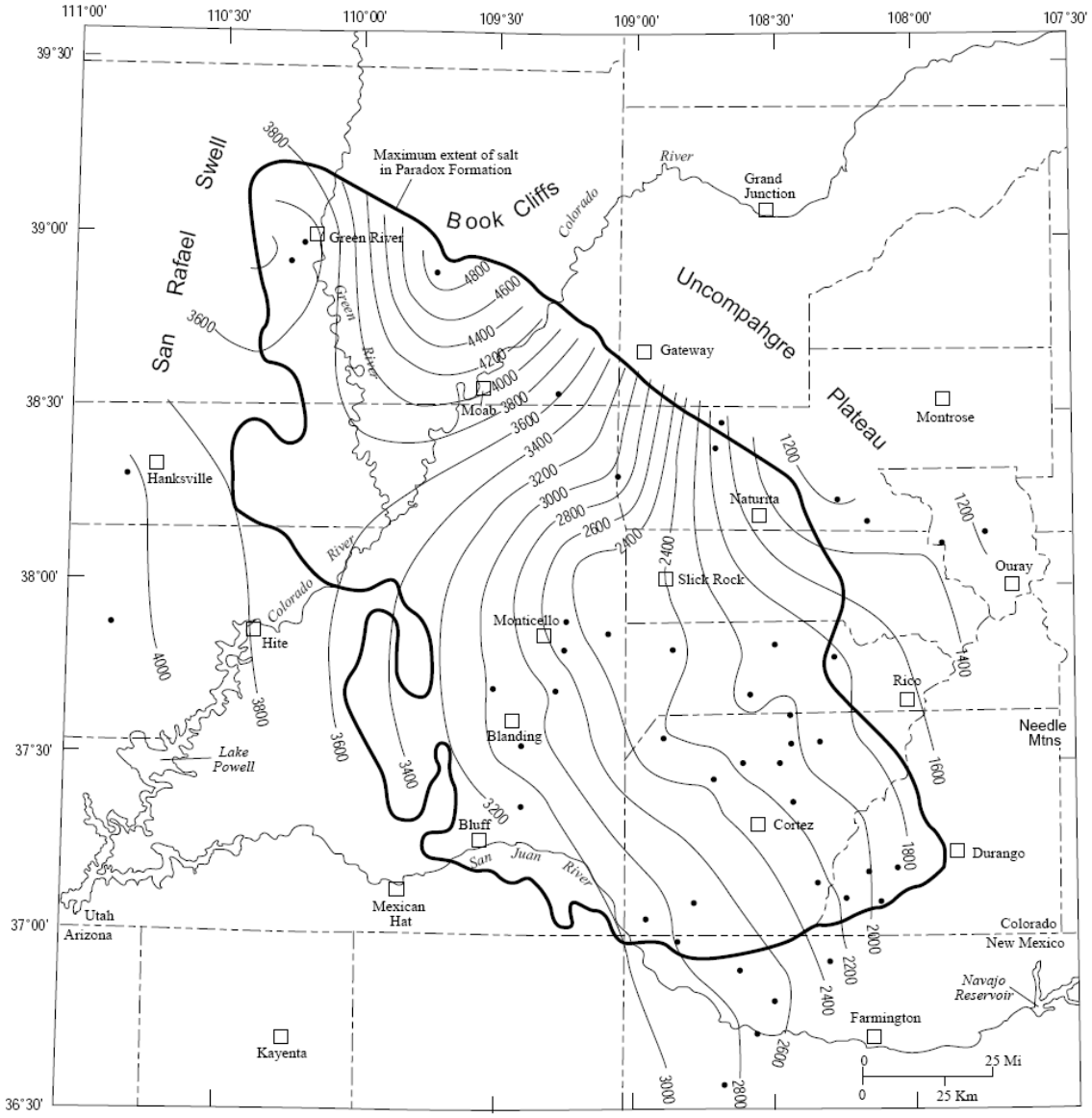

Figure 2.28: Isopach map totaling all Triassic and Jurassic stratigraphic units within the Paradox Basin (after Nuccio and Condon, 1996). Contour interval = 200 feet (61 m).

2.3.9 Early Jurassic Rocks

Glen Canyon Group (Sinemurian – Toarcian)

The Glen Canyon Group is comprised of the Wingate, Kayenta and Navajo formations (Figure 1.2). The Wingate Formation is a thick 300 foot (90 m), fluvial, cliff forming sandstone that lies unconformably over the underlying Chinle Formation (Molenaar, 1981). The Kayenta Formation is a fluvial dominated sandstone with a thickness range of 100 to 280 feet (30 to 85 m). It lies conformably over the Wingate sandstone (Molenaar, 1981; Doelling, 1988). The Navajo Formation is a heavily cross-bedded eolian sandstone. It can be up to 450 feet (137 m) thick in the western sections of the basin, but can vary greatly due to its unconformable relationship with the overlying Carmel Formation (Molenaar, 1981; Doelling, 1988).

2.3.10 Late Jurassic – Cretaceous Rocks

The middle and end of the Jurassic saw the deposition of several formations including, in ascending order: San Rafael Group consisting of the Carmel, Entrada, Curtis and Summerville formations (Bajocian – Oxfordian(?)), and the Morrison Formation (Kimmeridgian) (Figure 1.2) (Berman *et al*., 1980; Molenaar, 1981). The Cretaceous saw the deposition of Burrow Canyon and Cedar Mountaion formations (Aptian). The Dakota Sandstone was deposited by Albian time and is conformably overlain by the Late Cretaceous Mancos Shale (Berman *et al*., 1980; Molenaar, 1981). Tertiary-aged igneous intrusive centers of the Abajo, La Plata, La Sal and Sleeping Ute Mountains extend through all sedimentary units to an unknown depth (Condon, 1995) (Figure 2.1).

CHAPTER 3

EVAPORITE DEPOSITIONAL CYCLES AND ENVIRONMENTS, REGIONAL CORRELATIONS, CLASTIC INTERBEDS AND SALT (HALITE) LITHOLOGIES

The Paradox Formation contains at least 29 well defined evaporite cycles composed of halite beds in association with penesaline and siliciclastic rocks or interbeds (Hite, 1960). Each halite bed represents the final stage in a complete or partial evaporite cyclothem that also involves an ordered vertical sequence of shale, dolomite/siltstone and anhydrite. Depending on position within the basin, this same order of facies can also be observed laterally.

3.1 Evaporite Cycles and Regional Correlations

An idealized evaporite cycle would consist of (from bottom to top): anhydrite, silty dolomite, black shale, silty dolomite, anhydrite and halite (Figures 3.1 and 3.2). The upper and lower contacts of each cycle are disconformities caused by extreme changes in brine concentration. Some of the cycles are incomplete and are missing one of more lithologies within the clastic zones. However, other cycles have additional interbeds that are out of sequence from the idealized model.

Each cycle has been broken into transgressive and regressive phases (Figure 3.1) (Raup and Hite, 1992). The lower anhydrite bed marks the start of the transgressive phase (rising sea-level and decreasing salinity) due to an influx of seawater into the basin caused by a rapid rise in sea-level (probably both eustatic and tectonically controlled). Sea-level reached a maximum during the deposition of the black shale. This point marks the end of the transgression and the start of the regressive phase (falling sea-level and increasing salinity). The black shale could be considered a condensed section, but it is unclear how much time would be represented during such a highstand. The deposition of

the second half of the black shale marks the start of sea-level fall. After this point, the interbed depositional series reverses until the point where salinity concentrations reach halite saturation and thus halite is precipitated completing the cycle.

This same series of salinity and sea-level conditions can be observed in the carbonate cycles in the southern part of the Paradox Basin. The discovery of natural gas in 1945 at Barker Creek initiated a frenzy of hydrocarbon exploration (Malin, 1958). When additional discoveries were made in southeastern Utah and southwestern Colorado, important producing intervals or 'pay zones' were given informal names after the fields or locations where the first production was recorded. These intervals are all Pennsylvanian in age and include, from oldest to youngest, the Alkali Gulch, Barker Creek, Akah, Desert Creek and Ismay zones (Herman and Barkell, 1957; Malin, 1958; Peterson, 1966; Hite and Buckner, 1981; Reid and Berghorn, 1981). After Hite (1960) studied the evaporite sequences further north, regional correlations were possible between the evaporite and carbonate depositional environments (Figure 3.3). The black shales found in both systems make excellent time-sensitive rock units that can be correlated across the basin. Hite and Buckner (1981) were able to make this correlation using both outcrop and well data. They compared shale and carbonate facies of the Cane Creek Anticline south to the Raplee Anticline which is about 25 miles (40 km) west of the Aneth Field (Figure 3.4). From these correlations, they could associate the producing intervals (Barker Creek, Akah, Desert Creek, Ismay, etc.) in the southern part of the basin to the time-equivalent evaporite cycles located further north. It is important to note these producing zones don't represent complete cycles, only intervals of production. Therefore, direct correlations between producing intervals may not encompass complete evaporite cycles and vise versa.

Figure 3.5 is a diagrammatic section from north to south across the basin. It shows the correlation of the 29 evaporite cycles to the carbonate producing intervals found in the south. The Ismay interval is correlative to cycles 1 – 3 but can also makeup the lower portion of the Honaker Trail Formation. The Desert Creek matches with cycles 4 and 5 followed by the Akah zone with cycles 6 – 9. The Barker Creek zone is equivalent to cycles 10 – 19. The Alkali Gulch interval is mainly found on the Colorado side of the basin, but can roughly be time correlated to some of the oldest evaporite

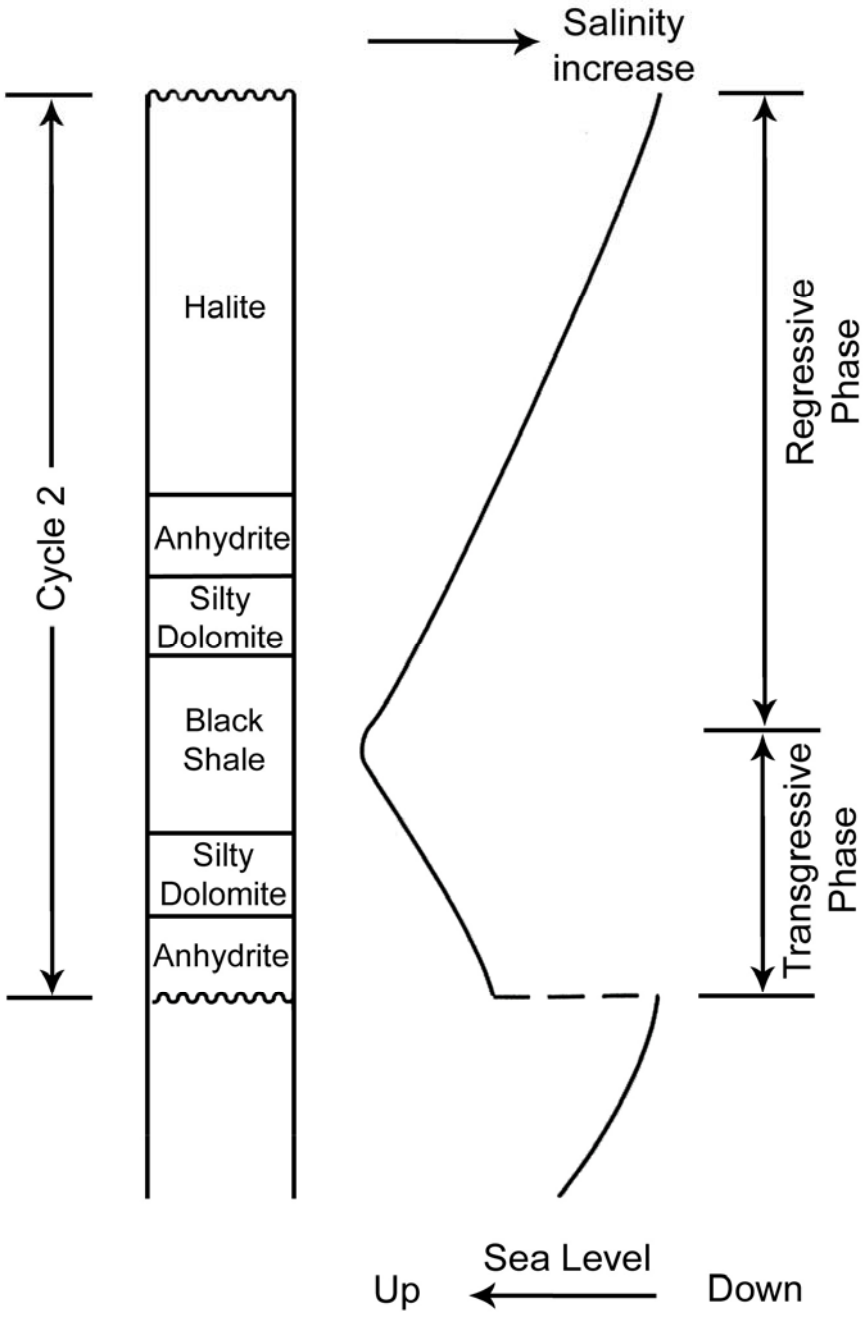

Figure 3.1: Facies stratigraphy of evaporite cycle 2 from the Cane Creek No. 1 core (T 26S, R 20E, sec. 25). The curve represents relative sea-level and salinity during the deposition of each facies. Notice how the change from transgressive to regressive occurs during the deposition of the middle of the black shale. This point also marks the reversal in order of facies (modified from Raup and Hite, 1992).

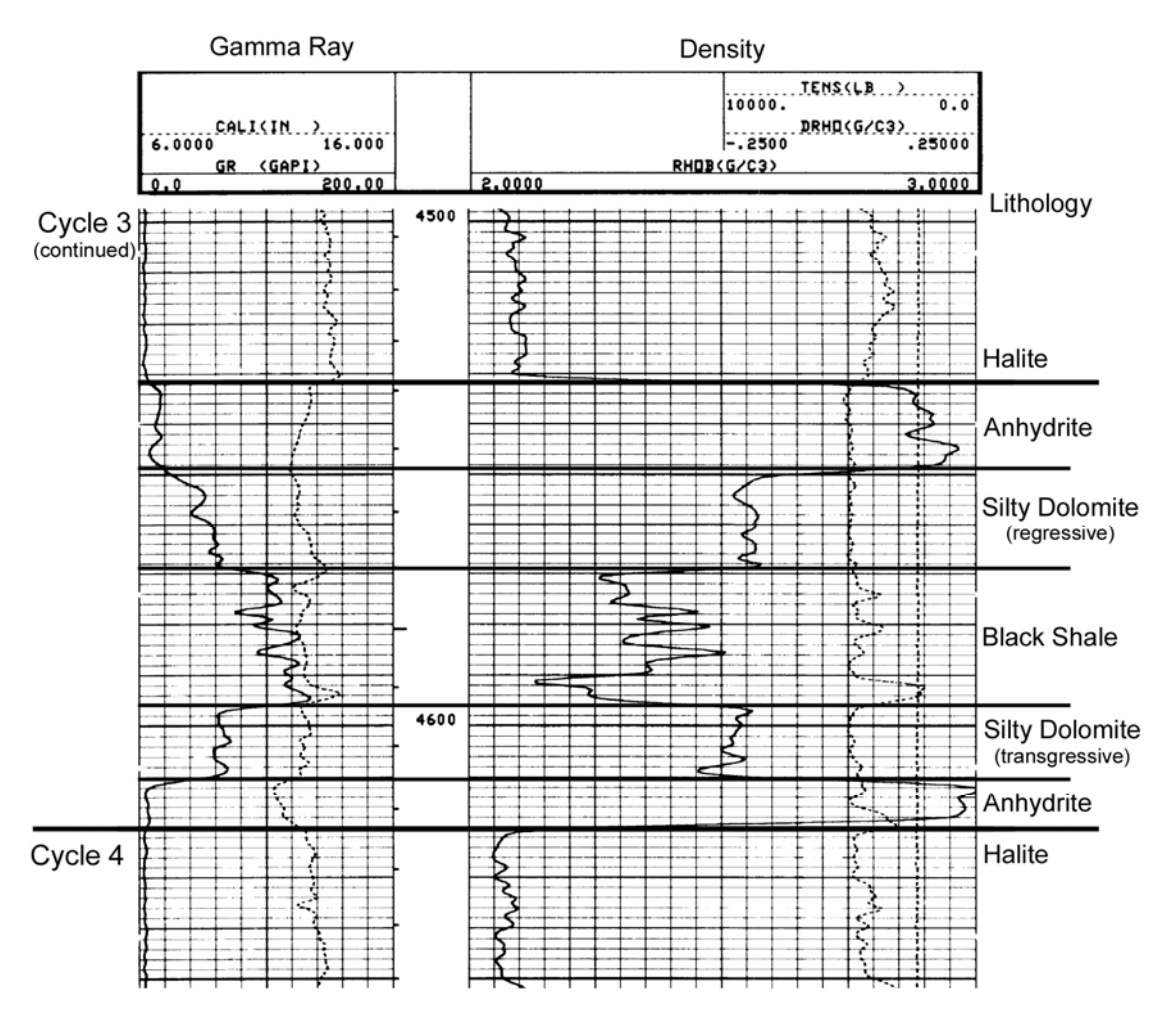

Figure 3.2: A type log from the Coors Energy Coors USA 1-10LC well (T 26S, R 20E, sec. 10) highlighting the clastic interval of evaporite cycle 3.

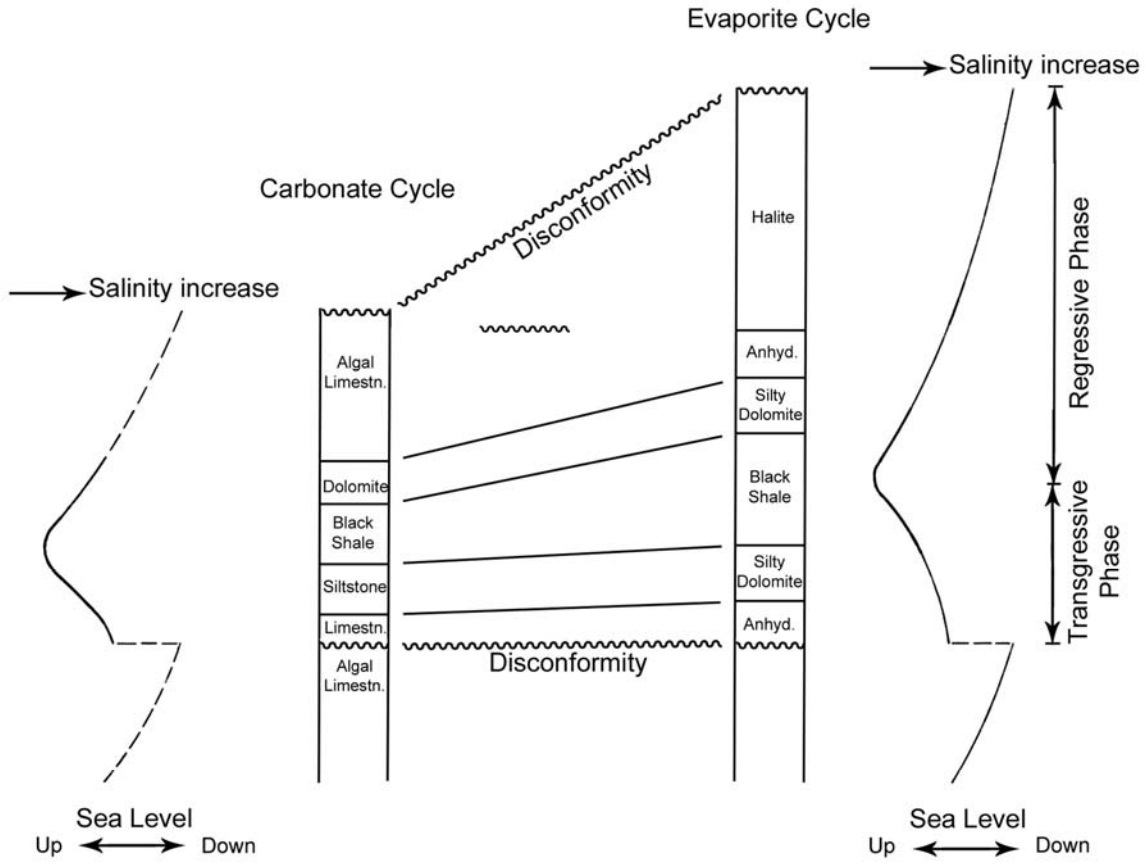

Figure 3.3: Diagram showing the regional correlation of facies from an idealized evaporite cycle (right) found in the northern half of the basin, to a carbonate cycle (left) typically found further south in the basin. The curves show relative sea-level and salinity conditions for each facies during deposition (modified from Hite and Buckner, 1981).

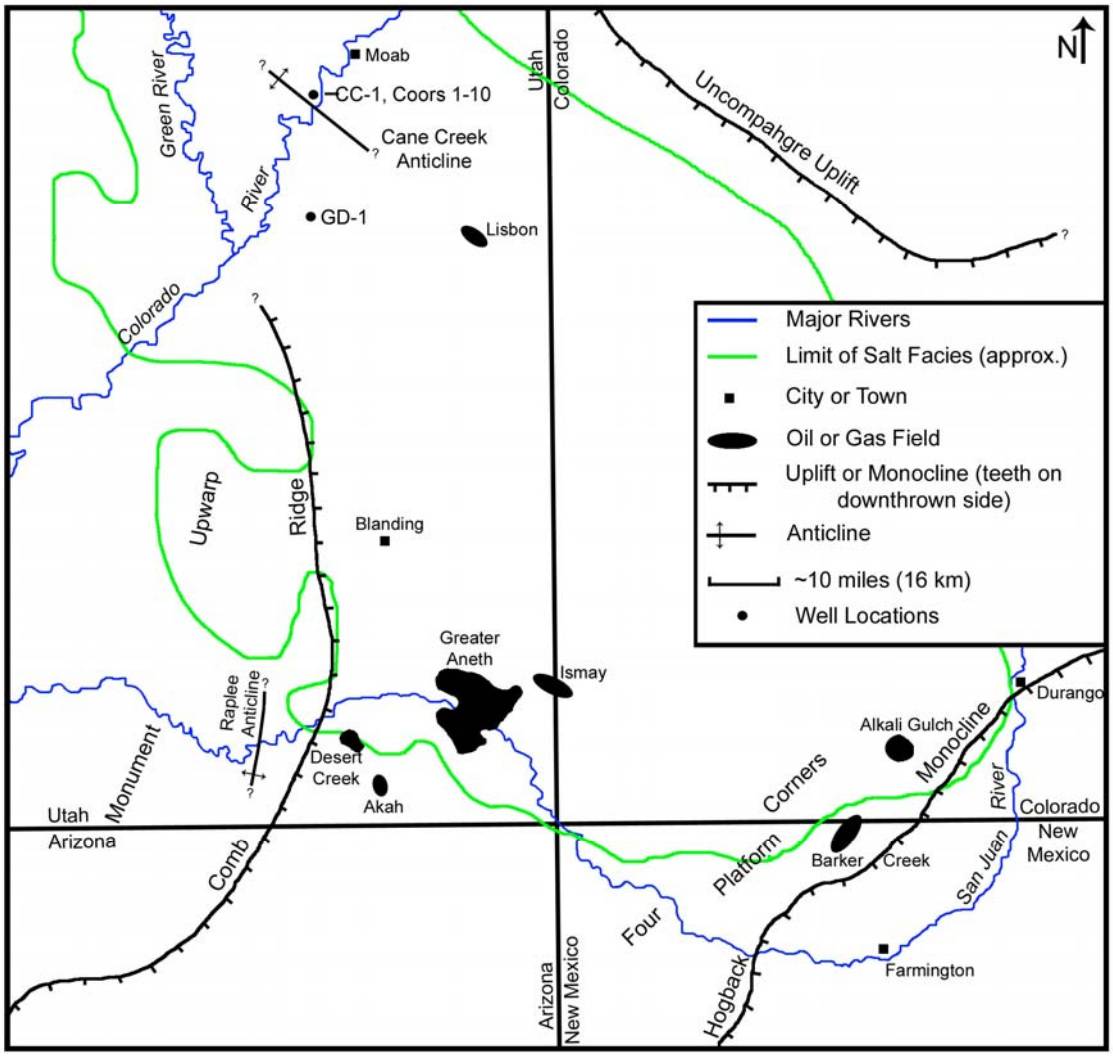

Figure 3.4: Index map showing the location of several prominent oil/gas fields, uplifts, monoclines, anticlines and three well locations (CC-1, Cane Creek No. 1 corehole; Coors 1-10, Coors Energy Coors USA 1-10LC well; GD-1, Gibson Dome No. 1 corehole) in the southern Paradox Basin (modified from Peterson, 1966).

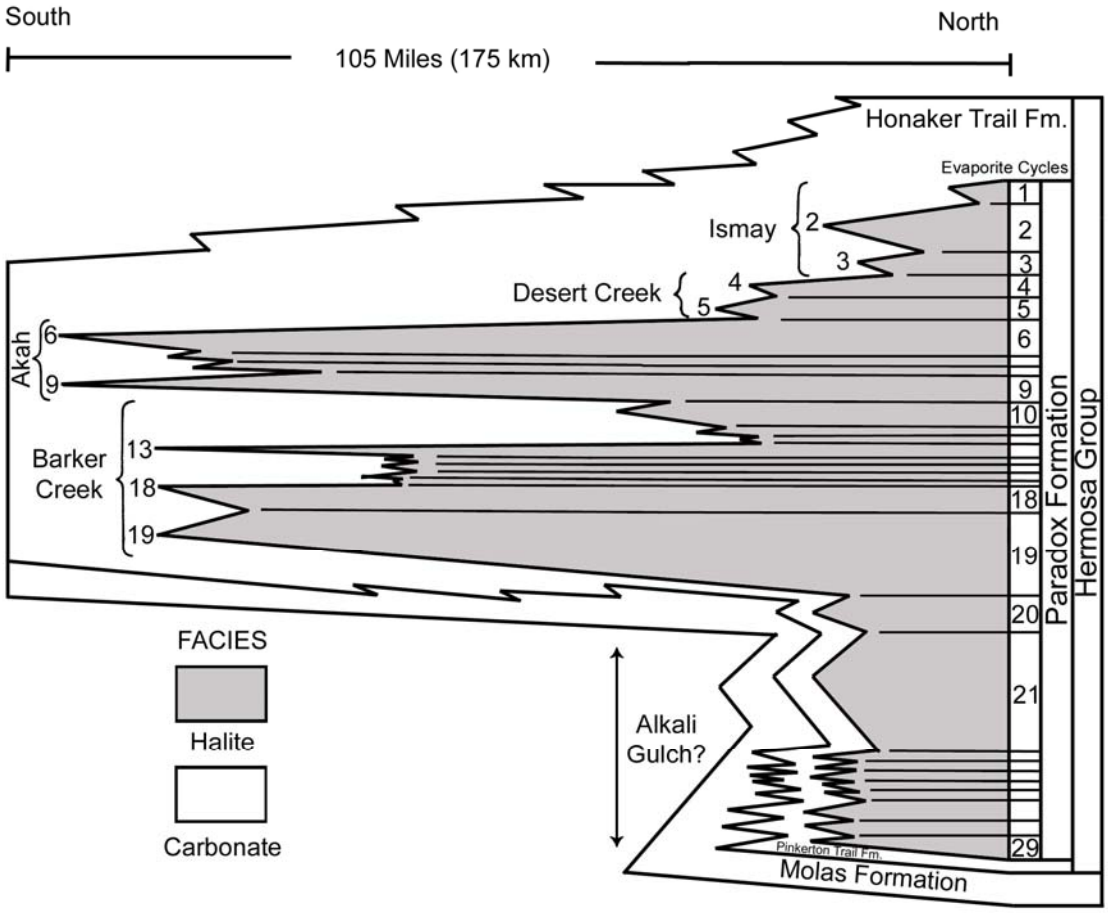

Figure 3.5: A diagrammatic section from north to south across the Paradox Basin. It shows the correlation of the 29 evaporite cycles in relationship to the carbonate producing intervals found in the south. Note how evaporite cycles 6, 9, 13, 18 and 19 mark the maximum extent of salt deposition into the southern half of the basin. Also note how cycles 20 – 29 are limited to only to the northern, deepest parts of the basin (modified from Hite and Buckner, 1981).

cycles (20 – 29) (Lockridge, 1958; Baars *et al*., 1967). Note that all 29 cycles can only be found in the older, deeper, northern half of the basin. In fact, many of the older cycles are not found south of the Gibson Dome area (Figure 3.4).

3.2 Salt and Interbed Precipitation/Deposition Sequence

In most basins, seawater often evaporates at temperatures between 25° and 55°C. Evaporation then brings the onset of mineral and salt precipitation as the brine solution reaches specific saturation levels. If any given quantity of normal marine seawater is allowed to evaporate, and no further influx of water occurs, then the brine volume during each precipitation stage can be represented by a series of consecutive circles (Figure 3.6) (Borchert and Muir, 1964). Figure 3.6 does not indicate actual changes in the volume of brine within the basin, but illustrates the brine concentration while salt deposition is occurring. Calcite starts precipitating when brine levels reach a 2 – 3 fold concentration followed by gypsum at 3 – 12 fold of the original brine (Bochert and Muir, 1964; Sonnenfeld, 1984). Halite precipitation begins only when 91.7% of the original seawater has evaporated. This represents a concentration increase starting at about 12 fold ranging to 64 fold the normal concentration of seawater.

Normal seawater contains approximately 4.24 moles of Na_2Cl_2, 0.633 mole of $MgCl_2$ and 0.088 mole of K_2Cl_2 per 1,000 moles of H_2O. Therefore once halite starts precipitating, calcium, magnesium and potassium levels begin to rise. Precipitation of potash salts begins when the brine reaches a density of around 1.3235 or when the $MgCl_2$:NaCl ratio exceeds 10:1. (Figure 3.7) (Sonnenfeld, 1984).

These situations are, however, idealized. In reality many other factors contribute to the dilution or concentration of the brine during the evaporation process. Most basins are not completely cut off from an open marine source or receive periodic influxes of seawater (an example of this is seepage, where marine water is able to pass through a sill or other type of barrier into the basin). Freshwater can also cause the brine solution to become diluted, but may not contain the minerals and salts found in typical marine waters. Temperature changes vary evaporation rates and thus affect deposition rates.

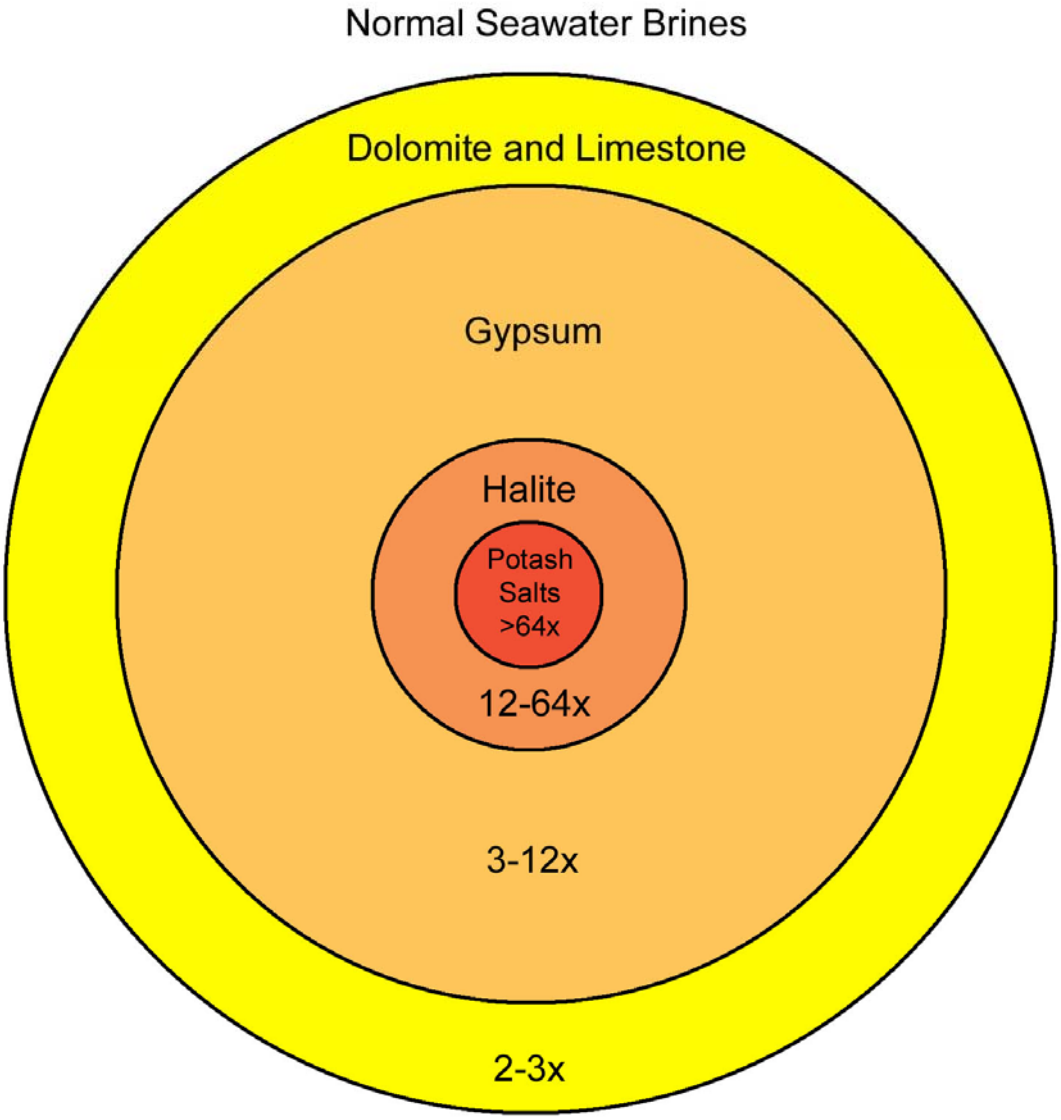

Figure 3.6: Diagram showing the relative brine concentration during salt precipitation within a marine basin. The area of each subsequent circle corresponds to the volume of brine remaining when various salts precipitate. It does not indicate actual water volume changes, only brine concentrations. The numbers in the lower half of the figure represent how many fold, from the concentration of normal marine water, the brine must be to start precipitating the associated salts. For example, it takes between 3 – 12 times the original brine concentration to start, and continue, depositing gypsum (modified from Borchert and Muir, 1964).

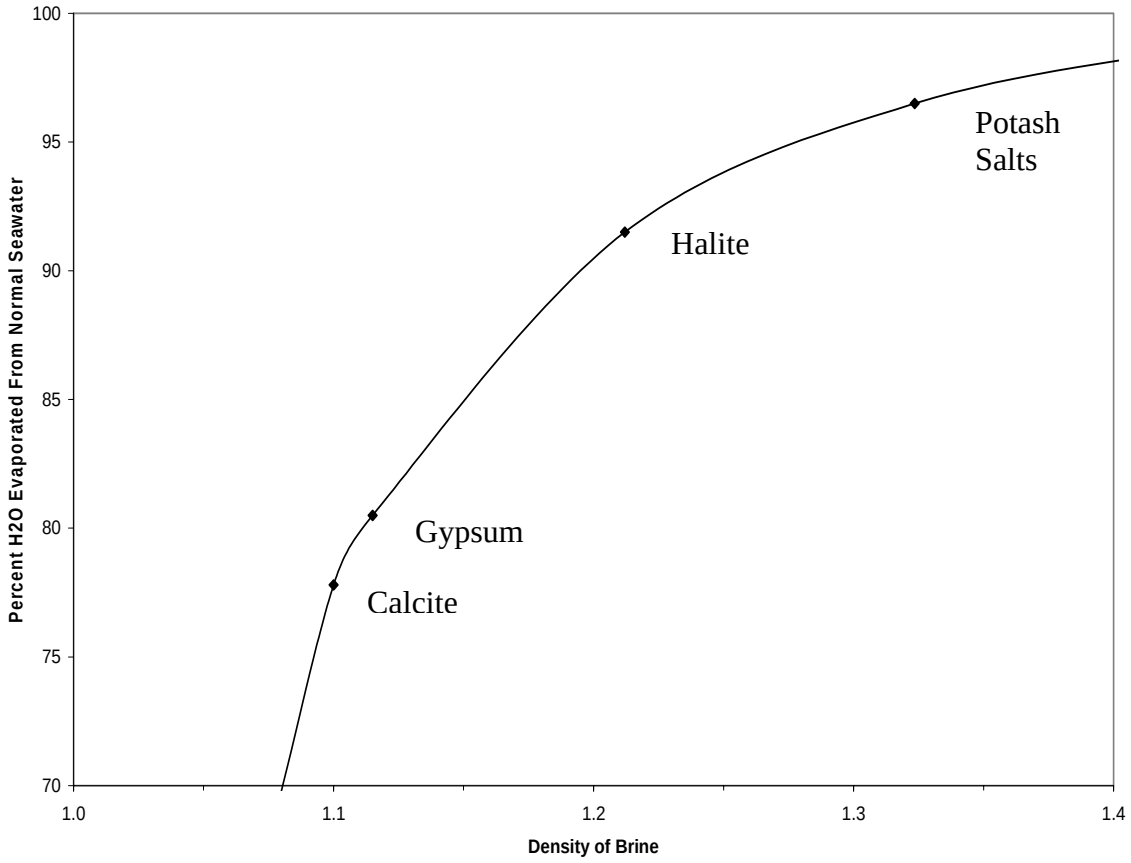

Figure 3.7: Precipitation path of calcite, gypsum, halite and potash from an anoxic marine brine (modified from Sonnenfeld, 1984).

Supersaturation can also occur with temperature variations disrupting the ideal precipitation sequence.

As brine concentrations become greater, evaporation rates decrease due to the decrease of fluids that are able to evaporate (mainly water). Currently only about 6 feet (2 m) of seawater is evaporated from normal marine water bodies annually. In more concentrated brine solutions there is typically a 1% decrease in total evaporation for every 1% increase in brine concentration. Considering this, halite precipitates at the waters surface, further hindering evaporation, so that evaporation of a halite-saturated solution is only about 4.5 feet (1.5 m) per year (Braitsch, 1971).

It is also important to understand how little salt would be deposited in a basin completely cutoff from open marine waters. About 3 feet (1 m) of salt would precipitate from only about 280 – 330 feet (85 – 100 m) of normal seawater (Bochert and Muir, 1964; Braitsch, 1971). Some of the thicker salt beds within the Paradox Formation exceed 330 feet (100 m) making it obvious there must have been at least some influx of marine waters into the basin during deposition.

3.3 Clastic Zone Interbeds

An exciting element of the Paradox evaporite cycles is the clastic intervals. Most of the clastic interbeds (as characterized and defined within this study) are composed of anhydrite, dolomite and/or siltstone, and organic-rich black shale (Figure 3.2). The contacts between each interbed are thought to be conformable and gradational (Raup and Hite, 1992). Some clastic zones are incomplete and may not incorporate all of the lithologies (generally the black shales) into each cycle. This may be dependent on location, as the lithologies for each cycle can change over short distances.

3.3.1 Anhydrite (Transgressive)

Anhydrite ($CaSO_4$) overlies the halite bed of the previous evaporite cycle. The anhydrite interval is composed mostly of anhydrite but also contains minor amounts of quartz, dolomite, mica, clay minerals and pyrite (Raup and Hite, 1992). It also can be divided into two textures; laminated and nodular. The laminated zones are purely depositional whereas the nodular zones are probably a result of the recrystallization process from gypsum ($CaSO_4 \cdot 2H_2O$) to anhydrite in a less saline solution and at temperatures above 50°C (Raup and Hite, 1992; Warren, 1999).

The contact with the underlying halite is very well defined and can be considered a solution disconformity. This boundary is caused by a rise in local sea-level that results in an influx of marine water, which lowers the salinity level and erodes the uppermost section of the underlying halite (Hite, 1968). The influx of marine water marks the beginning of the transgressive phase of each evaporite cycle. The marine waters not only dilute the remaining brine, but also re-supply it with calcium and sulfate. As a result, laminated calcium sulfate deposits accumulate (probably in the form of gypsum) as the brine becomes less saline. Over time, the entire zone is converted from gypsum to anhydrite (Raup and Hite, 1992).

Anhydrite precipitation rates vary depending on depositional environments. On average less than 0.04 inch (1 mm) of anhydrite is formed annually. Hite and Buckner (1981) suggest a rate of about 0.03 inch (0.8 mm) per year based on halite sedimentation rates. However, it is not uncommon to see annual layers around 0.2 inch (5 mm) thick. Precipitation of 0.2 inch (5 mm) requires the complete evaporation of about 46 feet (14 m) of normal seawater or about 13 feet (4 m) of brine saturated with calcium sulfate (Braitsch, 1971). Overall, an average of only about 3 feet (1 m) of gypsum/anhydrite would be precipitated from 3,280 feet (1,000 m) of seawater (Borchert and Muir, 1964). It is also important to note that some compaction (upwards of 40%) occurs during the dewatering of gypsum to anhydrite (Kupfer, 1989).

Transgressive anhydrite thicknesses within the northern Paradox Basin range from zero to >20 feet (>6 m).

3.3.2 Silty Dolomite (Transgressive)

In many of the evaporite cycles within the Paradox Basin, an interval of silty dolomite overlies the transgressive anhydrite beds. These dolomitic sequences are composed of mainly dolomite, but also contain significant amounts of quartz, feldspar (orthoclase and plagioclase) and mica. There are also small zones or stringers of halite, anhydrite and black shale. Considerable amounts of silt and clay are present within the dolomite. Most of the dolomite is fine- to very fine-grained with a sugary or sucrosic texture (Raup and Hite, 1992). These rocks usually lack bedding structures and are indistinct possibly due to bioturbation (Raup and Hite, 1992).

The transgressive dolomite precipitated as the brine within the basin became increasingly less saline due to an influx of seawater enriched with bicarbonate ions (HCO_3^-). It is unclear whether the dolomite is a result of primary or secondary precipitation. Raup and Hite (1992) proposed it was primary precipitation by referring to the sucrosic texture of the rock and how the reduced dissolved sulfate in the basin brines could contribute to the conditions needed for primary dolomite precipitation. However, changes in the physical properties of chemical sediments, like texture, can change drastically over geologic time and across relatively short distances. Some wells, in the same transgressive zone, have been reported to contain limestone in association with dolomite. This evidence suggests the dolomite formed due to secondary dolomitization processes from a silty limestone that was originally deposited. It is even plausible to suggest a process like seepage-reflux dolomitization could occur (Tucker and Wright, 1990). Here, porewaters rich in magnesium are released from under or overlying evaporite rocks (mainly from halite salt beds and the water lost during the gypsum to anhydrite dewatering reaction) to facilitate the dolomitization process.

Interestingly enough, both precipitation sequences can occur simultaneously in different sections of the basin. First, rapid changes of water level, in transgressive basins, are certainly possible especially near the basin margins. This could cause any subaqueously precipitated carbonates to become exposed and subject to syndepositional subaerial diagenesis (secondary precipitation). Secondly, the Mg/Ca ratio in hypersaline environments fluctuates as the salinity concentration fluctuates (Warren, 1999).

Therefore, during the early stages of carbonate precipitation a lower Mg/Ca ratio is dominant. As the brine becomes more saline, the Mg/Ca ratio is heightened due to the loss of calcium already exhausted during the precipitation of early, calcium-rich carbonates. Thus, subsequent carbonates are precipitated from brines with increasing amounts of magnesium, substituting for the lack of calcium in the system. The resulting carbonates are typically dolomites, enriched in magnesium that formed as a product of primary precipitation. Within the Paradox Basin, secondary precipitation might occur on the southern shelf and along the margins of the basin, whereas primary precipitation is more likely in the deeper areas of the basin.

The transgressive phase of the Paradox cycles consistently contains larger amounts of silt than the regressive sequence. Hite and Buckner (1981) attributed this to the incoming transgressive sea churning up sediments along the shores and low-lying areas of the basin. This matter would then become deposited along with the precipitation of, in this case, the carbonaceous dolomites. Also seen throughout the northern part of the basin is the presence of detrital quartz and feldspar within the dolomite. Some mineralogical estimates reach upwards of 40 percent the total mineralogy and can be observed in core (Raup and Hite, 1992). The origin of such a large quantity of material is debatable. The nearest known sources are the Uncompahgre Uplift bounding the northeast side of the basin, and the shelf margin in the southwest. Some possible transport methods include saline density currents, small scale turbidites and eolian systems. It is also important to note that during times of transition from glacial to interglacial periods (transgression) there is a significant increase in humidity. A greater amount of humidity would create increased precipitation levels (Van der Zwan, 2002). This would allow for a larger fluvial presence transporting any organic, clastic and detrital material into the basin (P. Plink-Björklund, 2008, personal communication).

If it is assumed that during dolomite precipitation the basin brine was at or very near calcium bicarbonate saturation, sedimentation rates can be calculated. Using an aggressive evaporation rate of about 13 feet (4 m) of brine water per year, with it being replaced constantly by marine water influxes, Hite and Buckner (1981) calculated a deposition rate of 0.007 inch (0.17 mm) per year. Yang (2000) and Kirkland and Evans (1981) also arrived at similar results of 0.004 – 0.008 inch/year (0.1 – 0.2 mm/year) and

0.006 inch/year (0.15 mm/year) respectively. With the addition of quartz, silt and other clastic material into the transgressive dolomite, the sedimentation rate should be increased to around 0.008 inch/year (0.2 mm/year). Transgressive silty dolomite thicknesses within the northern Paradox Basin range from zero to >30 feet (>9 m) per individual bed.

3.3.3 Black Shale (Transgressive and Regressive)

An organic-rich black shale overlies the transgressive silty dolomite. It tends to be very carbonaceous and is composed of dolomite, calcite, quartz, mica, clay minerals (illite) and minor amounts of sphalerite, feldspar and pyrite (can be abundant). The silt-sized quartz grains can account for as much as 40 percent of the total mineralogy along with carbonates ranging between 20 – 30 percent (Raup and Hite, 1992). The siliciclastic material found within the black shales probably was deposited by saline density currents, light turbidites or originated from an eolian source (Raup and Hite, 1992). Some small shells (brachiopods), and associated shell fragments, fern pinnules and carbonized plant stems, along with other conodonts indicate there was some biological activity during deposition (Herman and Barkell, 1957). It is very common to see vertical fractures within the shale ranging from <0.04 inch (<1 mm) to over 2.8 inches (7 cm) in width. These fractures are generally filled with halite or in some rare cases, carnallite (Hite, 1960). Some of the interbeded shales are highly radioactive reaching over 300 API on several of the gamma ray well logs. These hot shales are typically located within cycles 10, 13, and 21. The contact with the underlying dolomite is generally gradational, however in some wells it can be abrupt.

The black shales were deposited when sea-level was at its highest and thus the salinity was at its lowest throughout the basin. This allowed for the shales to be deposited basin-wide making them good time correlation units. The sometimes abundant pyrite, within the black shales, indicate the shales were deposited in a humid-reducing euxinic environment which is opposite of most evaporite settings where an arid-oxygenated environment is more prevalent (Hite, 1968). Interestingly, Herman and

Barkell (1957) report how some of the black shales thicken and grade into gray-green shales, siltstones and even redbeds as they near the Uncompahgre Uplift along the eastern margin of the basin. However, most of the shales change very little from north to south varying only in thickness with the thicker sections located on the southeastern shelf and in the basin interior (Hite and Buckner, 1981).

Most of the black shales range in organic matter from 0.5 to 13 weight percent. The organic matter was probably derived from algae and bacteria of both marine and terrestrial sources (Raup and Hite, 1992). There is also evidence of marine plankton and organic material that was swept into the basin via the Silverton fan delta as a result of fluviatile influxes (Hite *et al.*, 1984). RockEval pyrolysis data from several shale intervals in the upper Paradox Formation suggest a mixture of types II and III kerogen make up the organic matter (Hite *et al.*, 1984). The organic matter was preserved by dense, anoxic, highly saline brines that formed during the regressive phase of each evaporite cycle. There are three main shale intervals that have traditionally generated hydrocarbons. These include the Gothic Shale of cycle 3, the Chimney Rock Shale of cycle 5 and the Cane Creek Shale of cycle 23. However, many of the other shale intervals exhibit the same generation potential as the three listed above and need to be explored for and studied in further detail. The Gothic Shale has a total organic carbon (TOC) of 2 – 3 percent, while the Chimney Rock Shale has a TOC of about 1.46 percent (Hite *et al*., 1984). The Cane Creek Shale is more of a combination of anhydrite, shale and silty dolomite than a true shale. Nonetheless, several shale zones within the Cane Creek contain TOC values ranging from 0.42 – 3.96 percent. Vitrinite reflectance values (R_o) for shales within the Paradox Formation range from 0.42 – 0.54 which puts these rocks at the beginning of catagenesis and thus the start of the oil window. However, the thermal alteration index (TAI) of palynomorph data suggest these R_o values are minimal. An explanation of why the R_o values are suppressed involves the relationship of vitrinite and exinite macerals and bacterial reworking of organic matter in anoxic environments. This is discussed in further detail by Hite *et al*., (1984).

The black shales within the clastic interbeds represent the point in the evaporite cycle when the system transitions from transgressive to regressive. It is assumed the first half of the black shale interval is transgressive and the second half is regressive. This

transition point is difficult to determine because the mineralogy is fairly consistent throughout the bed. One could also assume the black shale represents a condensed section within the cycle, but again this would be hard to determine on a macro or microscopic level. However, sometime during the deposition of the shale, sea-level began to fall and was accompanied by an overall rise in salinity.

Black shale sedimentation rates are difficult to determine because the shales formed via a combination of chemical, clastic and organic components. One way to calculate the rate is to compare organic matter within the shales to organic carbon production rates (Hite and Buckner, 1981). Evaporite settings like the enormous saline lakes in eastern Africa or even the Great Salt Lake in northern Utah are modern analogs to what the Paradox Basin might have been like during shale deposition. These highly saline areas don't support normal marine life, but do facilitate an enormous amount of biologic activity that is greater than any upwelling zones located throughout the world (Kirkland and Evans, 1981). Unfortunately the organic carbon production rates in these extreme locations are tricky to determine because they are highly variable, so production rates in traditional marine waters are used. Modern oceanic waters produce between 50 g/m^3/year (open ocean) and 300 g/m^3/year (upwelling zones) of organic carbon (Tissot and Welte, 1984). Hite and Buckner (1981) note how the Paradox shales have an average density of 1.8 g/cm^3 and contain an average of 5.42 weight percent TOC (calculated from RockEval data in Hite *et al*., (1984)). Therefore each cubic meter of shale contains roughly 97,520 grams of organic carbon. This value of 97,520 grams is divided by the organic carbon production rates of 50 g/m^3/year and 300 g/m^3/year resulting in a deposition rate of 0.02 inch (0.51 mm) or 0.12 inch (3.08 mm) respectively for the black shales within the Paradox Formation.

Clastic zone shale thicknesses in the northern Paradox Basin vary greatly. Depending on location, a shale zone may not be represented in a particular cycle, but several miles away it can be measured in feet. With that said, shale thicknesses range between zero and >20 feet (>6 m). Since the Cane Creek interval is not a clean shale and is a mixed zone of shale, anhydrite and carbonates, its total thickness is not reported here.

3.3.4 Silty Dolomite (Regressive)

The black shale is overlain by a regressive dolomite that is very similar to the transgressive dolomite discussed above. Both have the same sucrosic texture, however the regressive dolomite contains less (but still abundant) detrital material. This is most likely a result of falling sea-level and the availability of additional clastic material entering into the basin, unlike the transgressive phase where new material is mobilized with rising water levels.

Although in less quantities, quartz and other silt-sized siliciclastic grains are still found within the dolomite. It is important to note that sedimentation rates for dolomites and black shales are rather slow compared to anhydrite or halite zones. Therefore, the abundance of siliciclastic material transported into the basin perhaps didn't increase substantially during transgressive times. If the rate of siliciclastic material entering the basin remained relatively unchanged throughout each cycle, it would accumulate in larger quantities within the sediments that have slower sedimentation rates like the black shales and dolomites.

The boundary between the overlying anhydrite and the dolomite is transitional with thin layers of altering anhydrite and dolomite. Raup and Hite (1992) noted the presence of small pseudomorphs of anhydrite and gypsum in this transition zone. These pseudomorphs are consistent with rising salinity levels.

Much like the transgressive dolomite, the regressive silty dolomite has a precipitation rate ranging from about 0.004 – 0.008 inch (0.1 – 0.2 mm) per year. Because there is less siliciclastic material a rate .0067 inch (0.17 mm) per year, suggested by Hite and Bucker (1981), is appropriate. Individual regressive dolomite zone thicknesses, within the northern Paradox Basin, range from zero to >30 feet (>9 m).

3.3.5 Anhydrite (Regressive)

Overlying the regressive dolomite is a zone of laminated anhydrite. The anhydrite here was precipitated as the brine concentration became more saline as water

levels fell. This zone is very similar to the transgressive anhydrite except for the textural features seen here. It is thought the fine and wavy laminations are a result of anhydrite replacement of carbonate algal mats (Raub and Hite, 1992). The upper portion of the zone contains pseudomorphs of anhydrite and is sometimes interlaced with the overlying halite. These pseudomorphs represent some sort of extreme change in salinity and their purpose and formation are not fully understood. The upper boundary, above the pseudomorphs is conformably overlain by halite beds.

Like the transgressive anhydrite discussed previously, precipitation rates for the regressive anhydrite are considered to be comparable at about 0.03 inch (0.8 mm) per year. Individual regressive anhydrite zone thicknesses, within the northern Paradox Basin, range from zero to >20 feet (>6 m).

3.3.6 Sandstone and Turbidities

Several wells drilled in the northern Paradox Basin have encountered sandstone beds within the clastic intervals of the evaporite cycles. The sandstones are fine- to medium-grained and are characterized by small scale cross-laminations (mainly clay), graded bedding, poor sorting and sole marks (Hite and Buckner, 1981). Fragments of vascular plants and clasts of gray shale are also found throughout the sandstone. These defining characteristics suggest the sandstone units found within the clastic intervals are turbidites (Bouma, 2000; D. L. Rasmussen, 2007, personal communication).

If these sandstones are indeed turbidites, then the grain size distribution does not coincide with clastic sources from the southern shelf of the basin. It has been noted by Hite and Buckner (1981) how the medium-grained, poorly-sorted sandstones lie adjacent to fine-grained, silt-sized rocks derived from the south. This suggests the turbidites originated from the Uncompahgre Uplift in the northeast.

The timing and position of the turbidites within the evaporite cycles is important and can give clues on how and why they formed. Some of the sandstone units identified in cores taken from the Salt Valley area are located above underlying halite beds thus placing the turbidites at the beginning of a transgression into the basin (Hite and Buckner,

1981). During transgressive times, a rising sea-level could initiate turbidity currents from fan deltas along the base of the Uncompahgre Uplift. Other sandstones are located randomly throughout the clastic interbed sequence. These turbidites might have been triggered by earthquakes, floods, storms or from slumping directly off the uplift (Hite and Buckner, 1981).

3.4 Halite Beds

Probably the most defining characteristic about the Paradox Basin is the presence of salt. Halite makes up most of these salt or saline facies and is equigranular with anhedral grains ranging from about 0.06 to 0.5 inch (1.5 to 12.5 mm) in diameter. The salt ranges in color between clear, white, orange, gray and amber (Hite, 1960). Color is determined by the amount of impurities within the halite including shale, anhydrite, clay, potash, organic matter and fluid hydrocarbons. The contact with the underlying regressive anhydrite is usually gradational and the contact with the overlying transgressive anhydrite is unconformable.

The halite beds were deposited during a time of sea-level lowstand where the influx of marine waters into the basin was minimal. This caused the remaining brine to become increasingly saturated with evaporite salts initiating the deposition of halite. However, there was still enough marine water entering the basin to recharge the remaining brine. This allowed for the halite intervals to reach impressive thicknesses. The halite beds also contain thin laminations of shale, silt, anhydrite or potash that are thought to mark seasonal changes in salinity, clastic sediment supply and temperature (Raup and Hite, 1992). Spacing between laminations ranges from 0.25 to 18 inches (0.64 to 46 cm) but averages around 2.5 inches (6.35 cm) (Hite, 1960; Raup and Hite, 1992).

As discussed earlier with the black shales, evaporite environments generate large amounts of organic material. Most of the organic matter that is produced or flows into a basin via marine influxes, is typically well preserved. Oxygen solubility is extremely low in saline rich brines and thus inhibits aerobic decay. Anaerobic sulfate-reducing bacteria use only minor amounts of organic matter in their metabolism and in doing so expel large

volumes of H_2S limiting the growth of other halophillic bacteria (Hite *et al*., 1984). Therefore during halite deposition much of this organic matter is captured and preserved within the salt and associated pore fluids. Halite beds can have up to 35 percent porosity (Ver Planck, 1958) trapping these organic-rich fluids which can contain anywhere from 250 ppm organic carbon in halite to upwards of 3,000 ppm organic carbon in potash beds (Hite *et al*., 1984). Overtime these beds became compacted and the organic rich fluids were expelled into the over and underlying clastic zones. These intervals, now charged with significant amounts of organic material, would make favorable source and reservoir rocks.

Halite sedimentation rates can range from 0.4 – 59 inches (1 – 150 cm) per year. Analysis in Saskatchewan, Canada by Wardlaw and Schwerdtner (1966) resulted in a reasonable deposition rate of about 2 inches (5 cm) per year. Similar results were calculated by Hite and Buckner (1981) by counting seasonal laminae composed of anhydrite and shale/silt. They concluded on an average precipitation rate of 1.57 inches (4 cm) per year. Halite bed thicknesses within the northern Paradox Basin range between 15 (4.5 m) feet near the edge of the evaporite facies to over and 990 feet (300 m) near the salt walls and anticlines (Hite, 1960). The halite bed within cycle 6 is usually the thickest individual interval at around 330 feet (100 m).

3.4.1 Potash

Potash is a generic term for ore-bearing minerals that contain potassium. These include carnallite, sylvite, polyhalite, langbeinite, kainite, kieserite and leonite just to name a few. Most potash in the Paradox Basin is in the form of sylvite (KCl) and carnallite ($KCl•MgCl_2•6H_2O$). It is primarily used for fertilizers but also has applications in the manufacturing of soap, synthetic rubber, ceramics, chemicals and even glass (Warren, 1999).

Potash has been identified in over half of the evaporite cycles within the Paradox Basin. These beds are generally located at the top of the halite beds and mark the final stage of salt deposition within the basin (Klingspor, 1966). Here salinity concentrations

increased beyond halite precipitation and characterize the basin as being extremely arid and desolate. Potash is mainly found in the northern and eastern half of the basin because it is much deeper then the southern, western and southwestern basin margins where shallow shelves are dominant (Goldsmith, 1969).

3.4.2 Caprock

Caprock is gypsum, anhydrite and calcite beds that generally overlie salt structures. It forms by dissolution of halite, leaving behind insoluble residues like anhydrite and any organic matter. Meteoric ground water rich in $CaCO_3$ often circulates through the caprock morphing the anhydrite into gypsum and/or calcite (Dutton and Kreitler, 1980; Dutton *et al*., 1982).

Caprock formation and the dissolution of halite, within the Paradox Basin, also leaves behind the clastic intervals (shale, silty dolomite, anhydrite, sandstone). Where available, this clastic material can be sampled and studied but several problems do arise. Since the caprock formed atop a salt structure the orientation of bedding and cycle number are near impossible to identify. The caprock also underwent several episodes of diagenesis and chemical weathering changing the original composition of the rock.

Caprock is exposed locally in several places in the northern Paradox Basin. The best exposure is along Onion Creek west of Moab, Utah. The creek itself, along with several other drainages have cut down through the Onion Creek salt wall revealing spectacular caprock exposures. An area north of Moab, Utah is another location of exposed caprock but the quality and quantity of revealed rocks is less then at Onion Creek.

3.4.3 The Significance of Bromide Distribution

The bromide content found within evaporites can indicate the degree of brine concentration (salinity) when the evaporites were formed. It also can help distinguish

between marine and non-marine waters in which deposition occurred. Bromide (Br^{-1}) is present in seawater as a naturally occurring anion and can substitute regularly for chloride (Cl^{-1}) when forming halite (NaCl). However, bromide concentrations (0.066 g/kg of seawater) are far less then chlorine (19.345 g/kg of seawater) which makes bromide a good indicator for salinity and brine concentration (Borchert, 1969). Halite found in evaporites has a bromide content ranging from 50 to 100 ppm for normal marine waters. Once concentrations elevate to around 150 ppm and greater, potash precipitation is likely to occur. Higher concentrations can also be a result of recycled or reworked evaporites. Variations in bromide content below 50 ppm suggest a strong presence of non-marine waters during deposition (Jenyon, 1986).

Bromide distribution profiles for four Paradox Formation halite beds can be seen in Figures 3.8 – 3.11. Salt beds/zones 2 and 3 are shallow cycles from the Cane Creek No. 1 core, Grand County, Utah (T 26S, R 20E, sec. 25) and salt beds 19 and 21 are from the Gibson Dome core, San Juan County, Utah (T 30S, R 21E, sec. 21).

Several observations can be made of the profiles. Bromide concentrations typically increase from bottom to top in most of the evaporite zones within the Paradox Basin (Raup and Hite, 1992). In cycles 2, 19 and 21 there is a sharp decrease of bromide content at the base of the zone. This is thought to be due to residual bromide rich-brines being expelled from the underlying clastic sediments during lithification. These cycles also exhibit a final decrease in bromide concentration in the upper few feet of the zone. This is due to an influx of seawater into the basin diluting the remaining brine and increasing circulation. Cycle 3 has a sharp increase in bromide concentration in the final few feet of section. Here it is likely the brine became extremely concentrated and the precipitation of potash minerals occurred.

Clearly seen in cycles 2 and 3 (and to some extent in cycles 19 and 21) there are several episodes throughout the zone where there is a rhythmic increase and decrease in bromide content. Four of these episodes can be easily seen in cycle 2 illustrated by the smoothed profile (Figure 3.8). A decrease in bromide content marks a decline in salinity and suggests there was an increase of water (probably brackish) into the basin (Raup and Hite, 1992).

The regularity of bromide distribution seen within many of the salt cycles indicates there was a large volume of brine within the basin. Shallow basins generally show erratic bromide distribution within halite zones (Raup and Hite, 1992). Such a regular distribution (and thus a significant volume of brine), combined with rapid salt deposition, would require adequate basin depth to accommodate such thick halite cycles.

3.4.4 Salt Rock Physical Properties

Salt rock is primarily formed from the mineral halite (NaCl) and has a density of around 2.17 g/cm^3 and a hardness of 2.5 (Klein, 2002). The density of salt is unique because is shows no change due to compaction with increasing depth. This property creates a constant seismic velocity independent of thickness and depth. Pure halite has a velocity of around 14,600 ft/s (4,500 m/s), but it is rare to see salt in a geologic environment without impurities (Jenyon, 1986). Anhydrite ($CaSO_4$) is often found in association with halite but far less in volume. It typically forms only thin stringers or near the boundaries, above and below, the salt beds. Anhydrite has a density of around 2.95 g/cm^3 and a seismic velocity of 19,500 ft/s (6,000 m/s) making it harder and more dense than halite (Jenyon, 1986; Klein, 2002). It is not uncommon to see a mixture of halite and anhydrite having a velocity of about 15,600 ft/s (4,800 m/s). Clastic sediments within the salt itself and interbedded clastic zones also cause a change in the overall density and thus seismic velocities.

The mobility of salt tends to be quite variable. Temperature, pressure, overburden, density and structural features can contribute to salt-body movement. Pure halite becomes plastic at around 200°C and will flow smoothly at 300°C (Jenyon, 1986). Pressure is caused by the weight of the overlying material pushing downward onto the salt. Jones (1959) calculated a shear strength that would cause salt to flow, using geologic conditions, of less then 30 kg/cm^2. This would be equivalent to about 1,000 feet (300 m) or less of overlying sediments. However, the density of the overburden would change how the underlying salt would react. As mentioned before, the density of the salt body itself can vary depending on imbedded impurities like anhydrite and clastic

material. Such impurities increase the density of the salt and also increase its strength and stability. Now obviously a larger volume of clastics and anhydrite would have much more of an impact on the overall strength then a smaller volume. Structural features, like faults, help salt to move. They provide an avenue of weaker stress in the overlying strata that mobile salt could follow.

These salt properties became extremely significant in the Paradox Basin involving the formation of the salt walls, pillows and anticlines. Differential loading from material shed off the Uncompahgre Uplift (undifferentiated Cutler Formation) onto the Paradox Formation caused the salt to squeeze and flow to the southwest (Paz Cuellar, 2006). The resulting salt structures and salt welds further influenced the deposition of overlying rocks along with adding pivotal time constraints to salt deposition.

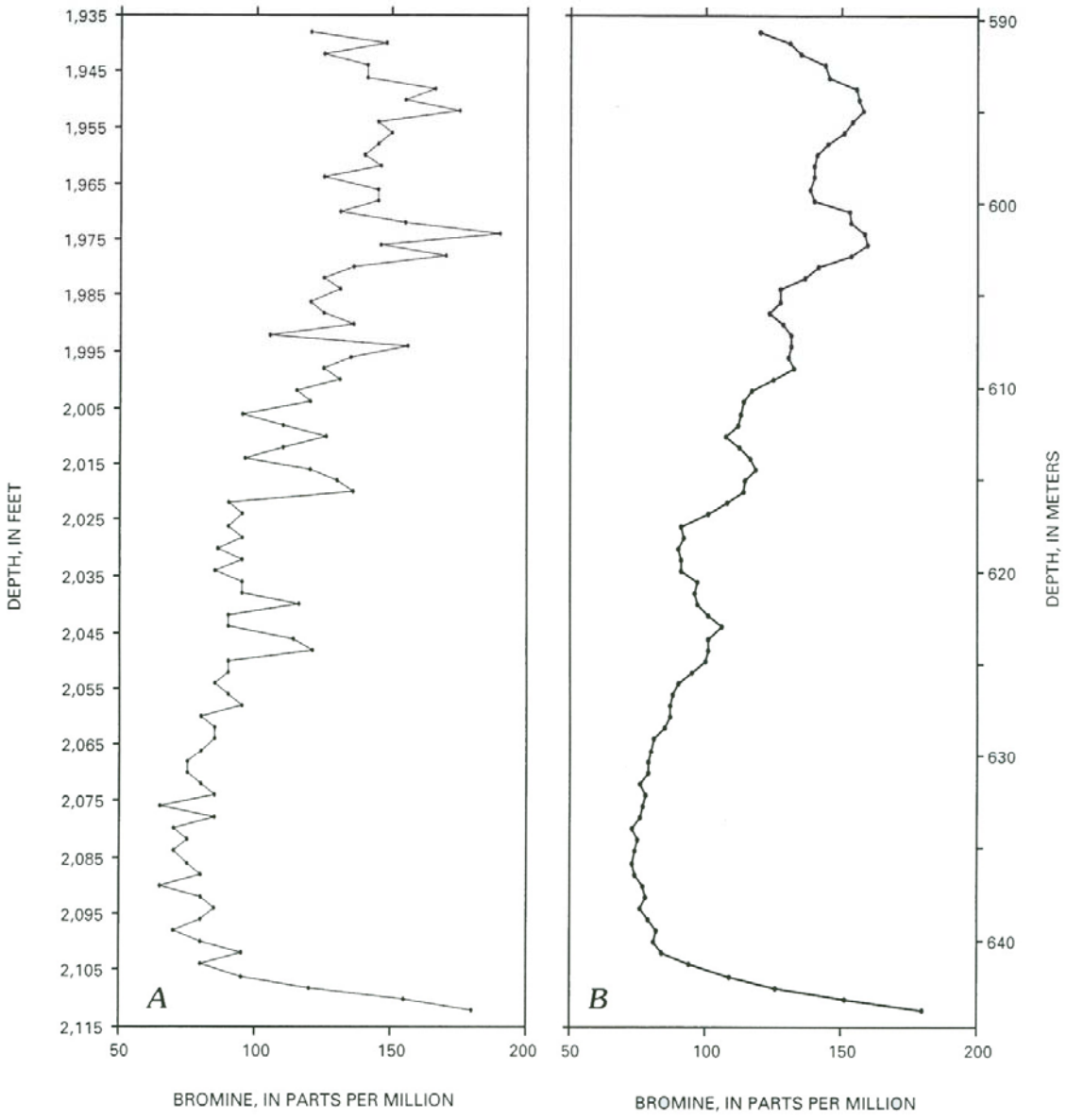

Figure 3.8: Bromide distribution within the halite bed of cycle 2, Cane Creek No. 1 core, Grand County, Utah. A) analytical results, B) Smoothed profile based on a moving average of five data points (from Raup and Hite, 1992).

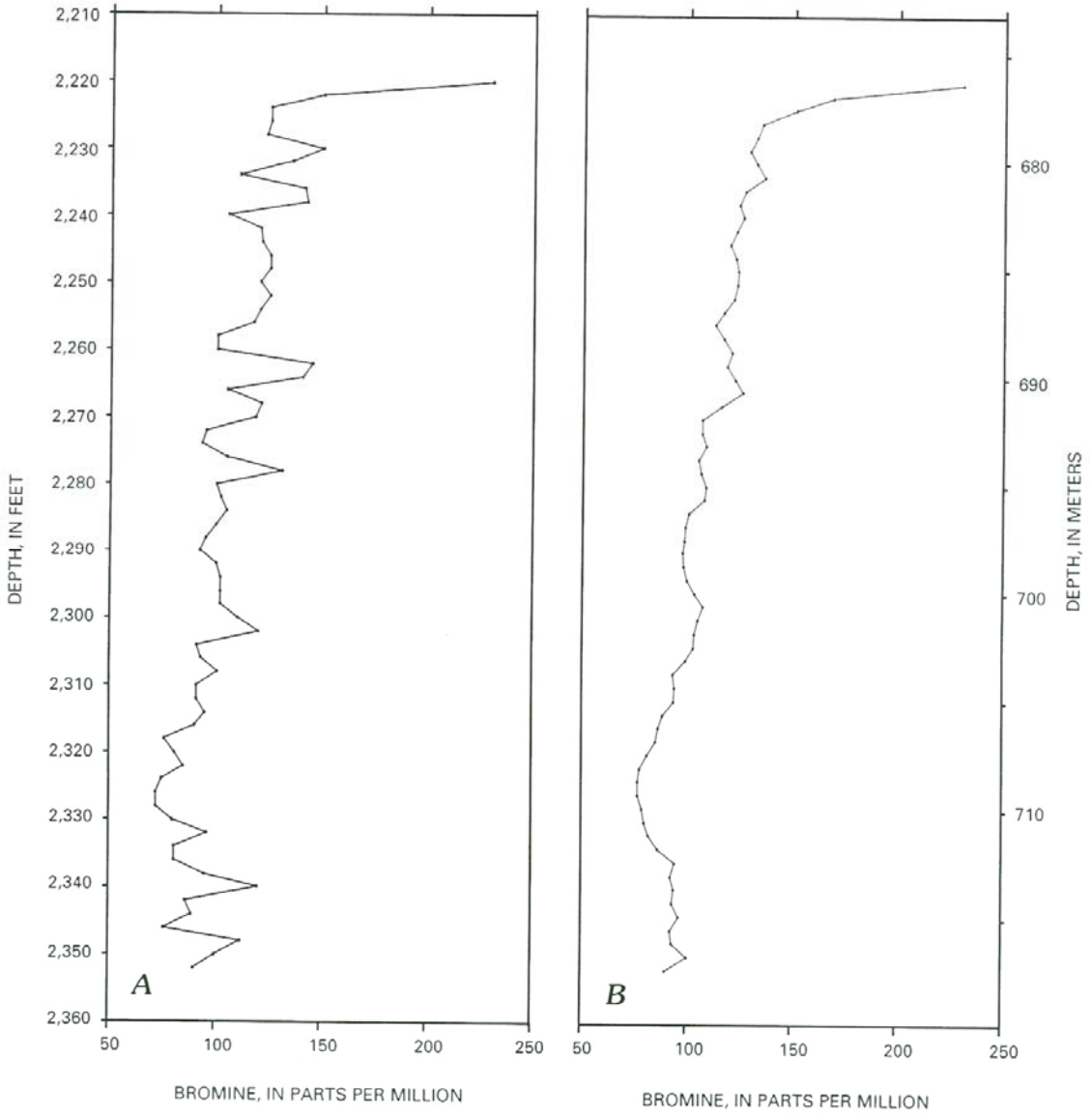

Figure 3.9: Bromide distribution within the halite bed of cycle 3, Cane Creek No. 1 core, Grand County, Utah. A) analytical results, B) Smoothed profile based on a moving average of five data points (from Raup and Hite, 1992).

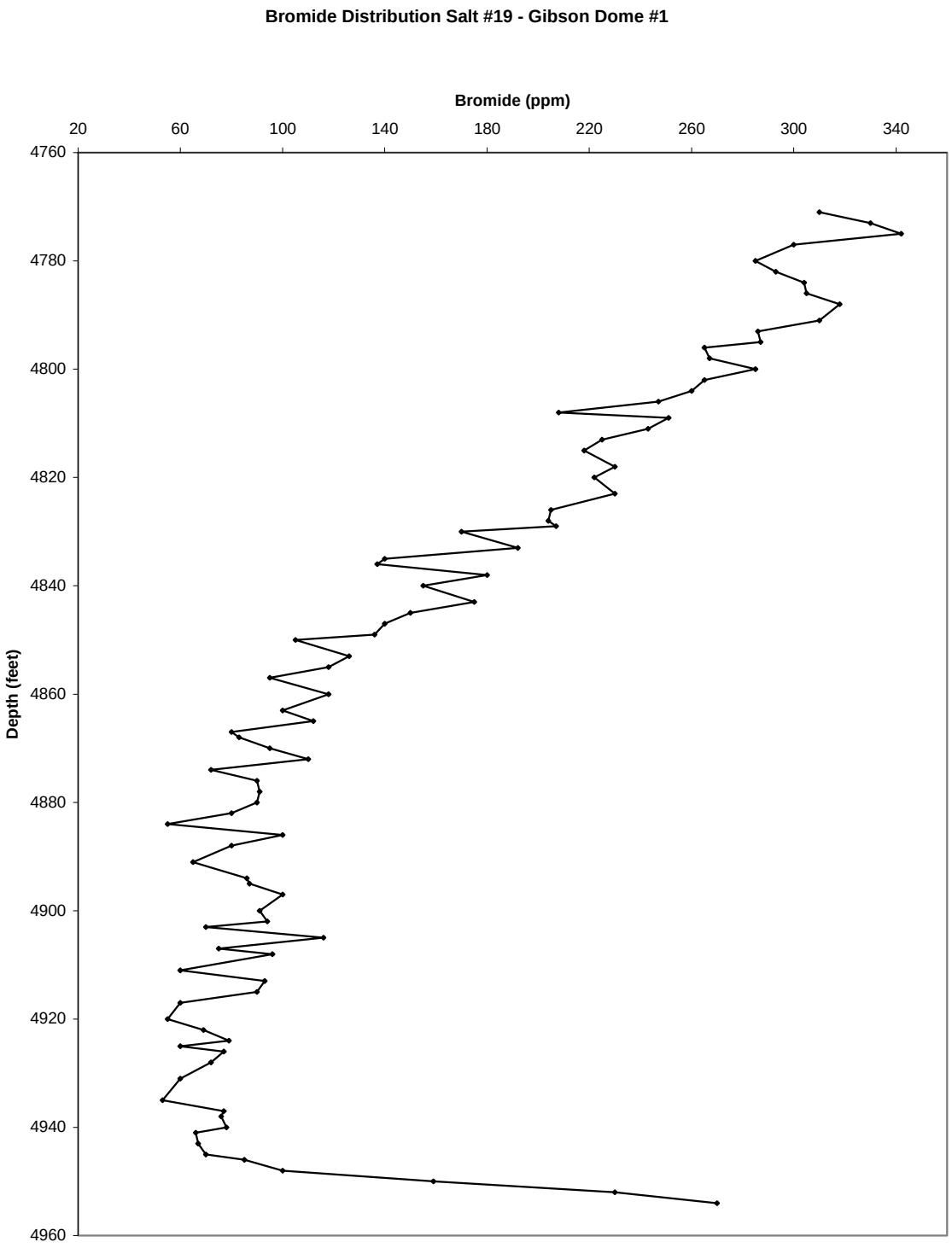

Figure 3.10: Bromide distribution in salt cycle 19 of the Paradox Formation, Gibson Dome #1 core, San Juan County, Utah (reproduced from Hite, 1983).

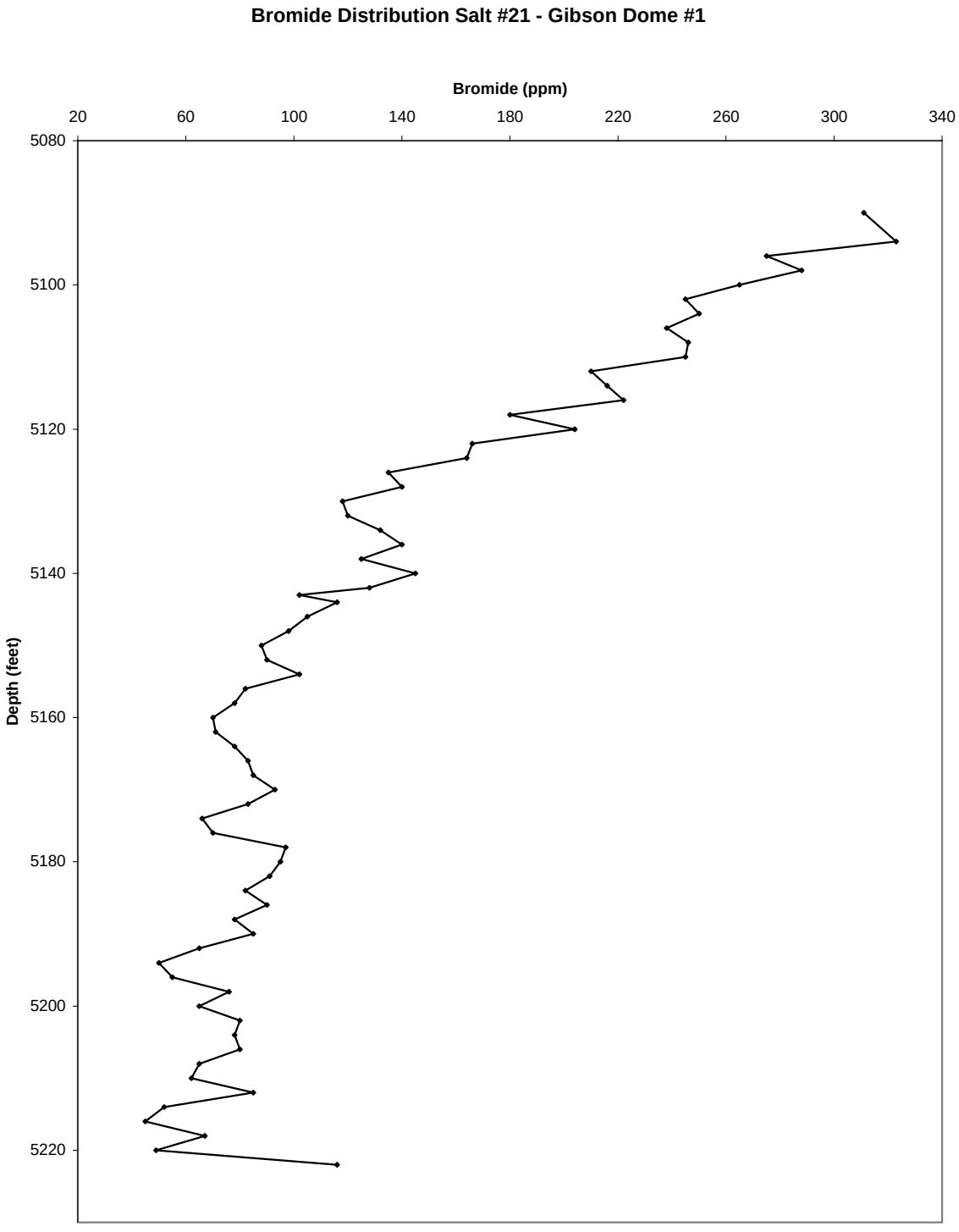

Figure 3.11: Bromide distribution in salt cycle 21 of the Paradox Formation, Gibson Dome #1 core, San Juan County, Utah (reproduced from Hite, 1983).

CHAPTER 4

CLIMATE AND CYCLICITY

The following chapter describes the climate and cyclicity during Pennsylvanian time and observed within the Paradox Basin.

4.1 Evaporites and Climate

Today evaporites typically form in areas on the world's surface where water is more likely to leave the system than to enter it. Therefore evaporites generally precipitate in dry, arid and semiarid regions of the world. Interestingly these regions almost always lie between 15° and 45° north and south latitudes. Here large convection cells of moist air are warmed near the equator causing them to rise, and then cool (losing moisture in the form of precipitation), where they descend back down to the earth's surface at around 30° latitude (Warren, 1989). The colder, dryer air absorbs available water particles as it falls creating a landscape that is deficient in moisture, thus resulting in a desert-like environment. These undersaturated air masses are the main driving force in the evaporation process and are also coupled with changes in air temperature, storm frequency, wind speed and direction, brine concentration and humidity (Sonnenfeld, 1984). The moving air masses that descend back down to the earths surface are known as prevailing easterlies or trade winds and are deflected westward due to the Coriolis effect (Sonnenfeld, 1984).

During the Desmoinesian (~309.4 – 305.5 Ma (Gradstein *et al*., 2004)), the Paradox Basin was situated in/near these arid zones. Maps created by Bambach *et al*. (1980) place the Paradox Basin roughly between about 8° and 14° north latitude. Similarly, a map published by Blakey (2007) situates the basin at roughly between 7° and 9° north latitude. Weber *et al*. (1995) illustrates the position of the northern Paradox

Basin to be at 15° north latitude during the Pennsylvanian. Although slightly different, these sources acknowledge that the position of the Paradox Basin, during Paradox Formation deposition, would be ideal for evaporite precipitation. Zharkov (1981) also notes how the position of these arid zones around the earth's surface can change depending on the location of the continents via continental drift. The arrangement of the continents, which also influence the position of seas, oceans, ocean currents and weather patterns, dictate paleoclimate zonations (Zharkov, 1981). Therefore, the arid zones we observe today (between 15° and 45° north and south latitudes) may not exactly be representative of the same arid zones exhibited during the Desmoinesian.

4.1.1 Global Climate During the Pennsylvanian

Changes in sea-level are dependent on the existence or absence of polar ice caps. The presence of the ice caps dictates the occurrence of high amplitude sea-level changes. During periods when the polar ice caps are non-existent, high amplitude sea-level fluctuations (controlled by tectonics and climate) are attributed to second- and third-order cycles that create oscillations in sea-level on the scale of tens of meters (Figure 4.1) (Vail *et al*., 1977; Warren, 1999). Smaller, but higher frequency fourth- and fifth-order cycles only occur on a scale of a few meters during greenhouse periods (times when little or no polar ice is present) because the change in sea-level is dominated by second- and third-order cycles.

By comparison, almost the opposite can be said during periods when thick polar ice caps are present (icehouse). Here high amplitude sea-level changes are dominated by fourth- and fifth-order cycles that are a result of ice volume fluctuations likely dictated by Milankovitch cycles (Figure 4.1) (Warren, 1999). The larger second- and third-order cycles that control the greenhouse periods are still present, but they experience a much longer period and a lower frequency thus having a smaller immediate effect then the fourth- and fifth-order cycles (Warren, 1999).

The late Paleozoic is characterized by a lowstand first-order cycle (Figure 4.2) (Fischer, 1984). This is attributed to icehouse conditions following the assembly of the

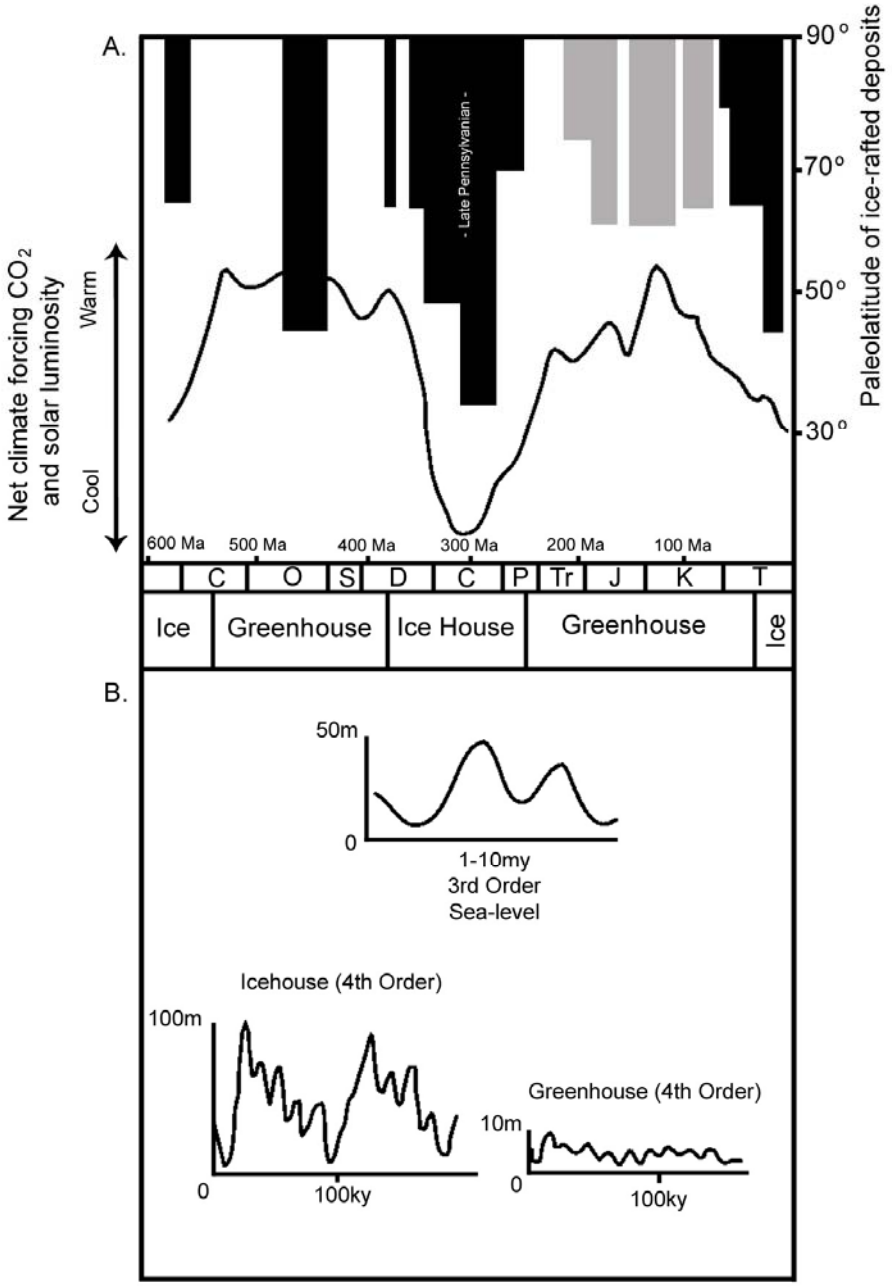

Figure 4.1: Diagram showing the relationship between greenhouse (periods of little to no polar ice) and icehouse (periods where polar ice exists) conditions, global CO_2 and eustasy. (A) Illustration showing paleolatitudinal extent of marine ice-rafted deposits (gray) and continental ice-rafted deposits (black). The curve plots net forcing of climate due to changes in CO_2 and solar luminosity. Ages, time periods and general greenhouse/icehouse episodes are shown on the horizontal axis. (B) Diagram showing typical third-order sea-level curves with a 1 – 10 million year period. There are also two examples of fourth-order cycles with superimposed fifth-order sea-level curves drawn during times of both icehouse and greenhouse environments (modified from Warren, 1999).

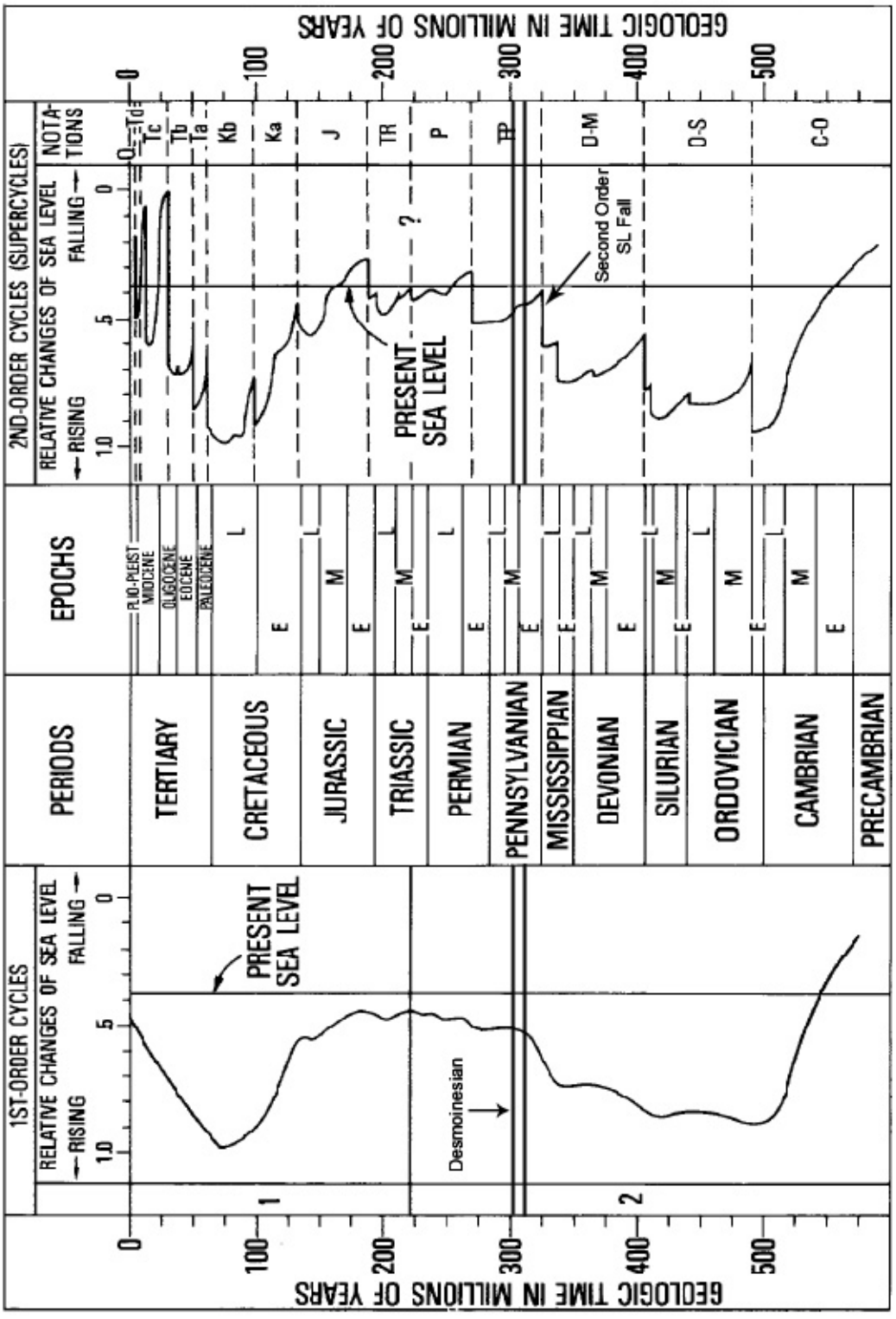

Figure 4.2: Figure illustrating first and second-order cycles of relative sea-level change during the Phanerozoic (modified from Vail *et al.*, 1977).

super-continents (Gondwanaland and Euramerica) in the southern hemisphere (Veevers and Powell, 1987). Vail *et al*. (1977) documented a second-order regression marking the end of the Mississippian (Figure 4.2) and highlighting an unconformity of approximately 4.5 million years (Hallam, 1992). The Pennsylvanian is characterized by a slight second-order rise or transgression in sea-level (Vail *et al*., 1977) which can be further broken down into several smaller third- and fourth-order cycles. These are observed in the evaporite and carbonate cycles of the Paradox Formation. This cyclical interval matches one of the glacial episodes proposed by Veevers and Powell (1987) undoubtedly linking glacio-eustatic influenced controls with the deposition of the evaporite cycles of the Paradox Formation.

4.2 Pennsylvanian Cyclicity and Climate Controlled Sedimentation

Pennsylvanian cyclicity has long been recognized in the central and western United States. Moore (1936) noticed cyclical repetition in marine limestones and shales in Kansas and how they created, what he deemed as, cyclothems. Hite and Buckner (1981) also recognized similar cyclic activity in the Paradox Basin involving both the evaporite sequences and related carbonate cycles in the southern part of the basin. It is evident today these cyclothems represent marine transgressions and regressions (Heckel, 1986).

Since the location of the Paradox Basin, during the Pennsylvanian, was roughly at 10° N latitude, it is likely the cyclic deposition of the Paradox Formation was climatically influenced (Rueger, 1996). Wanless and Shepard (1936) first suggested these Pennsylvanian cyclothems were caused by fluctuations in sea-level brought on by volume changes involving Gondwanaland glaciation. Their theory involves the increase and decrease of ice volume creating global, cyclic, climate change resulting in what we recognize today as periods of transgression and regression. As continental ice accumulated, both humidity and sea-level would fall restricting open marine contact with inland seas (Rueger, 1996) and basins much like the Paradox Basin. During this time the Paradox Formation evaporites would have been deposited. A loss in volume of

Gondwanaland glacial ice would result in an opposite situation, where inland seas and basins would have a direct connection with marine waters due to a rise in sea-level (Rueger, 1996). In the Paradox Basin, during times of higher eustatic sea-level, the organic rich black shales, within the clastic zones, would have been deposited.

Weber *et al*. (1995) were able to break the Desmoinesian into five stratigraphic sequences ranging between 800,000 years and two million years for the southern part of the Paradox Basin. The length of the sequences indicates they are associated third-order composite cycles or sequences (Figure 4.3). The sequence boundaries were determined by examining outcrop and seismic evidence involving subaerial exposure, onlapping of evaporite wedges, regionally correlated black laminated shales and mudstones, and aggradational growth of carbonates that likely formed during times of sea-level highstand.

The first (1) of these third-order sequences encompasses the entire Alkali Gulch evaporite interval which correlates to cycles 20 – 29 (Figure 3.5) and is defined as a lowstand evaporite wedge (Weber *et al*., 1995). The second (2) third-order sequence is characterized by the Barker Creek interval (cycles 10 – 18) (Figure 3.5) and is also described as a lowstand evaporite wedge (Weber *et al*., 1995). The Akah and Desert Creek zones (cycles 4 – 9) (Figure 3.5) together comprise the third (3), third-order sequence. The Akah interval represents a lowstand systems tract, but also contains what is thought to be the maximum flooding surface for the Desmoinesian – Lower Missourian second-order transgressive/regressive supersequence (Weber *et al*., 1995). The Desert Creek is identified as a highstand/transgressive systems tract that is responsible for the deposition of the Chimney Rock shale (cycle 5) and the carbonate buildups or mounds located on the southwestern shelf of the basin. The fourth (4) third-order sequence is defined as a progradational composite sequence and incorporates the Ismay (cycles 1 – 3) (Figure 3.5) and part of the lower Honaker Trail Formation. The final third-order sequence (5) identified by Weber *et al*. (1995) is a highstand systems tract and comprised of non-evaporite rocks within the Honaker Trail Formation.

Four of the five third-order Desmoinesian sequences (1 – 4) described above involve evaporite cycles of the Paradox Formation. It is important to note how each cycle can be characterized as a fourth-order sequence (Figure 4.3) ranging in duration

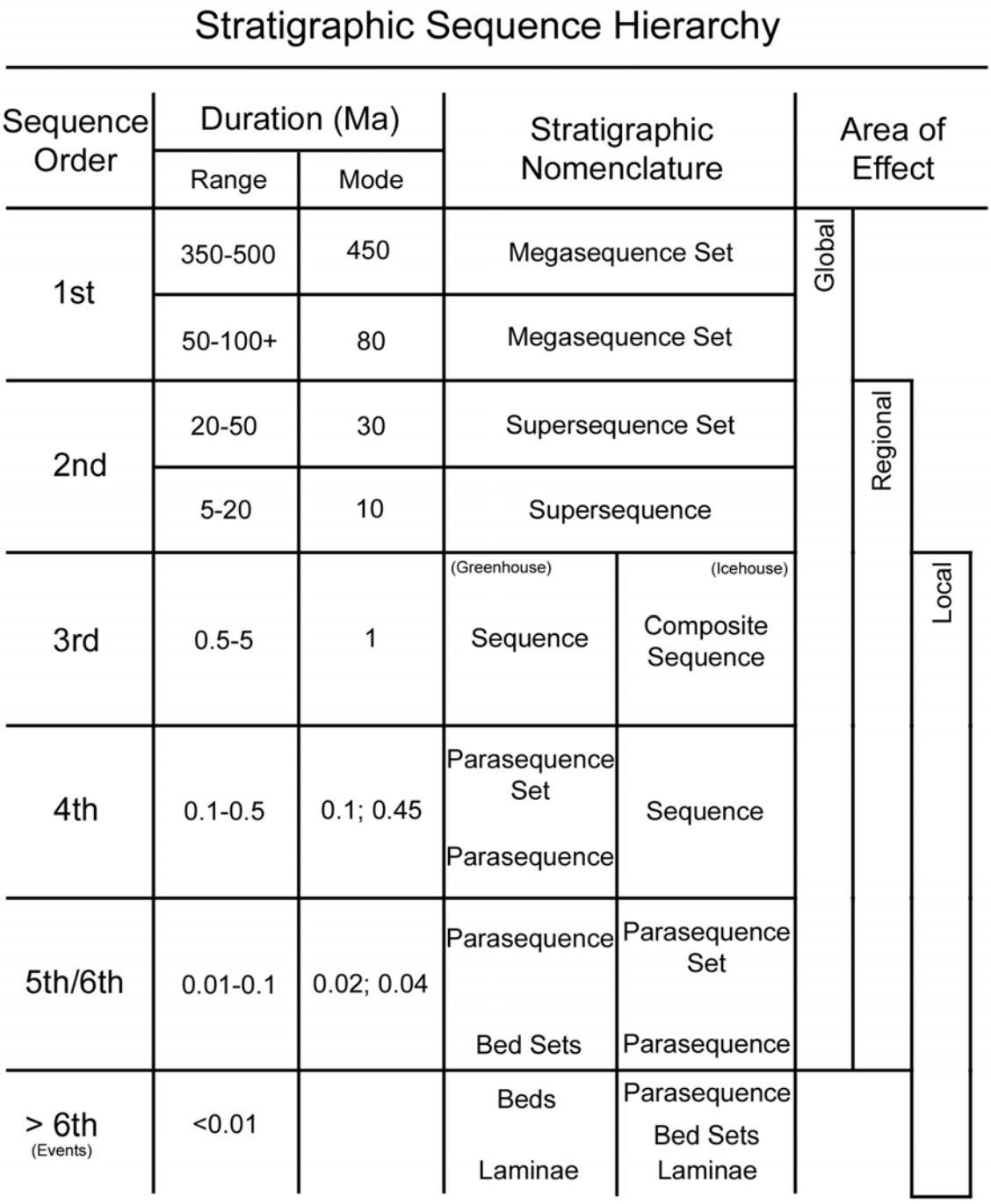

Figure 4.3: Chart showing the stratigraphic orders and cycle sequences and associated nomenclature, duration and area of effect (modified from Weber *et al*., 1995).

from 100,000 – 500,000 years with modes of 100,000 years and 450,000 years (Weber *et al*., 1995). These time intervals closely relate to eccentricity cycles defined by the Milankovitch theory.

Weber *et al*. (1995) were also able to correlate all of the third-order cycles (1 – 5) identified in the Paradox Basin with other third-order sequences characterized in the Midcontintent of North America using fusulinid and foraminifera correlation points. They were also able to tentatively match the third-order sequences in the Paradox Basin with major cycle boundaries identified by Heckel (1986) in Kansas using major transgressive/regressive black shales. They concluded that the Chimney Rock shale (evaporite cycle 5) and the Gothic Shale (evaporite cycle 3) were correlative to the Verdigris (Oakley shale) and Lower Fort Scott (Excello shale) cycles (Weber *et al*., 1995; Heckel, 1986).

4.2.1 Milankovitch Cycles

Although largely circumstantial, evidence of climate change stimulated by orbitally forced Milankovitch cycles in the Pennsylvanian, is becoming more persuasive. As we all know, the climate undergoes seasonal changes that involve the earth's orbit around the sun and the earth's axis being tilted at about 23 degrees. If all the factors that govern seasonal change remain fixed, then the average climate over a single year would be consistent through time (Schwarzacher, 1993). However since the earth is a dynamic system, changes in the elliptical orbit and inclination of the earth create dramatic cyclical variations in the earth's climate. The theory that explains these long term cyclic climate changes is known as the Milankovitch theory.

The three most important climate altering aspects of the Milankovitch theory involve the earth's eccentricity (elliptical orbit around the sun), obliquity (inclination of the earth's celestial axis; tilt) and precession (fluctuations in the earth's rotational momentum due to the sun and moon) all of which are directly affect the amount of solar energy (insolation) received by the earth from the sun (Figure 4.4) (Schwarzacher, 1993; House, 1995). Berger (1984) was able to calculate the development, timing and

frequency for each of the three parameters since the beginning of the Pleistocene. He noticed how the eccentricity of the earth has significant power intervals every 100,000 and 400,000 years. He added that the importance of the 100,000 and 400,000 year periods varies in significance from one to another. The same alternating succession is also observed with the precession which has a cyclical period of 19,000 to 23,000 years. Unlike the eccentricity and precession, the obliquity of the earth has a consistent period of 42,000 years, but can vary in strength (Berger, 1984).

Unfortunately, most detailed Milankovitch studies only involve data from about the last two million years. Schwarzacher (1993) discusses how pre-Pleistocene cyclicities, involving the earth's system, have changed over time. Precession is altered by the earth's rotational speed, inertia, angular momentum and tidal friction, all of which are effected by the distance between the earth and moon (Schwarzacher, 1993; House, 1995). These variables have decreased (as the distance between the earth and moon has increased) over geologic time slowing the rotation of the earth and thus extending the length of an individual day (Schwarzacher, 1993). Therefore in the past, a shorter distance between the earth and moon would have undoubtedly made both precession and obliquity cycles shorter then what they are today (Table 4.1 and Figure 4.5).

Age	Ma	Precession (years)		Obliquity (years)	
		Min.	Max.	Min.	Max.
Present	0	19,000	23,000	41,600	54,000
Upper Cretaceous	72	18,641	22,474	39,328	51,100
Middle Permian	270	17,545	20,868	34,227	42,250
Upper Carboniferous	300	17,272	20,468	32,954	40,403
Middle Devonian	380	16,562	19,428	29,649	34,309
Lower Silurian	440	16,014	18,625	27,097	29,884

Table 4.1: A table showing the estimated minimum and maximum lengths of paleoclimatic periods for six time intervals including today. Notice how the precession and obliquity have both decreased over time (after Schwarzacher, 1993 and Berger *et al*., 1989).

Hite and Buckner (1981) used individual sedimentation rates for anhydrite, dolomite, black shale and halite (all of which compose the evaporite cycles of the

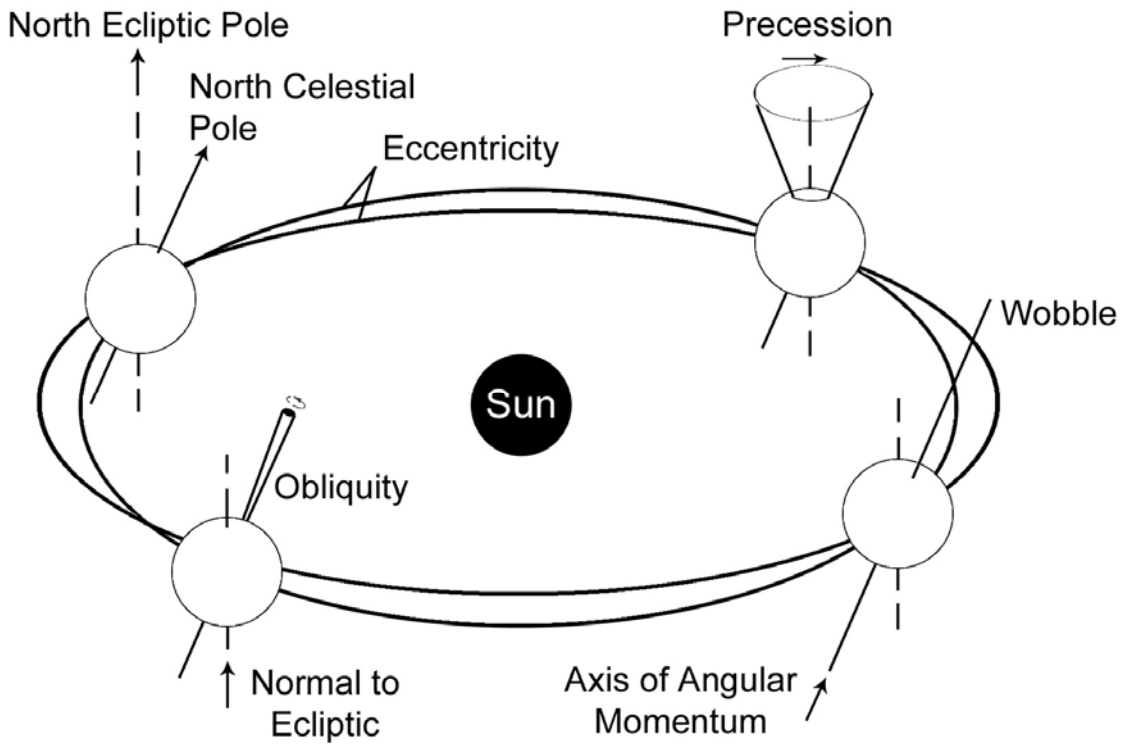

Figure 4.4: Diagram illustrating the three main Milankovitch cycle parameters: eccentricity, obliquity and precession. All three occur as oscillations involving the earth, sun and moon which directly affect the amount of insolation or energy received by the earth from the sun. Fluctuations in the earth's insolation can result in orbitally forced signatures or changes in the sedimentary record (modified from House, 1995).

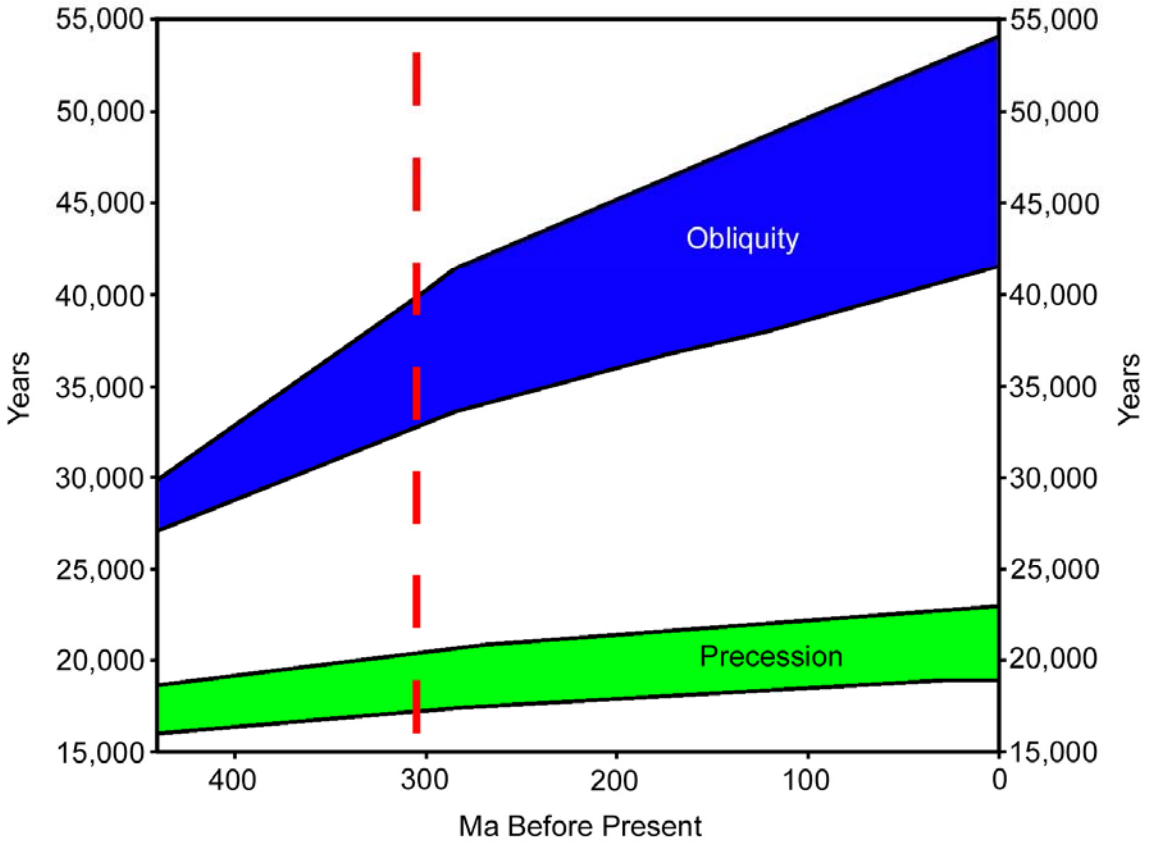

Figure 4.5: Change in precession and obliquity over the past 440 million years. Notice how both the precession and obliquity ranges have increased from past to present. The red dashed line marks the approximate timing of the Pennsylvanian Demoinesian (after Schwarzacher, 1993).

Paradox Formation) in an attempt to calculate the duration of each cycle. They concluded that the complete deposition of evaporite cycle 2 occurred in approximately a 100,000 year duration and believe this same time period can be applied to most of the complete cycles. Obviously this coincides with the perturbations of the earth's eccentricity which has a period of 100,000 years. This will be discussed in further detail later in this thesis. Hite and Buckner (1981) also studied global climate factors during the Pennsylvanian and concluded that the changes in water volume within the Paradox Basin (which caused the deposition of the evaporite sequences) were directly related to glacio-eustatic fluctuations involving ice volume in the southern hemisphere (Gondwanaland).

4.2.2 Palynology

Palynology is the study of spores and pollen generally deposited within an ancient sedimentary sequence. Changes in climate can be documented based upon the distribution of fossil spores and pollen which are called palynomorphs. Distinct palynomorph assemblages are abundant throughout all zones within the Paradox evaporite sequences.

Palynomorph specimens tend to be well preserved in halite rock due to the quick and un-abrasive deposition of the salt. Samples located in the silty dolomite and black shale facies range in quality. Most of the grains are unfortunately corroded due to the geochemical aspects of the rocks (Rueger, 1996). Few palynomorphs are observed in anhydrite. It is likely they are destroyed during the dehydration process of gypsum to anhydrite but some have been recovered in several zones within the Paradox Basin.

Rueger (1996) was able to identify, classify and categorize palynomorph taxa for evaporite cycles 4 – 26 from the U. S. Department of Energy Gibson Dome No. 1 core in San Juan County, Utah (T 30S, R 21E, sec. 21) (Figure 3.4). From these data he noticed how the palynomorph genera could be broken into biostratigraphic zones based on dominating taxa assemblages and matched those zones with the evaporite cycles (Figure 4.6). The lower zone consists of abundant *Vesicaspora* sp. and ranges from the bottom of the Paradox Formation through cycle 19 (i.e. cycles 19 – 26, for this well). Above the

Vesicaspora sp. is a zone of *Striatites* sp. which includes cycles 13 – 18. Additionally, a zone of *Potonieisporites* sp. encompasses evaporite cycles 7 – 10. Cycles 4 – 6 are represented by a mixed zone of *Striatites* sp. and *Potonieisporites* sp. which are co-dominant. These zones represent particular phases in a larger cyclical sequence responsible for the deposition and cyclicity of the Paradox Formation. The boundaries of these zones mark significant climatic changes that were severe enough to cause changes in the flora of the surrounding area (Figure 4.6).

Changes in the distribution of palynomorphs have even been documented in a single evaporite cycle. Several palynomorphs identified overall in a single cycle are not recognized within each of the lithological facies of that particular cycle (Rueger, 1996). This indicates there were small scale climate changes throughout the deposition of a single cycle.

Palynoflora in the Paradox Formation have been compared and correlated to other areas in an attempt to establish age relationships. Palynomorphs including *Lycospora pellucida* and *Calamospora breviradiata* are seen in both the Paradox Formation and in other rocks that have been identified as Pennsylvanian Desmoinesian in the central and eastern areas of the United States (Kosanke, 1995). This reconfirms the time period for the deposition of the Paradox Formation which was proposed by Baars *et al.* (1967) who analyzed fusulinids and black shale markers to create an age relationship.

4.2.3 Rhythmic Periodicity of Anhydrite Laminations and the 11 Year Solar Cycle

Within many of the halite zones, of the Paradox Formation, are distinct anhydrite laminations. These laminations are thin, ranging in thickness from 0.03 – 0.09 inches (0.5 – 2 mm) and are offset by intervals of halite varying in thickness from 0.75 – 6.0 inches (2 – 15 mm) (Figure 4.7) (Raup and Hite, 1992). The anhydrite layers exhibit a texture that Raup and Hite (1992) have termed ‘snow-on-the-roof’ which is described as the draping of anhydrite on top of the uneven surface of halite crystals much like snow would fall over uneven ground. This draping effect would imply the halite was in place before anhydrite deposition and the fine-grained texture of the anhydrite indicates

primary, subaqueous, rapid precipitation (Hite, 1985; Warren, 1985). It is not uncommon to have thin layers of clay, potash minerals and organic matter in combination with the anhydrite laminations (Figure 4.7). Hite (1968) hypothesized this detrital material occurred due to seasonal runoff. Sonnenfeld and Hudec (1985) expanded on the origin of the clay layers suggesting they are a result of flash flooding. The halite section of the anhydrite/halite couplets increase in thickness from bottom to top and also contain less depositional anhydrite, detrital material and organic matter (Raup and Hite, 1992). This was observed in the Delhi-Taylor Oil Company Cane Creek No. 1 core where halite intervals between laminae, at the base of an evaporite sequence, ranged from 0.8 – 1.7 inches (2 – 5 cm) compared to thicknesses near the top of an evaporite sequence which were much thicker exceeding 5.9 inches (15 cm).

It is likely the thin layers of anhydrite can be explained by cyclic temperature changes that create oscillations in the temperature of the brine. Since calcium sulfate precipitation is stimulated by temperature change (more soluble in cold solutions), anhydrite varves could have been deposited during warmer periods (Raup and Hite, 1992). Halite, which in turn is more soluble in hot water, would be deposited in cooler periods. This was also discussed by Stewart (1963) who suggested it is possible these periods of deposition occurred annually. Another possibility that could cause the precipitation of anhydrite laminations is the cyclic influx of meteoric waters abundant with calcium bicarbonate (Magaritz, 1987). The calcium bicarbonate would react with the sulfate in the remaining brine to create gypsum, or in this case, anhydrite (Raup and Hite, 1992). One might conclude these influxes are annual and would have a similar result as (if not tied to) the seasonal temperature changes described above.

Interestingly the 11 year solar cycle can also be interpreted within the anhydrite laminations. These larger scale cyclical rhythms are directly related to sunspot activity on the surface of the sun. Sunspot cycles occur on average during an 11 year period but can range between 8 and 15 years, during which the suns polarity reverses. Sunspots are darker ‘spots’ on the sun which are much cooler (by around 2,000° C) than surrounding areas (Pekarek, 2001). Sunspots form when the suns magnetic field limits the flow of gasses to the suns surface lowering the overall temperature of the effected areas. However, these cooler spots are counterbalanced and overshadowed by larger, hotter, and

brighter areas called faculae and plages that display much stronger magnetism then the sunspots (Pekarek, 2001). Therefore, during times of maximum sunspot activity the overall temperature of the sun increases. The opposite is true during times of sunspot minimums.

Such variations have been documented in evaporite sequences where every tenth to twelfth lamellae is generally thicker and more abrupt (Borchert and Muir, 1964; Borchert, 1969). Unfortunately, problems in relating small scale bedding anomalies with sunspot cycles do arise. Some of these problems involve accurate lamellae thickness measurements that can be subjective and the periodicity of the sunspot cycles varies depending on the suns magnetism and position (Braitsch, 1971; Pekarek, 2001). Therefore, attempting to correctly identify an 11 year cyclicity in fine-grained sediments can be very skewed and biased based on individual interpretation, however, recognizing the 11 year periodicity is well within the range of possibility.

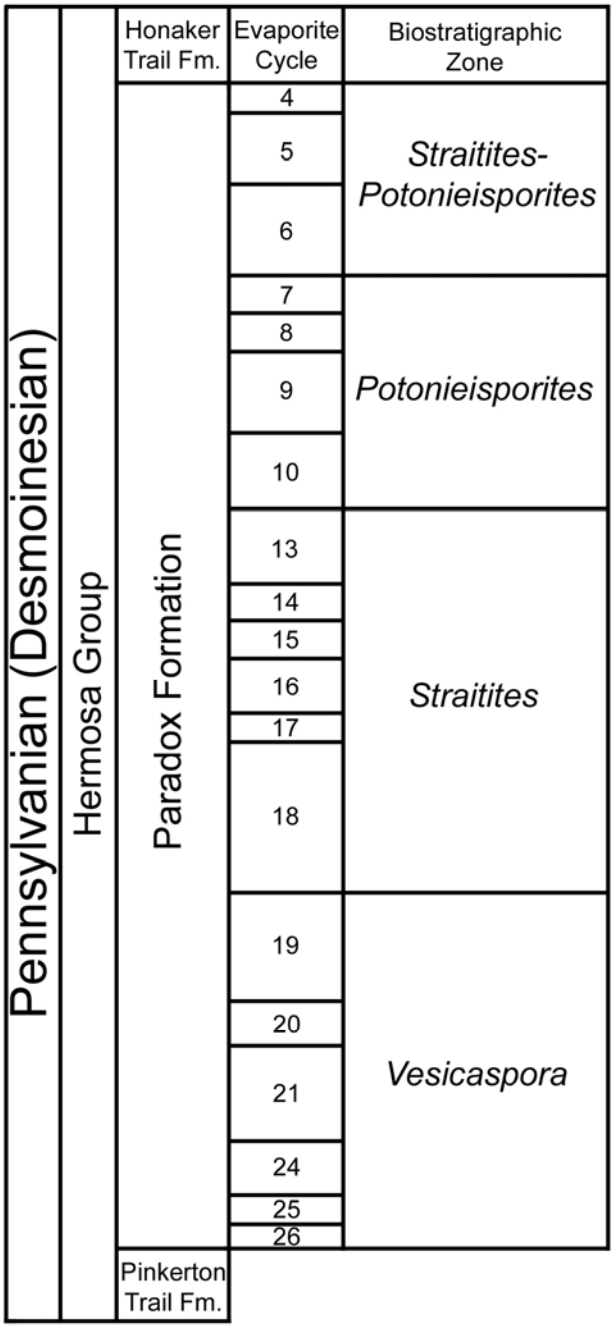

Figure 4.6: Biostratigraphic zones formulated from palynomorph data. Samples were taken from the U. S. Department of Energy Gibson Dome No. 1 in San Juan County, Utah (T 30S, R 21E, sec. 21). The change in palynomorph genera within the formation suggests drastic climatic changes took place (modified from Rueger, 1996).

Figure 4.7: A photograph of core taken from the Delhi-Taylor Oil Company Cane Creek No. 1 core (T 26S, R 20E, sec. 25). The interval is from the halite zone of evaporite cycle 2 at a depth of approximately 2,000 feet (610 m). Notice the anhydrite laminations (darker intervals) that are thought to represent seasonal periodicities within the basin. The laminae also contain significant amounts of detrital and organic material giving the intervals a darker color. A pencil is used for scale.

CHAPTER 5

METHODOLOGY AND DATA ACQUISITION

In order to better understand the complex structural and stratigraphic Pennsylvanian salt system and its relationship to the Uncompahgre Uplift, well logs, mud logs, outcrop samples, QEMSCAN data and core were all analyzed, and form the primary dataset for this study.

5.1 General Well Information

Well information for over 500 wells was obtained through the Utah State Oil and Gas (2007) website and incorporated wells from Grand, Emery and San Juan counties. These data include well locations (latitude, longitude, township, range, section, etc.), elevations (kelly bushing, ground, derrick floor), API numbers, well names, operators, total depths, completion dates, and well type/status. Any perforation and formation test data were also acquired along with information on cored, producing and pay/show intervals where available.

Formation top data were gathered from a variety of sources. The primary source was the Utah State Oil and Gas (2007) website. The tops were located from the well files listed under each individual well. Scout tickets reserved at the Denver Earth Resources Library (2007) were also used in the assembly of the formation tops database.

Unfortunately there are two major problems within the data set involving a lack of well information. First, there are an insufficient number of useful wells located east of the Salt Valley Anticline compared to the amount west of the structure. This creates problems when attempting to correlate from the west side of the study area to the east. Secondly, since Arches National Monument became a national park in 1971, (National

Park Service, 2007) no further exploration drilling as been authorized and thus creates a significant void within the study area.

The above well information was compiled into a *PETRA* (IHS) database specifically designed for this project.

5.2 Well Logs

Well logs for over 120 wells were acquired from the Utah State Oil and Gas (2007) website (Table A.1). Many of the wells within the study area were drilled pre-1990 and the qualities of the logs were at times unreadable and uninterpretable. Most of the available logs consisted of sonic, resistivity, gamma ray-neutron and density-neutron logs with a variety of other atypical logs. These were calibrated and added to the *PETRA* database mentioned above.

Available formation tops were then added to the logs and adjusted for errors. Additionally, any formation tops not already available were picked from the well logs. This included identifying the top and bottom of the Paradox salt plus each individual halite and clastic interval. These zones were labeled 1 – 29 (and beyond) following Hite's (1960) informal system of nomenclature where the evaporite cycles are identified numerically.

Well logs, in conjunction with geologic well reports obtained from the Utah State Oil and Gas (2007) website, were also used to identify the main lithological units within the clastic intervals for 10 wells (Table A.2). These specific 10 wells were used because of their geographical location, completeness of stratigraphy through the Paradox Formation, quality of well logs and the number of evaporite cycles identified. The lithological units included anhydrite, black shale, and silty dolomite (both transgressive and regressive). Individual facies thicknesses for each clastic zone, as well as total lithological thicknesses for the 10 wells, were calculated and tallied. These lithologies, along with their respective sedimentation rates, were used to calculate and estimate the time of total deposition for individual evaporite cycles and thus for the entire Paradox Formation.

5.3 Core

To augment the well data, the Delhi-Taylor Oil Company Cane Creek No. 1 core (T 26S, R 20E, sec. 25) was studied. The well was drilled approximately along the crest of the Cane Creek Anticline (Figure 3.4) in Grand County, Utah as a potash exploratory well (Raup and Hite, 1992). The cored interval starts at a depth of 1,825 feet (556 m) in the lower Honaker Trail Formation and proceeds to the bottom of the well at a depth of 2,805 feet (855 m) (evaporite cycle 5 of the Paradox Formation). The core encompasses complete cycles 2, 3, 4 and the halite section of cycle 5. Cycles 2 and 3 are typical, well preserved evaporite sequences that are described in Chapter 3. Cycle 4 is much thinner then the previous two cycles and lacks the repetitious clastic zone lithologies also observed in cycles 2 and 3. The halite of cycle 5 is roughly 127 feet (38.7 m) thick and the upper 10 – 12 feet (3 – 3.7 m) is chiefly composed of sylvite (KCl) in association with halite. This potash-bearing zone is currently being mined by Intrepid Mining, LLC (Raup and Hite, 1992; Intrepid Mining, 2006).

For the purposes of this study, describing and logging the core was deemed unnecessary, as this had already been thoroughly completed by several authors including Raup and Hite (1992). Instead, specific questions were addressed while studying the core which included observing thickness variations of interbedded anhydrite and detrital laminae within the halite zones, characterizing the boundary between cycles, identifying textures within the anhydrite intervals and noting the presence of fractures (cemented or un-cemented) within the organic-rich black shales.

5.4 Outcrop

Outcrop samples were gathered from the Onion Creek area south of Utah State Highway 128 (Figure 5.1). The exposed caprock is mainly composed of gypsum, anhydrite and the remains of what appears to be clastic intervals. Several tributaries or drainages feed into Onion Creek and have cut narrow canyons into the diapir. A side canyon along Onion Creek (N38° 41' 58.2", W109° 16' 48.2") offers good access to the

outcrops and cuts down vertically through the caprock revealing a cross-sectional profile. However, since the rocks have undergone chemical and physical changes during the caprock formation process, it is very difficult to identify the intervals within the stratigraphic sequence the clastic zones represent (Figure 5.2). Well control from several wells in the area suggest this outcrop is correlative to somewhere within the first 10 evaporite cycles. Samples of black shale, dolomite/siltstone and gypsum were collected from several locations along this canyon (Figure 5.3).

An exposed bed of fine-grained, fractured, laminated sandstone is located on the northern edge of the caprock (Figure 5.4). The sandstone might represent a turbidite bed, but because the area is so structurally distorted and complex it is difficult to ascertain the placement of the bed within the stratigraphic sequence. The sandstone is located adjacent to red-bedded shales considered to be part of the Moenkopi Formation. Therefore, because of the physical position next to the caprock and its relationship adjacent to the Moenkopi Formation, it is thought the sandstone bed represents part of the Cutler Formation (B. D. Trudgill, 2007, personal communication).

5.5 Mud Logs

Mud logs from several recently drilled wells were generously provided for this project by Gasconade Oil Company and Delta Petroleum Corporation. These wells include several drilled by Delta Petroleum in their Greentown (Greentown St. 36-11, T 21S, R 16E, sec. 26; Greentown St. 32-42, T 22S, R 17E, sec. 32; Samson Federal 28-11, T 22S, R 17E, sec. 28) and Salt Valley (Salt Valley St. 25-12, T 22S, R 19E, sec. 25) project areas (Delta Petroleum, 2008). Due to confidentiality restrictions, at the present time the information obtained and used from these wells cannot be recreated for public display within this thesis. However, the data were analyzed and used in this report.

Figure 5.1: Map showing the location of the caprock outcrop used for field study and sample collection along Onion Creek in the middle of the Onion Creek salt wall. Image modified from Google Earth (2007).

Figure 5.2: A clastic interbed overlain by caprock located along the Onion Creek salt wall. The distortion of the beds is attributed to salt wall and caprock formation processes. A rock hammer (left side of the image) is used for scale.

Figure 5.3: An example of a black shale overlain by a silty dolomite. The photograph was taken along the caprock of the Onion Creek salt wall. Rock hammer is used for scale.

Figure 5.4: A fine-grained, fractured, laminated sandstone about 10 feet (3.05 m) thick near the edge of the caprock exposure, Onion Creek salt wall, Utah.

5.6 QEMSCAN Sample Preparation and Investigation

This section describes the sample preparation, research objectives and results acquired using the QEMSCAN analysis machine.

5.6.1 QEMSCAN Research Objectives and Sample Preparation

Five samples were sent to the Advanced Mineralogy Research Center, Colorado School of Mines, Golden, Colorado for detailed mineralogical, porosity and grain size analysis. Four of the samples were chosen from the Delhi-Taylor Oil Company Cane Creek No. 1 core (T 26S, R 20E, sec. 25) and were generously borrowed courtesy of the USGS Core Research Center located at the Denver Federal Center, Denver, Colorado (Table 5.1). The fifth sample was taken from a hand specimen collected from caprock of the Onion Creek diapir.

Location	Depth (ft)	Cycle	Trans./Regres.	Lithology
Cane Creek Core	2134.8	2	Regressive	Silty Dolomite
Cane Creek Core	2184.0	2	Transgressive	Silty Dolomite
Cane Creek Core	2377.1	3	Regressive	Silty Dolomite
Cane Creek Core	2446.1	3	Transgressive	Silty Dolomite
Onion Creek	Outcrop	?	?	Silty Dolomite

Table 5.1: Table of the five samples used for QEMSCAN analysis.

The purpose of testing these five dolomitic samples was to determine their mineralogical composition. This involved two objectives: (1) to determine if there was a change in the quartz, feldspar, muscovite, etc. contents between transgressive and regressive dolomites of individual cycles and (2) to attempt a correlation from the Cane Creek No. 1 core, eastward across the basin toward the Uncompahgre Uplift, to the

Onion Creek area using the mineralogical composition (quartz and feldspar in particular) as the major correlative factor.

Sample preparation included using a diamond-studded saw to cut each sample into proper sized sections, which were then mounted in epoxy-resin and left to cure. The mounted samples were ground and polished using alcohol-based lubricants and suspensions to preserve water-sensitive materials like gypsum and halite. They were then carbon coated to establish an electrically conductive surface needed for the analysis. The QEMSCAN analysis machine uses x-rays and four detectors to examine each individual point on a grain or sample depending on the measurement size (25 and 10 microns were used for each sample). The data were then filtered through the QEMSCAN computer processors where a mineralogical spectrum was used to identify the mineral or mineral assemblage for that particular point. After the entire sample was scanned, a detailed picture of the sample including a mineralogical mode, was created.

5.6.2 QEMSCAN Sample Analysis

Four samples from the Delhi-Taylor Oil Company Cane Creek No. 1 core were analyzed. The samples were from two evaporite cycles (cycles 2 and 3) and from both transgressive and regressive lithological units (Table 5.1). As first postulated by Raup and Hite (1992) there is a significant difference in the mineralogical composition between transgressive and regressive dolomites, particularly involving the amount of quartz. There is an abundant amount of quartz in each transgressive sample (Figures 5.5 and 5.6) compared to its regressive counterpart (Figures 5.7 and 5.8). In fact there are increased amounts of plagioclase, alkali feldspar, muscovite, illite and kaolinite within the transgressive sequences (Figures 5.9, 5.10 and Table 5.2).

The fifth sample obtained from the Onion Creek diapir (Figure 5.11) was used in an attempt to correlate clastic zone mineralogical assemblages across the basin and is discussed in further detail in Chapter 7.

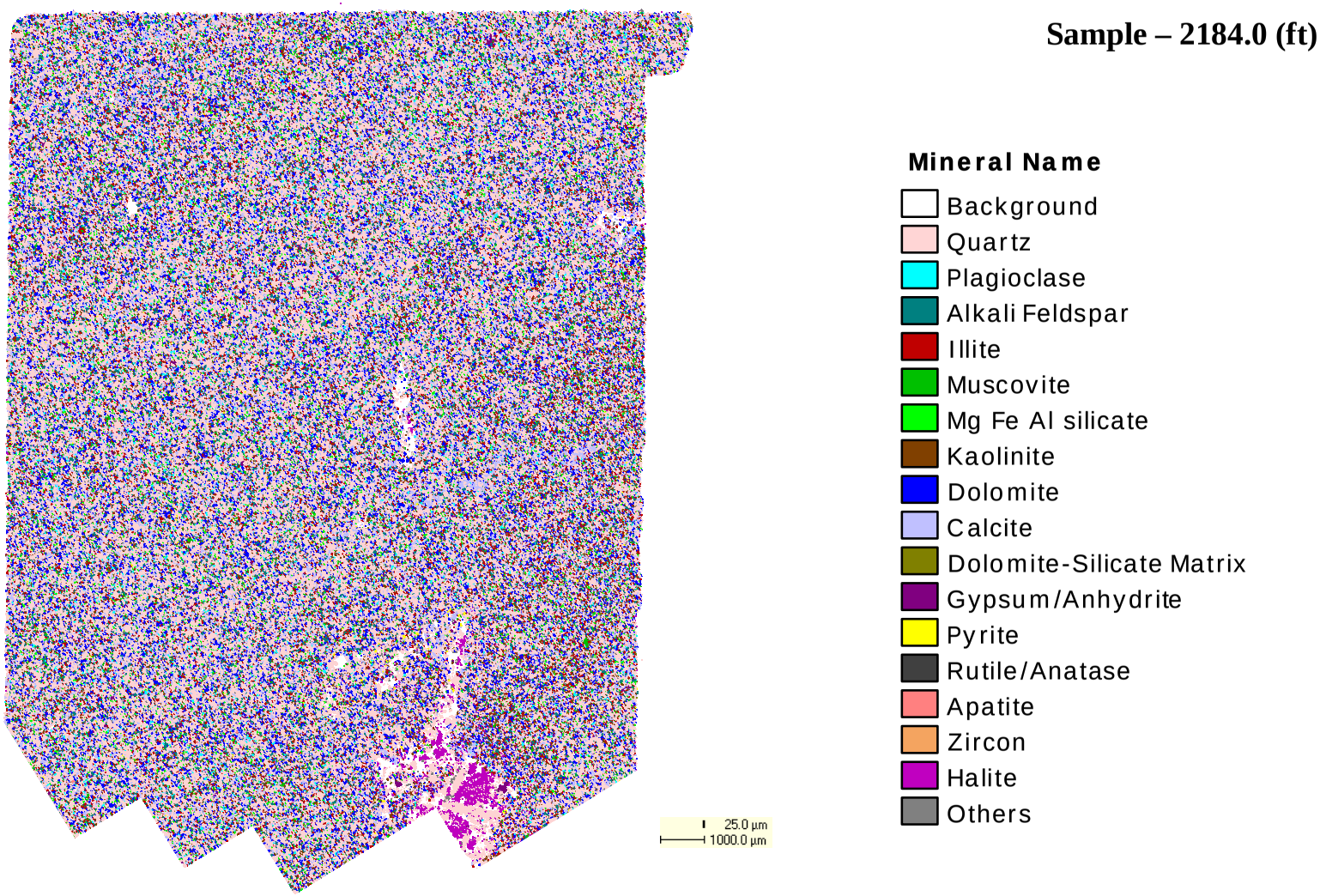

Figure 5.5: Figure showing the mineral compilation for transgressive sample 2184.0 (ft) (cycle 2) using a 25 µm measurement spacing. Background (white) is equal to porosity.

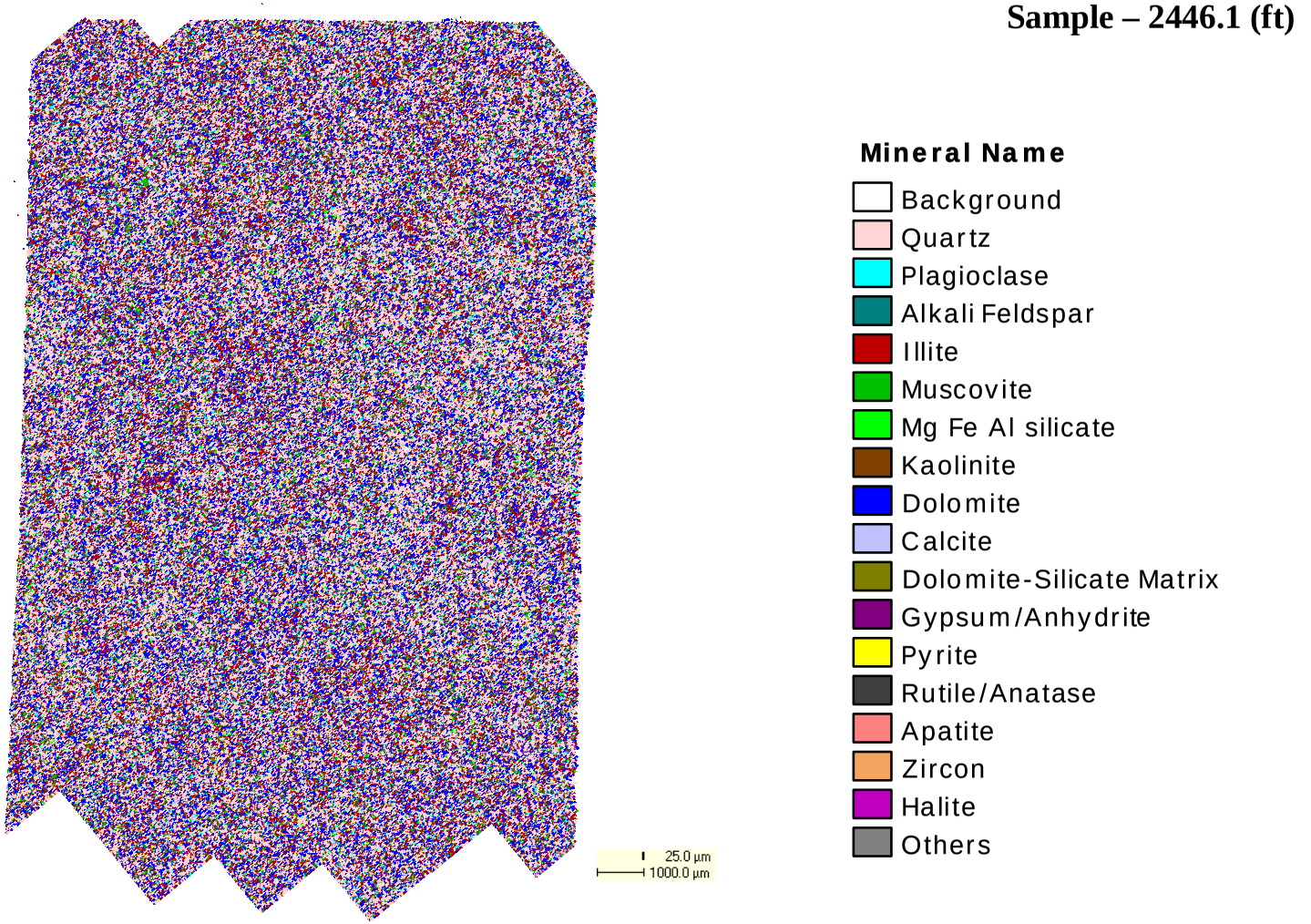

Figure 5.6: Figure showing the mineral compilation for transgressive sample 2446.1 (ft) (cycle 3) using a 25 µm measurement spacing. Background (white) is equal to porosity.

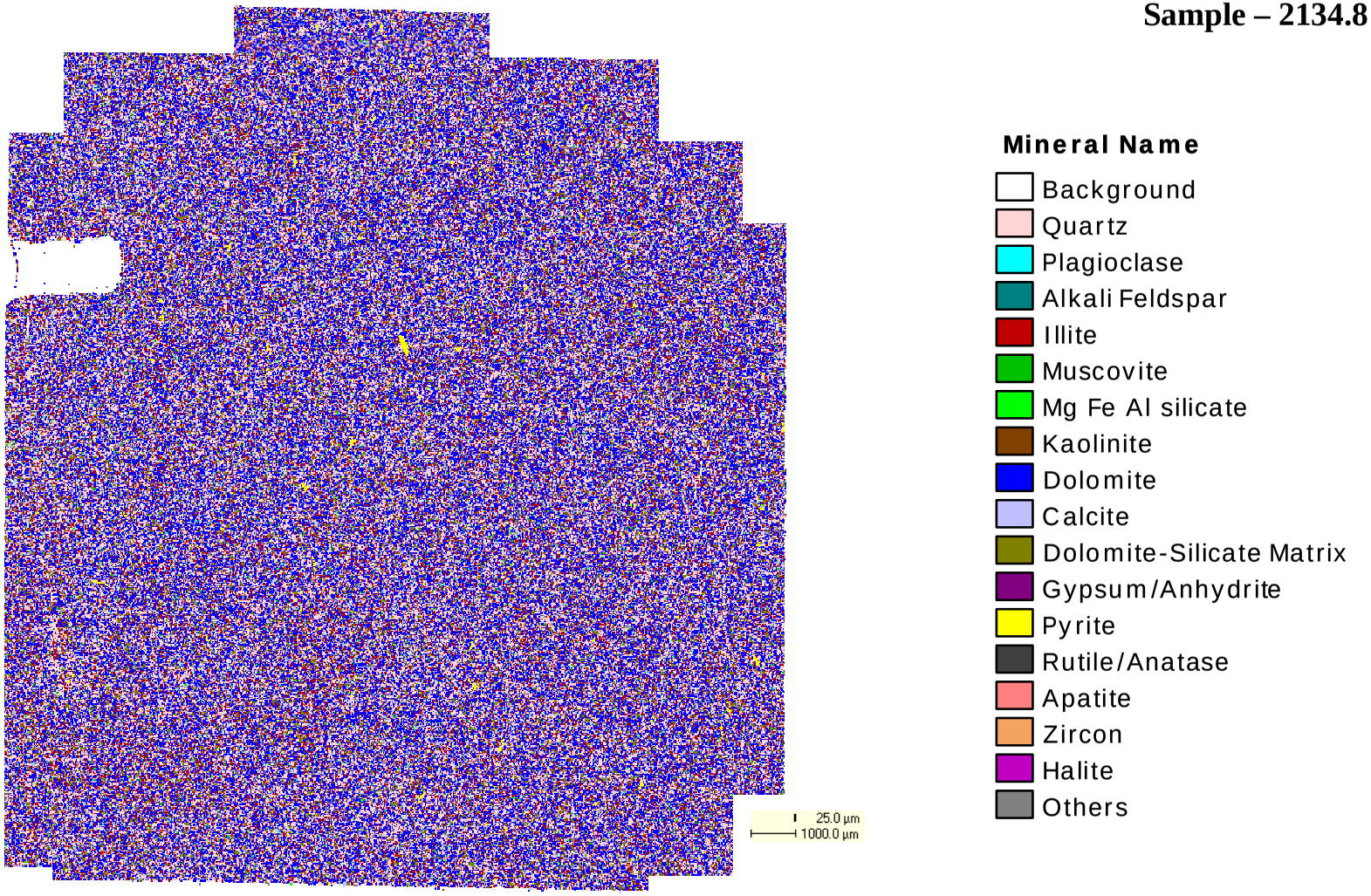

Figure 5.7: Figure showing the mineral compilation for regressive sample 2134.8 (ft) (cycle 2) using a 25 µm measurement spacing. Background (white) is equal to porosity.

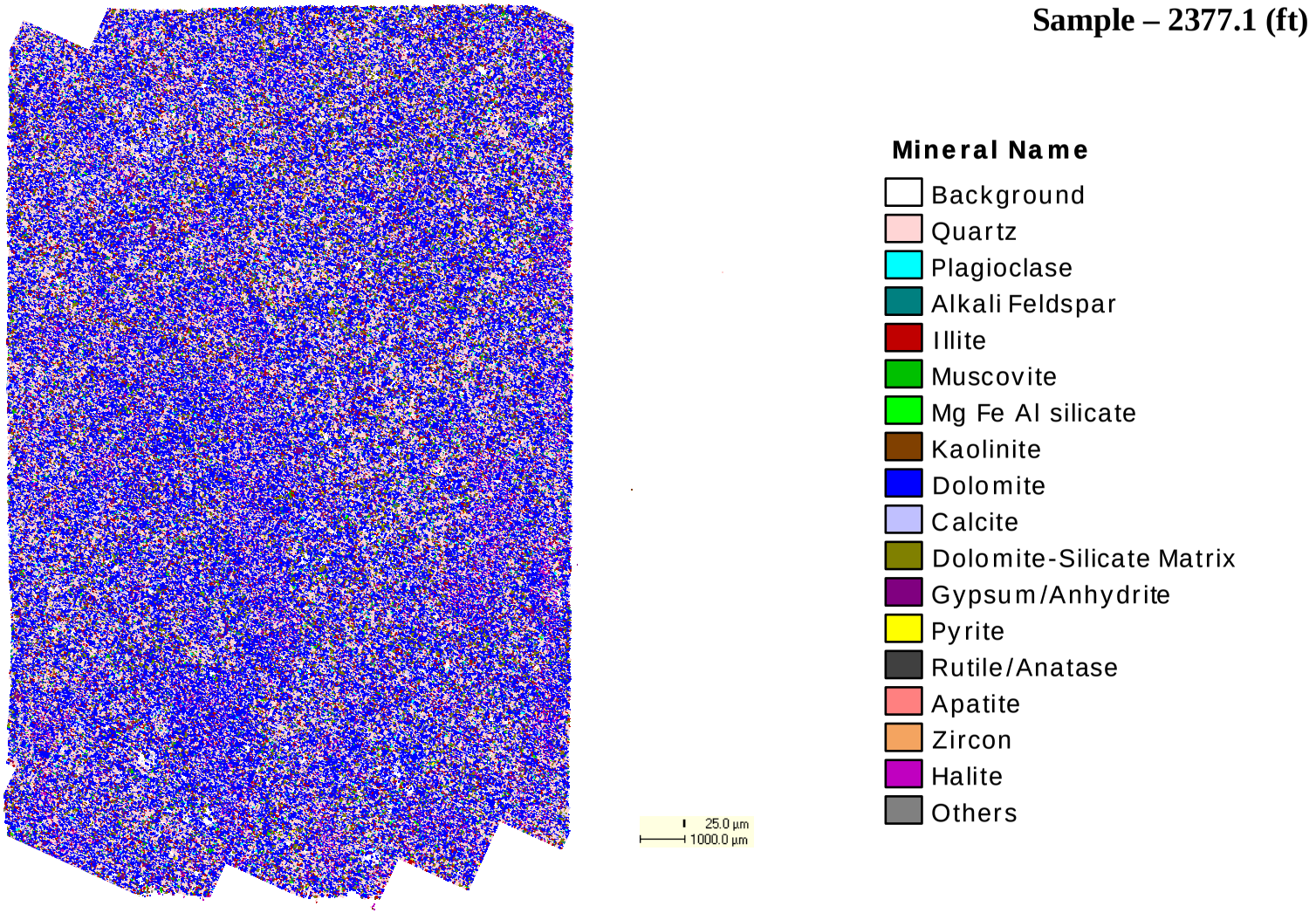

Figure 5.8: Figure showing the mineral compilation for regressive sample 2377.1 (ft) (cycle 3) using a 25 µm measurement spacing. Background (white) is equal to porosity.

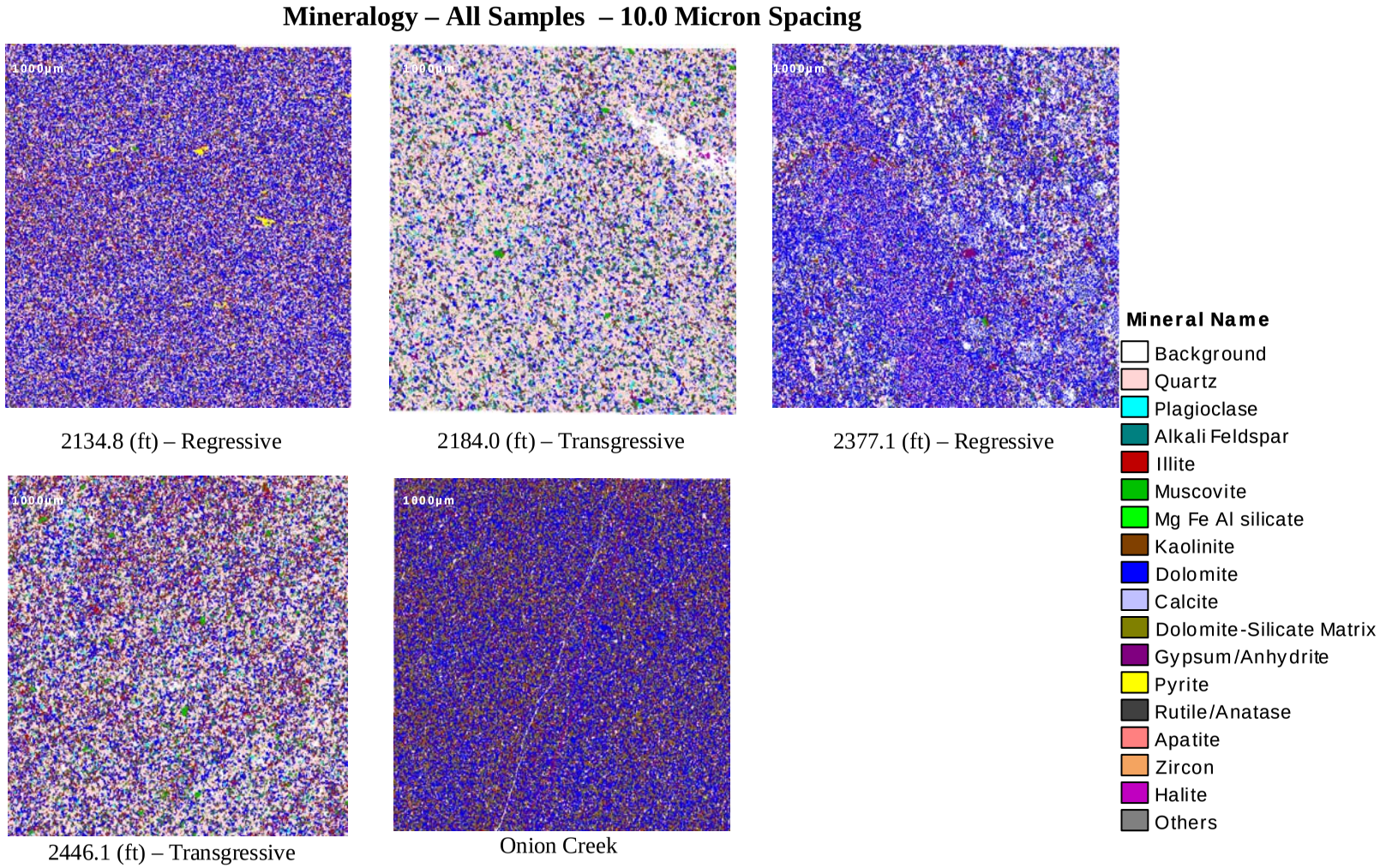

Figure 5.9: Figure showing the mineral assemblage for all five samples using a 10 µm measurement spacing. Background (white) is equal to porosity.

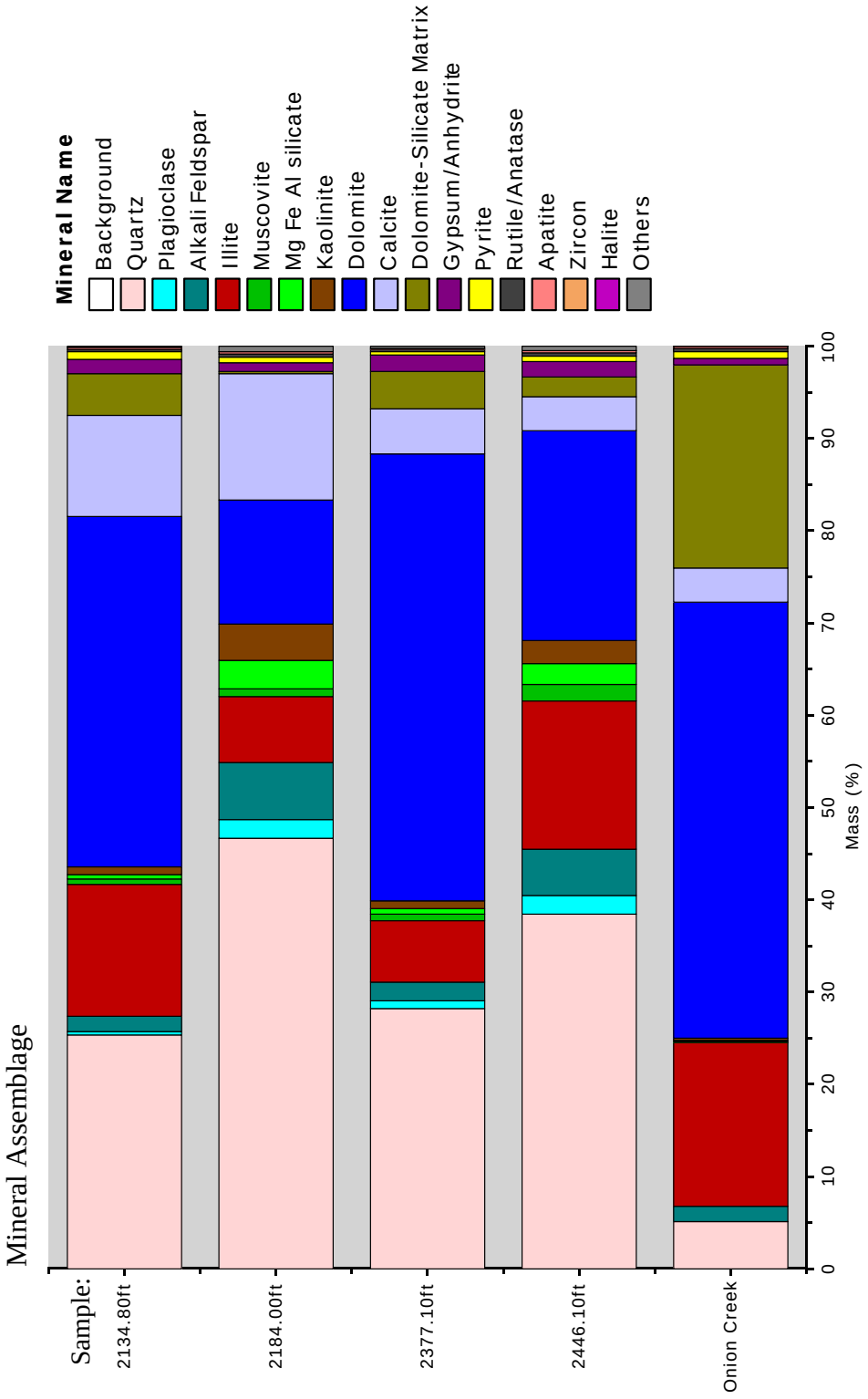

Figure 5.10: Figure graphically showing the mineral assemblage for the five QEMSCAN analyzed samples. Note the increased quartz, plagioclase, alkali feldspar, etc. content in the transgressive samples.

Minerals	Samples (%) 2134.8 (ft)	2184.0 (ft)	2377.1 (ft)	2446.1 (ft)	Onion Creek
Quartz	25.4	46.7	28.2	38.4	5.2
Plagioclase	0.3	1.9	0.9	2.0	0.0
Alkali Feldspar	1.6	6.2	2.1	5.0	1.6
Illite	14.2	7.2	6.7	16.1	17.7
Muscovite	0.6	0.8	0.7	1.7	0.2
Mg Fe Al Silicate	0.5	3.1	0.5	2.3	0.0
Kaolinite	0.8	3.9	0.9	2.5	0.2
Dolomite	38.1	13.5	48.4	22.7	47.3
Calcite	10.9	13.7	5.0	3.8	3.7
Dolomite-Silicate Matrix	4.5	0.3	4.0	2.1	22.0
Gypsum/Anhydrite	1.6	0.9	1.7	1.7	0.8
Pyrite	0.8	0.6	0.3	0.6	0.7
Rutile/Anatase	0.3	0.4	0.2	0.4	0.2
Apatite	0.2	0.2	0.1	0.2	0.3
Zircon	0.0	0.1	0.0	0.0	0.0
Halite	0.0	0.0	0.0	0.0	0.0
Others	0.2	0.5	0.3	0.5	0.1
Total %	100.0	100.0	100.0	100.0	100.0

Table 5.2: A table displaying the mineral assemblages for the five QEMSCAN analyzed samples. The Mg Fe Al silicate mineral listing represents minerals like chlorite and serpentine.

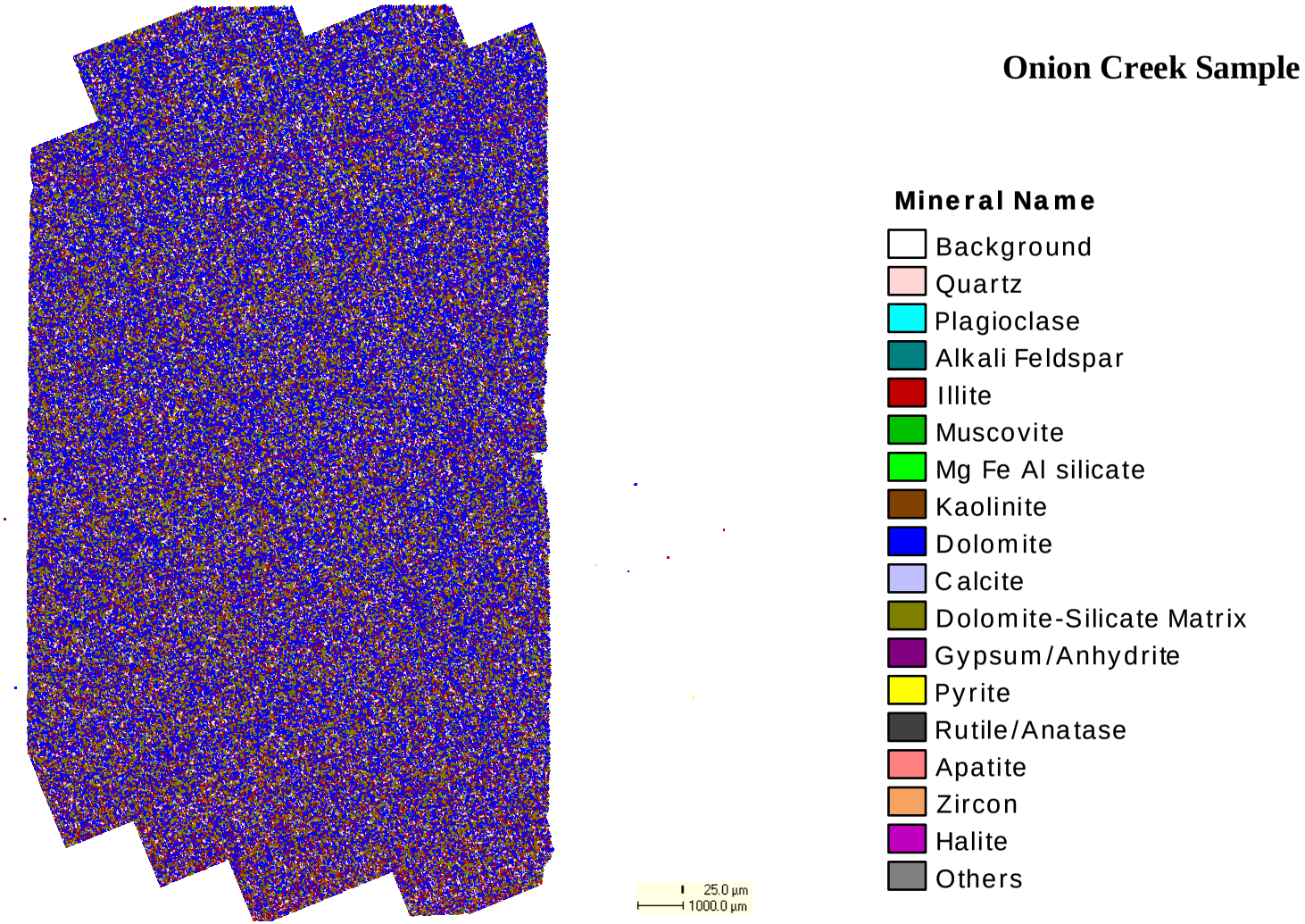

Figure 5.11: Figure showing the mineral compilation for the Onion Creek outcrop sample using a 25 µm measurement spacing. Background (white) is equal to porosity.

5.6.2.1 Grain Size, Grain Density, Porosity Estimations and Other

The average grain size, grain density and an estimated porosity were calculated for all five samples. The average grain size for the transgressive samples were larger than the regressive samples (Figure 5.12). This supports the hypothesis that as sea-level rose, the incoming waters collected and distributed coarser-grained material into the basin.

The grain density was calculated based on the mineral assemblage for each sample and is thus influenced by the most abundant minerals including quartz and dolomite (Figure 5.13). The grain density may have also been affected by several heavy minerals, like pyrite and zircon, boosting the sample density depending on representative percentages (Figure 5.14).

Porosity estimates were also conducted for the five samples and range from 0.43 to 10.68 percent (Figure 5.15). There is no clear correlation between transgressive and regressive samples. It is thought the porosity may be a factor of microfractures, grain overgrowths and cement content and abundance.

In regressive sample 2134.8 (ft) bacteria-produced framboidal pyrite was identified. This indicates there was organic material deposited within at least the regressive dolomites.

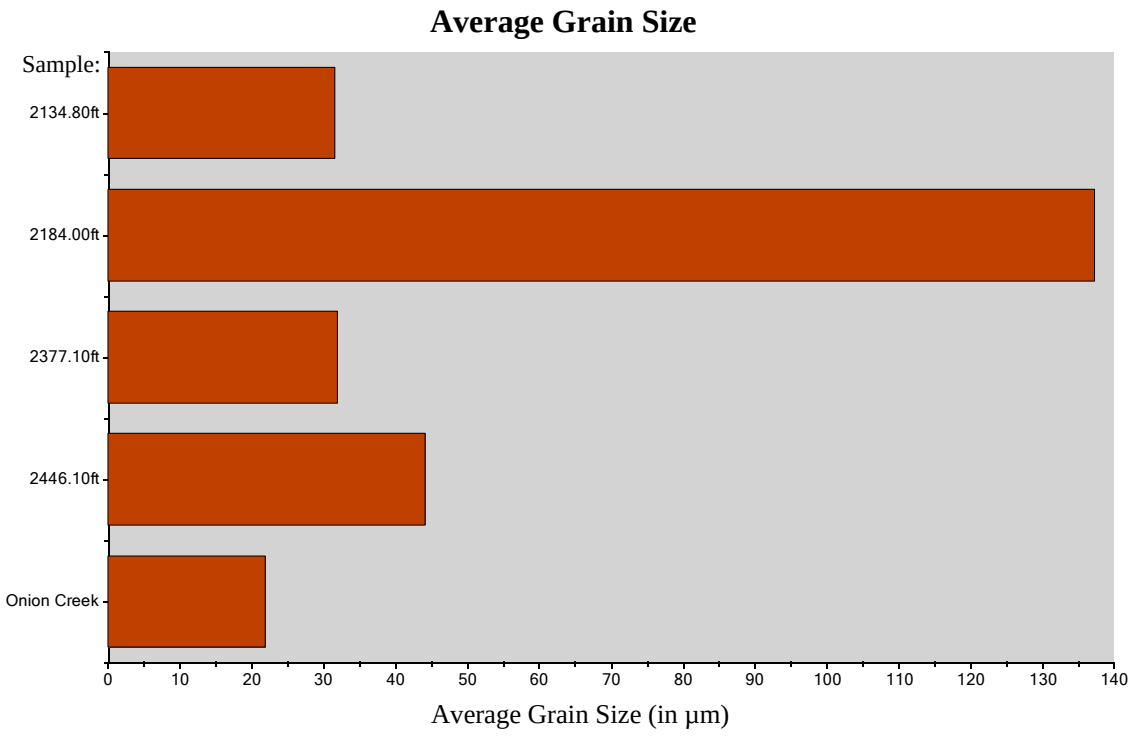

Sample (ft)		Average Grain Size (µm)
2134.8	Regressive	31.55
2184.0	Transgressive	137.28
2377.1	Regressive	31.86
2446.1	Transgressive	44.10
Onion Creek		21.88

Figure 5.12: Graph and table displaying the average grain size distribution for all five QEMSCAN analyzed samples. Note how the regressive samples (2134.8 (ft) and 2377.1 (ft)) tend to be finer-grained.

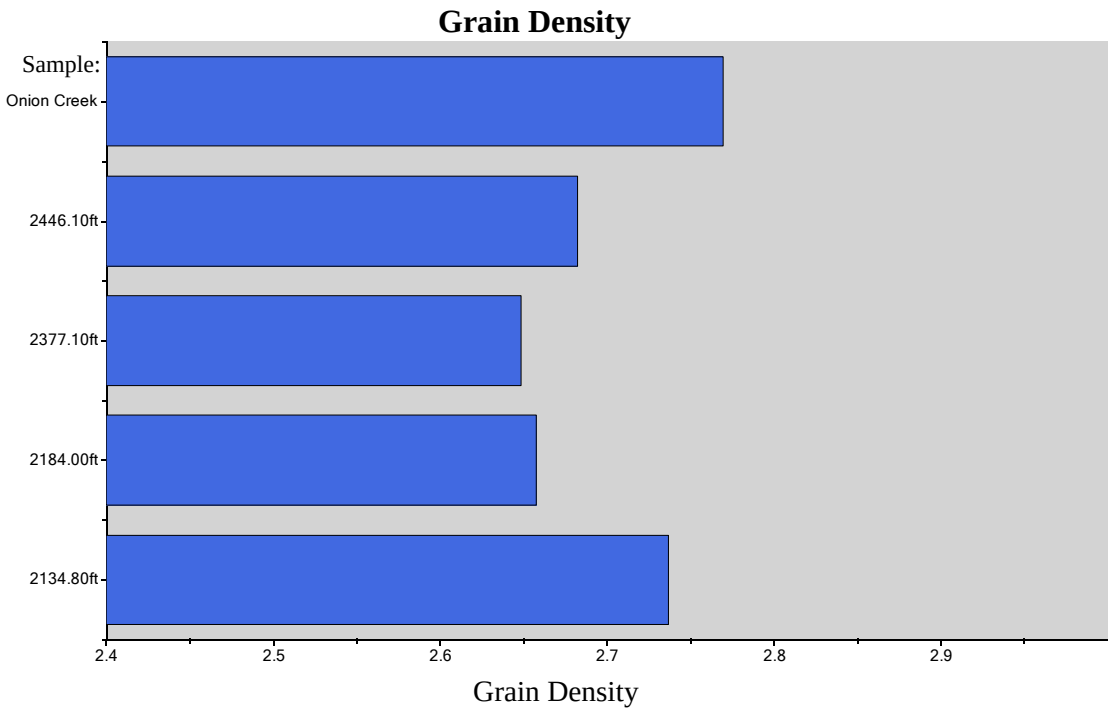

Sample (ft)		Grain Density
2134.8	Regressive	2.74
2184.0	Transgressive	2.66
2377.1	Regressive	2.65
2446.1	Transgressive	2.68
Onion Creek		2.77

Figure 5.13: Graph and table displaying the grain density distribution for all five QEMSCAN analyzed samples. It is possible the density calculations may be highly influenced by the amount of available pyrite.

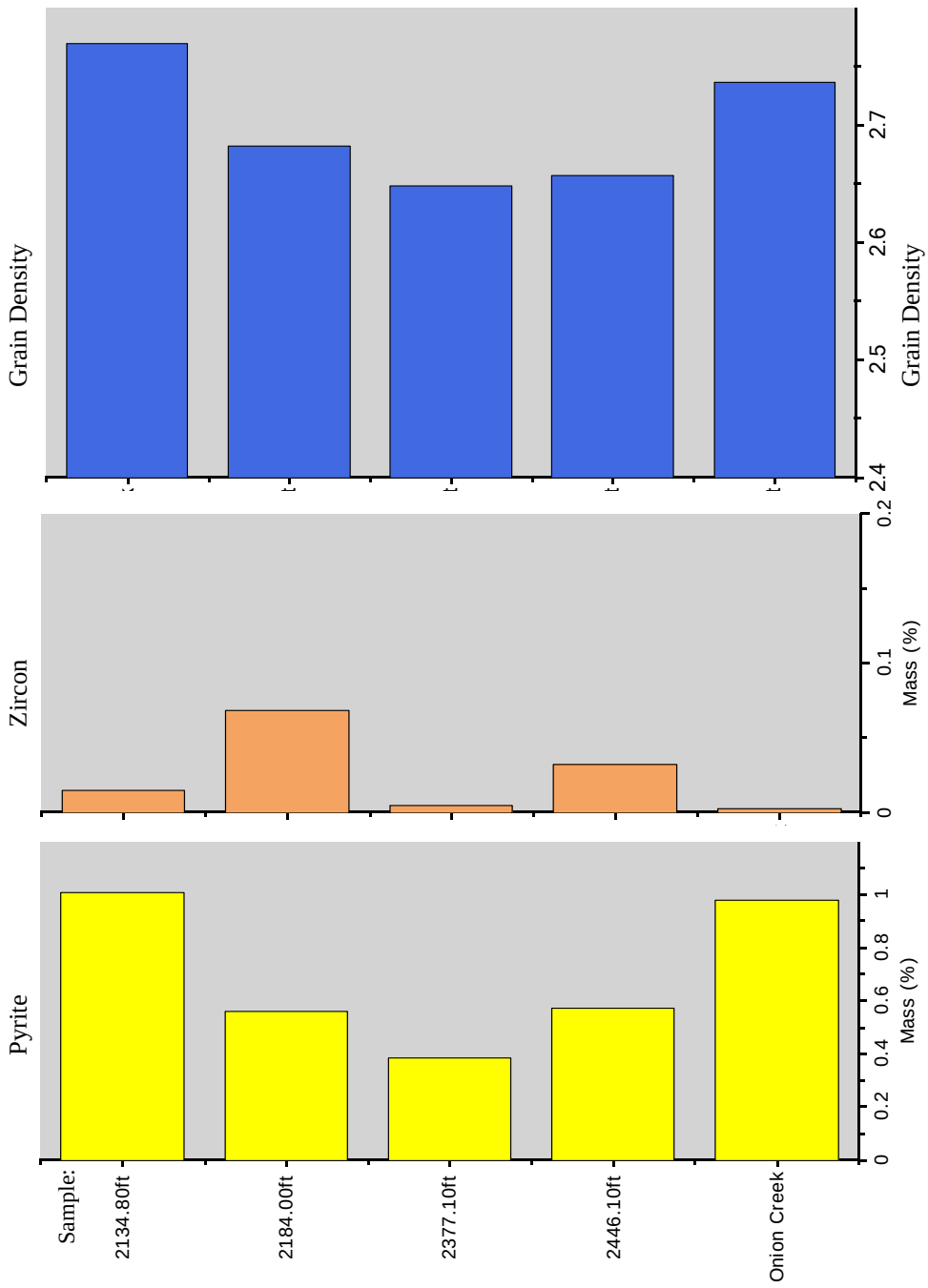

Figure 5.14: Figure comparing the pyrite content, zircon content and grain density for the five QEMSCAN analyzed samples. Note how an increased pyrite assemblage correlates to an increased grain density. Samples 2134.8 and 2377.1 are regressive samples. Samples 2184.0 and 2446.1 are transgressive samples.

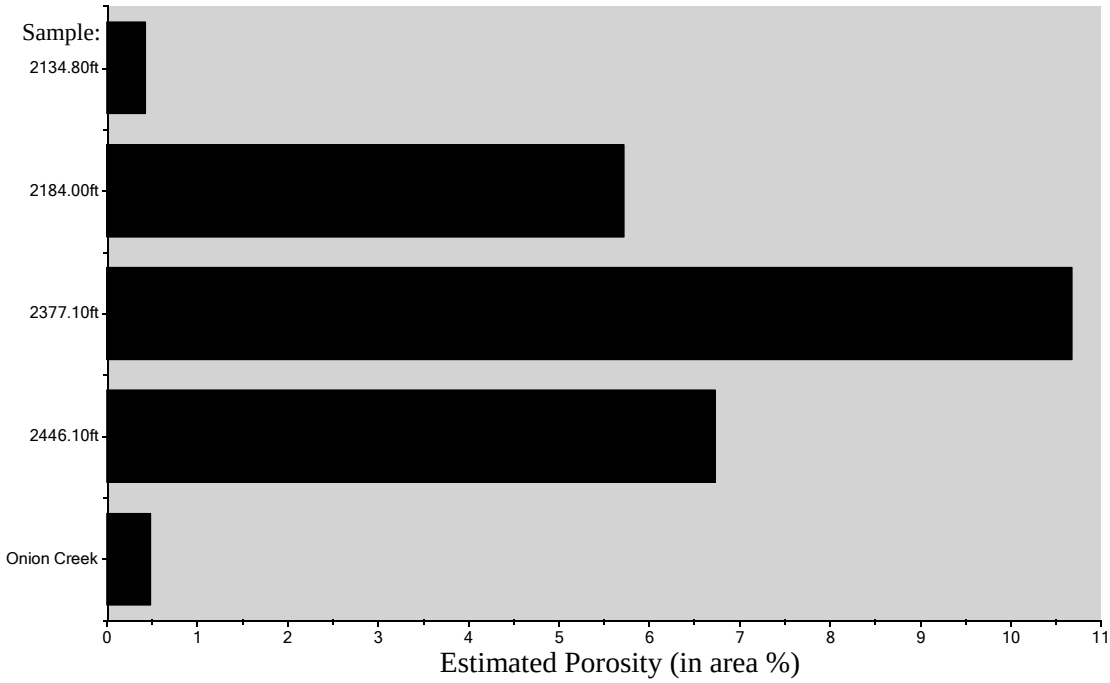

Sample (ft)		Estimated Porosity (in area %)
2134.8	Regressive	0.43
2184.0	Transgressive	5.72
2377.1	Regressive	10.68
2446.1	Transgressive	6.73
Onion Creek		0.49

Figure 5.15: Graph and table displaying the estimated porosity for all five QEMSCAN analyzed samples.

CHAPTER 6

EVAPORITE CYCLE ISOPACH MAPS AND ANALYSIS

To understand the spatial and correlative relationships of the Paradox Formation evaporite cycles, isopach maps were created for each individual evaporite sequence. These maps were created using *PETRA* (IHS) and incorporate both the halite and clastic intervals of each cycle.

The thickness for each individual cycle was calculated based upon the thicknesses of the different lithological facies (anhydrite, silty dolomite, black shale and halite) within each respective cycle. The calculations were based upon well log interpretations and correlations.

6.1 Map Suite

Below is a suite of isopach maps for 19 of the 29 evaporite cycles observed in the northern Paradox Basin (Figures 6.1 – 6.19) that include both the halite zone and clastic interval. The maps are organized based on their depositional order where cycle 29 was deposited first followed by cycle 28 and so on.

Isopach maps for all 29 cycles can be viewed in Appendix B. Maps displaying the location of the wells that were used to create the isopach maps can also be observed in Appendix B. Principal observations and analysis of the following maps are discussed in further detail in section 6.2.

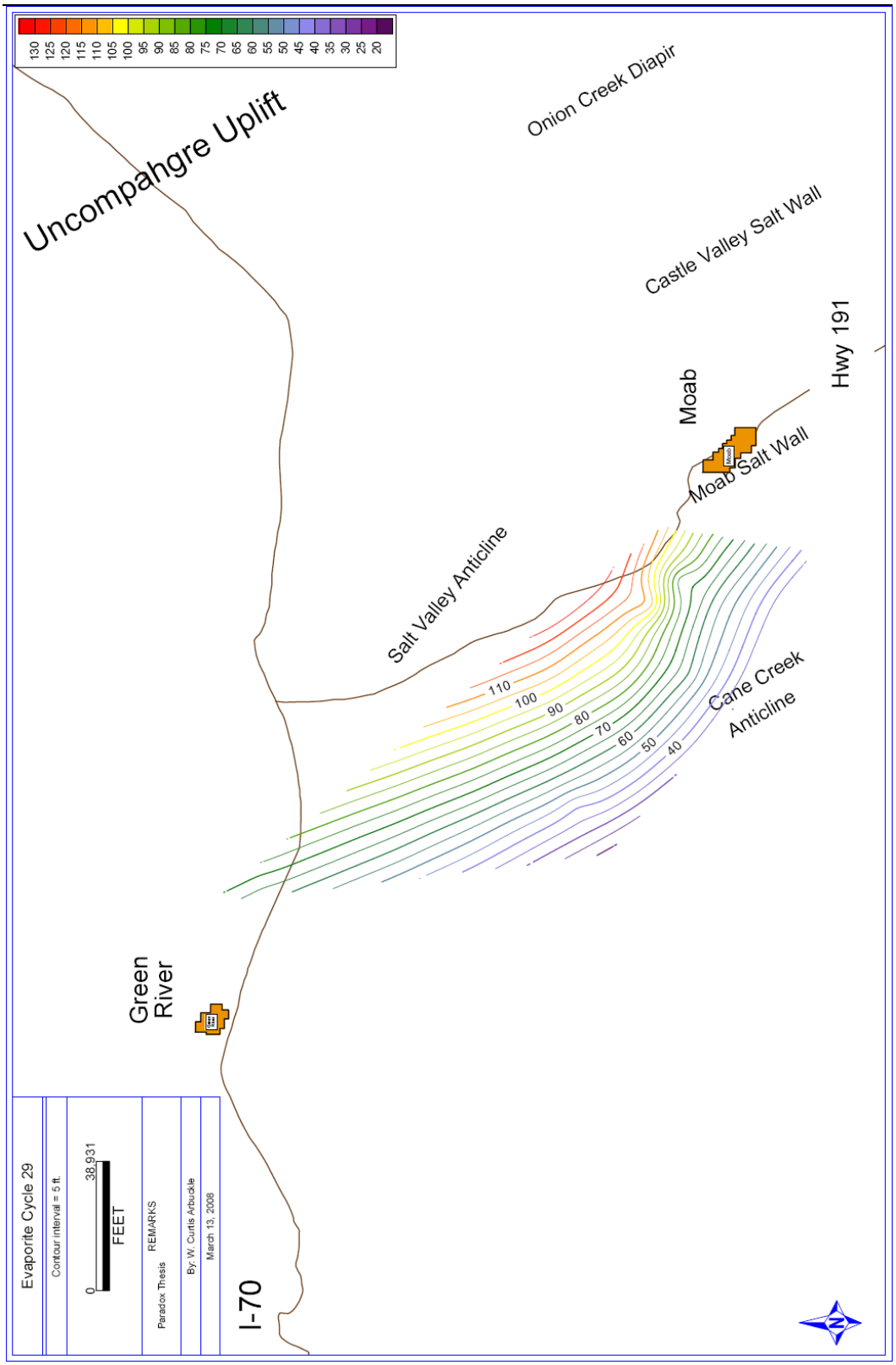

Figure 6.1: Isopach map of evaporite cycle 29 within the Paradox Formation. See text for analysis. Contour interval = 5 feet (1.52 m).

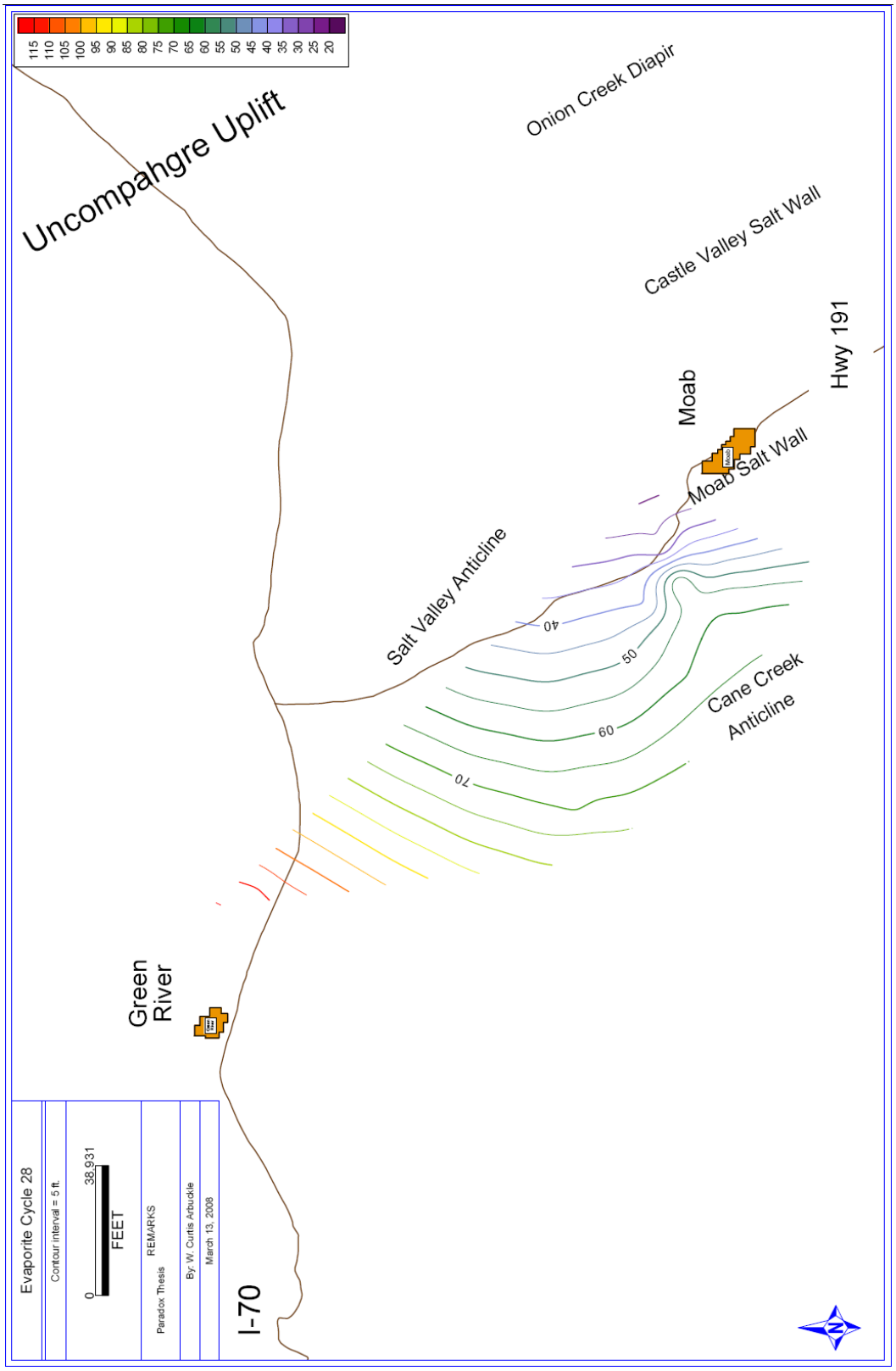

Figure 6.2: Isopach map of evaporite cycle 28 within the Paradox Formation. See text for analysis. Contour interval = 5 feet (1.52 m).

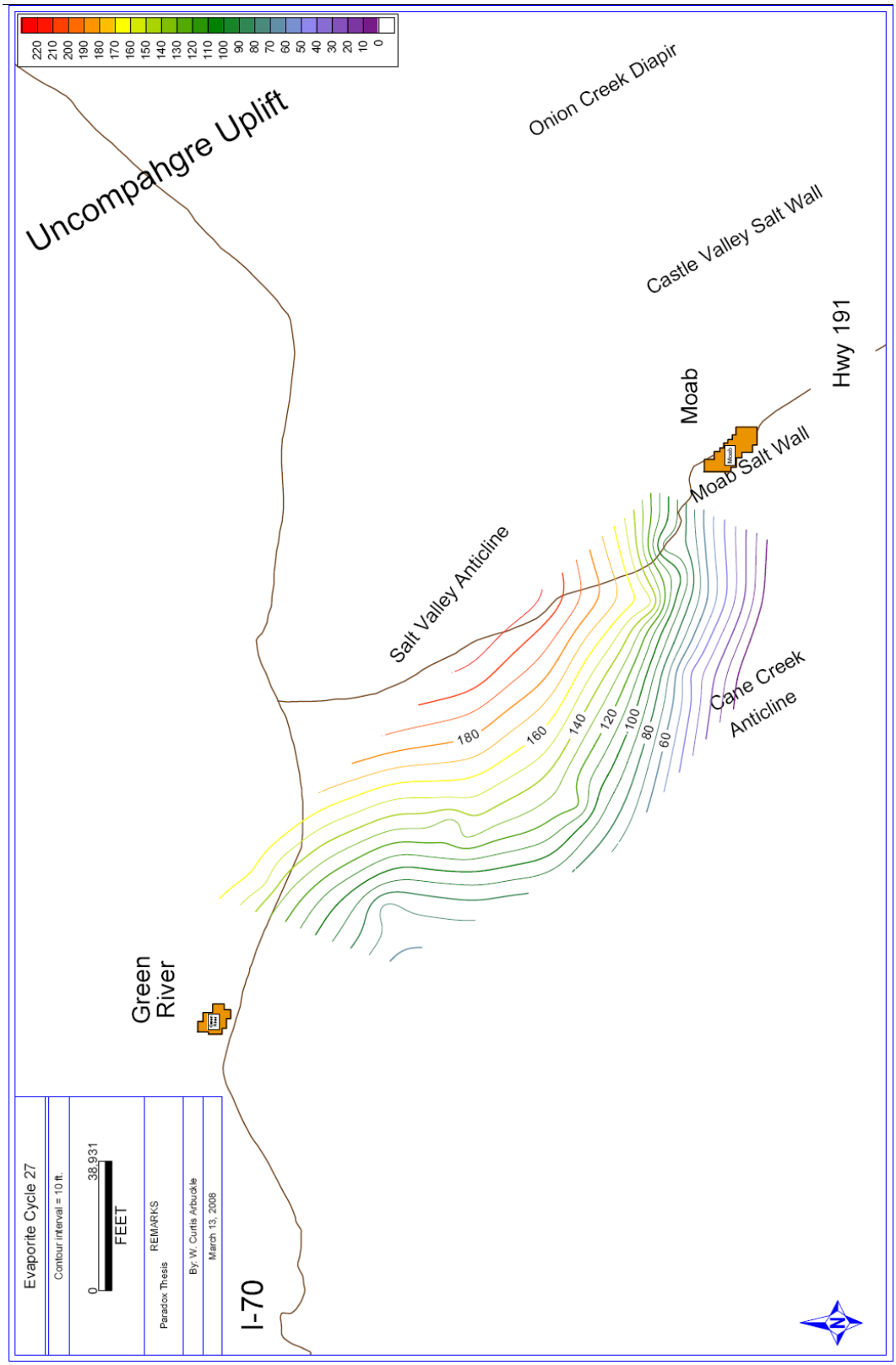

Figure 6.3: Isopach map of evaporite cycle 27 within the Paradox Formation. See text for analysis. Contour interval = 10 feet (3.05 m).

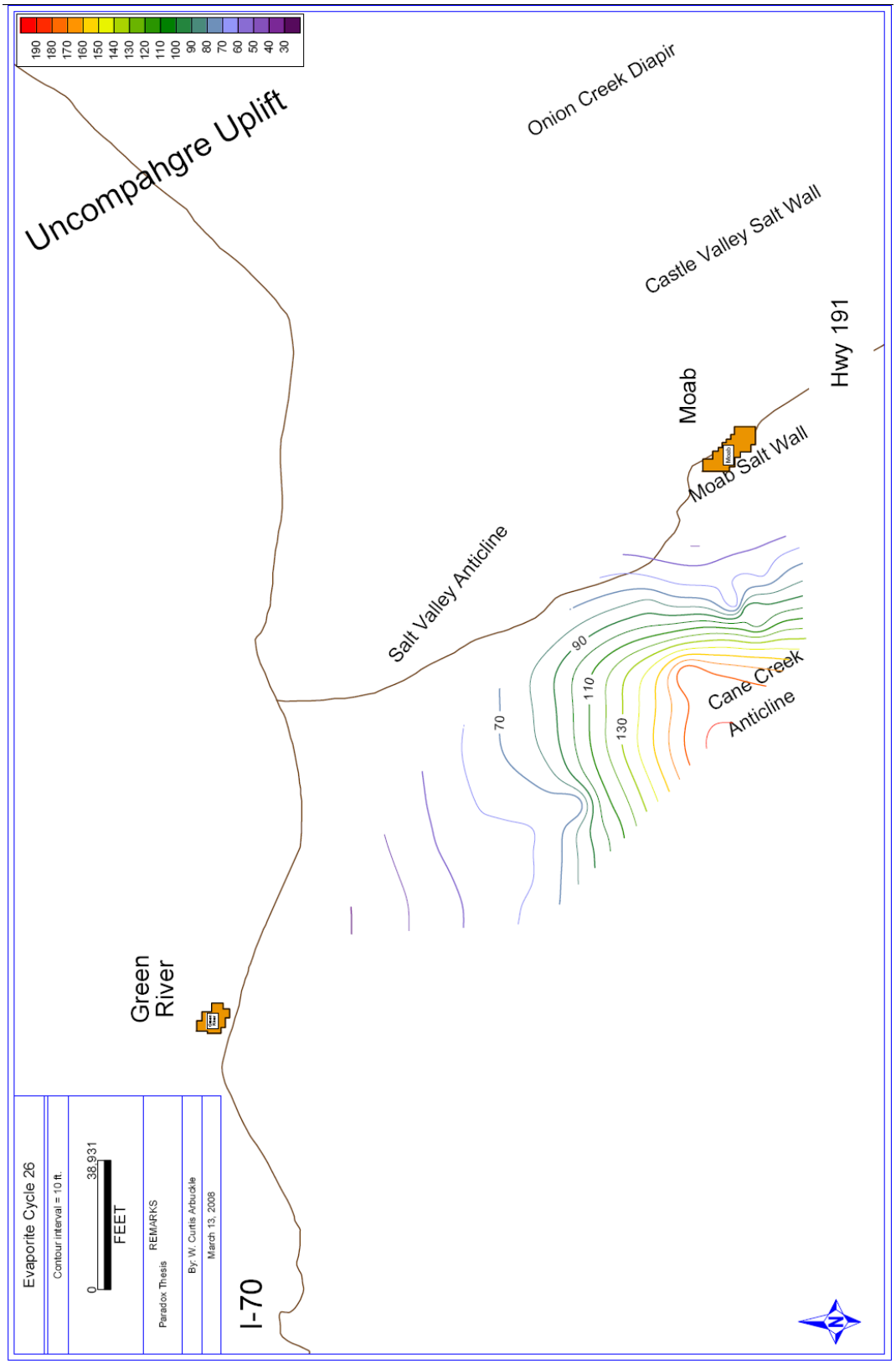

Figure 6.4: Isopach map of evaporite cycle 26 within the Paradox Formation. See text for analysis. Contour interval = 10 feet (3.05 m).

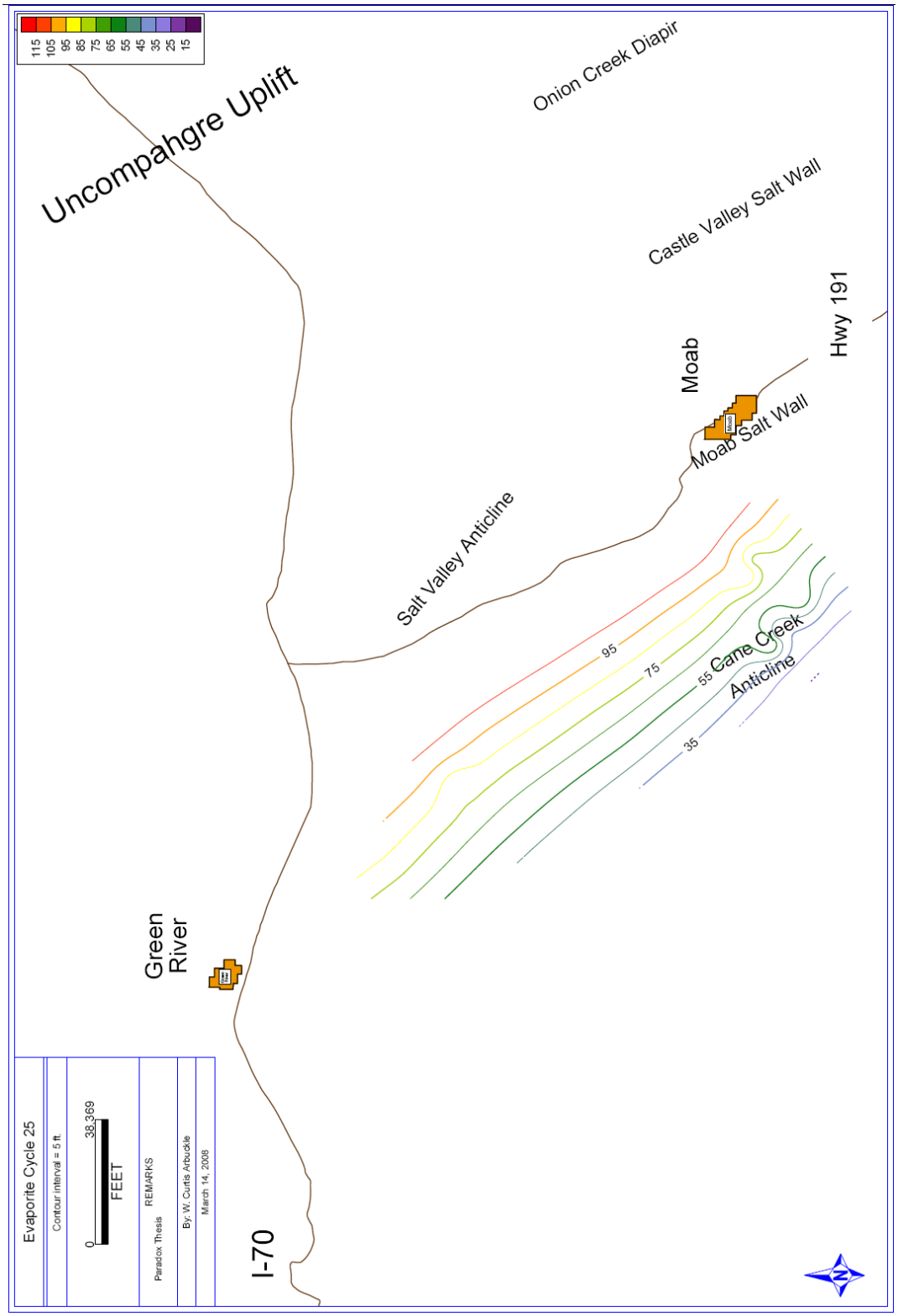

Figure 6.5: Isopach map of evaporite cycle 25 within the Paradox Formation. See text for analysis. Contour interval = 5 feet (1.52 m).

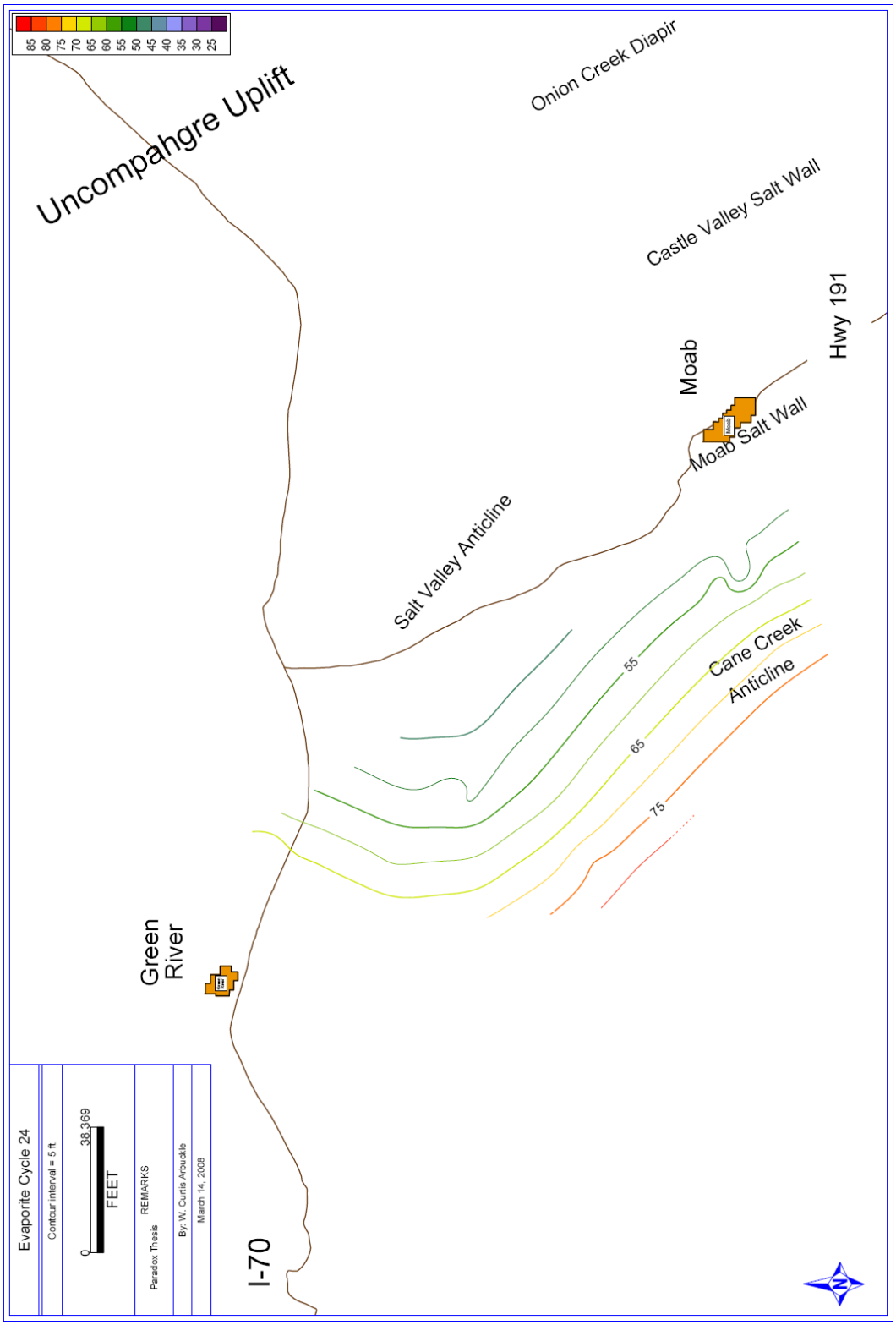

Figure 6.6: Isopach map of evaporite cycle 24 within the Paradox Formation. See text for analysis. Contour interval = 5 feet (1.52 m).

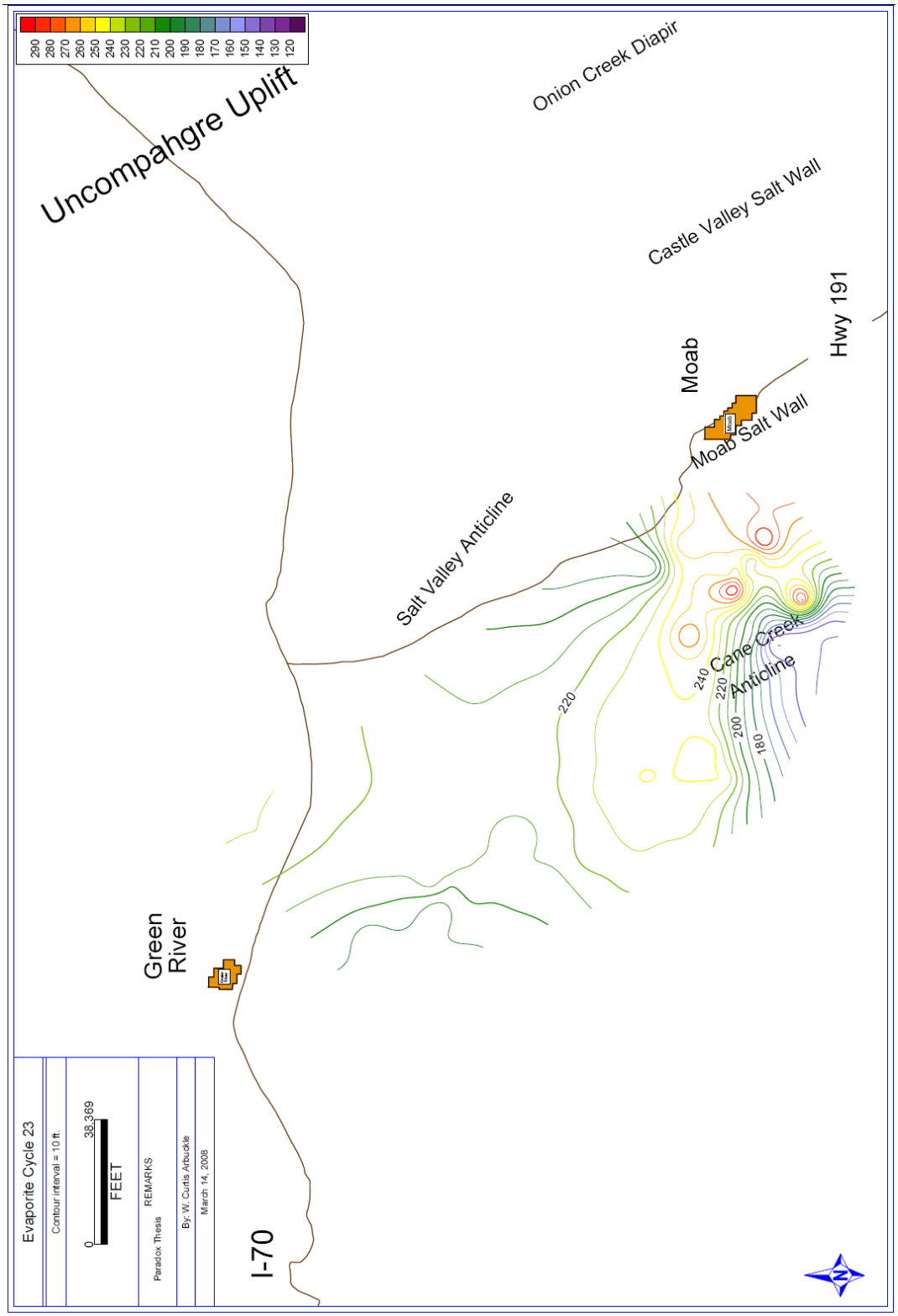

Figure 6.7: Isopach map of evaporite cycle 23 within the Paradox Formation. See text for analysis. Contour interval = 10 feet (3.05 m).

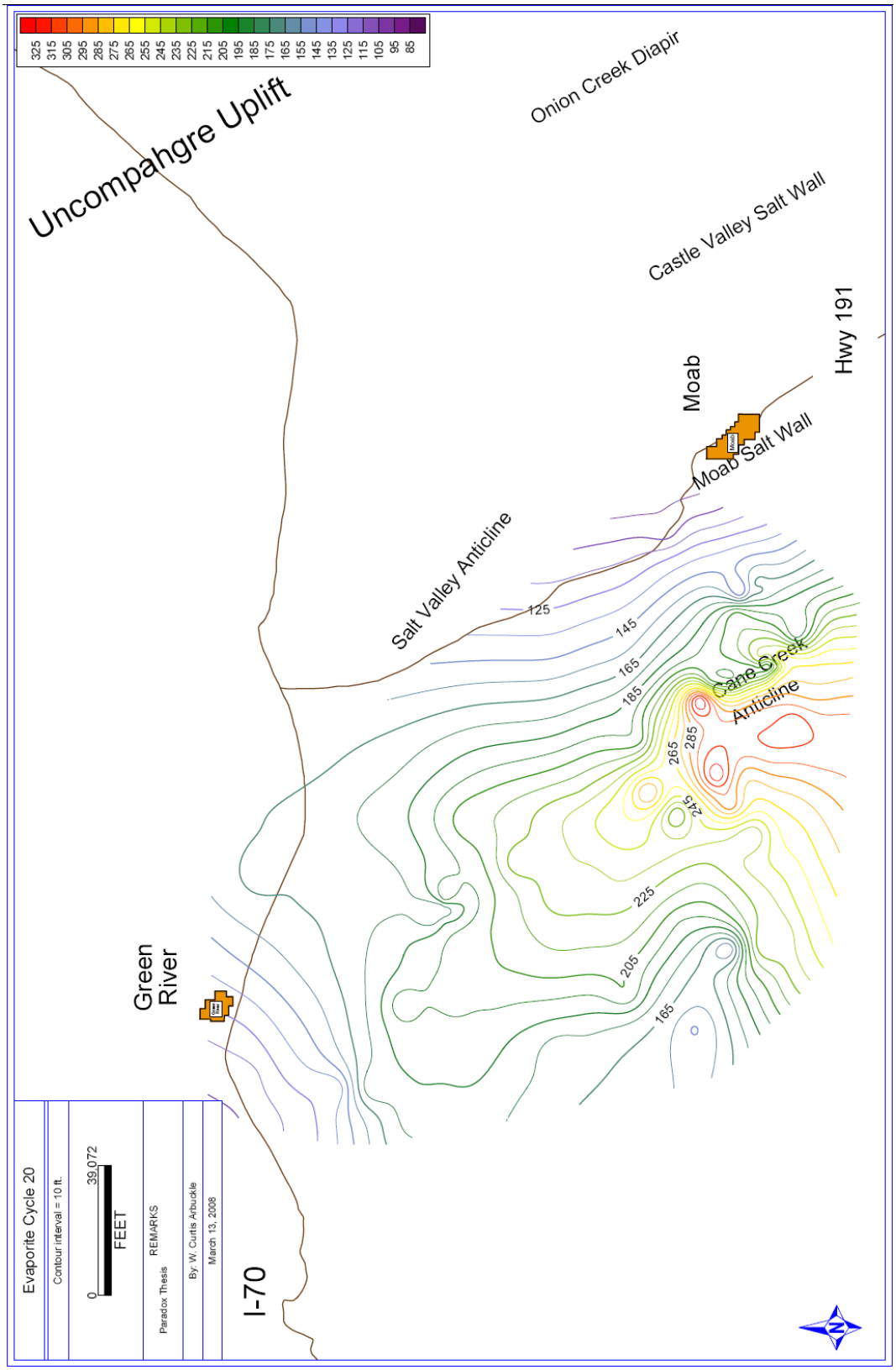

Figure 6.8: Isopach map of evaporite cycle 20 within the Paradox Formation. See text for analysis. Contour interval = 10 feet (3.05 m).

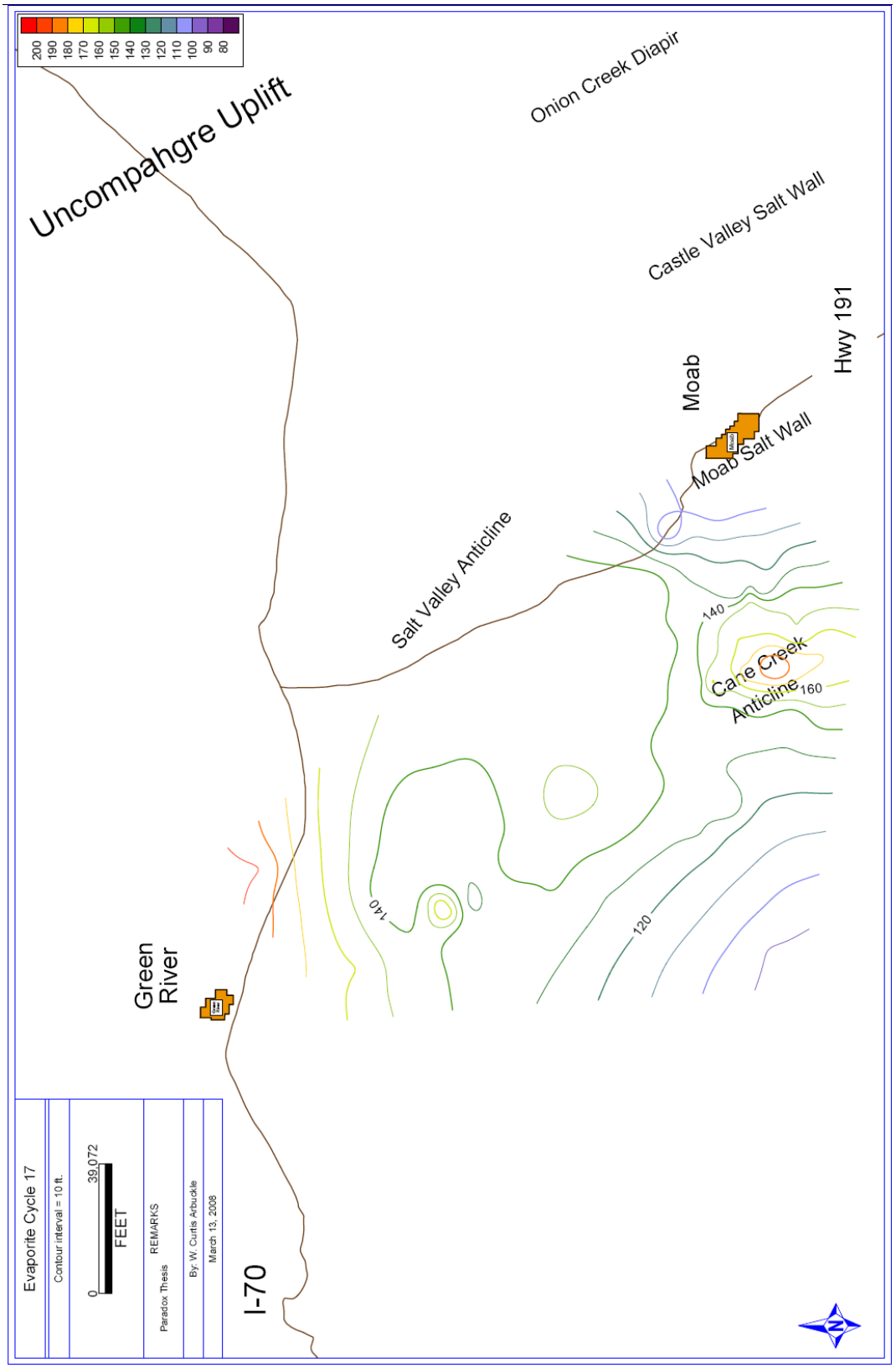

Figure 6.9: Isopach map of evaporite cycle 17 within the Paradox Formation. See text for analysis. Contour interval = 10 feet (3.05 m).

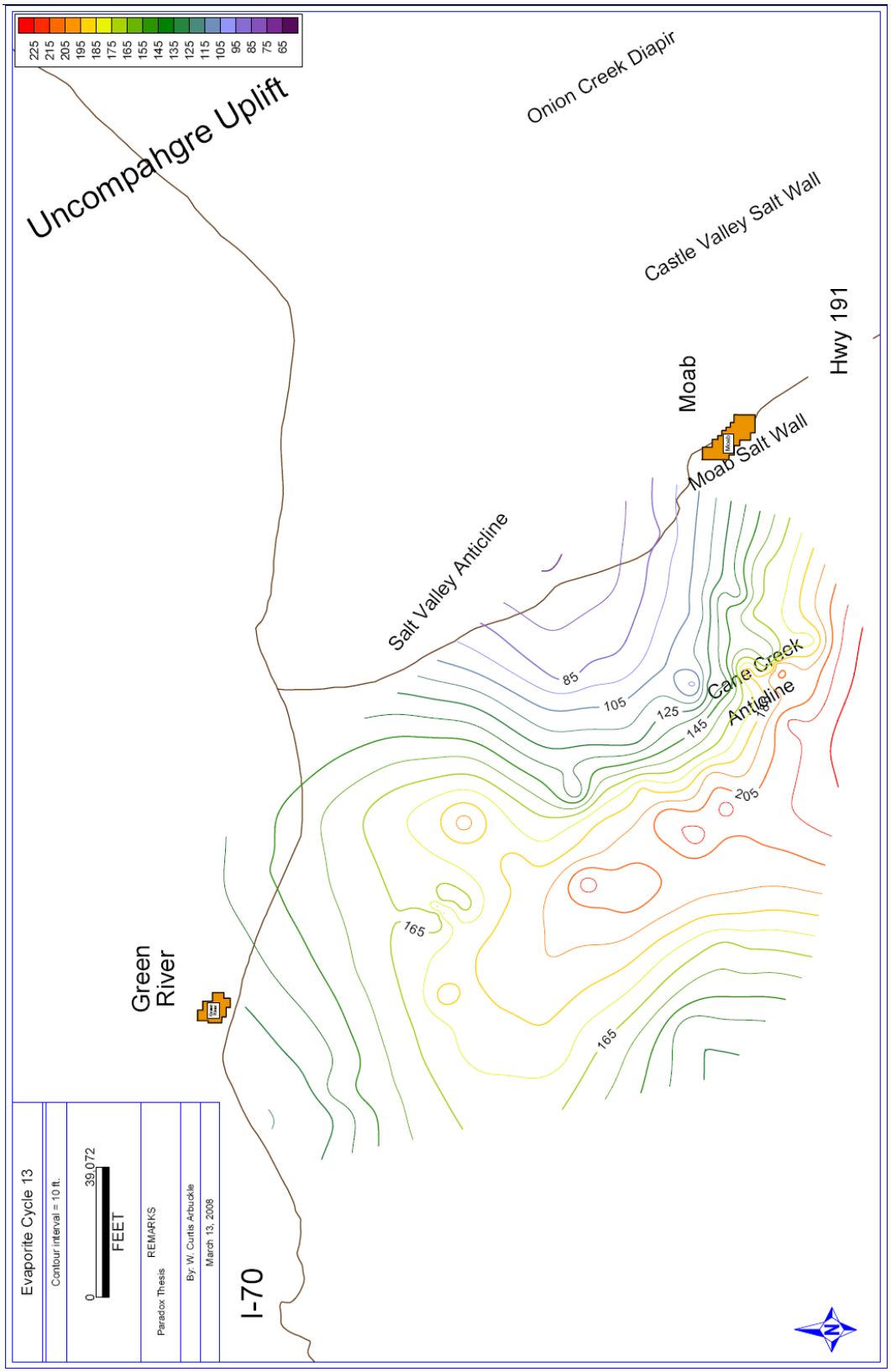

Figure 6.10: Isopach map of evaporite cycle 13 within the Paradox Formation. See text for analysis. Contour interval = 10 feet (3.05 m).

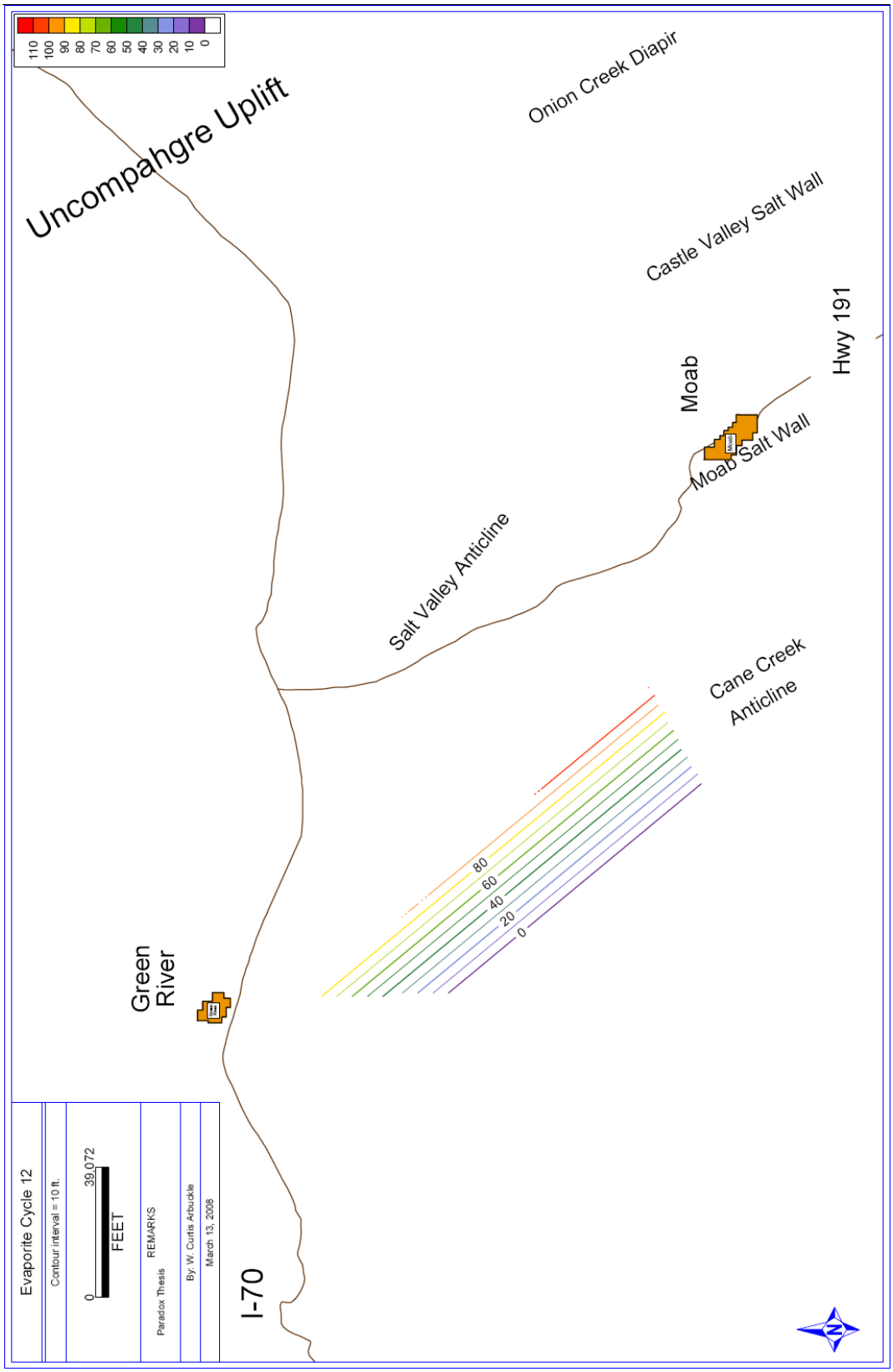

Figure 6.11: Isopach map of evaporite cycle 12 within the Paradox Formation. See text for analysis. Contour interval = 10 feet (3.05 m).

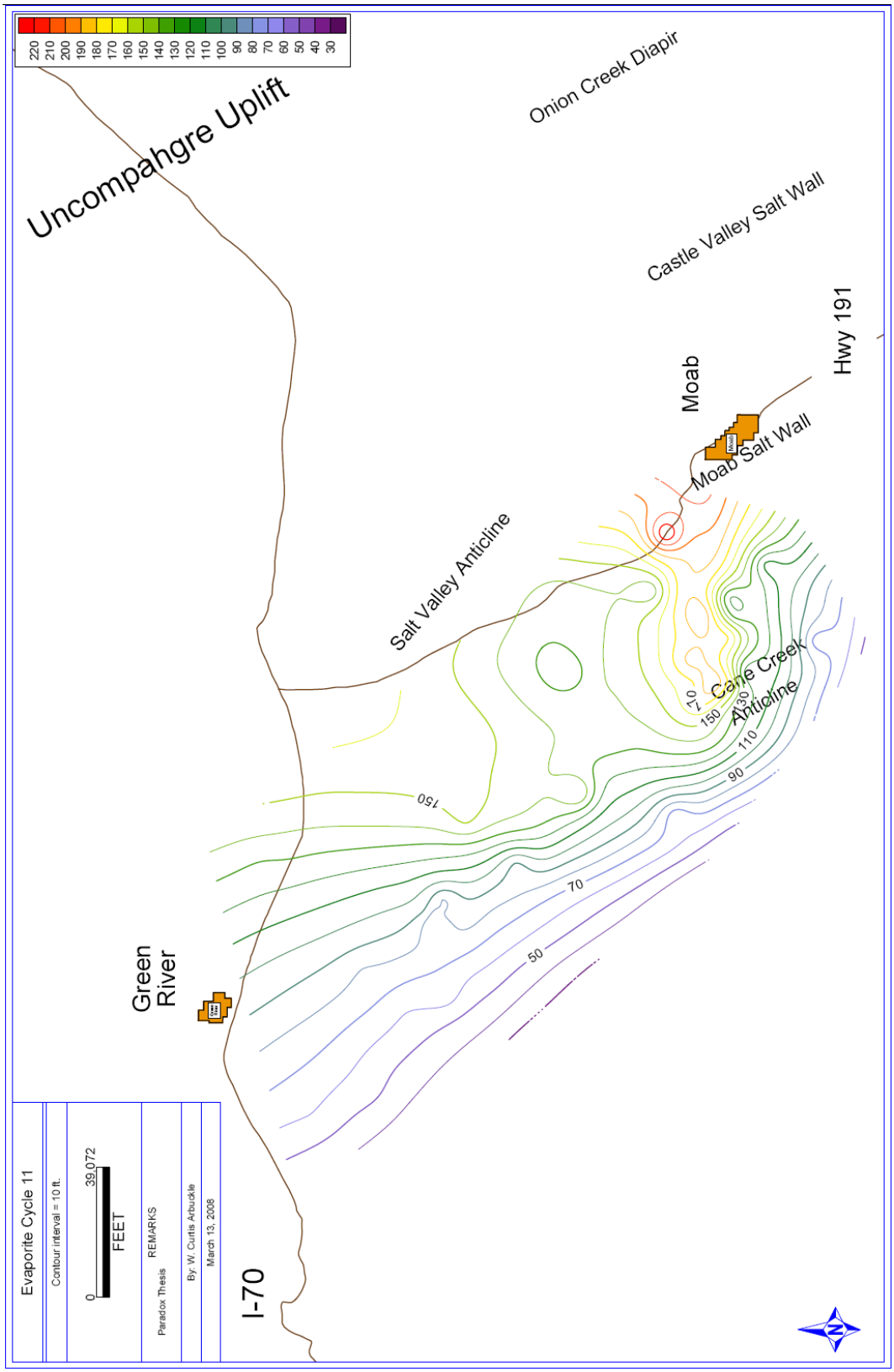

Figure 6.12: Isopach map of evaporite cycle 11 within the Paradox Formation. See text for analysis. Contour interval = 10 feet (3.05 m).

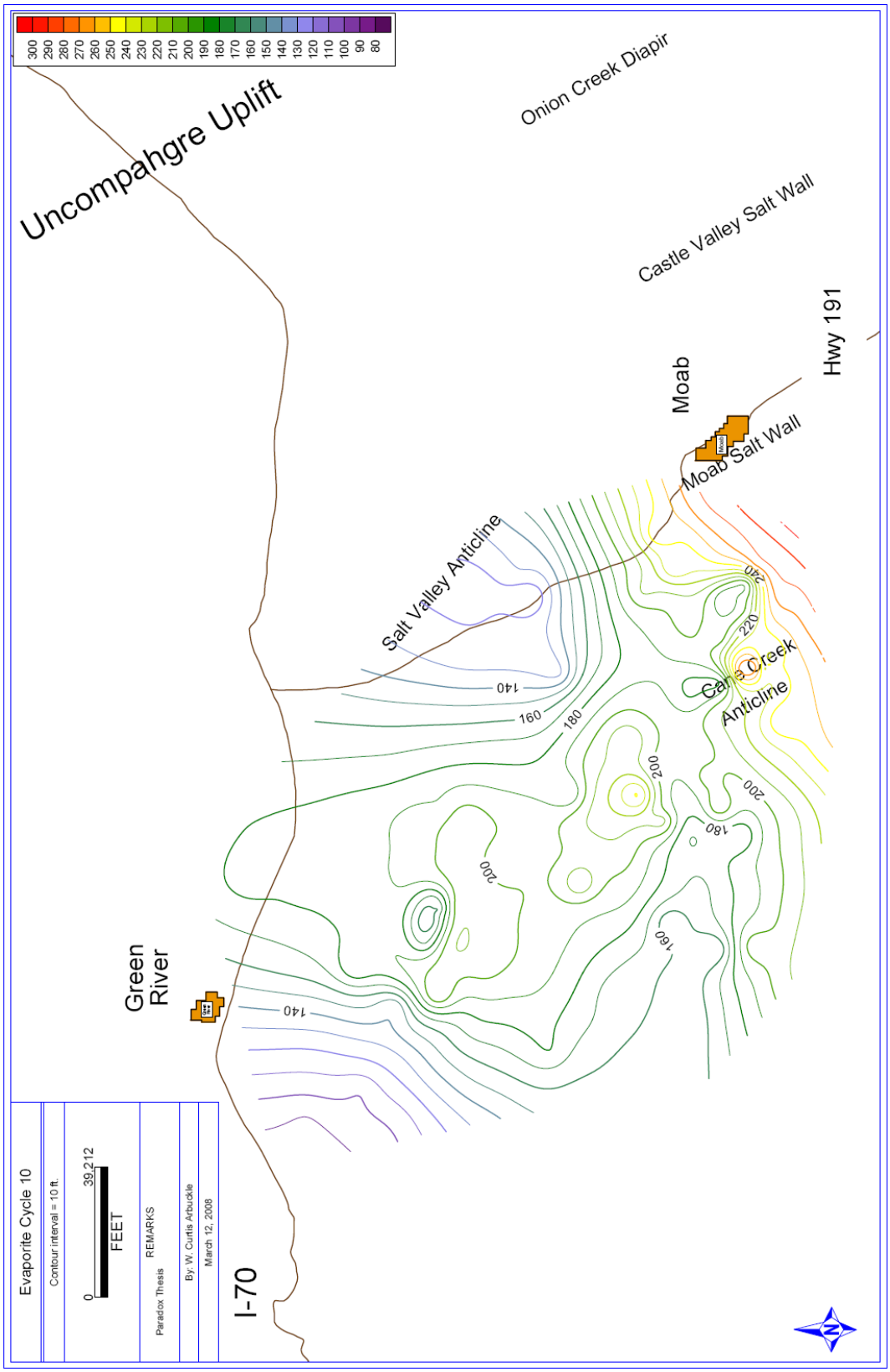

Figure 6.13: Isopach map of evaporite cycle 10 within the Paradox Formation. See text for analysis. Contour interval = 10 feet (3.05 m).

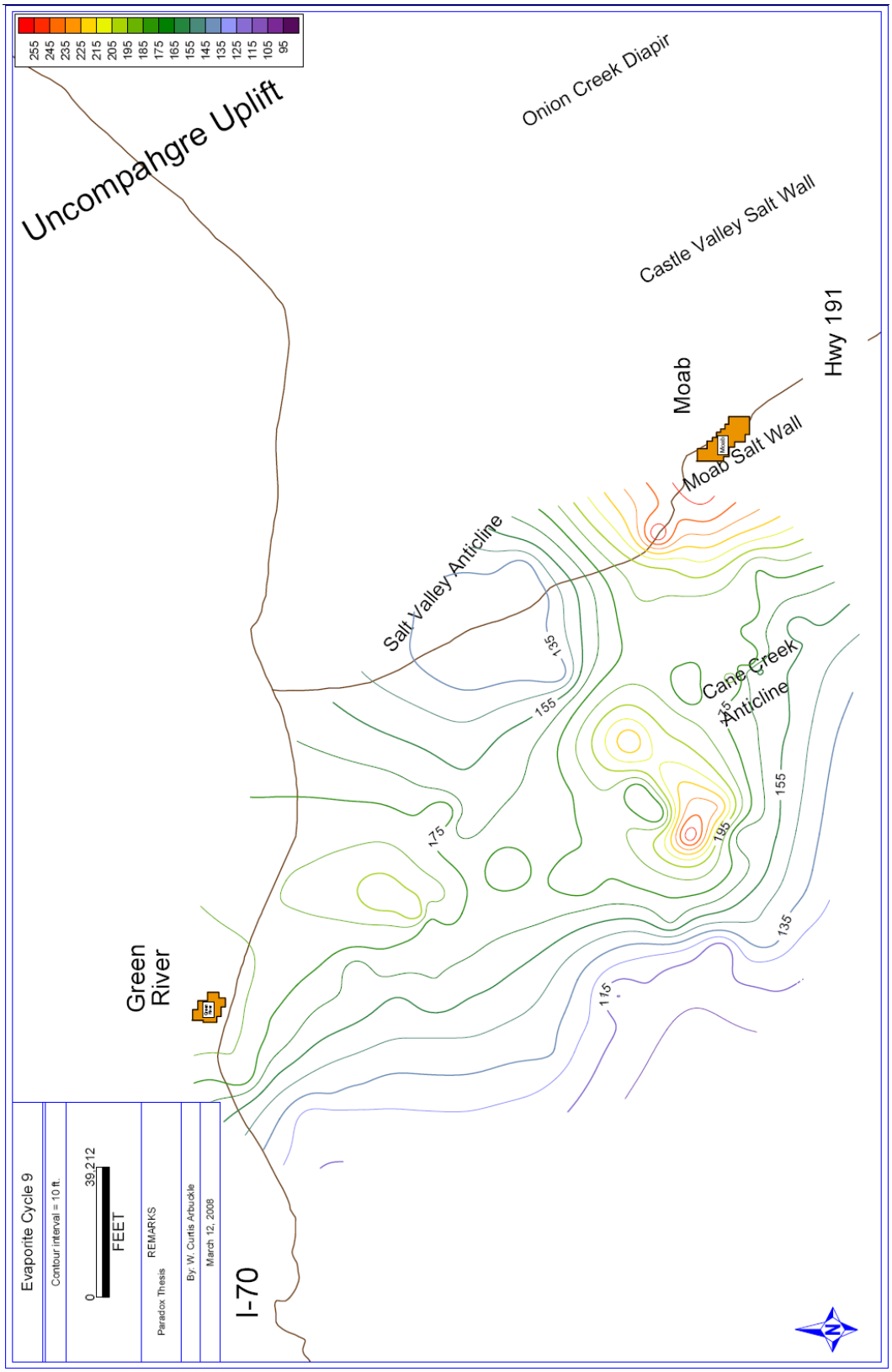

Figure 6.14: Isopach map of evaporite cycle 9 within the Paradox Formation. See text for analysis. Contour interval = 10 feet (3.05 m).

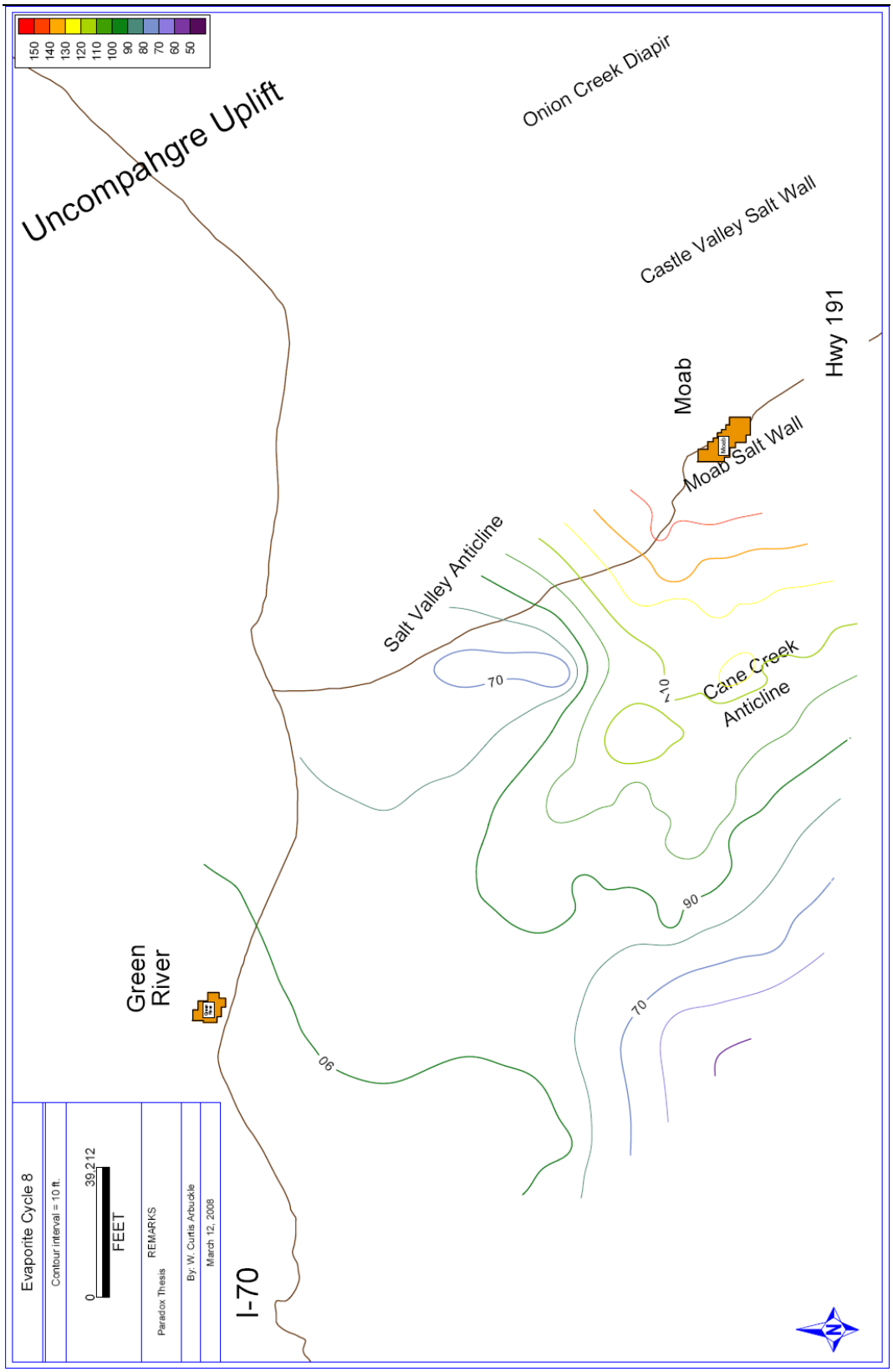

Figure 6.15: Isopach map of evaporite cycle 8 within the Paradox Formation. See text for analysis. Contour interval = 10 feet (3.05 m).

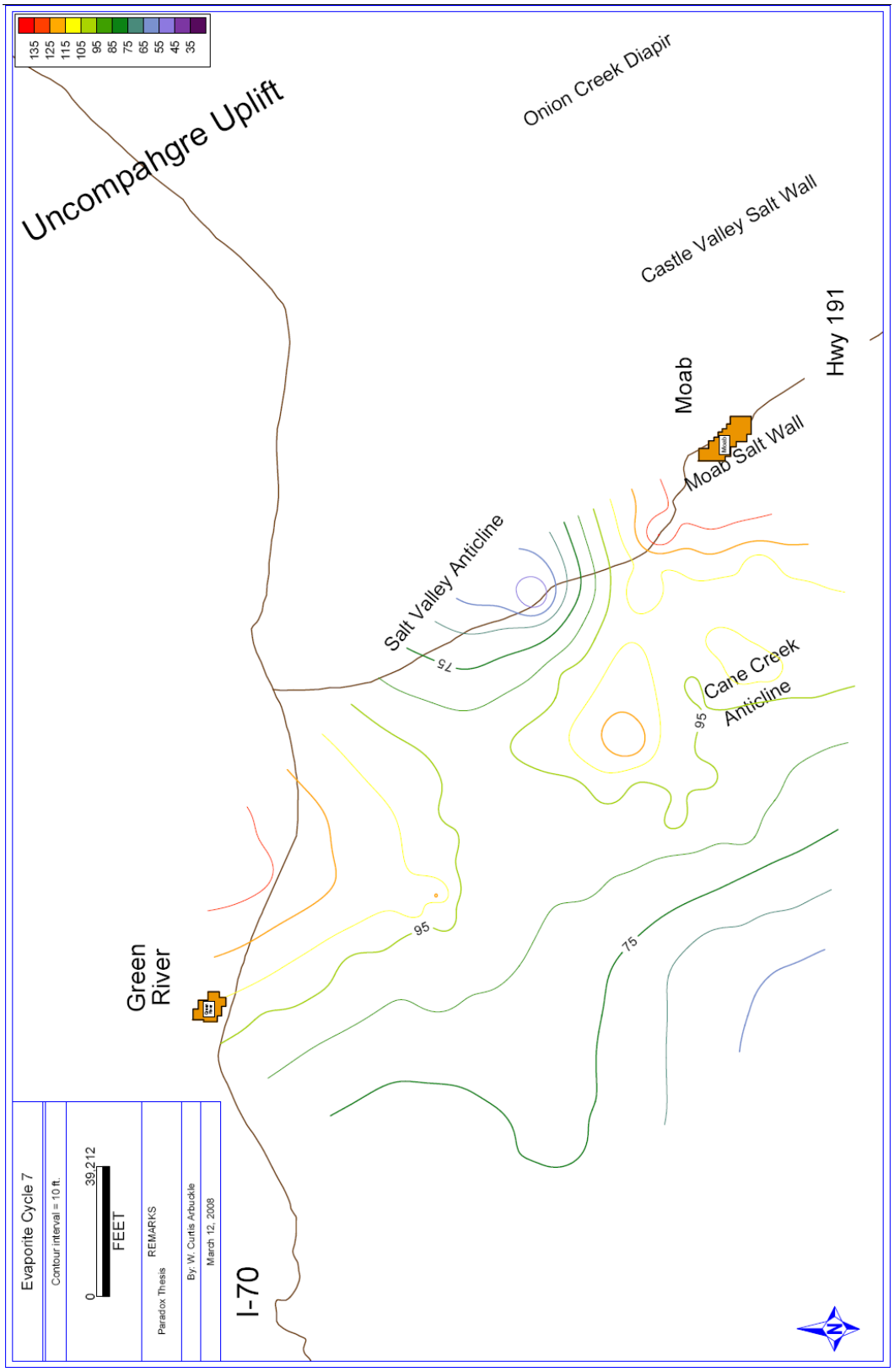

Figure 6.16: Isopach map of evaporite cycle 7 within the Paradox Formation. See text for analysis. Contour interval = 10 feet (3.05 m).

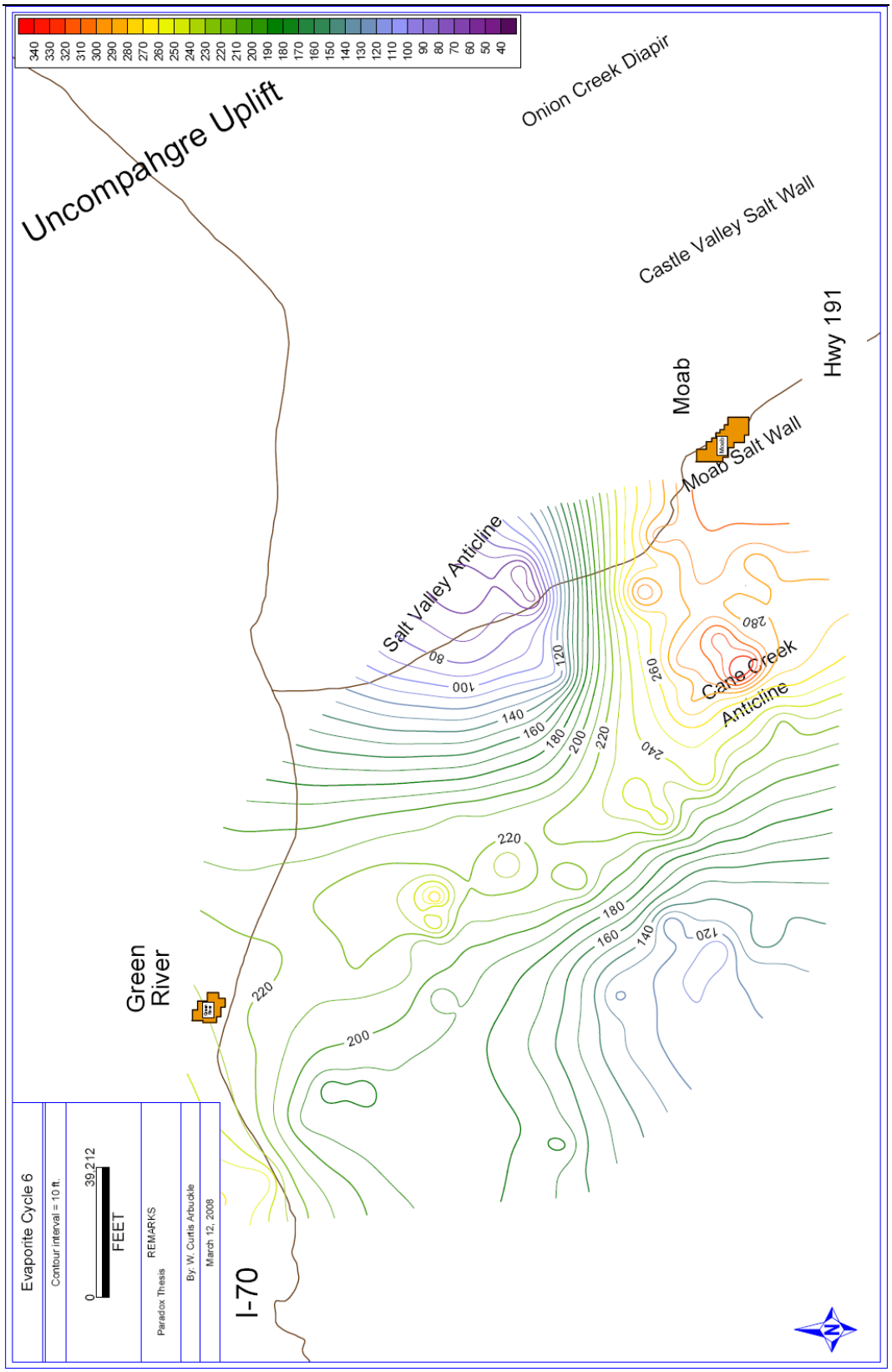

Figure 6.17: Isopach map of evaporite cycle 6 within the Paradox Formation. See text for analysis. Contour interval = 10 feet (3.05 m).

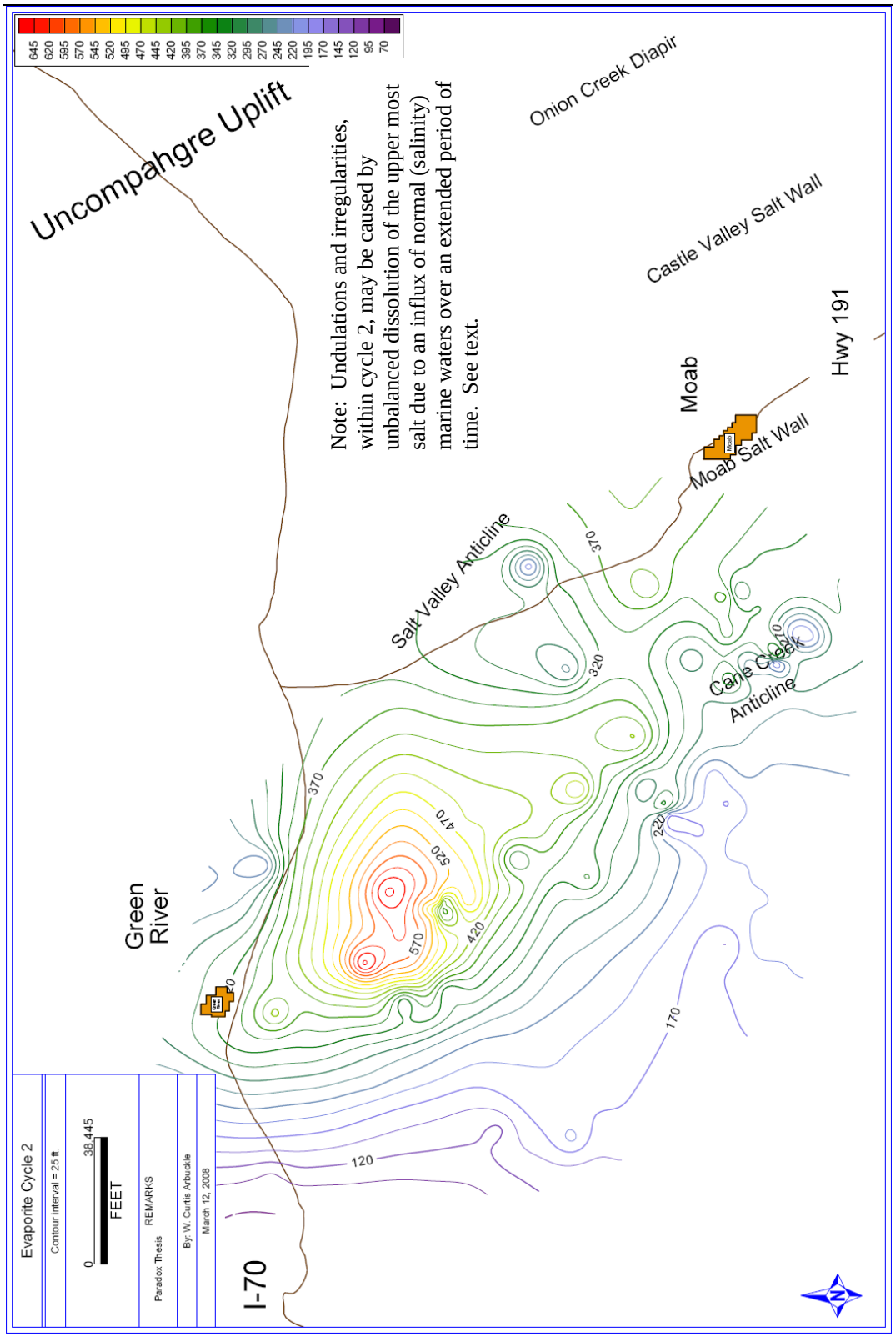

Figure 6.18: Isopach map of evaporite cycle 2 within the Paradox Formation. See text for analysis. Contour interval = 25 feet (7.62 m).

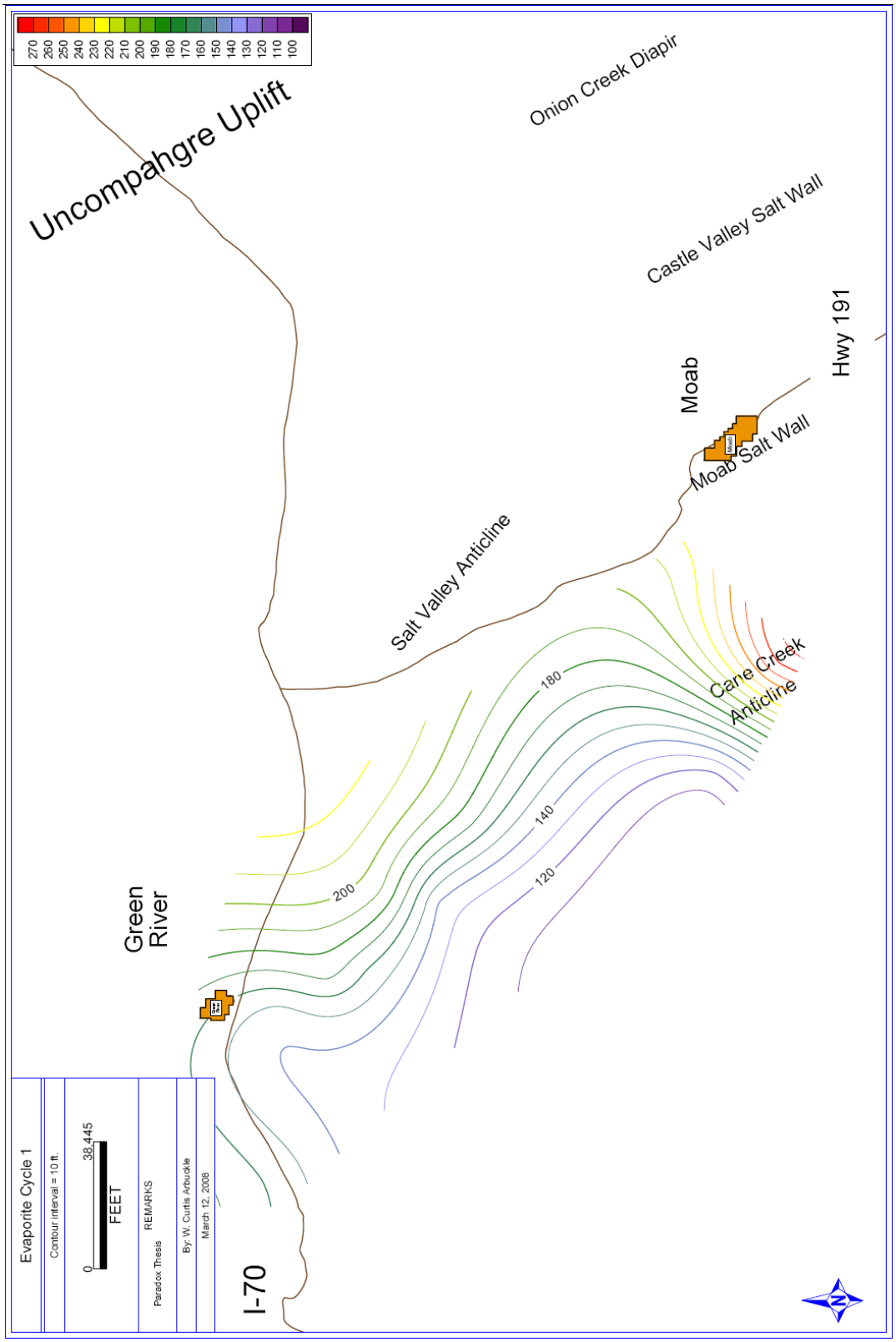

Figure 6.19: Isopach map of evaporite cycle 1 within the Paradox Formation. See text for analysis. Contour interval = 10 feet (3.05 m).

6.2 Map Analysis and Observations

Several key observations can be made from the 29 evaporite cycle isopach maps and are listed below.

1. Cycles 23, 20, 17, 13, 6 – 10 and 2 (Figures 6.7 – 6.10 and 6.13 – 6.18) all show a greater thickness beneath and along the northwest-southeast trend of the Cane Creek Anticline extending northwest towards Green River, Utah (Figures 6.20 – 6.23). These variations in thickness could be simply explained by post-depositional salt movement. However, Hite (1968) observed that Late Mississippian and Early Pennsylvanian (pre-Paradox Formation) age strata thicken slightly along the same regional zone, as do many of the individual clastic zones. This suggests that the area extending from the Cane Creek Anticline northwest towards the town of Green River, was a depositional low or trough, flanked to the northeast and southwest by slightly positive structures (Hite, 1968). It is likely this trough was tectonically controlled and the controlling structures were active before the deposition of the first salt bed. The trough must have still been actively down-dropping by at least the deposition of cycle 2 (Figure 6.18) but apparently stopped near or after the end of salt deposition. The conclusion of the down-dropping might have also been caused by differential compaction over rigid fault blocks, halting further movement.

2. The Cane Creek trough, described above, is also the only location where all of Hite's (1960) 29 cycles were deposited (Figures 6.21 and 6.23). In fact, several wells that were drilled down to the Mississippian encountered additional evaporite cycles numbering up through cycle 33.

3. Evaporite cycle 2, and specific rock units identified in the overlying Honaker Trail Formation are depositionally thinner over the Cane Creek Anticline, as first noticed by Hite (1968) (Figure 6.18). Hite attributes these thinner beds to folding and buckling of the upper salt beds into an anticlinal position that was likely a

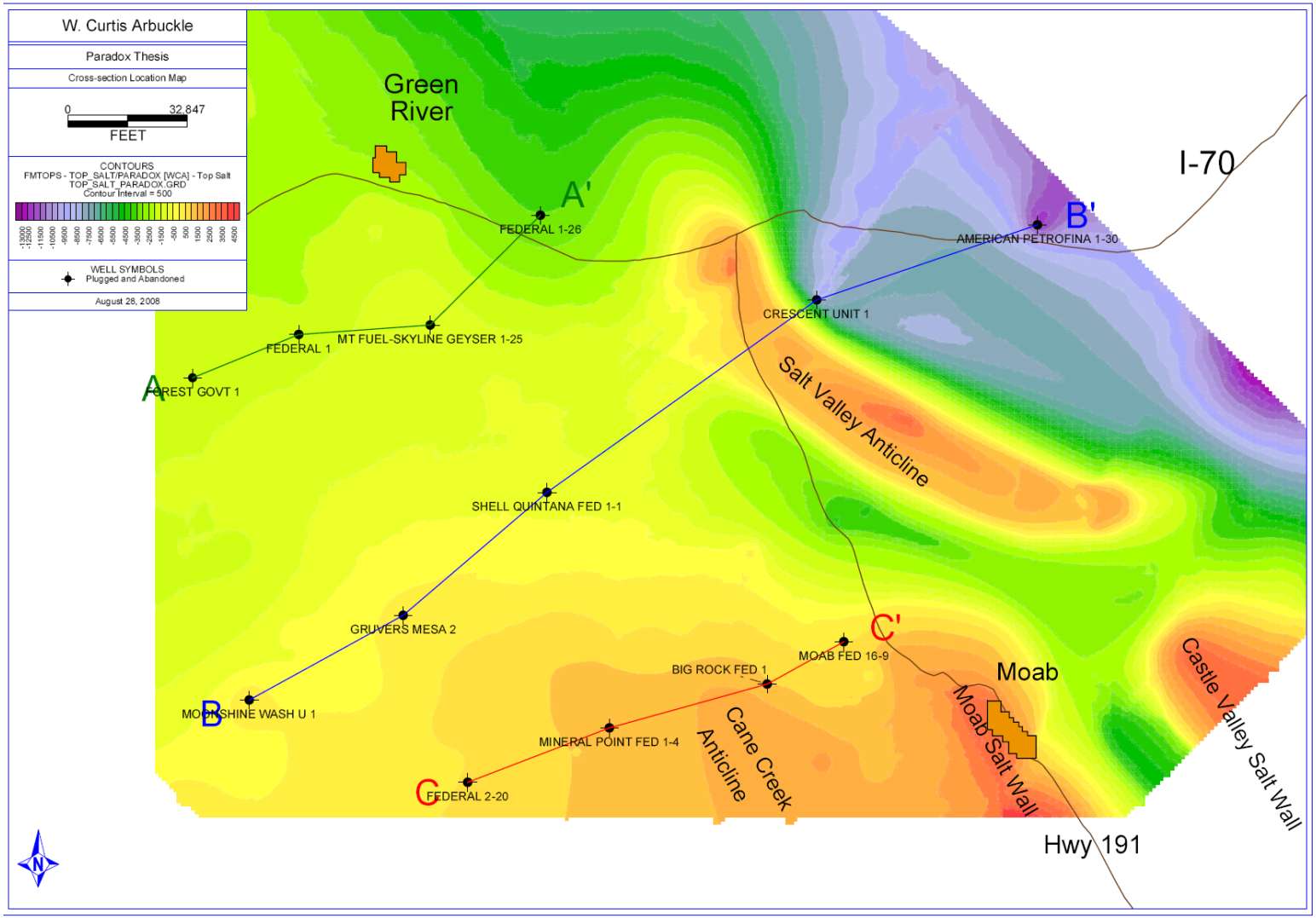

Figure 6.20: Map showing the location of well tied cross-sections A-A', B-B' and C-C'. The contoured interval represents the top of the Paradox salt.

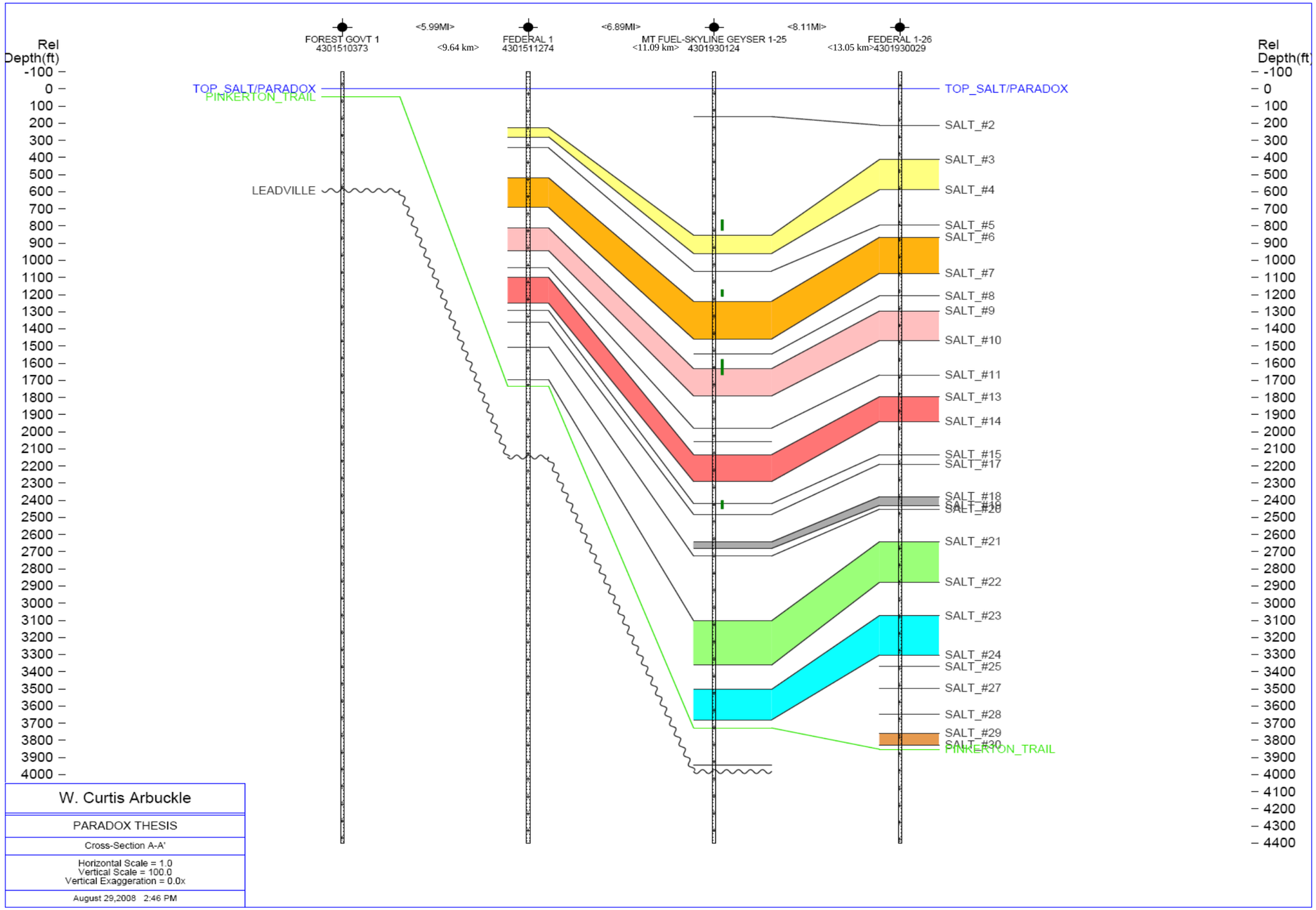

Figure 6.21: Cross-section A-A'.

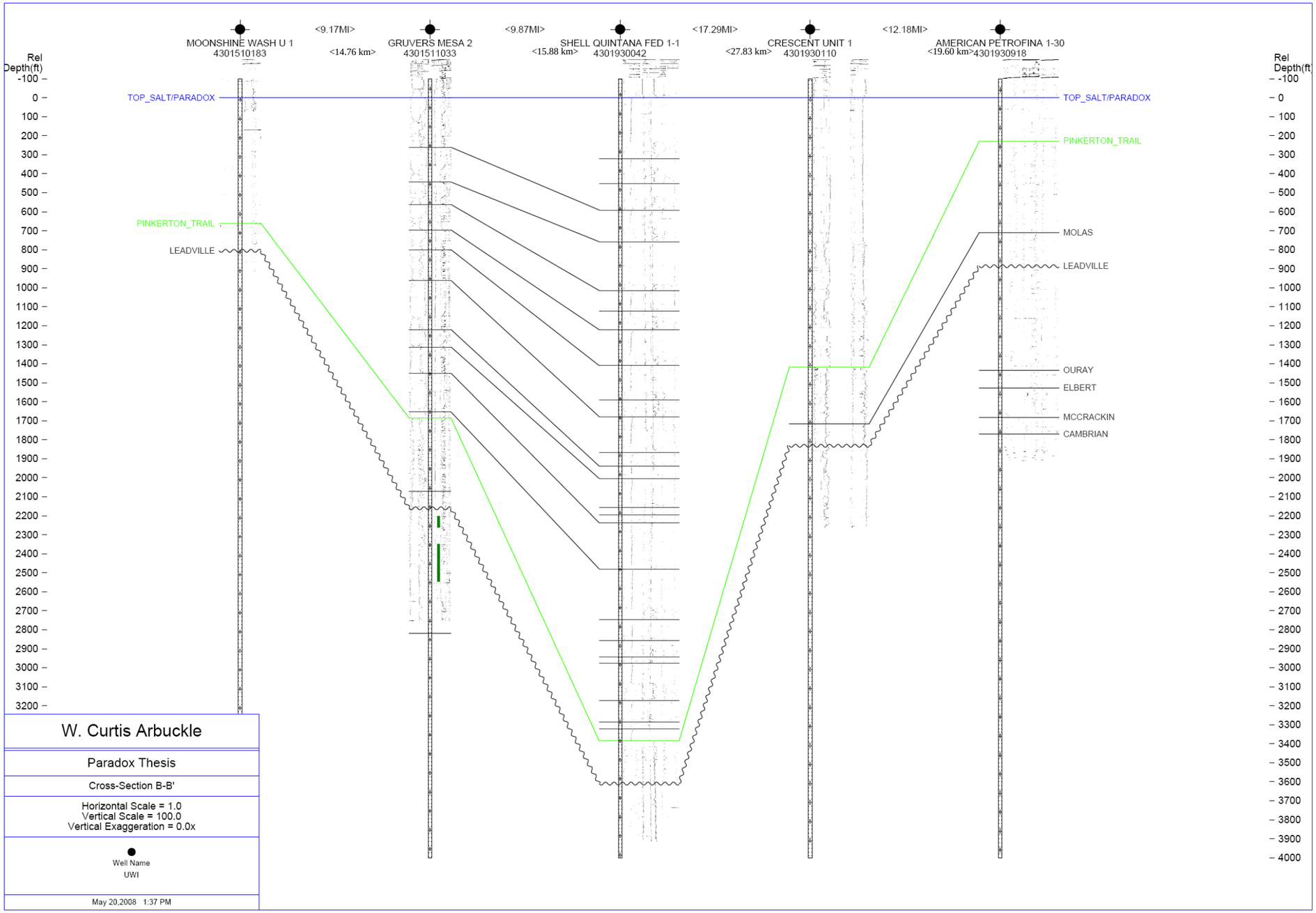

Figure 6.22: Cross-section B-B'.

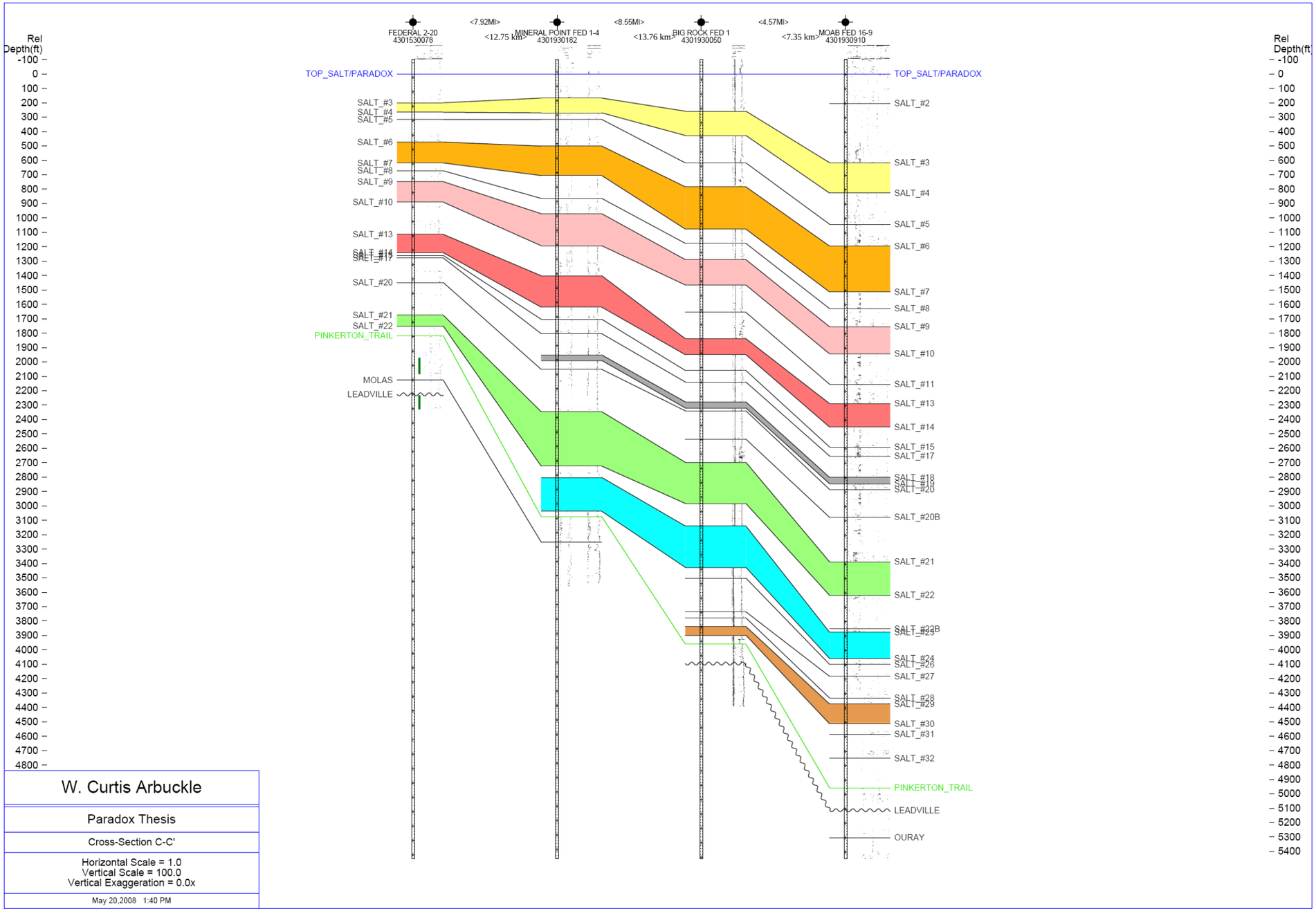

Figure 6.23: Cross-section C-C'.

result of greater salt movement further to the east towards the larger more abrupt salt walls.

4. Many of the maps show a distinctive low along the western flank of the Salt Valley Anticline. Initial thoughts might suggest this is solely attributed to salt evacuation into the growing salt wall (Crescent Unit #1 well, Figure 6.22). The resulting partial salt weld would therefore be misrepresentative of actual depositional cycle thicknesses. However, several of the isopach maps display thickening as they approach the salt wall. Well logs suggest there is considerable thinning along the western edge of the Salt Valley Anticline due to salt welding. The isopach maps that illustrate a thickening trend might be more representative of depositional thicknesses prior to salt tectonics.

5. An interesting relationship is observed with isopach maps involving cycles 29 – 24 (Figure 6.1 – 6.6). Cycle 29 thickens towards the east where as the following cycle, 28, thickens to the west. This pattern continues through cycle 24 creating an oscillating depositional pattern. It is interpreted that local tectonics (possibly the same basement faulting that controlled the deposition within the Cane Creek trough) is responsible for these thickness fluctuations within the early evaporite cycles.

6. The Mississippian Leadville Limestone (Figure 2.18) and the Pennsylvanian Pinkerton Trail Formation (Figure 2.21) display a regional dip to the east into the deepest part of the Paradox Basin, but are abruptly interrupted by the Uncompahgre Uplift (Figure 2.10). This regional down-dropping was a result of basin subsidence along the Uncompahgre Front. The Paradox Formation evaporite cycles generally don't follow the same depositional patterns as most clastic rocks and instead were precipitated in depressional areas where brine concentrations reached salt saturations. Therefore observing the same basin subsidence trend with the Paradox salt, while considering salt movement/tectonics, becomes difficult. The overlying Honaker Trail Formation

(Figure 6.24) also displays little evidence of basin subsidence. This is partly caused by the significant amount of coarse clastic material shed from the Uncompahgre Uplift into the basin. The resulting salt walls further shroud any detailed evidence of ongoing subsidence during the Pennsylvanian time.

7. The accuracy of the isopach maps involving cycles 1 and 2 is somewhat questionable. For cycle 1 (Figure 6.19), its areal extent does not cover the entire study area, particularly where the data are available west of the Salt Valley Anticline. The thickest accumulations were deposited along depositional lows mainly in an area just south of the town of Green River, Utah and along the Cane Creek Anticline (Figure 6.19). The subsequent isopach map is more of an interpretation between these two areas then an accurate representation.

   Cycle 2 (with the exception of cycle 1) is the upper most evaporite bearing sequence (Figure 6.18). Because cycle 2 is the last main, widely deposited evaporite interval it was probably in contact with open marine waters longer then most of the previous cycles. This change from a penesaline environment (Paradox Formation) to a marine environment (Honaker Trail Formation) (Hite, 1960) may have caused the upper section of cycle 2 (and/or cycle 1) to be eroded and dissolved away. It would be very difficult to estimate the loss in thickness due to this process and the resulting map is full of undulations that don't appear to be depositionally controlled.

8. Isopach maps involving cycles 12 – 10 (Figures 6.11 – 6.13) are very complex. For many of the wells within the database, cycles 11 and 12 are incomplete and lack a halite zone. Arguably, it can be considered that any clastic material deposited (without an associated halite zone) during these two cycles would be added to the assemblage of the previous cycle. For example, if cycle 11 was void of any related halite, any clastic material deposited during cycle 11 would be grouped into cycle 10. This creates correlation and thickness problems particularly where cycle 10 becomes locally much thicker in the absence of both the halite beds of cycles 11 and 12. These two cycles were restricted to a small

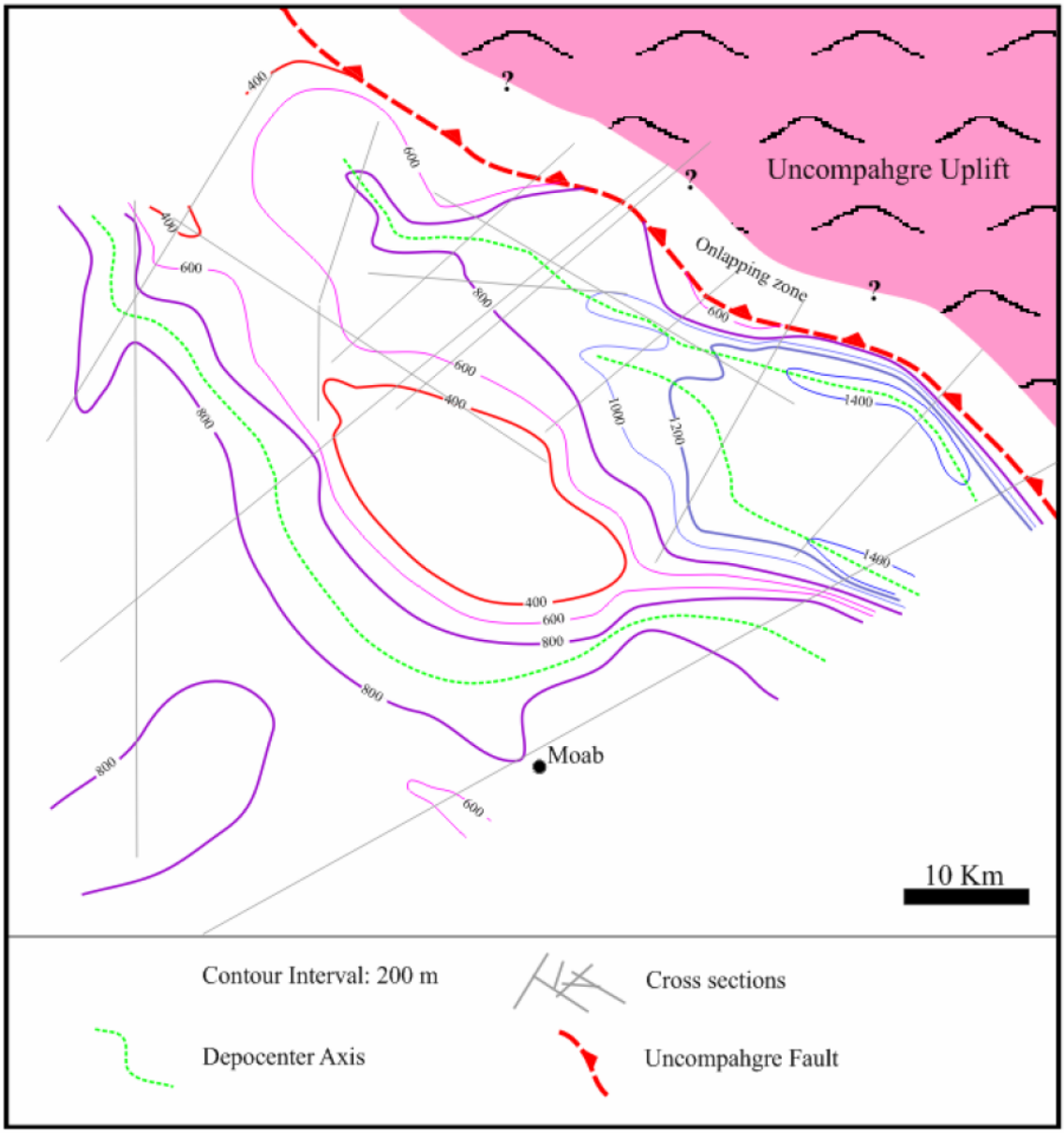

Figure 6.24: A paleogeographic and isopach map of the Honaker Trail Formation. Notice how the formation thins atop the Salt Valley salt wall (center of figure) but is much thicker along the flanks of the structure. These depocenters are also areas of significant salt movement and welding. West of the Salt Valley salt wall, the thickness of the Honaker Trail Formation is rather continuous (Paz Cuellar, 2006).

area north of the Cane Creek Anticline, especially cycle 12 (Figures 3.5 and 6.11). The same situation applies to cycles 16 and 15 (Figures B.14 and B.15) where cycle 16 was not widely deposited.

6.2.1 Mapping Problems and Potential Sources of Error

Unfortunately there are several problems when correlating and mapping the evaporite cycles across the northern part of the basin. The most serious issue involves the salt walls and anticlines. As the salt was evacuated into the deformed structures we observe today, the clastic zones within the salt were also forced upward. During this process the clastic intervals became distorted, broken and lost any recognizable orientation needed for correlation. Another correlation problem involving the salt wall structures are the associated synclines located adjacent to the salt walls (an example being the Courthouse Syncline (Figure 2.16)). These synclines are areas where the present day thickness of the salt is thinner, but they don't necessarily represent areas of thinner deposition. It is more likely the lack of salt is caused by the formation of the salt walls where any available salt was evacuated creating partial salt welds on either side of the structure. These problems involving salt movement become particularly relevant when attempting to correlate from the western side of the study area, across the Salt Valley Anticline (and Courthouse Syncline), to the eastern section of the study area (Figures 2.16 and 2.23). Correlations west of the anticline are relatively straight forward where as the opposite can be said along the salt structure. East of the Salt Valley salt wall correlations are also rather complex, mainly due to a lack of sufficient well data, salt welding and a large increase in coarse clastic material not observed west of the Salt Valley Anticline.

Another problem that arises when attempting to correlate the evaporite cycles involves the depositional relationships between each cycle. Because consecutive cycles are deposited on top of each other in a more or less sequential order, topographical variations in underlying cycles affect overlying depositional units. For example, if there was a local depression following the deposition of cycle 'X', it would be filled in by the

overlying cycle ‘Y’ thus allowing for cycle ‘Y’ to be locally thicker. Therefore correlations across areas of local thickness change are at times difficult to interpret and understand. It is also unclear how or why these local depressions or highs form, but correlations suggest salt movement and tectonics play an important role. Evidence for these types of occurrences becomes apparent within the evaporite cycles of the Paradox Basin.

Also, since the boundaries between cycles are deemed as solution unconformities, it is likely at least some of the upper-most section of each cycle would be removed or dissolved by the first transgressive waters entering the basin. Estimating how much of each cycle was lost becomes nearly impossible given a list of variables that include water depth, water temperature, water flow direction, water velocity, local and regional topography, clastic and organic material and the chemical makeup of the inflowing waters. If some areas of the basin experienced many of these formation changing variables, compared to other areas that were not at all affected, then the post-depositional thicknesses can vary greatly depending on location. This makes accurate correlation difficult.

Well data used for mapping of cycles 29 – 24 (Figures 6.1 – 6.6) are fairly inadequate. Many of the wells drilled east of Salt Valley targeted the Cane Creek shale (clastic zone 23) and were not drilled any deeper. Only six drilled through all 29 evaporite cycles of the Paradox Formation into underlying strata. These six wells (and thus data points) are enough to create isopach thickness maps of each interval, but prove to be an inadequate representation due to the expanse of the mappable area.

CHAPTER 7

DISCUSSION

Chapter 7 discusses the cyclicity of the Paradox Basin, depositional age and timing of the Paradox Formation and its evolutionary relationship with the Uncompahgre Uplift.

7.1 Pennsylvanian Cyclicity of the Northern Paradox Basin – Paradox Formation

Cyclicity can be controlled by a number of factors including tectonic, sedimentary, climate and eustatic controls and it is likely many of these factors contribute to the level and persistence of any cyclical patterns. Hite and Buckner (1981) concluded the cyclicity observed in the Paradox Basin evaporites was caused by periodic sea-level changes as a result of glacio-eustatic fluctuations involving Gondwanaland ice sheets during Pennsylvanian time. An increase of ice volume would have caused a lowering of global sea-level thus isolating the basin from open marine waters. This would result in a rise of brine salinities leading to the deposition of the Paradox Formation evaporites. In contrast, a melting of Gondwanaland glaciers would cause a rise in sea-level allowing for marine waters to flood and circulate within the Paradox Basin. The fresher water would cause some dissolution of the already deposited, uppermost halite layers creating a solution disconformity. During this time of higher sea-level, the clastic intervals would have been deposited.

It is possible that the glacio-eustatic driven evaporite cycles of the Paradox Formation can be correlated with the cyclothems from the Midcontinent of the United States even down to fourth- and fifth-order composite cycles (Raup and Hite, 1992; Olszewski and Patzkowsky, 2003). Cycles and cyclothems of glacio-eustatic origin should be synchronous and correlative with other basins throughout the world (Dickinson

et al., 1994). However, problems exist in making definitive correlations. The main problem is assuming that each major glacial-eustatic event left the same imprint and was of the same magnitude between basins. This is not observed within cycles documented during the Pleistocene and should also be discounted for cycles formed during the Pennsylvanian (Nadon and Kelly, 2004). The presence of paleosols between cycles during the Pennsylvanian suggests that deposition and exposure took place at slightly different times in many locations around the Midcontinent, Appalachian and Illinois basins (Olszewski and Patzkowsky, 2003; Nadon and Kelly, 2004). This implies there could be missing cycles that are thus non-correlative between basins, especially if one was to include silled basins like the Paradox Basin. These factors prevent high-resolution correlation between basins roughly of the same age and presumably affected by glacio-eustatic cyclical processes.

Tectonic controls on the cyclicity within the northern Paradox Basin are hard to determine. The Uncompahgre Uplift was at least mildly positive (above local sea-level) during the late stages of the deposition of the evaporites and was the source of at least some of the clastic material found within the cycles (Raup and Hite, 1992). The uplift may have also been the major cause of basin subsidence (based on basin structure, modeling and stratigraphic relationships), therefore creating accommodation space needed for each successive cycle. However, the Uncompahgre alone could not have caused the cyclicity observed within the evaporites, unless it was directly influencing the pathway and flow of seawater into the basin (Hite and Buckner, 1981). This is believed not to be the case based on the regularity of the cyclicity observed. Still, the regional tectonics of the Ancestral Rocky Mountains must have had some influence on cyclical deposition, but the effects are often overshadowed by evidence supporting strong glacio-eustatic control (Houck, 1997).

Climate-driven evaporite cycles should also be considered for the Paradox Basin. A change in the aridity of the climate would alter depositional patterns involving evaporation rates and seasonal precipitation (Hite and Buckner, 1981). However, these changes are considered minor compared to the much larger scale glacio-eustatic changes described above, but would still alter any cyclical pattern to some degree.

7.1.1 Sequence Stratigraphy and Palynomorphs: Relating to Milankovitch Periodicity

Sequence stratigraphic cycles in the southern part of the Paradox Basin were identified by Weber *et al*. (1995). They were able to divide the Paradox and lower Honaker Trail formations into five third-order stratigraphic sequences or composite cycles based on stratigraphic rock relationships (see section 4.2). The older four sequences are entirely grouped within the Paradox Formation where each individual evaporite cycle is considered to be a fourth-order sequence. These fourth-order sequences range in duration from 100,000 – 500,000 years (Weber *et al*., 1995) which closely mimics the eccentricity cycle durations defined in the Milankovitch theory.

Palynomorph data identified within the evaporite cycles gives several clues to the climate, age, depositional environment and cyclicity of the Paradox Basin. The presence of palynomorphs generally associated with Middle Pennsylvanian coal deposits indicates that locally the environment must have supported large, arborescent plants typically found in swamp-like environments during periods of highstand (Reuger, 1996). A lack of palynomorphs identified within regressive and lowstand rocks indicates there was climactic variability during the deposition of the cycles. This supports the theory that the cyclicity of the Paradox Formation was at least partially controlled by glacio-eustatic processes on roughly a 100,000 year (Milankovitch) succession.

7.1.1.1 Comparing Sequence Stratigraphy and Palynomorph Cycle Boundaries

Rueger (1996) identified and categorized palynomorph data, taken from the Paradox Formation, into four biostratigraphic zones based on sharp changes in taxa percentages (Figure 4.6). When compared to the third-order boundaries defined by Weber *et al*. (1995) a tentative correlation can be made (Figure 7.1). Interestingly many of the boundaries identified by both authors align and compare very well, especially since one is based on sequence stratigraphic rock relationships and the other from floral successions. What the comparison suggests is that these boundaries mark significant climatic changes within the basin on at least a third-order cyclical level.

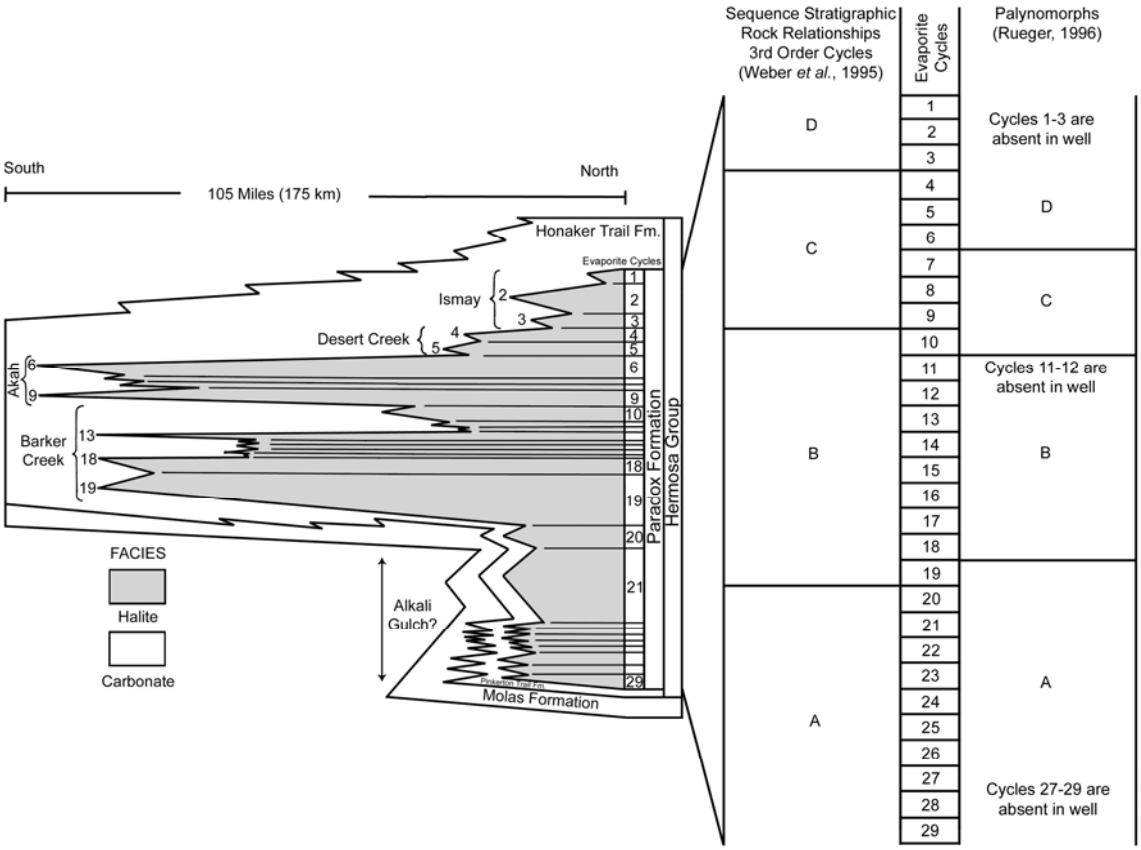

Figure 7.1: Diagram showing the comparison between third-order cycle boundaries identified by Weber *et al*. (1995) and palynomorph biostratigraphic zones recognized by Rueger (1996) (modified from Hite and Buckner, 1981).

7.2 Paradox Formation – Depositional Age and Timing

A key aspect of this thesis is to understand the timing and formation of the northern Paradox Basin with relation to the Uncompahgre Uplift. To achieve this goal, an age estimate calculated from the depositional duration of the Paradox Formation would provide a rough time approximation for basin formation and evolution. The Paradox Formation is thought to have been mostly deposited during the Desmoinesian (309.4 – 305.5 Ma according to Gradstein *et al*., 2004). By Late Desmoinesian time, and the end of Paradox deposition, massive amounts of coarse arkosic material were being shed from the Uncompahgre Uplift located to the northeast (Baars and Stevenson, 1981). This presents a rough time boundary estimate for the deposition of the Paradox Formation and timing of the Uncompahgre Uplift.

To calculate the age of the Paradox Formation, thicknesses of individual lithology types were tallied for 10 wells. These thicknesses were then multiplied by annual sedimentation rates, also unique to each lithology type, resulting in age duration estimates for individual evaporite cycles and also for the entire Paradox Formation. Age correlations can then be made from east to west across the basin and can also be related to global and local climate changes. It is however difficult to estimate the time of non-deposition during each cycle, although it can be estimated and included into the calculations.

7.2.1 Sedimentation Rates

It is often difficult to estimate halite sedimentation rates. The regularity of bromide profiles for the halite beds within the Paradox Basin suggests there was relatively continuous, uninterrupted deposition (Raup and Hite, 1992). Wardlaw and Schwerdtner (1966) analyzed several evaporite depositional provinces each having different halite sedimentation rates ranging from 0.4 – 59 inches (1 – 150 cm) per year. They closely examined the Middle Devonian Prairie Evaporite formation in Saskatchewan, Canada, and concluded that a halite sedimentation rate of 2.0 inches (5

cm) per year was reasonable. Similar rates were recorded in the tectonic setting of the Permian Zechstein Basin in Germany ranging from 1.18 – 4.0 inches (3 – 10 cm) per year (Borchert, 1969). Annual halite intervals measured between anhydrite laminae of the Delhi-Taylor Oil Company Cane Creek No. 1 core (T 26S, R 20E, sec. 25) averaged 1.57 inches (4 cm) per year in thickness and represents a good estimate of halite sedimentation rates within the Paradox Basin.

The thickest, consistent, in situ salt zone within the northern Paradox Basin is the halite section of cycle 6 at around 330 feet (100 m). Considering an average salt sedimentation rate of 1.57 inches (4 cm) per year, this bed would have been deposited in roughly 2,500 years. On a larger scale, a total of 5,000 – 6,000 feet (1,500 – 1,800 m) of depositional evaporites were precipitated within the Paradox Basin. Using the same average sedimentation rate, the total accumulation of evaporites would have been deposited in roughly 37,500 to 45,000 years. Therefore, the bulk of the depositional time for each individual evaporite cycle, and thus the entire formation, is contained within the clastic intervals. With much slower sedimentation rates, the black shales, anhydrites and silty dolomites become extremely important in the age estimates for each cycle and the formation in its entirety (Table 7.1).

Phase	Lithology	Average Annual Rate of Deposition	
		(inches)	(mm)
Regressive	Halite	1.575	40.00
	Anhydrite	0.031	0.80
	Silty Dolomite	0.007	0.17
----------	Black Shale	0.020 - 0.121	0.51 - 3.08
Transgressive	Silty Dolomite	0.008	0.20
	Anhydrite	0.031	0.80

Table 7.1: Table showing the depositional rates for each lithology within an ideal evaporite cycle of the Paradox Formation (Hite and Buckner, 1981). Sedimentation rates are further defined in Chapter 3.

7.2.2 Total Age of the Paradox Formation

The total age estimate for the entire Paradox Formation can be calculated using the sedimentation rates featured in Table 7.1 and utilizing the total thickness of each individual rock type (Table C.1). The age estimates for the 10 selected wells range from about 600,000 years to over 1.5 million years (Table 7.2). These estimates however, only account for periods of deposition and do not incorporate episodes of non-deposition that could have lasted much longer than the total time of salt and clastic deposition combined. Unfortunately, it is very difficult to determine the length of these periods of non-deposition, which are generally considered to be at the end of each subsequent cycle (following the last period of the halite/potash precipitation). If we consider the total time of non-deposition to be at least twice as long as the total time of complete deposition/precipitation, then the total age estimates for the Paradox Formation are recalculated to range from 1.8 million years to over 4.5 million years. These estimates therefore fit within the time period of the Desmoinesian, further quantifying that the Paradox Formation could have been completely deposited during the time interval of about 309.4 – 305.5 Ma (Gradstein *et al*., 2004).

When these ages for the 10 wells are plotted and contoured, very interesting relationships are established areally (Figure 7.2). Moving west to east, towards the Uncompahgre Uplift, and thus the deepest part of the basin, the total age of deposition for the Paradox Basin becomes increasingly greater. This indicates several key factors related to basin evolution. First, since the bulk of the age estimates are based on the clastic intervals (much slower sedimentation rates compared to halite), it is clear the further east, more clastic material is present. This signifies there was more clastic material supplied from the eastern (possibly from the Uncompahgre Uplift) side of the basin than from the west. It also might suggest there was a greater amount of accommodation in the east (i.e., the deepest part of the basin) possibly caused by basin subsidence in relation to the crustal flexure related to the rising Uncompahgre Uplift. Secondly, it is interesting to note how the area around the Cane Creek Anticline starts to change and become younger continuing further to the east (Figure 7.2). This might suggest that salt tectonics was active by at least the end of the Paradox salt deposition.

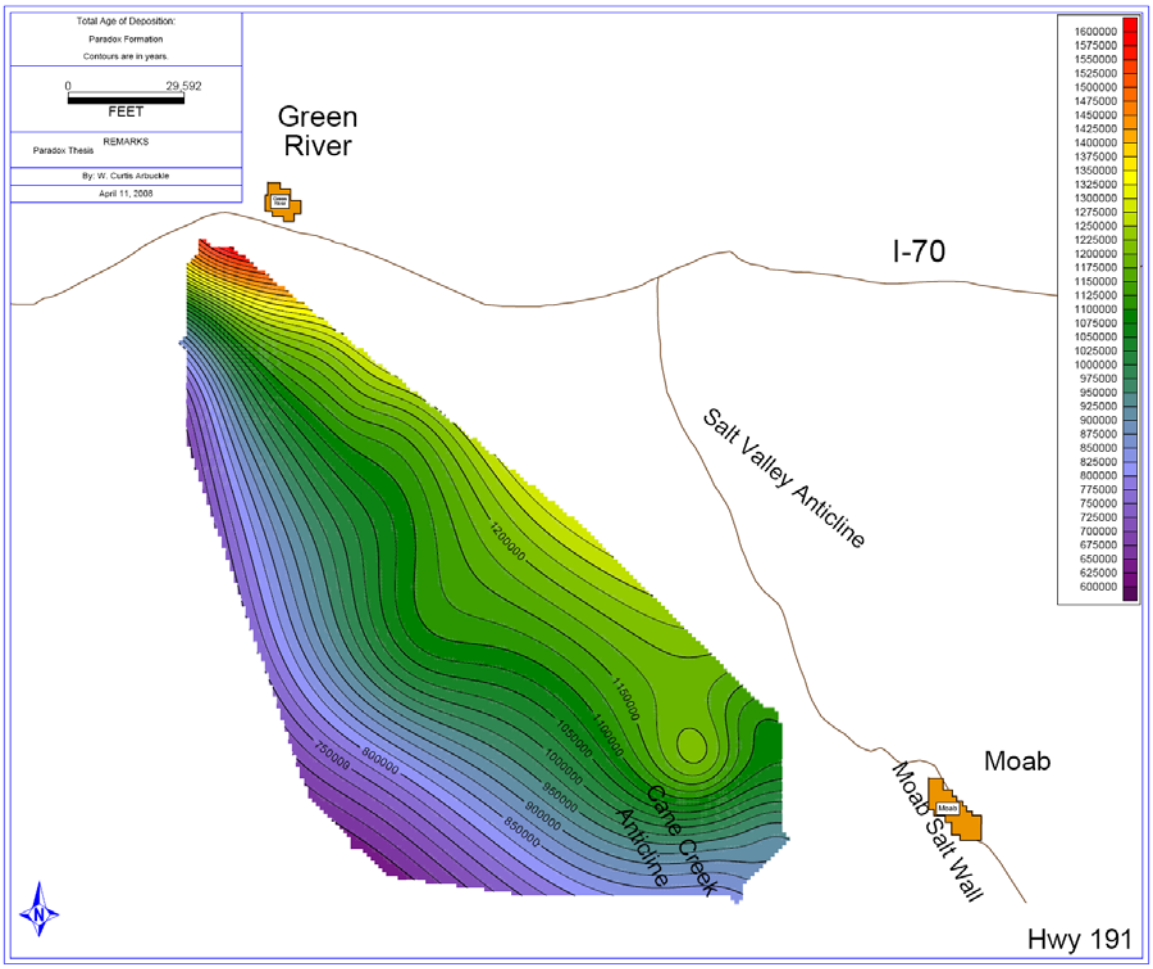

Figure 7.2: Map showing the total age duration estimate for the depositional units within the Paradox Formation. These ages were calculated using thicknesses tallied from well logs and sedimentation rates for each individual lithology. Contour intervals are in years.

Since the age estimates are based heavily on the clastic material and non-depositional time periods are almost impossible to ascertain, the Cane Creek Anticline may have started to become a more positive feature sometime during the Desmoinesian. The final few cycles appear to have been depositionally thinner over this structure, as mentioned previously in Chapter 6.

No.	API #	Operator	Well Name	Age (years)	
				(max.)	(min.)
1	4301511182	SUPERIOR OIL COMPANY	GRAND FAULT UNIT 14	1,544,000	1,476,000
2	4301530079	MEGADON ENTERPRISES	GEYSER DOME 1-14	873,000	830,000
3	4301930124	MOUNTAIN FUEL SUPPLY	MT FUEL-SKYLINE GEYS	1,181,000	1,089,000
4	4301930282	RESERVE OIL & GAS	SALT WASH NORTH 1	1,125,000	1,055,000
5	4301930688	MEGADON ENTERPRISES	FEDERAL 1-26	1,092,000	1,014,000
6	4301930050	GENERAL CRUDE OIL CO	BIG ROCK FED 1	1,203,000	1,116,000
7	4301930910	CHANDLER & ASSOCIATE	MOAB FED 16-9	1,104,000	1,023,000
8	4301530145	DAVIS OIL COMPANY	POOL UNIT 1	636,000	602,000
9	4301931190	COORS ENERGY	COORS USA 1-10LC	923,000	817,000
10	4301910767	MURPHY CONSTRUCTION	LITTLE VALLEY-FED 1	843,000	714,000

Table 7.2: A table showing the age estimates of the Paradox Formation for 10 wells based on calculations using lithology thicknesses and sedimentation rates. The table does not include estimated time of non-deposition. A maximum and minimum were calculated based on black shale sedimentation rates of 0.020 to 0.121 inches (0.51 to 3.08 mm) per year.

7.2.3 Age Per Depositional Cycle

If the sedimentation rates (Table 7.2) are applied to the sequence of rock types, in evaporite cycle 2 for example, the calculations suggest a depositional time interval of roughly 100,000 years (Table 7.3). This age estimate fits the 100,000 year eccentricity Milankovitch periodicity suggesting that the Paradox evaporite cycles were at least partially controlled or influenced by global 4^{th} and 5^{th} order climate cycle changes. Unfortunately, the age estimate for many of the other cycles, including cycle 2, 3, 5, 9 and 10 in several other wells, sometimes falls short of this 100,000 year boundary (Tables C.2 – C.6). Because there is such variability in the duration of the evaporite cycles, other

processes and factors must have influenced timing and sedimentation. It is also important to note the ages of the cycles become increasing longer as the cycles become younger. For example, cycle 9 has an average duration of 50 – 54 thousand years where as cycle 3 ranges from 70 – 79 thousand years. There are many reasons that could limit the duration of each cycle and probably could include a combination of fluctuating periods of localized tectonic activity, relative and eustatic sea-level changes, basin isolation, plate tectonics, subsidence, the influence of meteoric groundwater or seepage, varying periods of non-deposition, irregular erosional patterns, etc.

Lithology	Annual Rate of Deposition		Thickness		Age
	(inches)	(mm)	(feet)	(meters)	(years)
Halite	1.575	40.00	217.1	66.17	1,654
Anhydrite (total)	0.031	0.80	31.9	9.72	12,154
Silty Dolomite (R)	0.007	0.17	22.05	6.72	39,534
Black Shale	0.020-0.121	0.51-3.08	18.3	5.58	10,937 - 1,811
Silty Dolomite (T)	0.008	0.20	24.95	7.60	38,024
		Totals	314.3	95.8	102,303 - 93,177

Table 7.3: Table showing the estimated rates of sedimentation and age duration of deposition for evaporite cycle 2 of the Coors Energy, Coors USA 1-10LC well (T 26S, R 20E, sec. 10; Figure 3.4). (R) = regressive; (T) = Transgressive.

7.2.4 Subsidence

Subsidence in a present-day tectonically active region can be extremely variable making the calculation of subsidence rates inconsistent. Therefore, establishing a subsidence rate for the Paradox Basin, which formed roughly 300 millions of years ago, is a difficult task. Beloussov (1962) calculated subsidence rates, for stable crustal environments, of less than a few millimeters per year. Similarly, Donovan *et al*. (1985) produced comparable rates of 0.0004 – 0.02 inches (0.01 – 0.5 mm) per year for several geotectonic settings (Ouachitas, Southern Oklahoma Aulacogen, and Anadarko Basin) in

Oklahoma during the Paleozoic. However, there are examples of subsidence rates in collapsing basins of 16 – 19 feet (5 – 6 m) per 1,000 years which is about equal to 0.24 inches (6 mm) per year (Sonnenfeld, 1984).

If a subsidence rate of 0.04 inches (1 mm) per year is applied to the Paradox Basin, it is apparent that the average salt sedimentation rate of 1.57 inches (4 cm) per year far exceeds any subsidence totals. Therefore, the basin itself must have been deep enough to accommodate the deposition of each subsequent cycle and/or have a high enough rate of subsidence to counteract such rapid rates of precipitation. To summarize, the thickest salt accumulations would be located in areas with the greatest rates of subsidence (Sonnenfeld, 1984). Also, at this time the basin would have been relatively isolated from any open marine waters that would hinder the deposition of evaporites, but still have enough marine water influx to fuel and re-supply the brine with salt minerals.

One must also consider that when precipitation rates exceed basin subsidence rates, after halite saturation, the basin floor typically levels out creating a broad flat surface at the end of each cycle (Sonnenfeld, 1984). Therefore, any localized thickness changes within the halite interval of a cycle, could be explained by tectonic processes which include periods of rapid subsidence coupled with rapid uplift.

7.2.4.1 Subsidence Modeling

Subsidence modeling was conducted for five wells stretching across the basin (Figure 7.3 and Table 7.4) using *OSXBackstrip* (created by Nestor Cardozo). The purpose of the modeling was to understand the timing and degree of subsidence stretching from west (lower amount of subsidence) to east (greatest amount of subsidence) across the basin. Formation tops, lithologies, densities, formation ages, unconformities and relative sea-levels were all used to calculate subsidence amounts in each well.

No.	API #	Operator	Well Name	Township	Range	Section
1	4301530145	DAVIS OIL COMPANY	POOL UNIT 1	26S	17E	17
2	4301910368	FEDERAL OIL CO	FED BOWKNOT 1	25S	18E	30
3	4301930050	GENERAL CRUDE OIL CO	BIG ROCK FED 1	25S	19E	26
4	4301931112	LADD PETROLEUM CORP	SALT VALLEY 1	24S	20E	16
5	4301930918	MOBIL OIL CORPORATION	AMERICAN PETROFINA 1-30	21S	22E	30

Table 7.4: Table showing the name and location of the five wells used for subsidence modeling.

As expected, there was a significant increase in the amount of subsidence moving from west to east across the basin as the Uncompahgre Uplift and trough were approached (Figures 7.4 – 7.9). The modeling also suggests the most rapid rate of subsidence started around 311 million years ago (Figure 7.10). This correlates well to the start of the Desmoinesian through about the beginning of Early Permian time. This implies there was a substantial amount of upward movement or slip along the Uncompahgre Fault, which resulted in considerable flexural subsidence in the basin adjacent to the uplift. The Salt Valley #1 well is located west of the Salt Valley Anticline and is in an area that has been significantly affected by salt evacuation. It is assumed that if the salt thickness in this well was representative of its true depositional thickness, then the subsidence totals and rates would be greater than what is presented.

Using the modeling described above, a subsidence rate for each well, during the 10 million year interval, was calculated (Table 7.5). The rates range from 0.0039 – 0.0071 inch (0.0987 – 0.1814 mm) per year.

No.	API #	Operator	Well Name	Inches / yr	mm/yr
1	4301530145	DAVIS OIL COMPANY	POOL UNIT 1	0.0039	0.0987
2	4301910368	FEDERAL OIL CO	FED BOWKNOT 1	0.0055	0.1400
3	4301930050	GENERAL CRUDE OIL CO	BIG ROCK FED 1	0.0071	0.1814
4	4301931112	LADD PETROLEUM CORP	SALT VALLEY 1	0.0048	0.1210
5	4301930918	MOBIL OIL CORPORATION	AMERICAN PETROFINA 1-30	0.0054	0.1379

Table 7.5: Table displaying the subsidence rates during the time period of about 311 – 301 million years ago for the five wells used in the modeling.

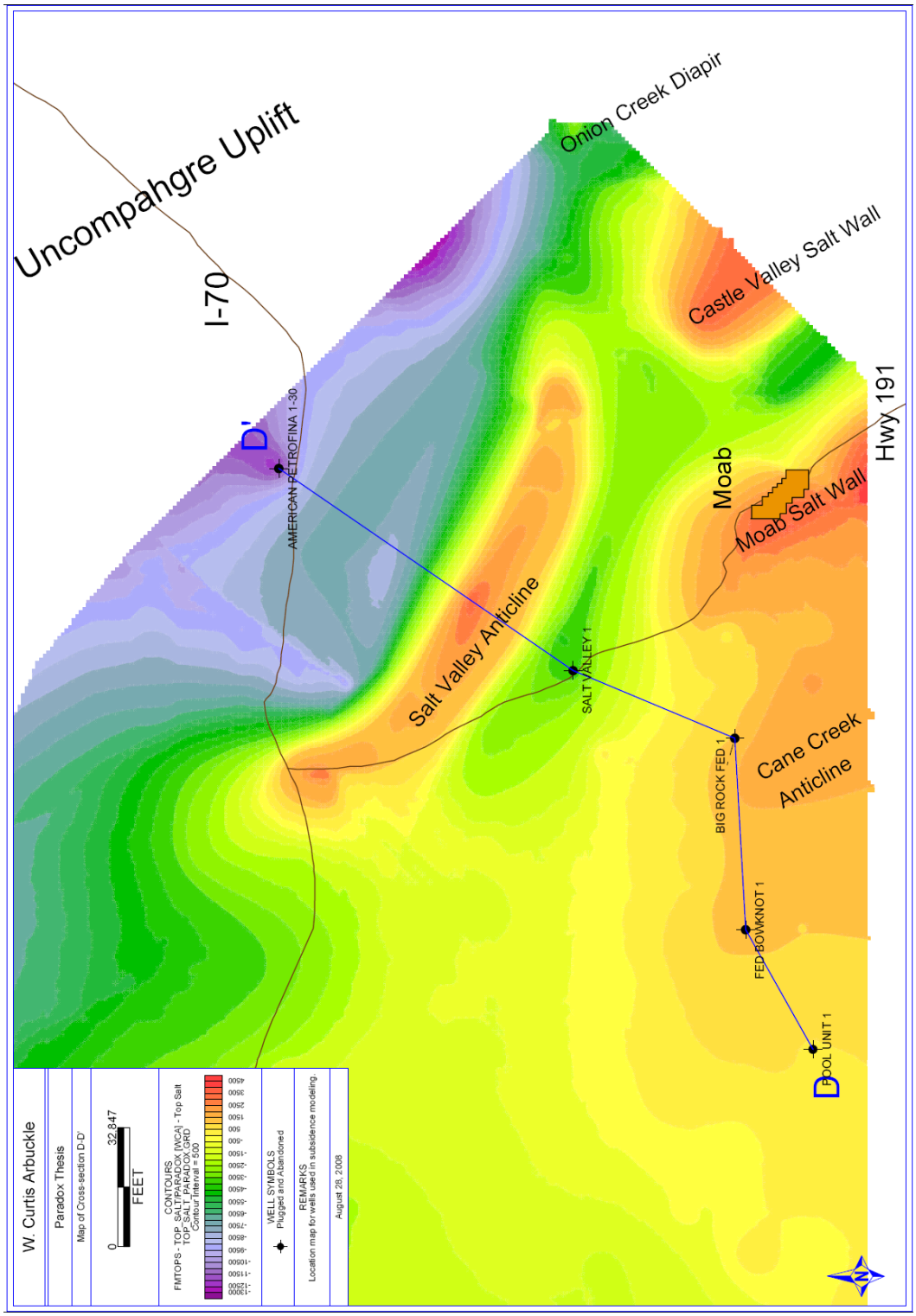

Figure 7.3: Map showing the location of cross-section D-D'. The contoured interval represents the top of the Paradox salt.

Pool #1

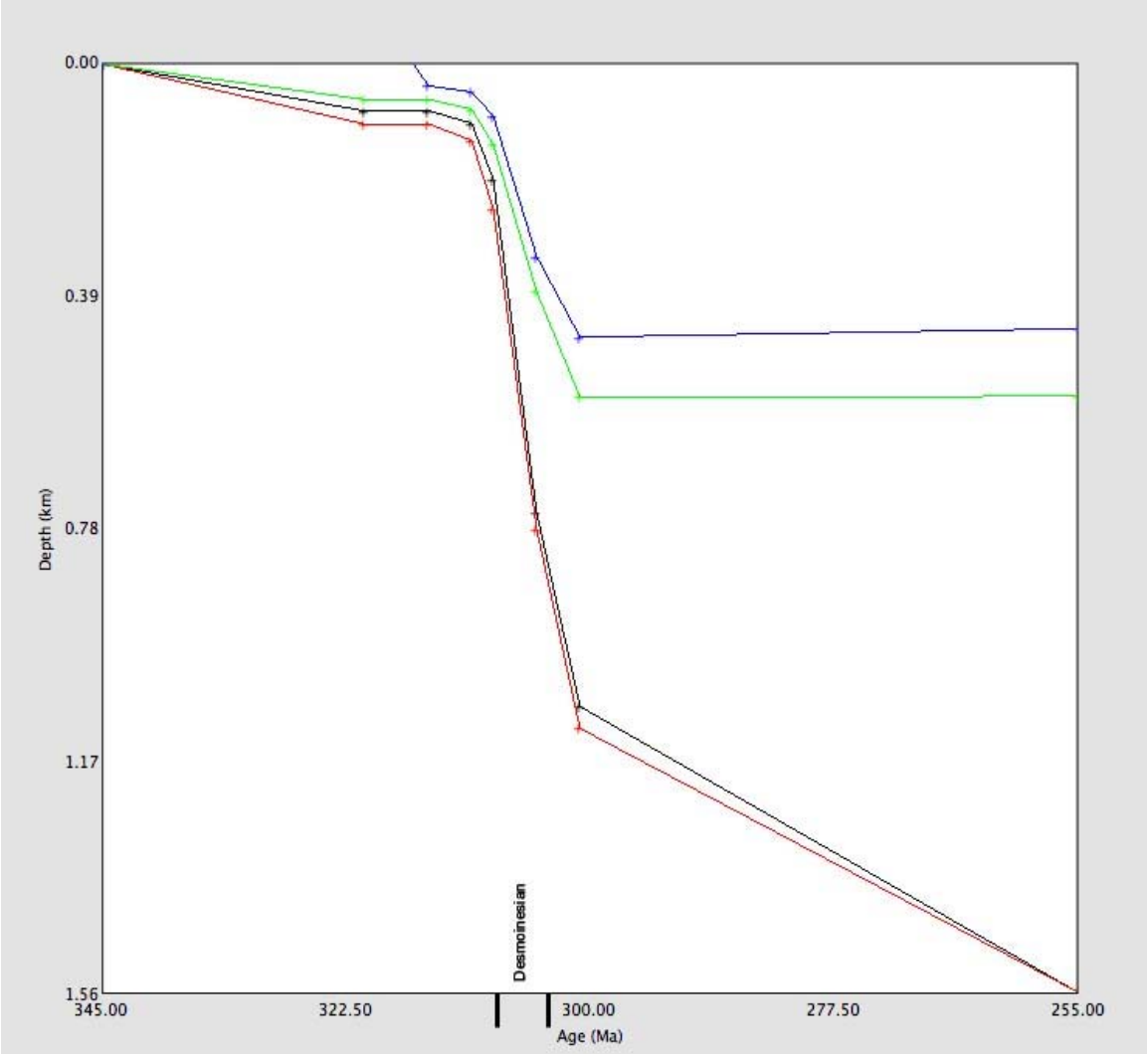

Figure 7.4: Subsidence plots for the Pool #1 well. The colored plots represent: black = compacted; red = decompacted; green = sediment corrected; and blue = with water correction.

Federal Bowknot #1

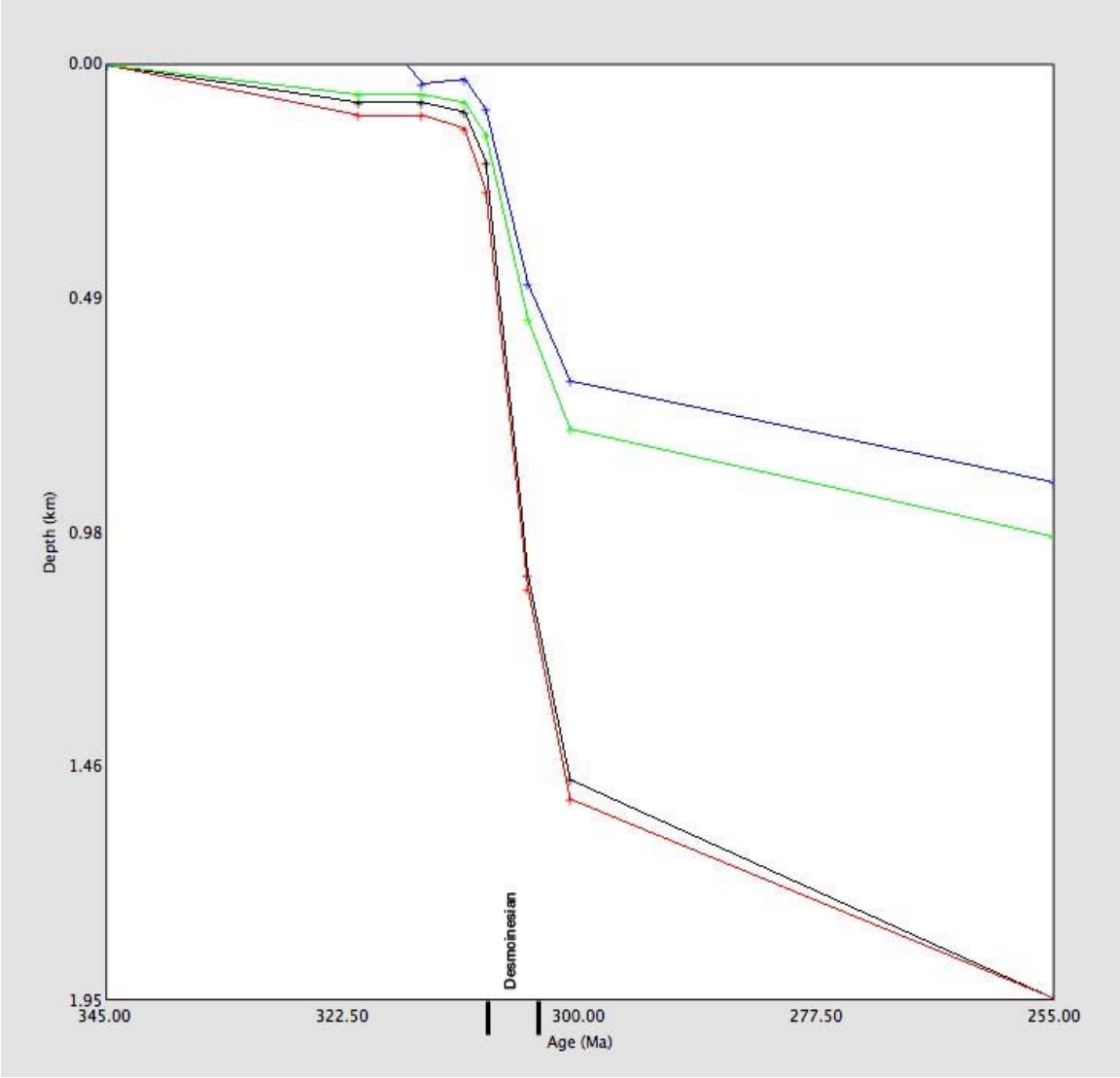

Figure 7.5: Subsidence plots for the Federal Bowknot #1 well. The colored plots represent: black = compacted; red = decompacted; green = sediment corrected; and blue = with water correction.

Big Rock Federal #1

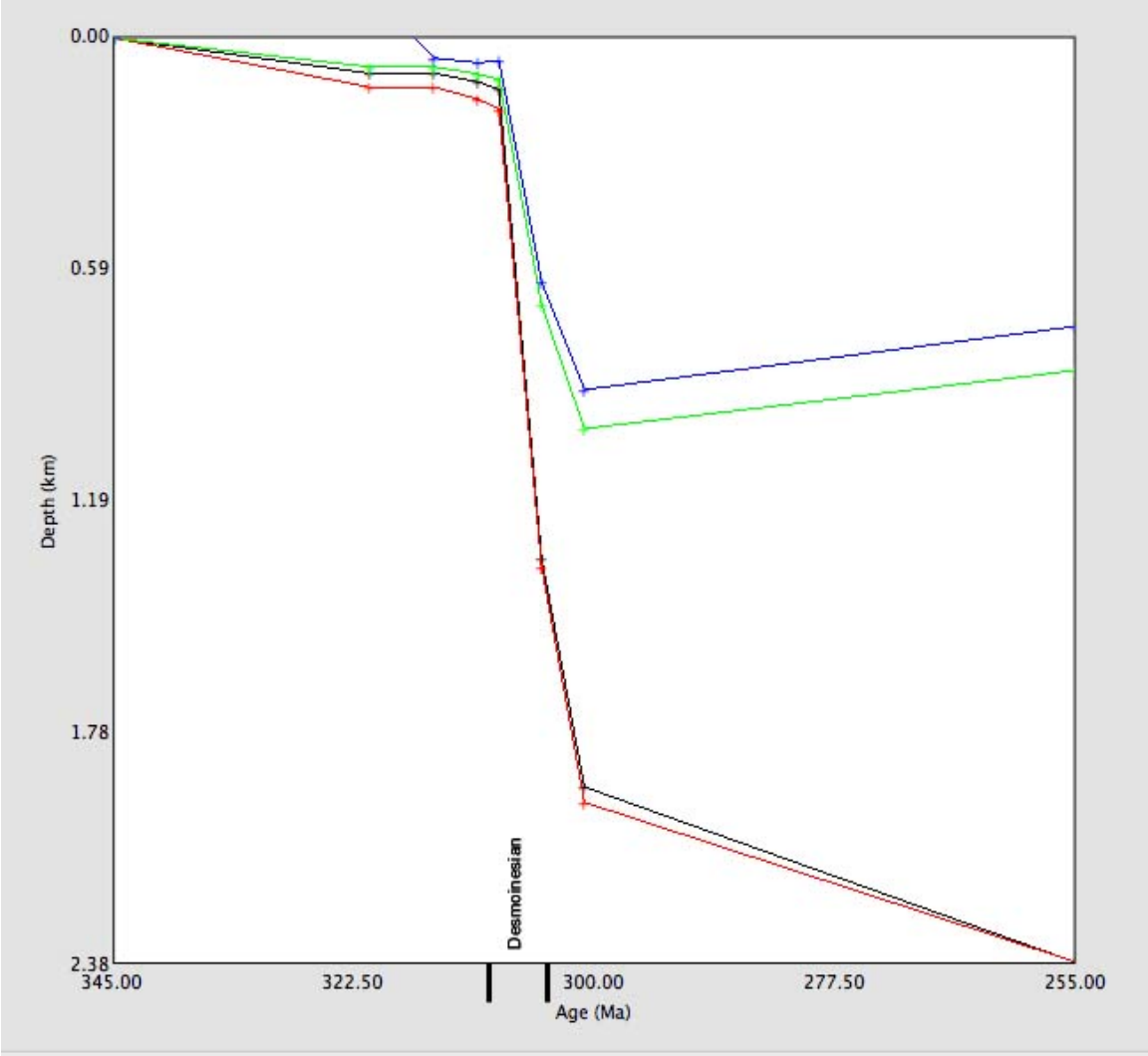

Figure 7.6: Subsidence plots for the Big Rock Federal #1 well. The colored plots represent: black = compacted; red = decompacted; green = sediment corrected; and blue = with water correction.

Salt Valley #1

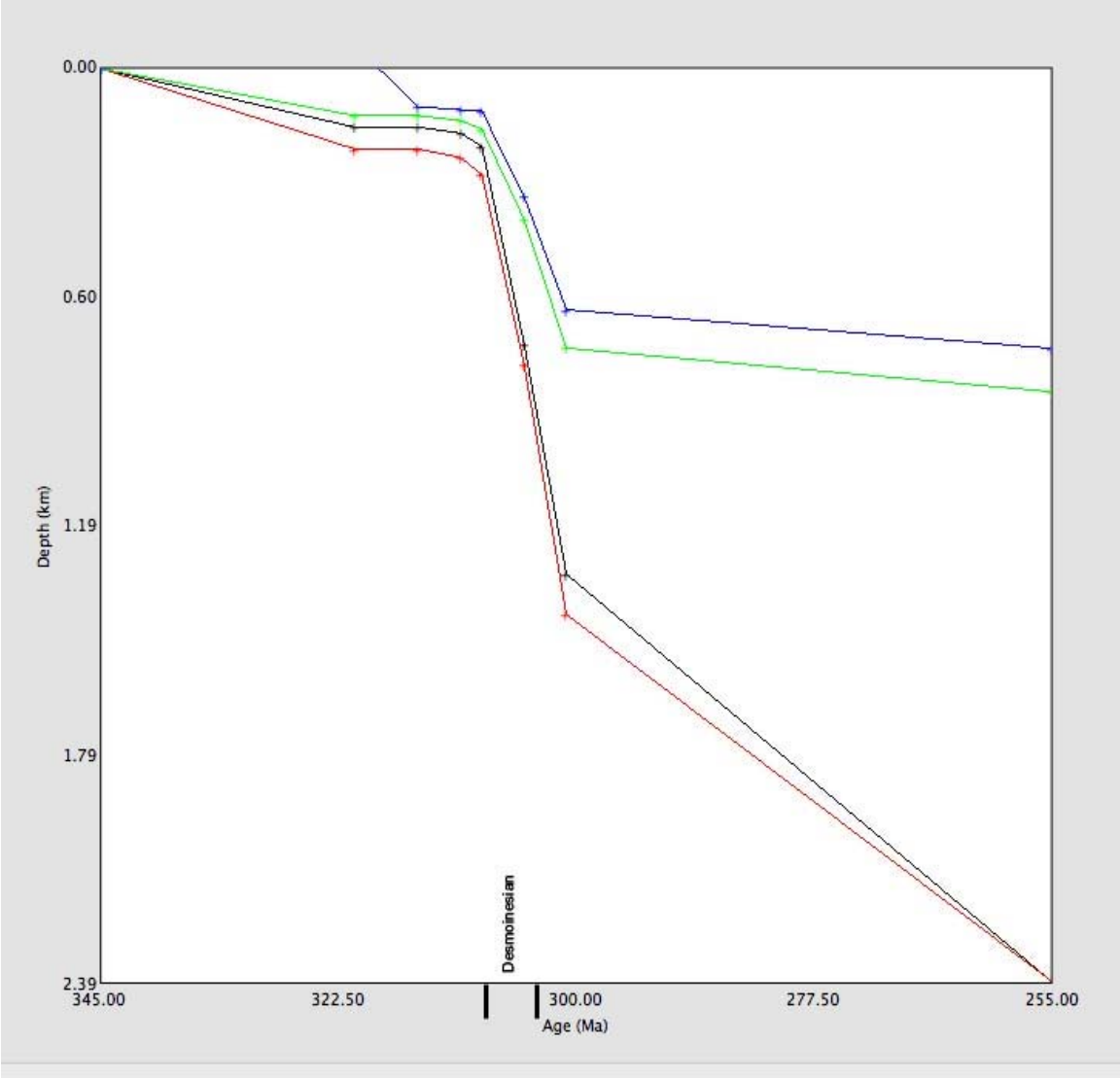

Figure 7.7: Subsidence plots for the Salt Valley #1 well. The colored plots represent: black = compacted; red = decompacted; green = sediment corrected; and blue = with water correction.

Elba Flats #1-30

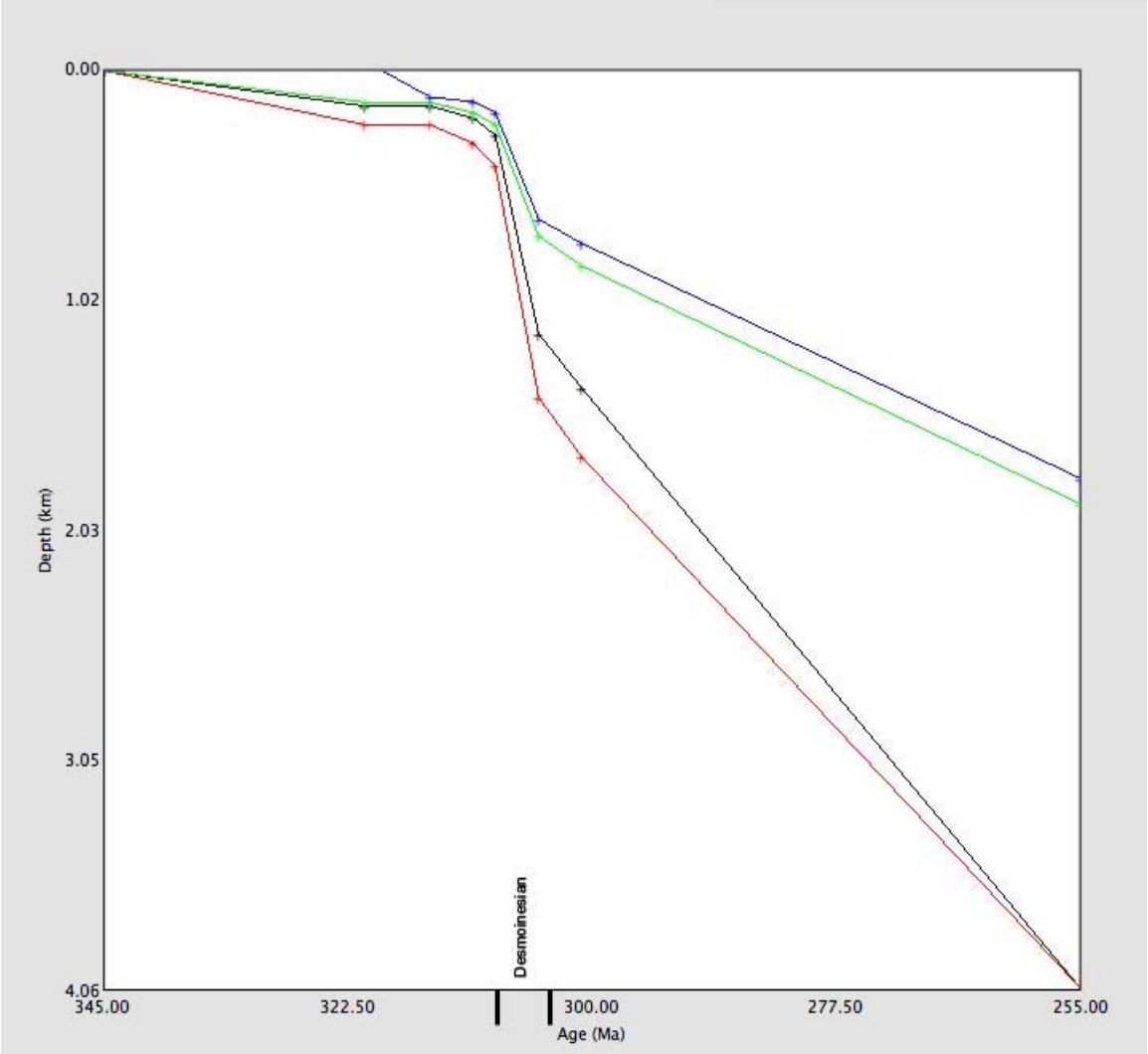

Figure 7.8: Subsidence plots for the American Petrofina Elba Flats #1-30 well. The colored plots represent: black = compacted; red = decompacted; green = sediment corrected; and blue = with water correction.

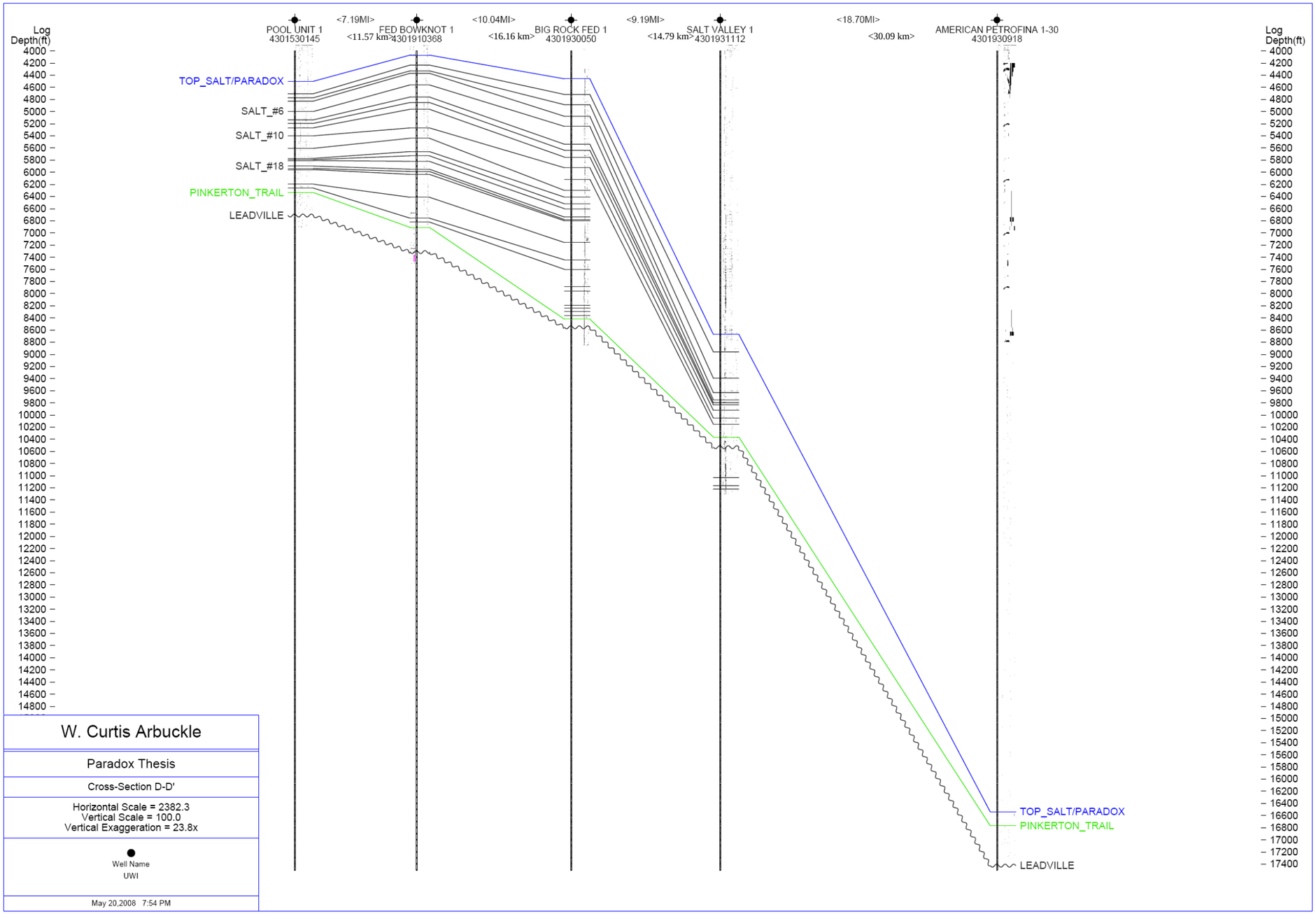

Figure 7.9: Cross-section D-D'.

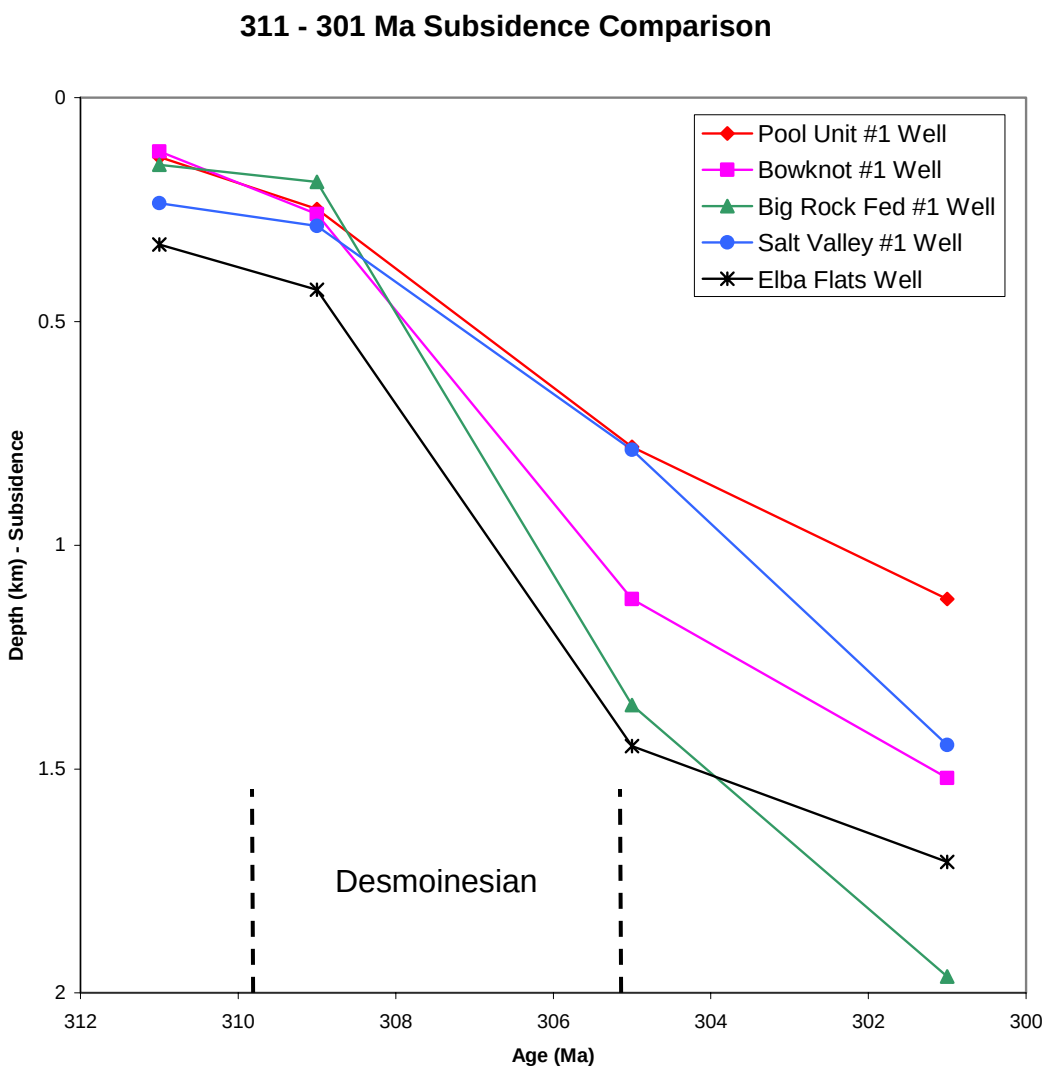

Figure 7.10: Graph illustrating the subsidence amount for five wells stretched across the northern Paradox Basin during the time interval of 311 – 301 Ma. A major subsidence event starts at about 309 Ma which corresponds to roughly the beginning of the Desmoinesian.

7.3 The Evolution of the Uncompahgre Uplift and the Paradox Basin

There have been several evolutionary models explaining and describing the formation of the Paradox Basin in relationship to the ARM Uncompahgre Uplift. These models are all supported by their own convincing evidence. However, they are all different from each other including the areas where each model has been applied.

Evidence including age estimates, isopach maps of individual evaporite cycles and subsidence modeling all indicate the Paradox Basin did not form due to a single evolutionary process and is likely the result of a progression of several complex processes.

7.3.1 Paradox and Uncompahgre Uplift Formation Model Comparison

There is no doubt the Paradox Basin and Uncompahgre Uplift shared a complex relationship during their respective formation. Whether or not they formed in a linked tectonic system is highly debatable and contested. Conflicting evidence supports ideas involving pull-apart tectonics, basin-wide flexural models, the development of the Uncompahgre Uplift after the formation of the basin and even implications for glacial-ice atop the uplift.

7.3.1.1 The Paradox Basin: A Pull-apart Basin

Stevenson and Baars (1986) believe the Paradox Basin and ARM formed due to extensional and pull-apart tectonics. During the Middle Pennsylvanian, east-west extensional strike-slip faulting along the Uncompahgre front, which is positioned at an intersection between regional and local basement faults and fracture zones (Figures 2.2 and 2.3), created a bend between the Uncompahgre and San Luis uplift(s). This bend released an area of strike-slip offset and extension creating basin subsidence (Stevenson and Baars, 1986). Sub-basins formed in response to local extension along the fault

lineaments, each having a varied amount of subsidence where the greatest occurred closer to the major controlling faults along the Uncompahgre front (Figure 2.12). The basin was deepened several times during the Middle Pennsylvanian due to further extensional basement faulting, but subsidence slowed during the Late Desmoinesian (Desert Creek stage) (Stevenson and Baars, 1986). At this juncture, minor amounts of wrench faulting created shoaling conditions in the southern part of the basin where the algal-carbonate mounds formed. Also, further basin subsidence occurred in the northern and eastern sections of the basin resulting in the deposition of marine and non-marine sediments by Early Permian time (Stevenson and Baars, 1986).

Based on the shape, structure and areal evidence presented by Stevenson and Baars (1986), accepting that the Paradox Basin and Uncompahgre Uplift were products of strike-slip extensional basement faulting seems plausible. Structural and tectonic features, including the local northeast-southwest and northwest-southeast trending basement faults and uplifts, support their theory. Resulting sub-basins and key evidence of a stress releasing bend/break in the Uncompahgre and San Luis uplift(s) compare well to other basins formed due to pull-apart tectonics.

Unfortunately, little data based on stratigraphic relationships were used in Stevenson and Baars' (1986) analysis. Utilizing well and seismic data could help solidify their theory which is primarily centered on tectonic associations. However, some stratigraphic and structural reconstructions, like those generated by Kluth and DuChene (2007), don't comply with Stevenson and Baars (1986) model.

7.3.1.2 The Paradox Basin: A Flexural Model

Barbeau (2003) interpreted the Paradox Basin as an intraforeland flexural basin formed due to flexural subsidence associated with the rise of the Uncompahgre Uplift. His model utilized subsidence history, shape, structural relationships and facies architecture to justify the interpretation of a foredeep zone that formed adjacent to the uplift as a result of crustal flexure (Figure 2.14). Barbeau (2003) also suggested there should be a positive crustal rebound structure called a forebulge that would form distally

to the foredeep. His model suggests this bulge coincides with the carbonate shelf located at the southern edge of the basin.

Barbeau's (2003) model contrasts with the previous pull-apart extensional interpretations made by Stevenson and Baars (1986) noting a lack of strike-slip offset. Barbeau (2003) also explains that the northwest-southeast trend of the Uncompahgre Uplift and the Paradox Basin suggest the two structures were formed together as a result of northeast-southwest shortening, again contrary to what Stevenson and Baars (1986) hypothesized.

Barbeau (2003) compared the Paradox Basin with other flexural-isolated foreland basins and the more closely related ARM basins. He explained how the northwest-southeast orientation of the Paradox Basin, combined with the major thrust fault system in the east (the Uncompahgre thrust) and the foreland basin facies architecture exhibited along the foredeep and forebulge, are analogous to other ARM basins. Furthermore, he implies that any model illustrating the formation of the ARM would consist of a system showing northeast-southwest contraction.

Barbeau's (2003) model raises several concerns including whether or not the Ouachita-Marathon thrust belt resulted in enough tectonic stress to cause shortening in the ARM uplifts and basins. The model and representative cross-section (Figure 2.14) strike roughly about 35 degrees south of perpendicular from strike of the Uncompahgre Uplift. Although this cross-section summarizes and fits the proposed model, it fails to incorporate much of the northern half of the basin. The northern half is by far the deepest and thus displays the greatest amount of subsidence. Therefore, to ignore these important features suggests the model may not be representative for the northern part of the basin. Additionally, strong evidence supporting a forebulge (which is structurally controlled) in the northwestern section of the basin is lacking, raising further questions about the accuracy of a flexural model for at least the northern Paradox Basin.

7.3.1.3 The Paradox Basin and Eagle Valley Evaporites

Recently, several authors including Kluth and DuChene (2006; 2007), Rasmussen (2006) and Kluth (2008) have speculated the Paradox Basin and the Eagle Valley evaporites were once connected, before the rise of the Uncompahgre Uplift. Rasmussen (2006) uses stratigraphic relationships of interlayered evaporites and carbonates abutting against the Uncompahgre Uplift, to suggest that the siliciclastics do not terminate against the uplift. This would only be possible if the Uncompahgre was not a positive feature at the beginning of Paradox Formation deposition. However, by late Desmoinesian and into Permian time, coarse arkosic material was being shed from the Uncompahgre Uplift into the basin. This suggests the uplift began to develop sometime during the Desmoinesian and escalated fast enough to erode the abundant amount of arkosic material into the basin by at least the beginning of Permian time.

Kluth and DuChene (2007) created several serial restorations of the Paradox Basin based upon one seismic line striking northeast-southwest across the Lisbon Valley, Gypsum Valley, Paradox Valley and Sinbad/Onion Creek salt structures. Their restorations involve removing the sediment load of the overlying Honaker Trail and Cutler formations, both of which caused significant differential loading and ultimately lead to salt wall/structure growth. Again, similar to Rasmussen (2006), the restorations illustrate the Uncompahgre Uplift was not a positive feature at the start of salt deposition, once more suggesting the Paradox Basin and Eagle Valley evaporites were connected.

Kluth (2008) suggested the San Luis Highlands were uplifted (Middle Pennsylvanian Desmoinesian time) before the Uncompahgre Uplift noting how some of the arkosic material shed from the highlands interfingers with several salt intervals in the southeastern section of the basin. Soon thereafter, the Uncompahgre began to develop further to the north but only after a significant percentage of the Paradox Formation, and maybe the Honaker Trail Formation, were already deposited.

The evidence presented by the authors described above is strikingly convincing, however there are several important questions that were not addressed and/or remain inconclusive. From what Kluth and DuChene (2007) presented in their restorations, there is no indication that basin-wide subsidence was incorporated into their model. Without

this information, it is hard to determine the timing, duration and thus evolution of the basin and Uncompahgre Uplift. Rasmussen (2006), Kluth and DuChene (2007) and Kluth (2008) together also fail to present any significant explanation(s) regarding basin formation prior to the development of the Uncompahgre Uplift. Their model therefore lacks, at least in the author's opinion, an important aspect of the Paradox Basin's evolution.

7.3.1.4 Late Paleozoic Glacial Evidence on the Uncompahgre Plateau

Soreghan *et al*. (2007) published an extensive study on the processes, timing and formation of Unaweep Canyon. Unaweep Canyon is about 0.62 miles (1 km) deep and 3.73 miles (6 km) wide and cuts perpendicular to the northwest-southeast trending Uncompahgre Uplift (Figure 7.11). It has been suggested that the ancient Gunnison River or the Colorado River once flowed through the area carving out the canyon, but a lack of (a large quantity of) typical river sediments and gravels poses additional questions.

Recent paleomagnetic, palynology and provenance data hint that the canyon fill is of late Paleozoic age (Soreghan *et al*., 2007). Further evidence of apparent Permo-Pennsylvanian glacial deposits (dropstones) within the canyon suggests the canyon itself was formed due to glacial processes (Sorgehan and Sorgehan, 2003). This implies there was ice at the equator (roughly) during canyon formation, thus appearing inconsistent with the late Paleozoic setting typically characterized for the region. If the climate of the late Paleozoic experienced rapid changes, then low-elevation, low-latitude glaciation could be possible. This however seems rather extreme based on global and regional climate studies and relationships. A more likely, but still unproven, hypothesis is that the Uncompahgre Uplift was much higher in elevation than previously thought. For modern tropical glaciation to occur, an elevation of 13,100 – 16,400 feet (4,000 – 5,000 m) is required (Soreghan *et al*., 2007). Although this is reasonable in theory, it may be implausible requiring a significant orogenic collapse of the Uncompahgre, following the conclusion of uplift, which has yet to be observed structurally (Soreghan *et al*., 2007).

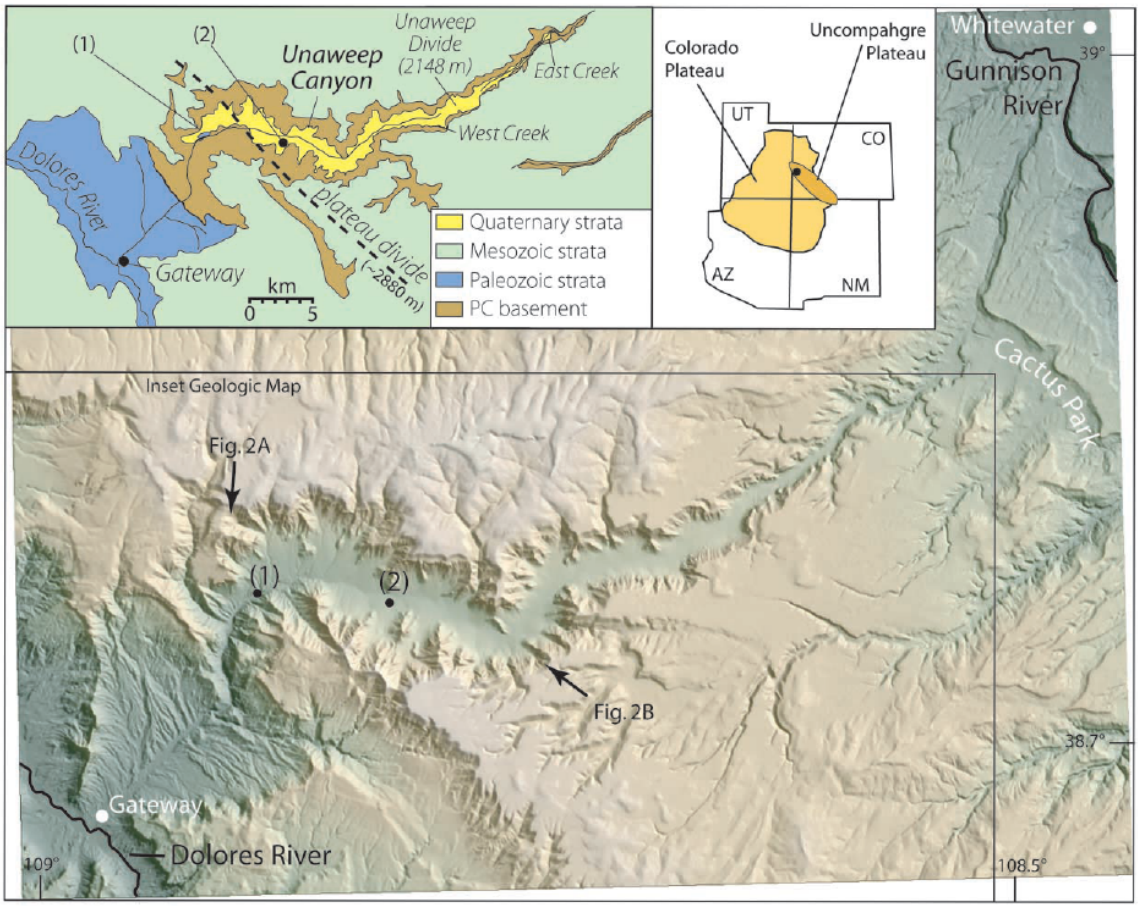

Figure 7.11: Figure and map showing the location and strata of Unaweep Canyon (after Soreghan *et al.*, 2007).

7.3.2 The Formation and Timing of the Uncompahgre Uplift – A New Perspective

The Uncompahgre and San Luis uplifts created a continuous Pennsylvanian tectonic highland stretching from southwestern Colorado to central-eastern Utah, and formed during the Late Paleozoic as part of the Ancestral Rocky Mountains.

By the end of Mississippian time there were probably several hundreds to thousands of feet of early and middle Paleozoic age strata extending across the current location of the Paradox Basin and Uncompahgre Uplift (Figure 7.12). Based on lithofacies data and stratigraphic relationships, the Uncompahgre and San Luis uplifts first became positive in their southern extremities by early Pennsylvanian time (Wengerd, 1958; Fetzner, 1960).

Evidence based upon basin reconstructions (Paz Cuellar, 2006), evaporite cyclicity isopach maps, subsidence modeling and stratigraphic relationships, suggest that by Middle Pennsylvanian (Desmoinesian) time the Uncompahgre front in the northern and eastern sections of the basin was in existence, but was not as tectonically active as the San Luis complex further to the south (Figure 7.12). At this time the Uncompahgre probably was not significantly elevated above local sea-level, if at all. However, the uplift itself and the associated trough or foredeep still likely affected the depositional patterns of the Paradox Formation. This will be discussed further in the next section.

A significant pulse of uplift along the central part of the Uncompahgre (in the vicinity of the Colorado-Utah state line) occurred near the end of evaporite deposition (Figure 7.12) (Elston and Shoemaker, 1960). This pulse is marked by arkosic and granitic material (as coarse as boulder size) interbedded with the upper part of the Paradox Formation in Sinbad Valley (Elston *et al*., 1962). Further tectonic pulses followed giving rise to the Uncompahgre Uplift, which by Late Desmoinesian/Early Missourian time, had become a strongly positive feature and was shedding arkosic material at least 20 miles (32.2 km) into the basin (Elston and Shoemaker, 1960).

The Uncompahgre experienced its most significant uplifting episode near the end of the Pennsylvanian and into Permian time (Figure 7.12). Evidence of an abundant influx of arkosic material into the Uncompahgre trough (undifferentiated Culter Formation) supports this important period of uplift. Several other tectonic pulses have

been documented following the major uplifting episode in Early Permian time. The deposition of the Late Triassic Moenkopi Formation marks the end of any further uplift or significant movement along the Uncompahgre (Molenaar, 1981; Doelling, 1983; Paz Cuellar, 2006).

7.3.2.1 The Uncompahgre Uplift and its Impact on the Northern Paradox Basin

There is strong evidence supporting the idea that the San Luis Uplift experienced greater amounts of uplift and tectonic activity before the northern part of the Uncompahgre became a positive feature (Fetzner, 1960). However, even if the structure wasn't exposed significantly above local sea-level, it still could have influenced sedimentation patterns.

A lack of an abundant amount of arkosic material located in the oldest evaporite cycles suggests the Uncompahgre was not exposed above sea-level and thus not subject to typical erosion processes early in Desmoinesian time. However, the Uncompahgre may have already begun thrusting upwards, but the majority of it remained below sea-level (Figure 7.13). Also at this time, the Paradox Basin and the Eagle Basin would have been connected at least in the northern part of the Paradox Basin.

If the Uncompahgre was a submerged structure, it, and the immediate surrounding area, could have been ideal locations for increased carbonate accumulations. This is observed by Paz Cuellar (2006) where he identified an area east of Onion Creek where there was a lack of significant arkosic material in Middle Pennsylvanian strata (and thus a greater accumulation of non-evacuated salt) and increased amounts of carbonates. Personal communication with Gary Nydegger (2007) also supports this conclusion noting how there were increased carbonate accumulations within the Paradox Basin #1 well, typically not found further west into the basin. Also, if the Uncompahgre was a low relief or submerged structure below relative sea-level (Figure 7.13), it still would have been accompanied by significant amounts of subsidence adjacent to the uplift. Basin subsidence probably began near the end or shortly after the deposition of the Pinkerton

Figure 7.12: Diagrammatic series of cartoons showing the evolutionary progression of the northern half of the Paradox Basin. (A) Pre 318 Ma – Regional thickening to the west and northwest of pre-Pennsylvanian strata (Nuccio and Condon, 1996). No evidence supporting the existence of the basin. (B) ~315-310 Ma – Regional thickening to the south and southwest of the Pennsylvanian Pinkerton Trail Formation (Hite, 1960; Frahme and Vaughn, 1983; Doelling, 1988). There is little to no evidence supporting significant basin subsidence. (C) ~310 Ma – Start of major subsidence within the basin accompanied by the deposition of the oldest evaporite cycles (29-20) of the Paradox Formation. Uplift along the San Luis Highlands in the south and the beginning of uplift along the Uncompahgre front (although it may not have been a positive feature). There was likely a connection between the Paradox and Eagle basins at this time. (D) ~305 Ma – The end of Paradox Formation evaporite deposition. Continued uplift along the Uncompahgre and San Luis uplifts, but there could have been several connection pathways still joining the Paradox and Eagle basins. Also at this time, carbonates were accumulating along the peripheral forebulge adjacent to the southern and southwestern margins of the Paradox Basin. (E) ~300 Ma – Continued uplift along the Uncompahgre and San Luis uplifts during the deposition of the Pennsylvanian Honaker Trail Formation. Increased amounts of alluvial material were being shed into the basin. Any previous connection(s) between the Paradox Basin and Eagle basins would have been severed by this time. (F) ~Middle Permian time – Continued uplift along the Uncompahgre/San Luis uplift(s) with increased amounts of coarse arkosic material deposited into the basin as evidence given by the deposition of the proximal Cutler Formation.

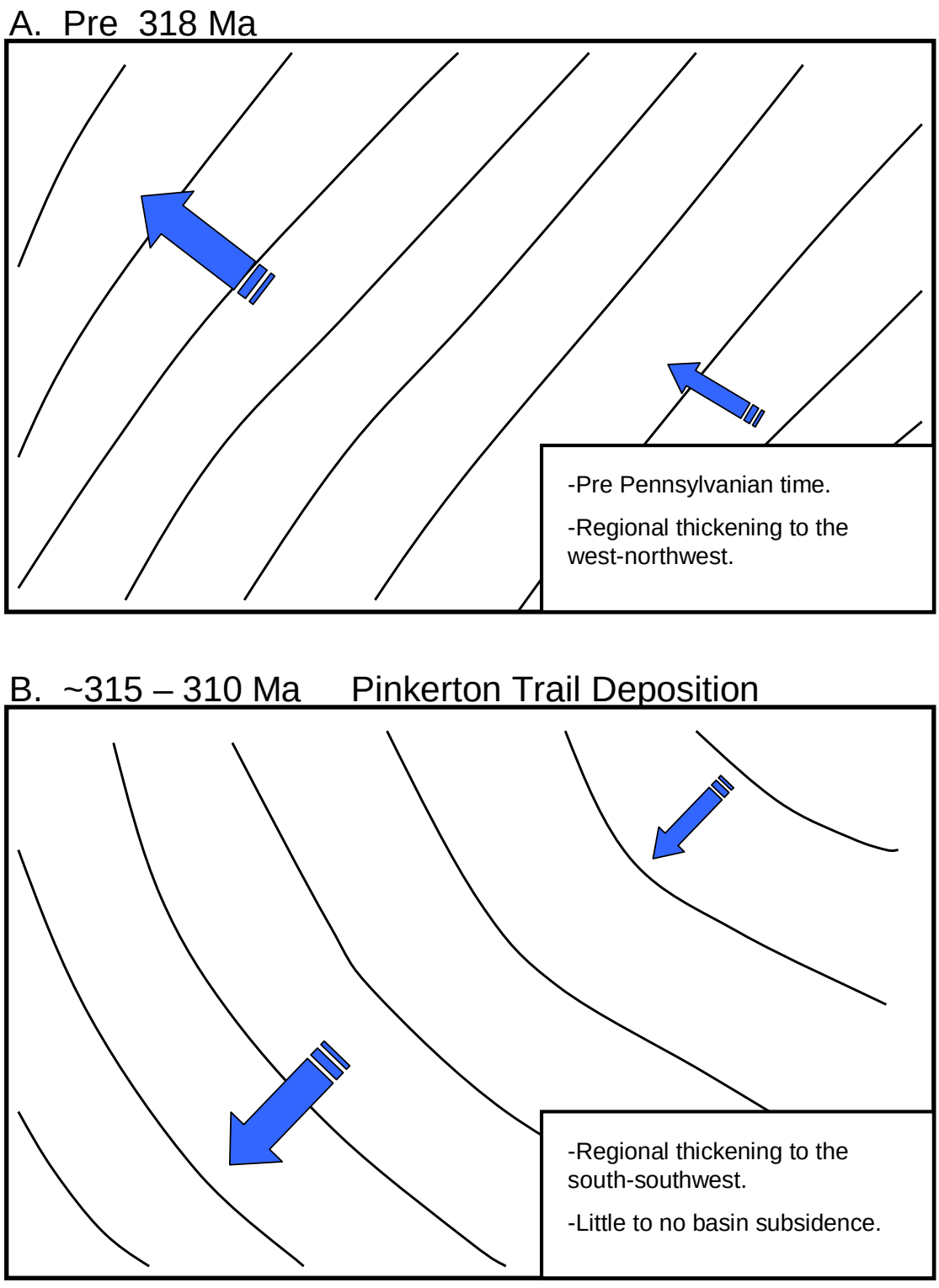

Figure 7.12a: For caption and explanation, see previous page.

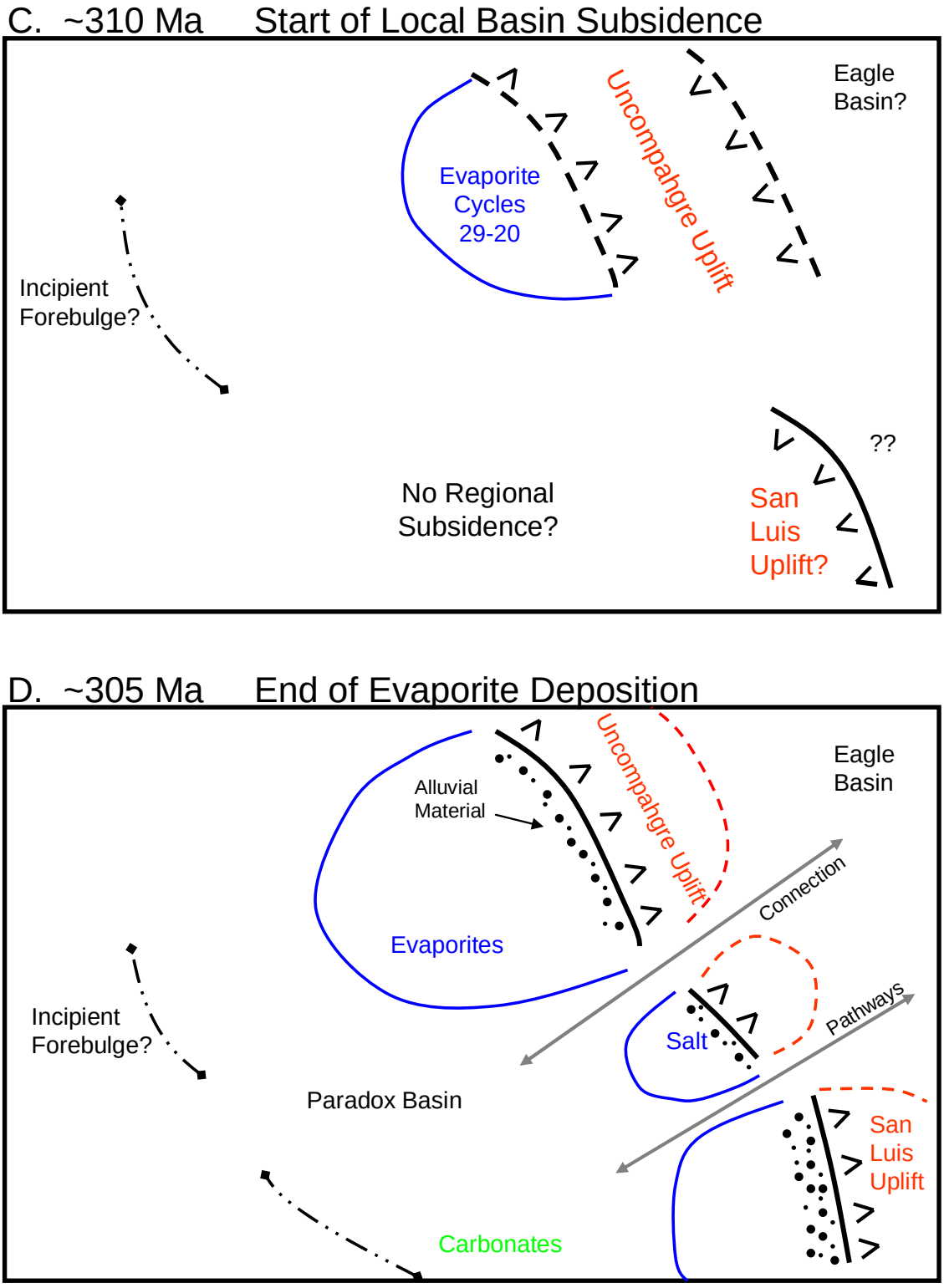

Figure 7.12b: Continued.

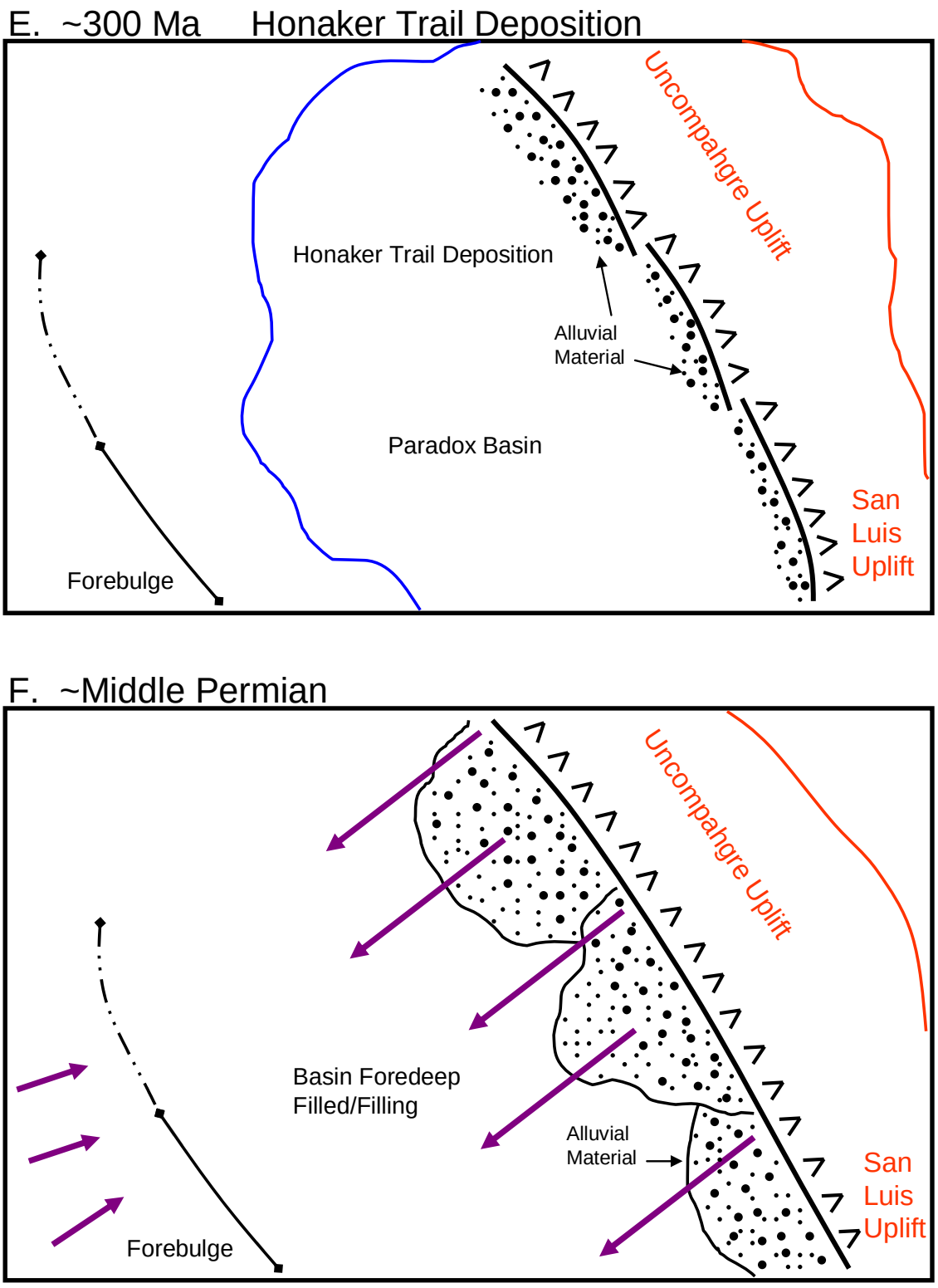

Figure 7.12c: Continued.

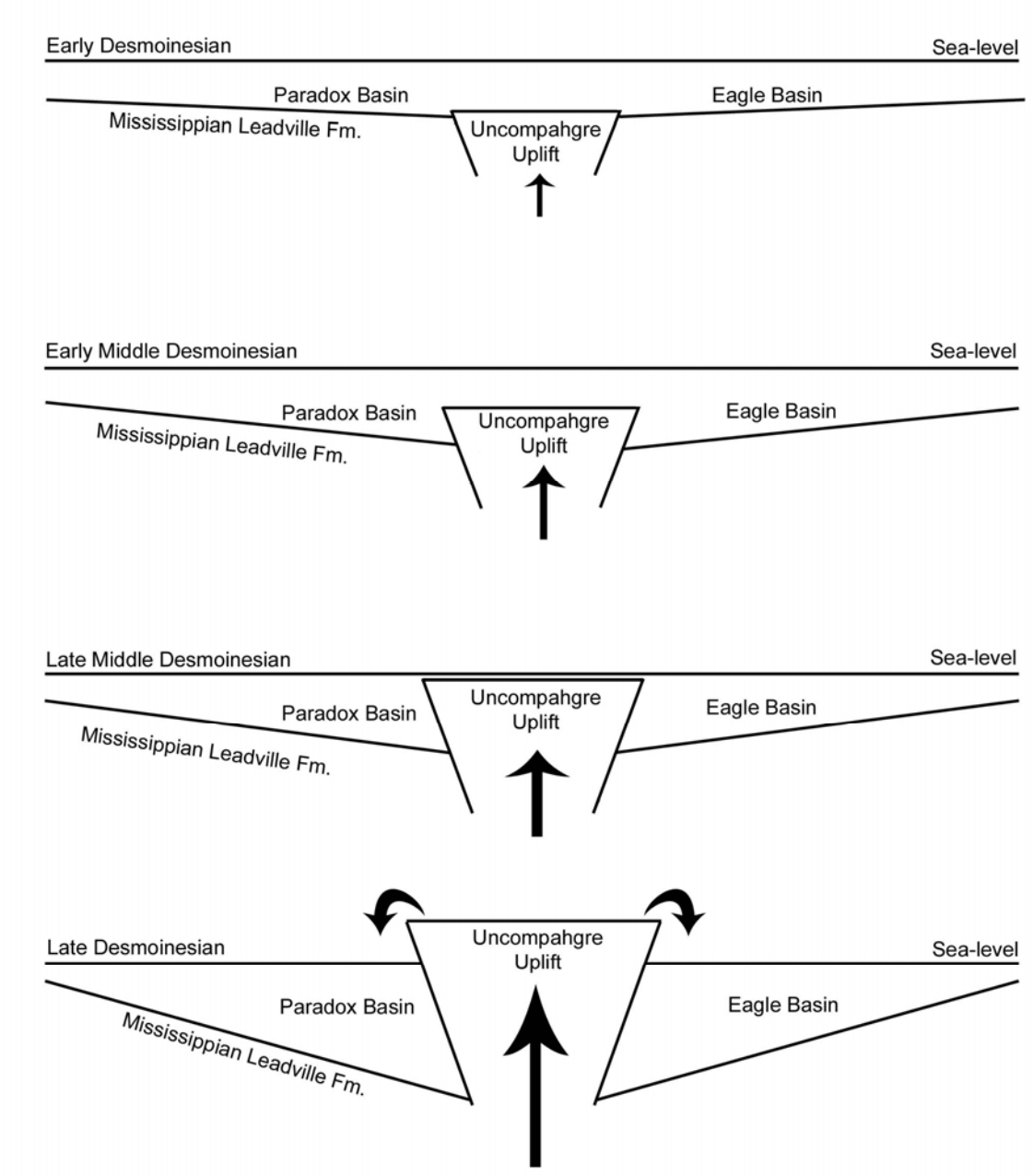

Figure 7.13: A schematic diagram illustrating the possible progression of the Uncompahgre Uplift throughout Desmoinesian time. Notice that although the uplift was not above sea-level during Early Desmoinesian time, it was still affecting basin subsidence. This diagram also suggests the Paradox Basin and the Eagle Basin (Eagle Valley evaporites) were once connected early in the basin(s) evolution.

Trail Formation as illustrated by the consistent and continuous structural dip of the formation (Figure 2.21).

By Middle Desmoinesian time, the Uncompahgre was at or near sea-level and had enough associated subsidence, partly driven by sediment loading, to create the initial stages of the foredeep we observe today. It is also important to note that at this time the Paradox and Eagle basins may have still been connected and were not completely separated from each other. Portions of the Uncompahgre Uplift may have been above local sea-level acting almost like small islands with channels between them still allowing the two basins to be connected (Figure 7.12).

Near the end of the Pennsylvanian and into Permian time, evidence from basin reconstructions, evaporite cyclicity isopach maps, subsidence modeling and stratigraphic relationships all indicate the Uncompahgre Uplift had become a strongly positive structure (Figure 7.12). By this time the basin had subsided over 12,000 feet (3,650 m) (Figures 2.10 and 2.18) within the foredeep located adjacent to the uplift, and was completely disconnected from the Eagle Basin located in Colorado.

7.3.2.2 Uncompahgre Uplift – Unanswered Questions

Questions still remain about the elevation achieved by the Uncompahgre Uplift. Wells drilled in the north-eastern section of the basin contain significant amounts of arkosic material in what is interpreted as age-equivalent Paradox Formation. One could argue that the majority of salt has been evacuated from this part of the basin, and that the overlying arkosic material is not part of the Paradox Formation but rather Late Pennsylvanian in age or part of the Cutler Formation (Permian). If indeed the clastic material was deposited as part of the Paradox Formation, then there must have been a local, positive, granitic structure shedding material into the basin. The GCRL Energy LTD Seismosaur Federal #1 well (T 21S, R 20E, sec. 20) is an interesting data point (Figure 7.14). It is an unusual well having clastic intervals, between salt zones, over 500 feet (152 m) in thickness (Utah State Oil and Gas, 2007). These intervals are also composed of sandstones, limestones, shales, dolomites, marlstones as well as glauconite

Figure 7.14: Map showing the location of the GCRL Energy Ltd. Seismosaur Federal #1 well. Image modified from Google Earth (2007).

which is altered from detrital biotite in shallow marine waters under reducing conditions (Nesse, 2000). This again might suggest there was a positive granitic structure locally available to source the deposition of these clastic zones. It is possible there were some sections of the Uncompahgre Uplift that were above relative sea-level creating islands that were able to shed this localized clastic material.

7.3.2.3 Early Clastic Sediment Supply

It is still unclear where much of the clastic material came from in the lower, older, evaporite cycles. Within the silty dolomite interbeds (transgressive and regressive), there are abundant amounts of quartz and feldspar (near 40 percent of the total mineralogy). These grains are well sorted and very-fine to fine-grained much like the hosting dolomite. It is unclear how and why these detrital grains were deposited with the dolomite and how they reached such a distance from the available and known source areas.

There were two known main source areas for the clastic material during the time of deposition; the Uncompahgre Uplift to the east and the shelf margin in the south. Undoubtedly both sources supplied clastic material to the basin synchronously by the end of the Pennsylvanian (Wengerd, 1962).

The quartz and other related minerals may have reached the center of the basin by low density currents over the top of dense salinity brines circulating down to the bottom of the basin. Raup and Hite (1992) suggest these currents may have collected clastic material as they advanced along the rising shoreline and past the arkosic alluvial fans that formed adjacent to the rising Uncompahgre Uplift. Such movement across significant distances may have led to the high degree of sorting within the clastic grains. Harms and Williamson (1988) proposed a similar mechanism of transport into deep water involving the Delaware Mountain Group in the Delaware Basin, Texas and New Mexico. The extreme level of sorting might also suggest the clastic grains are eolian in origin (Raup and Hite, 1992).

It is also important to note that during times of sea-level transgression, amplified humidity levels created an increase in fluvial input into the basin. A lack of substantial

vegetation, combined with warmer temperatures and higher humidity levels would favor increased chemical and physical weathering rates (Scheffler *et al*., 2003). This is especially true when eroding younger features (Van der Zwan, 2002) and applies directly to the Uncompahgre and the San Luis uplift(s) adjacent to the Paradox Basin. Therefore, much of the arkosic material, terrestrial organic matter and other related material found within the center of the basin may have been transported by fluvial processes. This would also account for the high degree of sorting identified within the clastic grains.

Most of the sandstones, sometimes classified as turbidites, are located in the northern part of the basin. If the Uncompahgre was not a strongly positive feature during sandstone deposition, an alternative source is required. These sandstones may have been transported into the basin via the Freemont embayment or through the Oquirrh passageway.

7.4 QEMSCAN Analysis

The main purpose of testing the five dolomitic samples using the QEMSCAN analysis instrument was to compare the mineralogical composition of each sample between transgressive and regressive sequences and to attempt a correlation across the basin.

7.4.1 Transgressive and Regressive Comparisons

Four samples from the Delhi-Taylor Oil Company Cane Creek No. 1 core, specifically from the transgressive and regressive lithological units of evaporite cycles 2 and 3, were analyzed (Table 5.1). As discussed previously in Chapter 5, there is an abundant amount of quartz and other related detrital material identified with each transgressive sample (Figures 5.5 and 5.6) compared to the regressive samples (Figures 5.7 and 5.8). It is believed the increased amount of detrital grains is a result of rising water levels within the basin stirring up and collecting any material that had been

deposited into the basin after halite deposition and before the start of the next sea-level transgression. It is also likely any loose material located along the edge of the basin, possibly from alluvial fans, would be collected and mobilized by the incoming transgressive waters and thus deposited into basin.

7.4.2 Basin Correlation

In an attempt to correlate clastic zone mineralogical assemblages across the basin, the samples from the Cane Creek core (west) were compared to one outcrop sample collected from the Onion Creek diapir (east). The preliminary thinking, before the samples were analyzed, involved the Onion Creek sample comprising significant amounts of granitic-derived material, compared to the samples from the Cane Creek core, if the detrital source was the nearby Uncompahgre Uplift. The results however, were rather inconclusive and can possibly be related to several problems involving the outcrop and rock/sample characterization.

The Onion Creek sample compares better to the regressive dolomitic samples identified in cycles 2 and 3 of the Cane Creek core (Figures 5.9 – 5.11 and Table 5.2). It is composed mostly of dolomite, illite and a dolomite-silicate matrix which has been analyzed as an extremely fine-grained assortment of dolomite and quartz material. It is also the only sample of the five analyzed that displayed any identifiable laminations.

There are several problems that limit the effectiveness and accuracy of using the Onion Creek sample for a basin-wide comparison. The sample was collected from one of a very few outcrops of the Paradox Formation in the northern half of the basin. In addition, the outcrop was highly altered and distorted due to caprock formation processes. The sample was also selected from an atypical dolomitic bed (very thin) compared to the carbonate intervals sampled from the core. Finally, it is unclear from which clastic zone, let alone evaporite cycle, the sample was taken. Because of the diapiric and caprock structural and chemical formation processes, it may not be possible to ascertain this vital information. Therefore, to create a better basin-wide correlation using the clastic zone

mineral assemblages, the Onion Creek specimen should be replaced by several samples taken from a cored interval located away from any major salt-related structure.

7.5 Hydrocarbon Exploration – Economic Potential

The hydrocarbon potential of the Pennsylvanian age rocks within the northern Paradox Basin is once again being recognized. Increased leasing and drilling activity, signifies the potential for significant hydrocarbon accumulations. Recently, Delta Petroleum has drilled several wells targeting the clastic intervals within the Paradox Formation (Delta Petroleum, 2008) and Golden State Resources has completed a successful well targeting what appears to be carbonate reservoirs within the upper Paradox Formation (Golden State Resources, 2002).

7.5.1 Source Rocks

The hypersaline environmental setting of the Paradox Basin is ideal for the preservation of organic material which became the ultimate source for much of the regions hydrocarbons. The most important Pennsylvanian source rocks are the black organic-rich shales. Hite *et al.* (1984) and Nuccio and Condon (1996) did extensive studies based on these shales and concluded many are ideal for hydrocarbon generation noting how TOC values, thermal maturity trends and genetic potential ($S_1 + S_2$) relationships all indicate favorable conditions. Nuccio and Condon (1996) used this information to create burial, thermal and hydrocarbon generation potential models for several areas throughout the basin (Figures 7.15 and 7.16).

For much of the petroleum-rich southern part of the basin, the black shales from clastic cycles/intervals 2, 3 (the Gothic shale), and 5 (the Chimney Rock shale) are the most significant because of their high kerogen content and stratigraphic location below many of the carbonate algal mounds (Hite *et al.*, 1984). In the northern part of the basin these same shales show similar hydrocarbon generation potential. However, along with

Figure 7.15: Burial, thermal and hydrocarbon generation potential model for the area around the town of Green River, Utah. A) Cambrian time through present day. Notice how there is a significant burial period during the Middle Pennsylvanian. This likely corresponds to the uplift of the Uncompahgre Front. B) Expanded time scale illustrating 100 Ma to present and displaying the phases of hydrocarbon generation (after Nuccio and Condon, 1996).

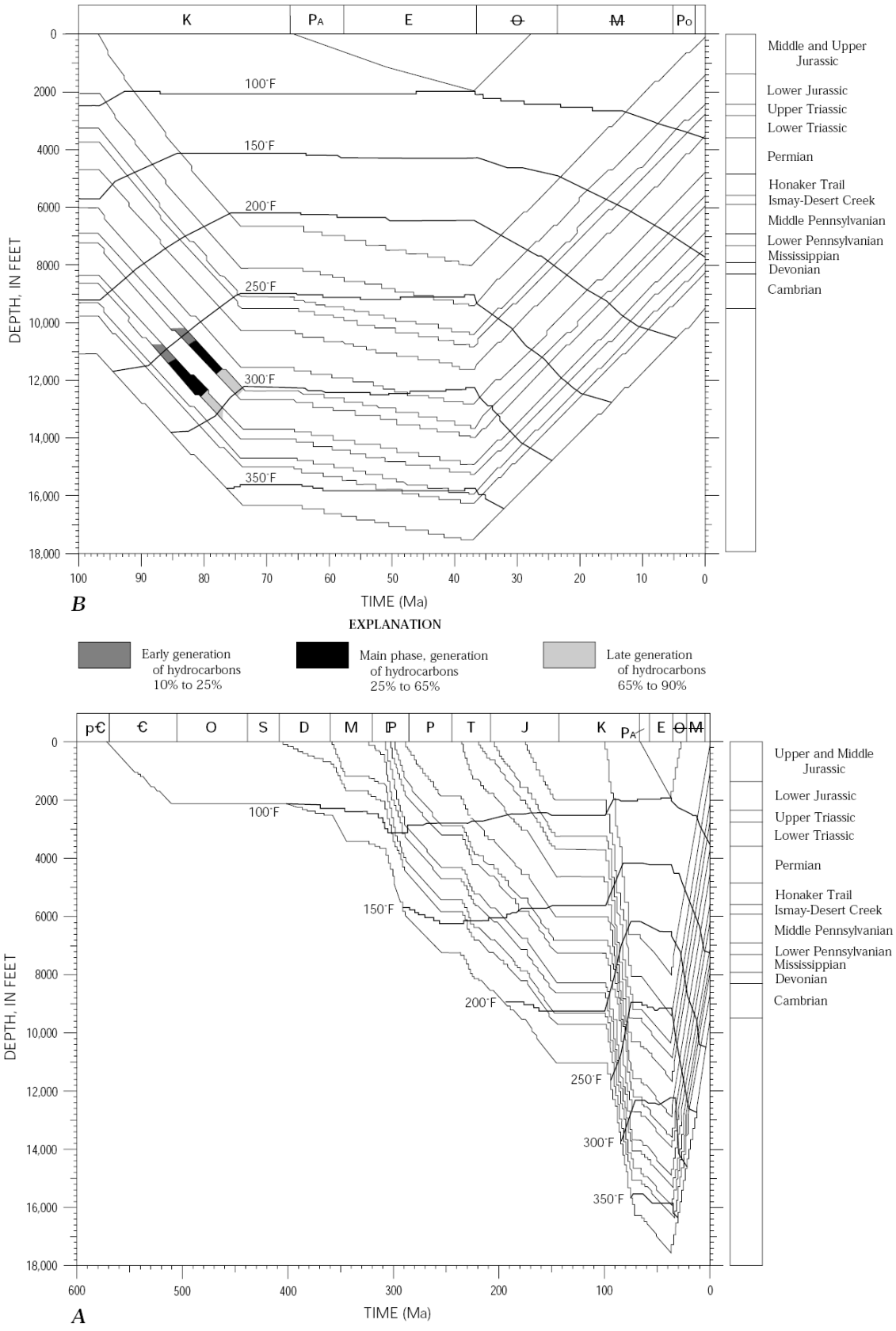
K
PA
E
O
M
PO
0
2000
4000
6000
8000
10,000
12,000
14,000
16,000
18,000
DEPTH, IN FEET
100°F
150°F
200°F
250°F
300°F
350°F
100
90
80
70
60
50
40
30
20
10
0
TIME (Ma)
B
Middle and Upper Jurassic
Lower Jurassic
Upper Triassic
Lower Triassic
Permian
Honaker Trail
Ismay-Desert Creek
Middle Pennsylvanian
Lower Pennsylvanian
Mississippian
Devonian
Cambrian
EXPLANATION
Early generation of hydrocarbons 10% to 25%
Main phase, generation of hydrocarbons 25% to 65%
Late generation of hydrocarbons 65% to 90%
pЄ
Є
O
S
D
M
IP
P
T
J
K
PA
E
O
M
0
2000
4000
6000
8000
10,000
12,000
14,000
16,000
18,000
DEPTH, IN FEET
100°F
150°F
200°F
250°F
300°F
350°F
600
500
400
300
200
100
0
TIME (Ma)
A
Upper and Middle Jurassic
Lower Jurassic
Upper Triassic
Lower Triassic
Permian
Honaker Trail
Ismay-Desert Creek
Middle Pennsylvanian
Lower Pennsylvanian
Mississippian
Devonian
Cambrian

Figure 7.16: Burial, thermal and hydrocarbon generation potential model for the area around the town of Moab, Utah. A) Cambrian time through present day. Notice how there is a significant burial period during the Middle Pennsylvanian. This likely corresponds to the uplift of the Uncompahgre Front. B) Expanded time scale illustrating 100 Ma to present and displaying the phases of hydrocarbon generation (after Nuccio and Condon, 1996).

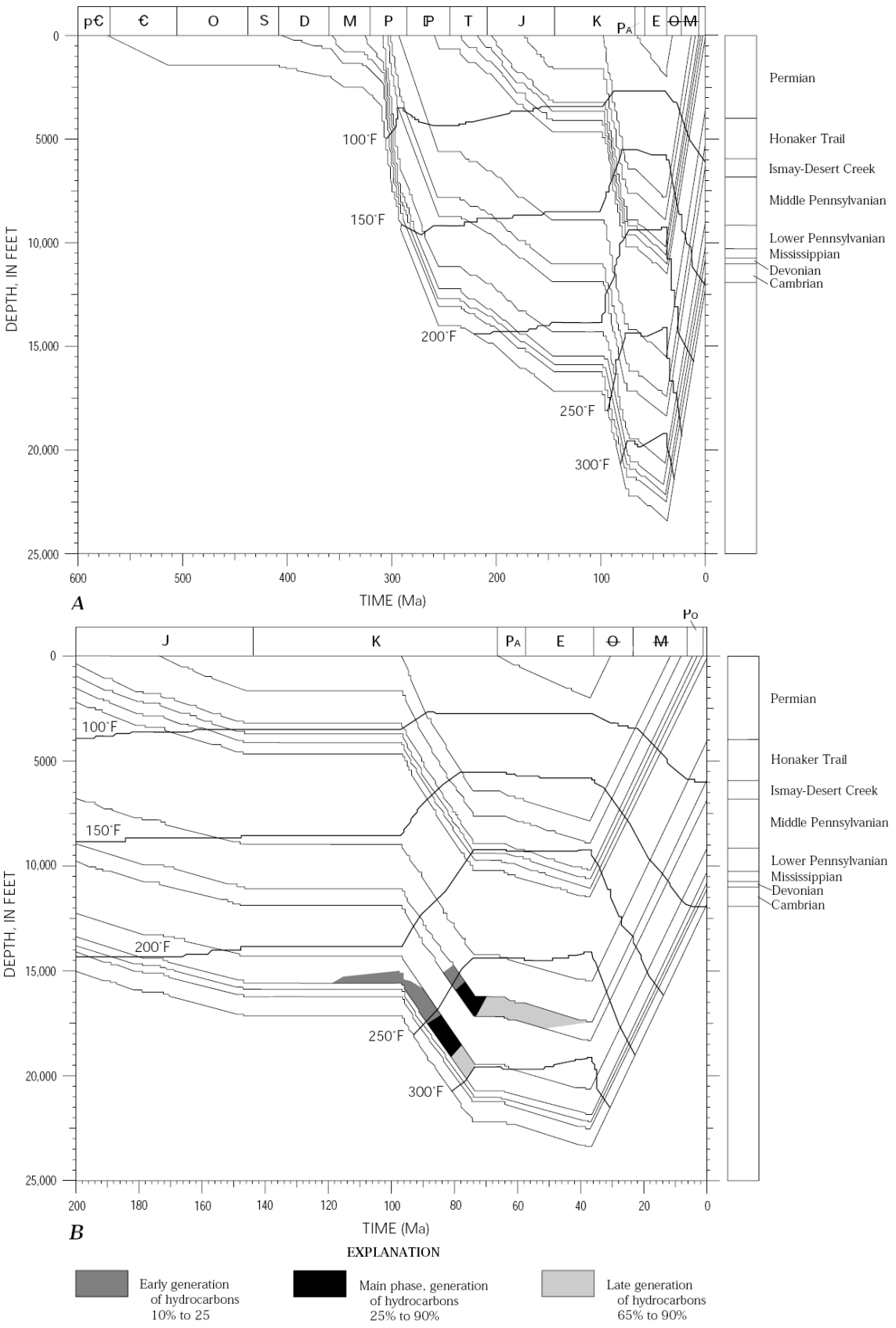
pЄ
Є
O
S
D
M
P
IP
T
J
K
PA
E
O
M
100˚F
150˚F
200˚F
250˚F
300˚F
DEPTH, IN FEET
TIME (Ma)
A
Permian
Honaker Trail
Ismay-Desert Creek
Middle Pennsylvanian
Lower Pennsylvanian
Mississippian
Devonian
Cambrian
PO
B
EXPLANATION
Early generation of hydrocarbons 10% to 25
Main phase, generation of hydrocarbons 25% to 90%
Late generation of hydrocarbons 65% to 90%

most of the other clastic zone black shales, they tend to be much thinner averaging less than 15 feet (4.57 m) thick (Hite *et al.,* 1984). Traditionally the Cane Creek shale (clastic zone 23) has been the most productive of the clastic intervals. Although much of the Cane Creek cycle is over-mature (due to a greater depth of burial in a rapidly subsiding basin) for oil (Nuccio and Condon, 1996), the potential for gas from thermally cracked oil, thermogenic gas and condensate is considerable and is currently being produced.

During the drilling of several wells within the northern part of the Paradox Basin, extreme over-pressured clastic zones (saturated with brine water, oil and/or gas) were encountered (Hite *et al.,* 1984; Walter K. Arbuckle and Elliott A. Riggs, 2007, personal communication). It is likely these intervals are over-pressured due to the generation of large volumes of hydrocarbons. It is also important to note almost all of the hydrocarbons generated from the black shales are retained within the source rocks themselves. The overlying anhydrite and halite zones act as perfect sealing layers and the transgressive and regressive dolomites are very non-porous having an average porosity of 5.9% (QEMSCAN analysis). Therefore identifying and locating zones of natural fractures and utilizing horizontal drilling techniques may increase the exploration potential of these black shales (Walter K. Arbuckle, 2007, personal communication).

As mentioned previously, the halite zone within the evaporite cycles is not pure, but is interlaced with anhydrite intervals, clastic material and large quantities of organic matter. Interestingly, the presence of such abundant organic matter within the halite could be considered a potential source rock (mainly for gas) (Walter K. Arbuckle, 2007, personal communication), but would have had to of migrated into a reservoir facies rather early (Friedman, 1982).

7.5.2 Carbonate Reservoirs

Carbonate reservoirs in the northwestern portion of the basin are currently being explored. Golden State Resources drilled the Paradox Basin #1 well (T 23S, R 23E, sec. 16) on top of an up-thrown basement fault block (Figures 7.17 and 7.18). Their targeted

intervals included sub-Pennsylvanian reservoirs, but they encountered shows within Pennsylvanian-aged strata. Most of these shows are thought to be within carbonate rocks and/or within carbonate buildups (Figure 7.18) (Golden State Resources, 2002). The absence of major salt accumulations (either non-depositional or welded) (Gary Nydegger, 2007, personal communication) and the presence of significant thicknesses of carbonates, highlight the possibility of considerable hydrocarbon accumulations atop these fault blocks.

7.5.3 Fine Grained Sands – Turbidites

The fine-grained sands facies, which have often been characterized as turbidites, could be highly significant potential reservoirs. However, most of these sands tend to be thin and laterally inconsistent making exploration and identification difficult. Further petroleum exploration near the Uncompahgre Uplift would provide a better understanding of the economic potential of the turbidites.

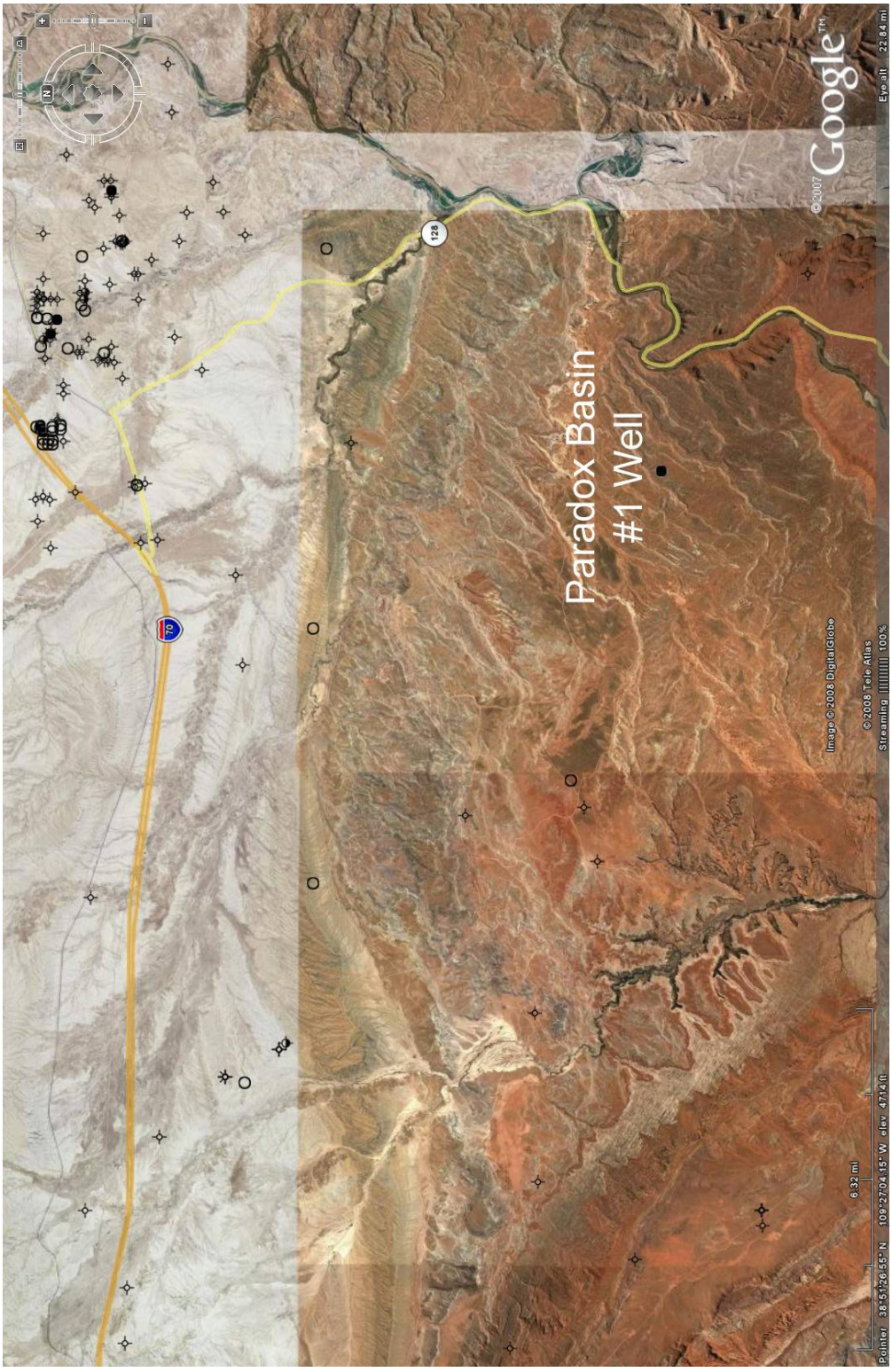

Figure 7.17: Map showing the location of the Paradox Basin #1 well (modified from Google Earth, 2007).

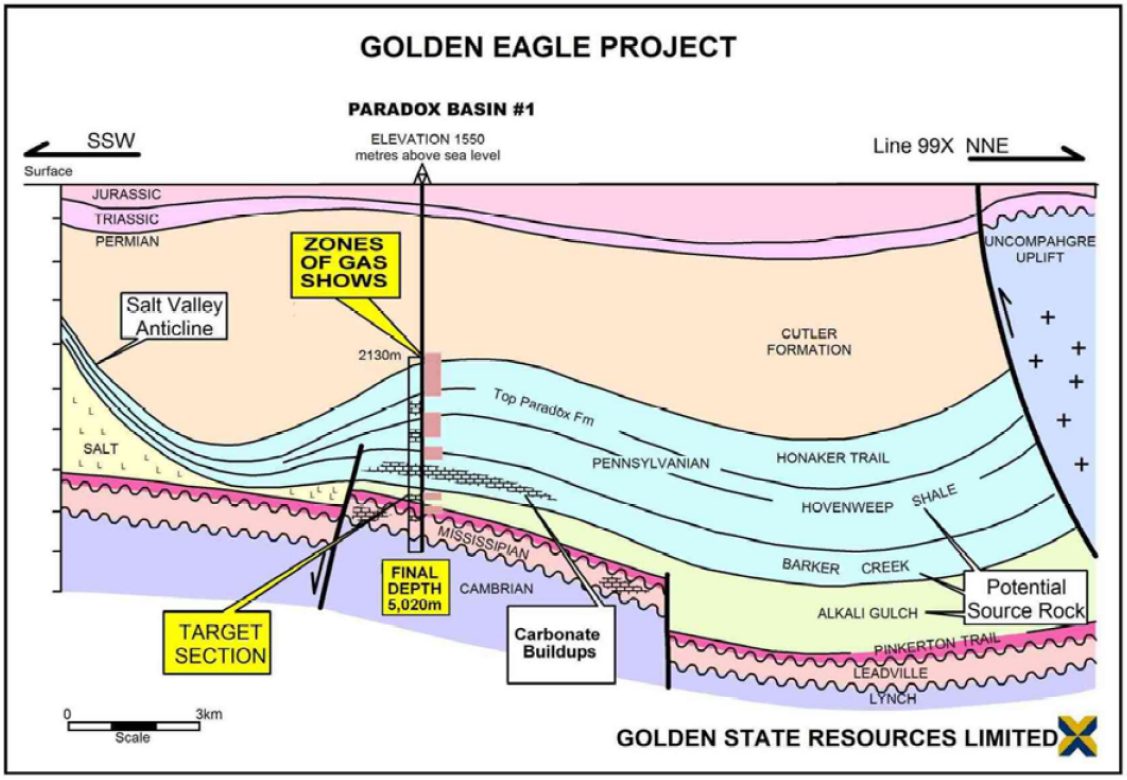

Figure 7.18: Illustration of the lithologies encountered in the Golden State Resources Paradox Basin #1 well (Golden State Resources, 2002).

CHAPTER 8

CONCLUSIONS AND RECOMMENDATIONS

The Pennsylvanian Paradox Formation was a pivotal factor in determining the formation of the northern Paradox Basin. Its relationship to the evolution of the ARM Uncompahgre Uplift played an integral part in determining the evolution, timing and formation of the basin itself. The following are conclusions from this study:

8.1 Periodicity and Mechanisms Involving Pennsylvanian Cyclicity – Paradox Formation

1. The cyclicity observed within the Paradox Formation is a result of several related factors including regional and local tectonics, subsidence, sediment availability and supply, climate and glacio-eustatic sea-level fluctuations.

2. It seems highly plausible, based on the evidence presented, that Gondwanaland glaciations ultimately caused the eustatic sea-level fluctuations thus becoming the main influencing factor on the Paradox evaporite/carbonate facies cyclicity.

3. Stratigraphic rock relationships and palynomorph data both indicate there are five third-order sequences comprising the Paradox and lower Honaker Trail formations. Therefore, it is deemed that each individual evaporite cycle was roughly deposited as a fourth-order sequence having a 100,000 – 500,000 year duration.

4. Unfortunately one cannot produce undisputable evidence that Milankovitch cyclicity dominated Pennsylvanian systems like the cyclical sequences deposited

with the Paradox Formation. However, it is clear that orbitally forced cycles strongly influenced sedimentation within the basin. Perhaps such a short interval of 100,000 years, or less, makes reliable identification and correlation of like cycles too problematic.

5. Age estimates for the entire Paradox Formation are highly affected by the thickness and lithology types of the clastic zones. Greater thicknesses within the clastic zones (particularly with the black shales and dolomites) indicate longer depositional sequences and thus provide further indication about sediment source and supply.

6. Individual age estimates calculated using sedimentation rates indicate cycle age durations range upwards of 100,000 years which is in agreement with Milankovitch influenced cyclicity. Transgressive and regressive lithologies also give clues to the amount and length of each respective cycle.

8.2 Basin Formation and the Evolution of the Uncompahgre Uplift

1. Isopach thickness maps of individual evaporite cycles clearly illustrate the northern Paradox Basin formed due to several dynamic processes. The maps suggest the basin was somewhat tectonically active even before Pennsylvanian time. They also indicate there could have been salt movement as early as the end of the Desmoinesian implying there was greater salt movement further to the east as a result of early Cutler deposition (sediment loading).

2. Subsidence modeling of the northern Paradox Basin highlights a four-million year period (309 – 305 Ma) of major, rapid subsidence within the basin. The start of this time interval coincides with the beginning of the Desmoinesian and therefore subsidence occurred during the deposition of the Paradox Formation. Major subsidence appears to end by Early Permian time.

3. The Uncompahgre was slower to develop compared to the San Luis Uplift further to the south. However, even though the Uncompahgre was not areally exposed until near the end of the Pennsylvanian, it still was influencing depositional patterns and was accompanied by significant basin subsidence. Further evidence of early eroded arkosic material suggests the Uncompahgre went through several stages or pulses of uplift with the largest occurring near the end of Desmoinesian Time.

4. There are several models that propose different ideas involving the formation of the Uncompahgre Uplift. Each model uses convincing evidence to support its conclusions, however, it is unlikely all of the models are entirely correct because each have conflicting results with the other models. Therefore, it is more reasonable to conclude that each model is accurate to some extent (depending on location within the basin) and that a combination of these models probably creates a more complete and accurate representation. Stratigraphic evidence and subsidence modeling support the conclusion that the Paradox and Eagle basins were at one time connected early, during the initial cycles of salt deposition. However, the Uncompahgre started to uplift soon thereafter, but never reached any significant height above sea-level (for long durations of time) until near the end of Pennsylvanian time.

5. Age estimations of the Paradox Formation further support conclusions made that the eastern half of the basin is much older, deeper and started to develop earlier then the rest of the basin (possibly starting in Late Atokan or Early Desmoinesian time).

6. The two main sources of sediment supply into the basin are the Uncompahgre Uplift to the east and the San Luis Uplift near the southern margin of the basin. Evidence suggests both sources added substantial material into the depths of the basin. However, once the Uncompahgre became a strongly positive structure it

had by far a greater impact on clastic supply, at least in the northern half of the basin. Much of the clastic material may have been transported into the basin by means of fluvial processes. However, a lack of sufficient data limits the accuracy of identifying all possible means of sediment transport.

8.3 Recommendations for Future Work

1. To help compliment and complete a northern Paradox Basin correlation based upon rock type lithologies, additional samples from drill cores or cuttings from the easternmost section of the basin are needed. These samples would allow for better correlations of individual evaporite cycles and/or transgressive regressive sequences unlike what is available in outcrop and used for the QEMSCAN analysis in this study.

2. Additional detailed analysis on fine-grained clastic sediments within the clastic zones of the evaporite cycles would help identify the provenance for these detrital sediments. Only then could their true source perhaps be identified.

3. Many of the wells drilled within the northern Paradox Basin, and used in this study, have unreliable formation top picks for the Honaker Trail Formation which are often confused with beds from the lower Cutler Formation. Accurate top information would provide additional details on salt movement, timing and give clues to when the Cutler was deposited in relation to the formation of the Uncompahgre Uplift.

4. Additional interpreted seismic lines across the Uncompahgre may provide further insight to the correlativeness of the genetic relationship between the Paradox and Eagle basins.

REFERENCES

Baars, D. L., 1962, Permian systems of Colorado Plateau, American Association of Petroleum Geologists Bulletin, vol. 46, no. 2, pages 149-218.

Baars, D. L., 1966, Pre-Pennsylvanian paleotectonics – key to basin evolution and petroleum occurrences in Paradox Basin, Utah and Colorado, American Association of Petroleum Geologists Bulletin, vol. 50, no. 10, October, pages 2082-2111.

Baars, D. L., 1987, Paleozoic rocks of Canyonlands country, *in* J. A. Campbell, ed., Geology of Cataract Canyon and vicinity, A field symposium – guidebook of the Four Corners Geological Society, Tenth Field Conference, May 14th-17th, pages 11-17.

Baars, D. L., J. W. Parker, and J. Chronic, 1967, Revised stratigraphic nomenclature of Pennsylvanian system, Paradox Basin, American Association of Petroleum Geologists Bulletin, vol. 51, no. 3, March, pages 393-403.

Baars, D. L., and G. M. Stevenson, 1981, Tectonic evolution of the Paradox Basin, Utah & Colorado, *in* D. L. Wiegand, ed., Geology of the Paradox Basin, Rocky Mountain Association of Geologists, 1981 Field Conference, pages 23-31.

Baars, D. L., and G. M. Stevenson, 1982, Subtle stratigraphic traps in Paleozoic rocks of Paradox Basin, American Association of Petroleum Geologists Special Volumes, M32, The deliberate search for the subtle trap, pages 131-158.

Baker, F., 1969, Precambrian geology of the Needle Mountains, southwestern Colorado, United States Geological Survey Professional Paper 644-A, 35 pages.

Barbeau, D. L., 2003, A flexural model for the Paradox Basin: Implications for the tectonics of the Ancestral Rocky Mountains, Basin Research, vol. 15, pages 97-115.

Beloussov, V. V., 1962, Basic problems in geotectonics, New York, McGraw-Hill Book Company, Inc., 816 pages.

Berger, A., 1984, Accuracy and frequency stability of the earth's orbital elements during the quaternary, *in* A. Berger, J. Imbrie, J. Hays, G. Kukla, B. Saltzman, eds., Milankovitch and climate: Part 1, D. Reidel Publishing Company, Dordrecht, Netherlands, pages 3-39.

Berger, A., M. F. Loutre, and V. Dehant, 1989, Influence of the changing lunar orbit on the astronomical frequencies of pre-Quaternary insolation patterns, Paleoceanography, vol. 4, no. 5, October, pages 555-564.

Berman, A. E., D. Poleschook Jr., and T. E. Dimelow, 1980, Jurassic and Cretaceous systems of Colorado, *in* H. C. Kent, and K. W. Porter, eds., Colorado Geology, Rocky Mountain Association of Geologists, Denver Colorado, pages 111-128.

Blakey, R., 2007, Paleogeography and tectonic evolution of late Paleozoic sedimentary basins, southwestern North America, < http://jan.ucc.nau.edu/~rcb7/>, accessed March 25, 2008.

Borchert, H., 1969, Principles of oceanic salt deposition and metamorphism, Geological Society of America Bulletin, vol. 80, no. 5, May, pages 821-864.

Borchert, H., and R. O. Muir, 1964, Salt deposits: The origin, metamorphism and deformation of evaporites, D. Van Nostrand Company, LTD., London, 333 pages.

Bouma, A. H., 2000, Fine-grained, mud-rich turbidite systems: Model and comparison with coarse-grained, sand-rich systems, *in* A. H. Bouma and C. G. Stone, eds., Fine-grained turbidite systems, American Association of Petroleum Geologists Memoir 72/Society of Sedimentary Geology Special Publication, no. 68, pages 9-20.

Bradish and Clair, 1956, Geological report, Paradox Basin and related areas: Part 1, Subsurface geology of the Paradox Basin, prepared for Vega Corporation, Denver, Colorado, 38 pages.

Braitsch, O., 1971, Salt deposits; their origin and composition, Springer-Verlag, New York, 297 pages.

Brambach, R. K., C. R. Scotese, and A. M. Zeigler, 1980, Before Pangea: The geographies of the Paleozoic World, American Scientist, vol. 68, no. 1, January-February, pages 26-38.

Brown, H. H., 1960, Pennsylvanian of the Paradox Basin salt structure area, *in* Geology of the Paradox Basin fold and fault belt, Four Corners Geological Society – Guidebook, Third Field Conference, page 79.

Cater, F. W., 1970, Geology of the Salt Anticline region in southwestern Colorado, Geological Survey Professional Paper 637, United States Atomic Energy Comission, Washington, 80 pages.

Cater, F. W., and D. P. Elston, 1963, Structural development of salt anticlines of Colorado and Utah, American Association of Petroleum Geologists, Memoir 2, Backbone of the Americas, pages 152-159.

Condon, S. M., 1995, Geology of pre-Pennsylvanian rocks in the Paradox Basin and adjacent areas, southeastern Utah and southwestern Colorado, United States Geological Survey Bulletin 2000-G, 53 pages.

Condon, S. M., 1997, Geology of the Pennsylvanian and Permian Cutler Group and Permian Kaibab Limestone in the Paradox Basin, southeastern Utah and southwestern Colorado, United States Geological Survey Bulletin 2000-P, 46 pages.

Currie, B. S., 1998, Upper Jurassic-Lower Cretaceous Morrison and Cedar Mountain formations, NE Utah-NW Colorado: Relationships between nonmarine deposition and early cordilleran foreland-basin development, Journal of Sedimentary Research, vol. 68, no. 4, July, pages 632-652.

Delta Petroleum, 2008, Delta Petroleum Corporation, < http://www.deltapetro.com/rockymountainregion.html>, accessed February 10, 2008.

Denver Earth Resources Library, 2007, 730 17th St # B1, Denver, CO 80202, (303) 825-5614.

Dickinson, W. R., G. S. Soreghan, and K. A. Giles, 1994, Glacio-eustatic origin of Permo-Carboniferous stratigraphic cycles: Evidence from the southern cordilleran foreland region, Tectonic and Eustatic Controls on Sedimentary Cycles, SEPM Concepts and Paleontology #4, pages 25-34.

Doelling, H. H., 1983, Observations on Paradox Basin salt anticlines, *in* W. R. Averett, ed., Northern Paradox Basin Uncompahgre Uplift, Grand Junction Geological Society Field Trip, pages 81-90.

Doelling, H. H., 1988, Geology of Salt Valley Anticline and Arches National Park, Grand County, Utah, *in* H. H. Doelling, C. G. Oviatt, and P. W. Huntoon, Salt deformation in the Paradox region, Utah Geological and Mineral Survey Bulletin 122, 58 pages.

Doelling, H. H., 2001, Geologic map of the Moab and eastern part of the San Rafael Desert 30’ X 60’ quadrangles, Grand and Emery counties, Utah, and Mesa county Colorado, Utah Geological Survey Map 180, scale 1:100,000.

Donovan, R. N., W. Beachamp, T. Ferraro, C. Lajek, D. McConnell, M. Munsil, D. Ragland, B. Sweet, and D. Taylor, 1985, Subsidence rates in Oklahoma during the Paleozoic, Oklahoma City Geological Society, The Shale Shaker Digest XI, vol. XXXIII-XXXV (1982-1985), pages 14-16.

Draut, A. E., 2005, The geology of central and southeastern Utah: Itinerary for a one-day field trip, Geological Society of America, Penrose Conference Field Trip Guide – Lessons in tectonics, climate, and eustasy from the stratigraphic record in arc collision zones, Price, Utah, 10-14 October, 20 pages.

Dutton, S. P., and C. W. Kreitler, 1980, Caprock formation and diagenesis, Gyp Hill Salt Dome, south Texas, Gulf Coast Association of Geological Societies Transactions, vol. 30, pages 333-339.

Dutton, S. P., C. W. Kreitler, and B. R. Bracken, 1982, Formation and diagenesis of salt-dome cap rock, Texas Gulf Coast, *in* C. R. Handford, R. G. Loucks, and G. R. Davies, eds., Depositional and diagenetic spectra of evaporites – a core workshop, Society for Sedimentary Geology core workshop no. 3, Calgary, Canada, June 26-27, pages 100-129.

Elston, D. P., and E. M. Shoemaker, 1960, Late Paleozoic and Early Mesozoic structural history of the Uncompahgre Front, *in* Geology of the Paradox Fold and Fault Belt, Four Corners Geological Society – Guidebook, Third Field Conference, pages 47-55.

Elston, D. P., E. M. Shoemaker, and E. R. Landis, 1962, Uncompahgre Front and salt anticline region of Paradox Basin, Colorado and Utah, American Association of Petroleum Geologists Bulletin, vol. 46, no. 10, October, pages 1857-1878.

Epis, R. C., G. R. Scott, R. B. Taylor, and C. E. Chapin, 1980, Summary of Cenozoic geomorphic, volcanic and tectonic features of central Colorado and adjoining areas, *in* H. C. Kent, and K. W. Porter, eds., Colorado Geology, Rocky Mountain Association of Geologists, Denver Colorado, pages 135-156.

Fetzner, R. W., 1960, Pennsylvanian paleotectonics of Colorado Plateau, American Association of Petroleum Geologists Bulletin, vol. 44, no. 8, August, pages 1371-1413.

Fischer, A. G., 1984, The two Phanerozoic supercycles, *in* W. A. Berggren and J. A. Van Couvering, eds., Princeton University Press, Princeton, New Jersey, pages 129-150.

Frahme, C. W., and E. B. Vaughn, 1983, Paleozoic geology and seismic stratigraphy of the northern Uncompahgre Front, Grand County, Utah, *in* J. D. Lowell, and R. Gries, Rocky Mountain foreland basins and uplifts, Rocky Mountain Association of Geologists, pages 201-211.

Friedman, G. M., 1982, Evaporites as source rock for petroleum, *in* C. R. Handford, R. G. Loucks, and G. R. Davies, eds., Depositional and diagenetic spectra of evaporites – a core workshop, SEPM Core Workshop No. 3, Calgary, Canada, June 26-27, pages 385-395.

Geology, 2008, Geology.com, <http://geology.com>, accessed May 23, 2008.

Golden State Resources, 2002, Golden State Resources Limited, < http://www.goldenstate.com.au>, accessed April 16, 2008.

Goldsmith, L. H., 1969, Concentration of potash salts in saline basins, American Association of Petroleum Geologists Bulletin, vol. 53, no. 4, April, pages 790-797.

Goggle Earth, 2007, Google Earth, *in* <http://earth.google.com/>.

Gradstein, F. M., J. G. Ogg, A. G. Smith, F. P. Agterberg, W. Bleeker, R. A. Cooper, V. Davydov, P. Gibbard, L. A. Hinnov, M. R. House, L. Lourens, H. P. Luterbacher, J. McArthur, M. J. Melchin, L. J. Robb, J. Shergold, M. Villeneuve, B. R. Wardlaw, J. Ali, H. Brinkhuis, F. J. Hilgen, J. Hooker, R. J. Howarth, A. H. Knoll, J. Laskar, S. Monechi, K. A. Plumb, J. Powell, I. Raffi, U. Röhl, P. Sadler, A. Sanfilippo, B. Schmitz, N. J. Shackleton, G. A. Shields, H. Strauss, J. Van Dam, T. van Kolfschoten, J. Veizer, and D. Wilson, 2004, A Geologic Time Scale 2004, Cambridge University Press, Cambridge, United Kingdom, 589 pages.

Gustafson, V. O., 1981, Petroleum geology of the Devonian and Mississippian rocks of the Four Corners region, *in* D. L. Wiegand, ed., Geology of the Paradox Basin, Rocky Mountain Association of Geologists, 1981 Field Conference, pages 101-109.

Hallam, A., 1992, Phanerozioc sea-level changes, Columbia University Press, New York, 266 pages.

Harms, J. C., and C. R. Williamson, 1988, Deep-water density current deposits of Delaware Mountain Group (Permian), Delaware Basin, Texas and New Mexico, American Association of Petroleum Geologists Bulletin, vol. 72, no. 3, March, pages 299-317.

Harrison, T. S., 1927, Colorado-Utah salt domes, American Association of Petroleum Geologists Bulletin, vol. 11, no. 2, February, pages 111-133.

Heckel, P. H., 1986, Sea-level curve for Pennsylvanian eustatic marine transgressive-regressive depositional cycles along mid-continent outcrop belt, North America, Geology, vol. 15, April, pages 330-334.

Herman, G., and C. A. Barkell, 1957, Pennsylvanian stratigraphy and productive zones, Paradox salt basin, American Association of Petroleum Geologists, vol. 41, no. 5, May, pages 861-881.

Hite, R. J., 1960, Stratigraphy of the saline facies of the Paradox Member of the Hermosa Formation of southeastern Utah and southwestern Colorado, *in* Geology of the Paradox Basin fold and fault belt, Four Corners Geological Society – Guidebook, Third Field Conference, pages 86-89.

Hite, R. J., 1968, Salt deposits of the Paradox Basin, southeast Utah and southwest Colorado, *in* R. B. Mattox, ed., Saline deposits: A symposium based on papers from the international conference on saline deposits, Houston, Texas, 1962, Geological Society of America Special Papers 88, pages 319-330.

Hite, R. J., 1983, Preliminary mineralogical and geochemical data from the Department of Energy Gibson Dome corehole no. 1, San Juan County, Utah, U.S. Geological Survey Open-File Report 83-780, 57 pages.

Hite, R. J., 1985, The sulfate problem in marine evaporites, *in* B. C. Schreiber and H. L. Harner, eds., Sixth International Symposium On Salt, vol. 1, pages 217-230.

Hite, R. J., and D. H. Buckner, 1981, Stratigraphic correlations, facies concepts, and cyclicity in the Paradox Basin, *in* D. L. Wiegand, ed., Geology of the Paradox Basin, Rocky Mountain Association of Geologists, 1981 Field Conference, pages 147-159.

Hite, R. J., D. E. Anders, and T. G. Ging, 1984, Organic-rich source rocks of Pennsylvanian age in the Paradox Basin of Utah and Colorado, *in* J. Woodward, F. F. Meissner, and J. L. Clayton, eds., Hydrocarbon source rocks of the greater Rocky Mountain region, Rocky Mountain Association of Geologists, pages 255-274.

Houck, K. J., 1997, Effects of sedimentation, tectonics, and glacio-eustasy on depositional sequences, Pennsylvanian Minturn Formation, north-central Colorado, American Association of Petroleum Geologists Bulletin, vol. 81, no. 9, September, pages 1510-1533.

House, M. R., 1995, Orbital forcing timescales: And introduction, *in* M. R. House and A. S. Gale, eds., Orbital forcing timescales and cyclostratigraphy, Geological Society Special Publication No. 85, pages 1-18.

Intrepid Mining, 2006, Intrepid Potash, Intrepid Mining, LLC, < http://www.intrepidpotash.com/index.html>, accessed on March 11, 2008.

Jenyon, M. K., 1986, Salt tectonics, Elsevier Applied Science Publishers, London and New York, 191 pages.

Joesting, H. R., J. E. Case, and D. Plouff, 1966, Regional geophysical investigations of the Moab-Needles area, Utah, Geological Survey Professional Paper 516-C, 21 pages.

Jones, R. W., 1958, Origin of salt anticlines of Paradox Basin, American Association of Petroleum Geologists Bulletin, vol. 43, no. 8, August, pages 1869-1895.

Kamola, D. L., and M. A. Chan, 1988, Coastal dune facies, Permian Cutler Formation (White Rim Sandstone), Capital Reef National Park area, southern Utah, Sedimentary Geology, vol. 56, Elsevier Science Publishers B. V., Amsterdam, Netherlands, pages 341-356.

Kelley, V. C., 1955, Regional tectonics of the Colorado Plateau and relationship to the origin and distribution of uranium, University of New Mexico Press, Albuquerque, 120 pages.

Kelley, V. C., 1958, Tectonics of the region of the Paradox Basin, *in* A. F. Sanborn, ed., Guidebook to the geology of the Paradox Basin, Intermountain Association of Petroleum Geologists, Ninth Annual Field Conference, pages 31-38.

Kirkland, D. W., and R. Evans, 1981, Source-rock potential of evaporitic environment, American Association of Petroleum Geologists Bulletin, vol. 65, no. 2, pages 181-190.

Klein, C., 2002, Mineral science, John Wiley and Sons, Inc., New York, 641 pages.

Klingspor, A. M., 1966, Cyclic deposits of potash in Saskatchewan, Canadian Petroleum Geology Bulletin, vol. 14, no. 2, June, pages 193-207.

Kluth, C. F., 1986, Plate tectonics of the Ancestral Rocky Mountains, *in* J. A. Peterson, ed., Paleotectonics & sedimentation in the Rocky Mountain region, United States, American Association of Petroleum Geologists, Memoir 41, Tulsa Oklahoma, pages 353-369.

Kluth, C. F., 2008, A new look at the Ancestral Rocky Mountains, Rocky Mountain Association of Geologists Friday Luncheon Lecture Series, April 18th, 2008.

Kluth, C. F., and H. R. DuChene, 2006, The geometry and tectonics of the Uncompahgre mountain front, western Colorado, abstract, Geological Society of America abstract with programs, vol. 38, no. 6, page 29.

Kluth, C. F., and H. R. DuChene, 2007, The tectonic development of the Uncompahgre Uplift and the Paradox Basin, Utah and Colorado, Geological Society of America Annual Meeting Denver, October 28-31, Poster.

Kosanke, R. M., 1995, Palynology of part of the Paradox and Honaker Trail formations, Paradox Basin, Utah, United States Geological Survey Bulletin 2000-L, 9 pages.

Kupfer, D. H., 1989, Gypsum dehydration, agent of salt diapirism, Gulf Coast Association of Geological Societies Transactions, vol. 39, Pages 171-181.

Lockridge, J. P., 1958, Alkali Gulch gas field, La Plata County, Colorado, *in* A. F. Sanborn, ed., Guidebook to the geology of the Paradox Basin, Intermountain Association of Petroleum Geologists, Ninth Annual Field Conference, pages 245-246.

Loope, D. B., and G. B. Kuntz, 1987, Evidence of evaporate growth within marine limestones of the upper member of the Hermosa Formation (Pennsylvanian), Cataract Canyon, southeastern Utah, *in* J. A. Cambell, ed., Geology of Cataract Canyon, Four Corners Geological Society Guidebook, Tenth Field Conference, pages 75-79.

Magaritz, M., 1987, A new explanation for the cyclic deposition in marine evaporite basins: Meteoric water input, Chemical Geology, vol. 62, pages 239-250.

Malin, W. J., 1958, A preliminary informal system of nomenclature for a part of the Pennsylvanian of the Paradox Basin, *in* A. F. Sanborn, ed., Guidebook to the geology of the Paradox Basin, Intermountain Association of Petroleum Geologists, Ninth Annual Field Conference, pages 135-137.

Martin, G. W., 1981, Patterson Field, *in* D. L. Wiegand, ed., Geology of the Paradox Basin, Rocky Mountain Association of Geologists, 1981 Field Conference, pages 61-69.

Maughan, E. K., and W. J. Perry Jr., 1986, Lineaments and their tectonic implications in the Rocky Mountains and adjacent plains region, *in* J. A. Peterson, ed., Paleotectonics & sedimentation in the Rocky Mountain region, United States, American Association of Petroleum Geologists, Memoir 41, Tulsa Oklahoma, pages 41-53.

Merrill, W. M., and R. M. Winar, 1958, Molas and associated formations in San Juan Basin-Needle Mountains area, southwestern Colorado, American Association of Petroleum Geologists Bulletin, vol. 42, no. 9, September, pages 2107-2132.

Molenaar, C. M., 1981, Mesozoic stratigraphy of the Paradox Basin – an overview, *in* D. L. Wiegand, ed., Geology of the Paradox Basin, Rocky Mountain Association of Geologists, 1981 Field Conference, pages 119-127.

Moore, R. C., 1936, Stratigraphic classification of the Pennsylvanian rocks of Kansas, State Geological Survey of Kansas Bulletin 22, 256 pages.

Nadon, G. C., and R. R. Kelly, 2004, The constraints of glacial eustatic and low accommodation on sequence-stratigraphic interpretations of Pennsylvanian strata, Conemaugh Group, Appalachian Basin, U.S.A., *in* J. C. Pashin, and R. A. Gastaldo, eds., Sequence stratigraphy, paloeclimate, and tectonics of coal-bearing strata, American Association of Petroleum Geologists Studies in Geology 51, pages 29-44.

Nation Park Service, 2007, Arches National Park, <http://www.nps.gov/arch/>, accessed March 9, 2008.

Neff, A. W., 1960, Comparisons between the salt anticlines of south Persia and those of the Paradox Basin, *in* Geology of the Paradox Basin fold and fault belt, Four Corners Geological Society – Guidebook, Third Field Conference, pages 56-64.

Nesse, W. D., 2000, Introduction to mineralogy, Oxford University Press, Inc., New York, 442 pages.

Nuccio, V. F., and S. M. Condon, 1996, Burial and thermal history of the Paradox Basin, Utah and Colorado, and petroleum potential of the Middle Pennsylvanian Paradox Formation, United States Geological Survey Bulletin 2000-O, 47 pages.

Olszewski, T. D., and M. E. Patzkowsky, 2003, From cyclothems to sequences: The record of eustasy and climate on an icehouse epeiric platform (Pennsylvanian-Permain, North America Midcontinent), Journal of Sedimentary Research, vol. 73, no. 1, January, pages 15-30.

Paz Cuellar, M. G., 2006, Restoration of mountain front and salt structures in the northern Paradox Basin, Colorado School of Mines masters thesis, 142 pages.

Pekarek, A. H., 2001, Solar forcing of earth's climate, *in* L. C. Gerhard, W. E. Harrison and B. M. Hanson, eds., Geological perspectives of global climate change, pages 19-34.

Peterson, J. A., 1966, Genesis and diagenesis of Paradox Basin carbonate mound reservoirs, *in* Symposium on Recently Developed Geologic Principles and Sedimentation of the Permo-Pennsylvanian of the Rocky Mountains, Wyoming Geological Association, Twentieth Annual Conference, Casper College, Casper, Wyoming, August to September, pages 67-86.

Prommel, H. W. C., and H. E. Crum, 1927, Salt domes of Permian and Pennsylvanian age in southeastern Utah and their Influence on oil accumulation, American Association of Petroleum Geologists Bulletin, vol. 11, no. 4, April, pages 373-393.

Raup, O. B., and R. J. Hite, 1992, Lithology of evaporite cycles and cycle boundaries in the upper part of the Paradox Formation of the Hermosa Group of Pennsylvanian age in the Paradox Basin, Utah and Colorado, United States Geological Survey Bulletin 2000-B, 37 pages.

Rasmussen, D. L., 2006, Escalation of Pennsylvanian-Permian Uncompahgre Uplift revealed by progression of siliciclastic wedges in the Paradox Basin, Colorado and Utah, abstract, Geological Society of America abstract with programs, vol. 38, no. 6, page 29.

Reid F. S., and C. E. Berghorn, 1981, Facies recognition and hydrocarbon potential of the Pennsylvanian Paradox Formation, *in* D. L. Wiegand, ed., Geology of the Paradox Basin, Rocky Mountain Association of Geologists, 1981 Field Conference, pages 111-117.

Reuger, B. F., 1996, Palynology and its relationship to climatically induced depositional cycles in the Middle Pennsylvanian (Desmoinesian) Paradox Formation of southeastern Utah, United States Geological Survey Bulletin 2000-K, 30 pages.

Scheffler, K., S. Hoernes, and L. Schwark, 2003, Global changes during Carboniferous-Permian glaciation of Gondwana: Linking polar and equatorial climate evolution by geochemical proxies, Geological Society of America, Geology, July, vol. 31, no. 7, pages 605-608.

Schwarzacher, W., 1993, Cyclostratigraphy and the Milankovitch theory, Developments in Sedimentology 52, Elesevier Science Publishers B. V., Amsterdam, Netherlands, 225 pages.

Shoemaker, E. M., J. E. Case, and D. P. Elston, 1958, Salt anticlines of the Paradox Basin, *in* A. F. Sanborn, ed., Guidebook to the geology of the Paradox Basin, Intermountain Association of Petroleum Geologists, Ninth Annual Field Conference, pages 39-59.

Sonnenfeld, P., 1984, Brines and evaporites, Academic Press Inc., Orlando, 613 pages.

Sonnenfeld, P., and P. P. Hudec, 1985, Clay laminations: Their cause and effect, *in* B. C. Schreiber and H. L. Harner, eds., Sixth International Symposium On Salt, vol. 1, pages 51-56.

Soreghan, M., and G. Soreghan, 2003, Ice at the equator: A Paleozoic Yosemite lurking in western Colorado?, Earth Scientist Magazine, University of Oklahoma, pages 28-31.

Soreghan, G. S., D. E. Sweet, K. R. Marra, C. F. Eble, M. J. Soreghan, R. D. Elmore, S. A. Kaplan, and M. D. Blum, 2007, An exhumed Late Paleozoic canyon in the Rocky Mountains, The Journal of Geology, vol. 115, pages 473-481.

Stevenson, G. M., and D. L. Baars, 1986, The Paradox: A pull-apart basin of Pennsylvanian age *in* J. A. Peterson, ed., Paleotectonics & sedimentation in the Rocky Mountain region, United States, American Association of Petroleum Geologists, Memoir 41, Tulsa Oklahoma, pages 513-539.

Stewart, F. H., 1963, Chapter Y: Marine evaporites, *in* M. Fleischer, ed., Data of geochemistry-sixth edition, United States Geological Survey Professional Paper 440-Y, Y52 pages.

Stokes, W. L., 1948, Geology of the Utah-Colorado salt dome region with emphasis on Gypsum Valley, Colorado, Guidebook to the Geology of Utah, no. 3, Utah Geological Survey, 50 pages.

Tillman, R. W., 1971, Petrology and paleoenvironments, Robinson Member, Minturn Formation (Desmoinesian), Eagle Basin, Colorado, American Association of Petroleum Geologists Bulletin, vol. 55, no. 4, April, pages 593-620.

Tissot, B. P., and D. H. Welte, 1984, Petroleum formation and occurrence, second revised and enlarged edition, Springer-Verlag, Berlin, Heidelberg, New York, Tokyo, 699 pages.

Trudgill, B., N. Banbury, and J. Underhill, 2004, Salt evolution as a control on structural and stratigraphic systems: Northern Paradox foreland basin, SE Utah, USA, in GCSSEPM 24th Annual Research Conference.

Tucker, M. E., and V. P. Wright, 1990, Carbonate sedimentology, Blackwell Science Ltd., London, 482 pages.

Tweto, O., 1980a, Precambrian geology of Colorado, *in* H. C. Kent, and K. W. Porter, eds., Colorado Geology, Rocky Mountain Association of Geologists, Denver Colorado, pages 37-46.

Tweto, O., 1980b, Tectonic history of Colorado, *in* H. C. Kent, and K. W. Porter, eds., Colorado Geology, Rocky Mountain Association of Geologists, Denver Colorado, pages 5-9.

Tweto, O., 1980c, Summary of the Laramide Orogeny in Colorado, *in* H. C. Kent, and K. W. Porter, eds., Colorado Geology, Rocky Mountain Association of Geologists, Denver Colorado, pages 129-134.

Tweto, O., 1987, Rock units of the Precambrian basement in Colorado, United States Geological Survey Professional Paper 1321-A, 54 pages.

Utah State Oil and Gas, 2007, Utah Department of Natural Resources Division of Oil, Gas and Mining, <http://oilgas.ogm.utah.gov/index.htm>, last accessed April 23, 2008.

Vail, P. R., R. M. Mitchum Jr., and S. Thompson III, 1977, Seismic stratigraphy and global changes of sea level, Part 4: Global cycles of relative changes of sea level, American Association of Petroleum Geologists Memoir 26: Seismic stratigraphy – applications to hydrocarbon exploration, pages 83-97.

Van der Zwan, C. J., 2002, The impact of Milankovitch-scale climatic forcing on sediment supply, Sedimentary Geology, vol. 147, pages 271-294.

Veevers, J. J., and C. McA. Powell, 1987, Late Paleozoic glacial episodes in Gondwanaland reflected in transgressive-regressive depositional sequences in Euramerica, Geological Society of America Bulletin, vol. 98, April, pages 475-487.

Ver Planck, W. E., 1958, Salt in California, California Division of Mines Bulletin, vol. 175, 168 pages.

Wanless, H. R., and F. P. Shepard, 1936, Sea level and climatic changes related to late Paleozoic cycles, Geological Society of America Bulletin, vol. 47, no. 8, pages 1177-1206.

Wardlaw, N. C., and W. M. Schwerdtner, 1966, Halite-anhydrite seasonal layers in the Middle Devonian Prairie Evaporite Formation, Saskatchewan, Canada, Geological Society of America Bulletin, vol. 77, April, pages 331-342.

Warner, L. A., 1978, The Colorado Lineament: A middle Precambrian wrench fault system, Geological Society of America Bulletin, vol. 89, pages 161-171.

Warner, L. A., 1980, The Colorado Lineament, *in* H. C. Kent, and K. W. Porter, eds., Colorado Geology, Rocky Mountain Association of Geologists, Denver Colorado, pages 11-21.

Warren, J. K., 1985, On the significance of evaporite laminations, *in* B. C. Schreiber and H. L. Harner, eds., Sixth International Symposium On Salt, vol. 1, pages 161-170.

Warren, J. K., 1989, Evaporite sedimentology, Prentice Hall, New Jersey, 285 pages.

Warren, J. K., 1999, Evaporites: Their evolution and economics, Blackwell Science Ltd., Oxford, 438 pages.

Weber, L. J., J. F. (Rick) Sarg, and F. M. Wright, 1995, Sequence stratigraphy and reservoir delineation of the Middle Pennsylvanian (Desmoinesian), Paradox Basin and Aneth Field, southwestern USA, *in* Milankovitch sea level changes, cycles and reservoirs on carbonate platforms in greenhouse and ice-house worlds, SEPM short course notes, no. 35, pages 1-81.

Weir, G. W., and W. P. Puffett, 1981, Incomplete manuscript on stratigraphy and structural geology and uranium-vanadium and copper deposits of Lisbon Valley area, Utah-Colorado, United States Geological Survey, open-file report 81-39, 292 pages.

Wengerd, S. A., 1958, Pennsylvanian stratigraphy, southwest shelf, Paradox Basin, *in* A. F. Sanborn, ed., Guidebook to the geology of the Paradox Basin, Intermountain Association of Petroleum Geologists, Ninth Annual Field Conference, pages 109-134.

Wengerd, S. A., 1962, Pennsylvanian sedimentation in Paradox Basin, Four Corners Region, *in* Pennsylvanian systems in the United States, American Association of Petroleum Geologists, Special Volumes 23, pages 264-330.

Wengerd, S. A., and J. W. Strickland, 1954, Pennsylvanian stratigraphy of Paradox salt basin, Four Corners region, Colorado and Utah, American Association of Petroleum Geologists Bulletin, vol. 38, no. 10, October, pages 2157-2199.

White, M. A., and M. I. Jacobson, 1983, Structures associated with the southwest margin of the Ancestral Uncompahgre Uplift, *in* W. R. Averett, ed., Northern Paradox Basin-Uncompahgre Uplift, Grand Junction Geological Society Field Trip, October 1-2, pages 33-39.

Wright, J. C., D. R. Shawe, and S. W. Lohman, 1962, Definition of members of Jurassic Entrada Sandstone in east-central Utah and west-central Colorado, American Association of Petroleum Geologists Bulletin, vol. 46, no. 11, November, pages 2057-2070.

Yang, W., 2000, Carbonate sedimentation rates in mixed siliciclastic and carbonate cycles, Cisco Group (Virgillian and Wolfcampian), eastern shelf, Texas, American Association of Petroleum Geologists Annual Meeting Abstract, New Orleans, Louisiana, April 16-19.

Young, R. G., 1983, Petroleum in northeastern Grand County, Utah, *in* W. R. Averett, ed., Northern Paradox Basin-Uncompahgre Uplift, Grand Junction Geological Society Field Trip, October 1-2, pages 1-7.

Zharkov, M. A., 1981, History of Paleozoic salt accumulation, Springer-Verlag, Berlin, 309 pages.

APPENDIX A

WELL LOCATIONS

No.	API #	Operator	Well Name	Township	Range	Section
1	4301510928	PLACID OIL COMPANY	MARSH FLAT UNIT 1	17S	14E	29
2	4301520053	DIAMOND SHAMROCK EXP	WITTER FED 1	18S	15E	19
3	4301530014	CHEVRON USA INC	NORRIS FED 1	18S	16E	8
4	4301530001	CALIFORNIA-TIME PET	BARRIER BANK 1	19S	14E	11
5	4301510504	HUMBLE OIL & REFININ	SPHINX UNIT 1A	19S	14E	35
6	4301530003	TOLEDO MINING CO	TOLEDO FEDERAL 1	20S	14E	33
7	4301530018	DENISON MINES LTD	DENISON MINES-SKYLIN	21S	14E	5
8	4301530089	MEGADON ENTERPRISES	SALERATUS FED ST 2-3	21S	14E	36
9	4301511182	SUPERIOR OIL COMPANY	GRAND FAULT UNIT 14	21S	15E	24
10	4301511138	TEXAS EASTERN SKYLIN	GREEN RIVER UNIT 1	21S	16E	33
11	4301930029	SHELL OIL COMPANY	FEDERAL 1-26	21S	17E	26
12	4301931357	GCRL ENERGY LTD	GCRL SEISMOSAUR FED	21S	20E	20
13	4301911485	PACIFIC WESTERN OIL	THOMPSON 1	21S	21E	33
14	4301930328	TXO PRODUCTION CORP	KLOTZ FEDERAL 1	21S	22E	11
15	4301930918	MOBIL OIL CORPORATION	AMERICAN PETROFINA 1	21S	22E	30
16	4301510021	AMAX PETROLEUM CORP	GREEN RIVER DESERT U	22S	15E	9
17	4301530079	MEGADON ENTERPRISES	GEYSER DOME 1-14	22S	15E	14
18	4301511274	TEXAS EASTERN TRANS	FEDERAL 1	22S	15E	26
19	4301520342	EQUITY OIL COMPANY	FEDERAL 1	22S	15E	28
20	4301910030	KERN COUNTY LAND CO	AMERADA GREEN RIVER	22S	16E	2
21	4301930074	FERGUSON OIL CO	U-TEX ET AL 1-14	22S	16E	14
22	4301930124	MOUNTAIN FUEL SUPPLY	MT FUEL-SKYLINE GEYS	22S	16E	25
23	4301911188	SUPERIOR OIL COMPANY	SALT WASH UNIT 22-34	22S	17E	34
24	4301930110	CONOCO INC	CRESCENT UNIT 1	22S	20E	17
25	4301510373	FOREST OIL CORP	FOREST GOVT 1	23S	14E	11
26	4301511030	SHELL OIL COMPANY	CHAFFIN UNIT 1	23S	15E	21
27	4301510736	MOBIL OIL CORPORATION	JAKEY'S RIDGE 12-3	23S	16E	3
28	4301510737	MOBIL OIL CORPORATION	JAKEY'S RIDGE 34-15	23S	16E	15
29	4301930282	RESERVE OIL & GAS	SALT WASH NORTH 1	23S	17E	9
30	4301910086	BELCO DEVELOPMENT CO	FLOY UNIT 1	23S	17E	11
31	4301910831	PAN AMERICAN PETROLE	SALT WASH UNIT 1	23S	17E	15
32	4301930752	MEGADON ENTERPRISES	FEDERAL 1-15	23S	17E	15
33	4301910832	PAN AMERICAN PETROLE	SUNILAND STATE A 1	23S	17E	16
34	4301910833	S W ENERGY CORP	SUNILAND STATE A-2	23S	17E	16
35	4301915819	SMOOT, RICHARD P	CF&I 22-16	23S	17E	16
36	4301915820	SMOOT, RICHARD P	CF&I 42-16	23S	17E	16
37	4301930783	S W ENERGY CORP	STATE 1-16A	23S	17E	16
38	4301916047	S W ENERGY CORP	GOVT SMOOT 1	23S	17E	17
39	4301930044	S W ENERGY CORP	GOVT SMOOT 3	23S	17E	17
40	4301930679	S W ENERGY CORP	GOVT 18-2	23S	17E	18
41	4301930327	PEASE OIL & GAS COMP	FEDERAL SKYLINE 1A S	23S	17E	21
42	4301930647	CITIES SERV OIL & GA	FEDERAL DE-1	23S	18E	20
43	4301930038	SHELL OIL COMPANY	MT FUEL FEDERAL 1-21	23S	18E	21
44	4301930251	HILLIARD OIL & GAS	KLONDIKE U 1	23S	18E	24
45	4301920146	UNION OIL CO OF CALI	DEVILS GARDEN USA 1	23S	21E	5

Table A.1a: Wells with available well log information used for maps, cross-sections and correlations. Well logs were obtained through the Utah State Oil and Gas (2007) website.

No.	API #	Operator	Well Name	Township	Range	Section
46	4301930055	QUINTANA PETROLEUM	YELLOW CAT USA 1-9	23S	22E	9
47	4301910980	ARCO OIL & GAS COMPA	ONION CREEK U 1	23S	24E	31
48	4301510116	GENERAL PETROLEUM CO	45-56	24S	15E	5
49	4301530235	COORS ENERGY	FEDERAL 1-29MW	24S	15E	29
50	4301511031	SHELL OIL COMPANY	GRUVERS MESA 1	24S	16E	19
51	4301930042	SHELL OIL COMPANY	SHELL QUINTANA FED 1	24S	17E	1
52	4301930688	MEGADON ENTERPRISES	FEDERAL 1-26	24S	17E	26
53	4301930276	LADD PETROLEUM CORPO	FEDERAL 1-27U	24S	18E	27
54	4301930272	MOUNTAIN FUEL SUPPLY	KLONDIKE UNIT 2	24S	19E	22
55	4301930455	TIGER OIL CO	STATE 12-11	24S	20E	11
56	4301931112	LADD PETROLEUM CORP	SALT VALLEY 1	24S	20E	16
57	4301910905	PHILLIPS PETROLEUM	ONION CREEK UNIT 2	24S	23E	13
58	4301931180	CONOCO INC	CONOCO FED 31 1	24S	23E	31
59	4301930206	MOBIL OIL CORPORATION	FEDERAL SECTION 7-1	24S	25E	7
60	4301930937	EXXON CORPORATION	ONION CREEK FED 1	24S	25E	18
61	4301511184	SUPERIOR OIL COMPANY	N SPRING WASH 31-15	25S	15E	15
62	4301510229	CONTINENTAL OIL CO	MOONSHINE WASH U 2	25S	15E	22
63	4301510183	STANDARD OIL CO	MOONSHINE WASH U 1	25S	15E	32
64	4301511033	SHELL OIL COMPANY	GRUVERS MESA 2	25S	16E	10
65	4301510182	STANDARD OIL CO	LOOKOUT POINT UNIT 1	25S	16E	29
66	4301911187	SUPERIOR OIL COMPANY	BOWKNOT UNIT 43-20	25S	17E	20
67	4301910715	MCRAE OIL & GAS CORP.	MCRAE-FEDERAL 1	25S	18E	10
68	4301931331	INTREPID OIL & GAS	KANE SPRINGS FED 10	25S	18E	10
69	4301931341	INTREPID OIL & GAS	KANE SPRINGS 16-1	25S	18E	16
70	4301930043	SHELL OIL COMPANY	FEDERAL 1-20	25S	18E	20
71	4301930033	SHELL OIL COMPANY	FEDERAL 1-21	25S	18E	21
72	4301930170	READ & STEVENS INC	SH. BOWKNOT 1	25S	18E	21
73	4301910368	FEDERAL OIL CO	FED BOWKNOT 1	25S	18E	30
74	4301930045	SHELL OIL COMPANY	SHELL-QUINTANA FED 1	25S	18E	35
75	4301931363	HUNT PETROLEUM AEC	CANE CREEK FED 7-1	25S	19E	7
76	4301930050	GENERAL CRUDE OIL CO	BIG ROCK FED 1	25S	19E	26
77	4301910154	CALVERT EXPLORATION	BIG FLAT UNIT 6	25S	19E	27
78	4301911333	UNION OIL CO OF CALI	BIG FLAT UNIT 5	25S	19E	27
79	4301930379	HUSKY OIL COMPANY	FED BARTLETT FLAT 10	25S	19E	27
80	4301931310	INTREPID OIL & GAS	KANE SPRINGS FED 27	25S	19E	27
81	4301931325	INTREPID OIL & GAS	KANE SPRINGS FED 28	25S	19E	28
82	4301931334	INTREPID OIL & GAS	KANE SPRINGS FED 25	25S	19E	34
83	4301930910	CHANDLER & ASSOCIATE	MOAB FED 16-9	25S	20E	9
84	4301930810	DAVIS OIL COMPANY	GOLD BAR UNIT 2	25S	20E	23
85	4301930795	DAVIS OIL COMPANY	GOLD BAR UNIT 1	25S	20E	29
86	4301931018	SAMSON RESOURCES CO	ARCHES FEDERAL 1	25S	21E	18
87	4301910397	GOLD BAR RESOURCES	CASTLE VALLEY U 1	25S	23E	16
88	4301530205	BOSWELL ENERGY CORP	N SPRING CREEK FED 1	26S	15E	21
89	4301530010	HUNT PETROLEUM CORP	USA FED 1	26S	16E	31
90	4301511181	SUPERIOR OIL COMPANY	BOW KNOT UNIT 14-5	26S	17E	5

Table A.1b: continued.

No.	API #	Operator	Well Name	Township	Range	Section
91	4301530145	DAVIS OIL COMPANY	POOL UNIT 1	26S	17E	17
92	4301530078	MEGADON ENTERPRISES	FEDERAL 2-20	26S	17E	20
93	4301930182	GRYNBERG, JACK J	MINERAL POINT FED 1	26S	18E	4
94	4301911335	PURE OIL CO	MINERAL POINT USA 1	26S	18E	7
95	4301931119	EP OPERATING COMPANY	MINERAL CANYON FED 1	26S	19E	3
96	4301911565	RUBY, GLEN ET AL	GLEN M RUBY 1-A	26S	19E	11
97	4301911578	TIDEWATER OIL CO	TIDEWATER OIL CO 74	26S	19E	11
98	4301920409	KING OIL CO	KING OIL COMPANY 1 R	26S	19E	11
99	4301931364	INTREPID OIL & GAS	CANE CREEK FED 11-1	26S	19E	11
100	4301911002	RUBY, GLEN ET AL	BIG FLAT UNIT 2	26S	19E	14
101	4301915777	RUBY, GLEN ET AL	BIG FLAT UNIT 1	26S	19E	14
102	4301930357	ENERGY RESERVES GR	SUNBURST 1	26S	19E	14
103	4301931156	EP OPERATING COMPANY	MINERAL CANYON U 1-1	26S	19E	14
104	4301931332	INTREPID OIL & GAS	KANE SPRINGS FED 20	26S	19E	20
105	4301911332	UNION OIL CO OF CALI	BIG FLAT UNIT 4	26S	19E	23
106	4301915778	RUBY, GLEN ET AL	BIG FLAT UNIT 3	26S	19E	23
107	4301930620	DAVIS OIL COMPANY	MATTHEW FED 1	26S	20E	4
108	4301930823	DAVIS OIL COMPANY	MATTHEW FED 2	26S	20E	4
109	4301930796	DAVIS OIL COMPANY	SKYLINE UNIT 1	26S	20E	5
110	4301910155	CALVERT EXPLORATION	BIG FLAT UNIT 7	26S	20E	6
111	4301930273	MINERALS MANAGEMENT	SKYLINE FEDERAL 8-44	26S	20E	8
112	4301911143	SOUTHERN NATURAL GAS	LONG CANYON UNIT 2	26S	20E	9
113	4301915925	INTREPID OIL & GAS	LONG CANYON 1	26S	20E	9
114	4301931190	COORS ENERGY	COORS USA 1-10LC	26S	20E	10
115	4301910987	MOAB OIL CO	WHITE CLOUD 1	26S	20E	14
116	4301910767	MURPHY CONSTRUCTION	LITTLE VALLEY-FED 1	26S	20E	29
117	4301911336	PURE OIL CO	HOBSON USA 1	26S	20E	30
118	4301910145	CABEEN EXPLORATION	BIG FLAT-GOVT 1	26S	20E	31
119	4301930076	UNION OIL CO OF CALI	BURKHOLDER UNIT 1-G	26S	22E	1
120	4301930113	CITIES SERV OIL & GA	CSO-FED WEAVER 1	26S	22E	28
121	4301910830	PAN AMERICAN PETROLE	PACE STATE 1	26S	25E	12
122	4301931157	AMOCO PRODUCTION CO	TAYLOR CREEK U 2	26S	25E	12

Table A.1.c: continued.

No.	API #	Operator	Well Name	Township	Range	Section
1	4301511182	SUPERIOR OIL COMPANY	GRAND FAULT UNIT 14	21S	15E	24
2	4301530079	MEGADON ENTERPRISES	GEYSER DOME 1-14	22S	15E	14
3	4301930124	MOUNTAIN FUEL SUPPLY	MT FUEL-SKYLINE GEYS	22S	16E	25
4	4301930282	RESERVE OIL & GAS	SALT WASH NORTH 1	23S	17E	9
5	4301930688	MEGADON ENTERPRISES	FEDERAL 1-26	24S	17E	26
6	4301930050	GENERAL CRUDE OIL CO	BIG ROCK FED 1	25S	19E	26
7	4301930910	CHANDLER & ASSOCIATE	MOAB FED 16-9	25S	20E	9
8	4301530145	DAVIS OIL COMPANY	POOL UNIT 1	26S	17E	17
9	4301931190	COORS ENERGY	COORS USA 1-10LC	26S	20E	10
10	4301910767	MURPHY CONSTRUCTION	LITTLE VALLEY-FED 1	26S	20E	29

Table A.2: List of wells used for lithology classification and age estimate relationships.

APPENDIX B

EVAPORITE CYCLE ISOPACH MAPS

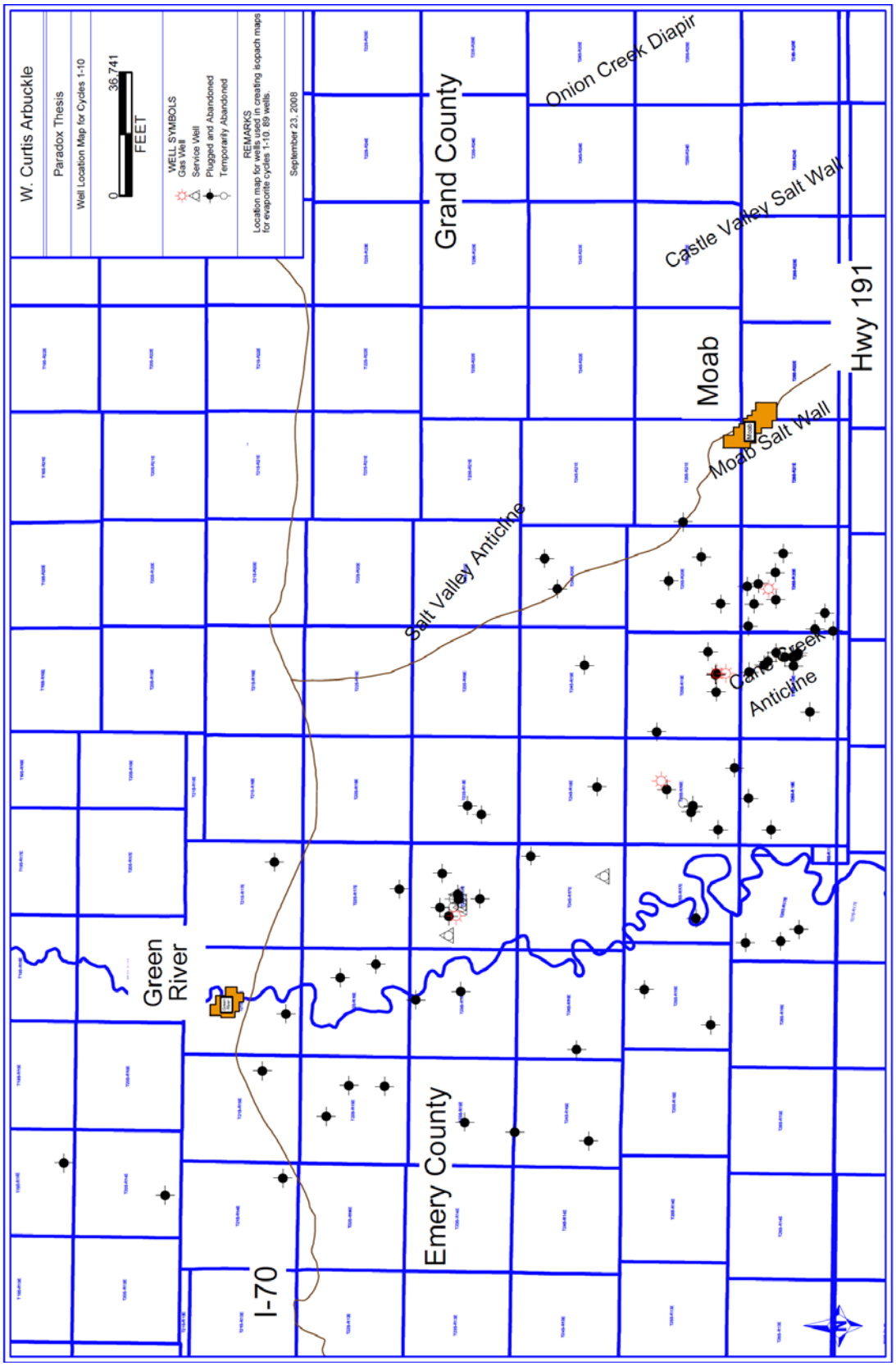

Figure B.1: Map showing the location of the wells used to create evaporite cycle maps 1-10.

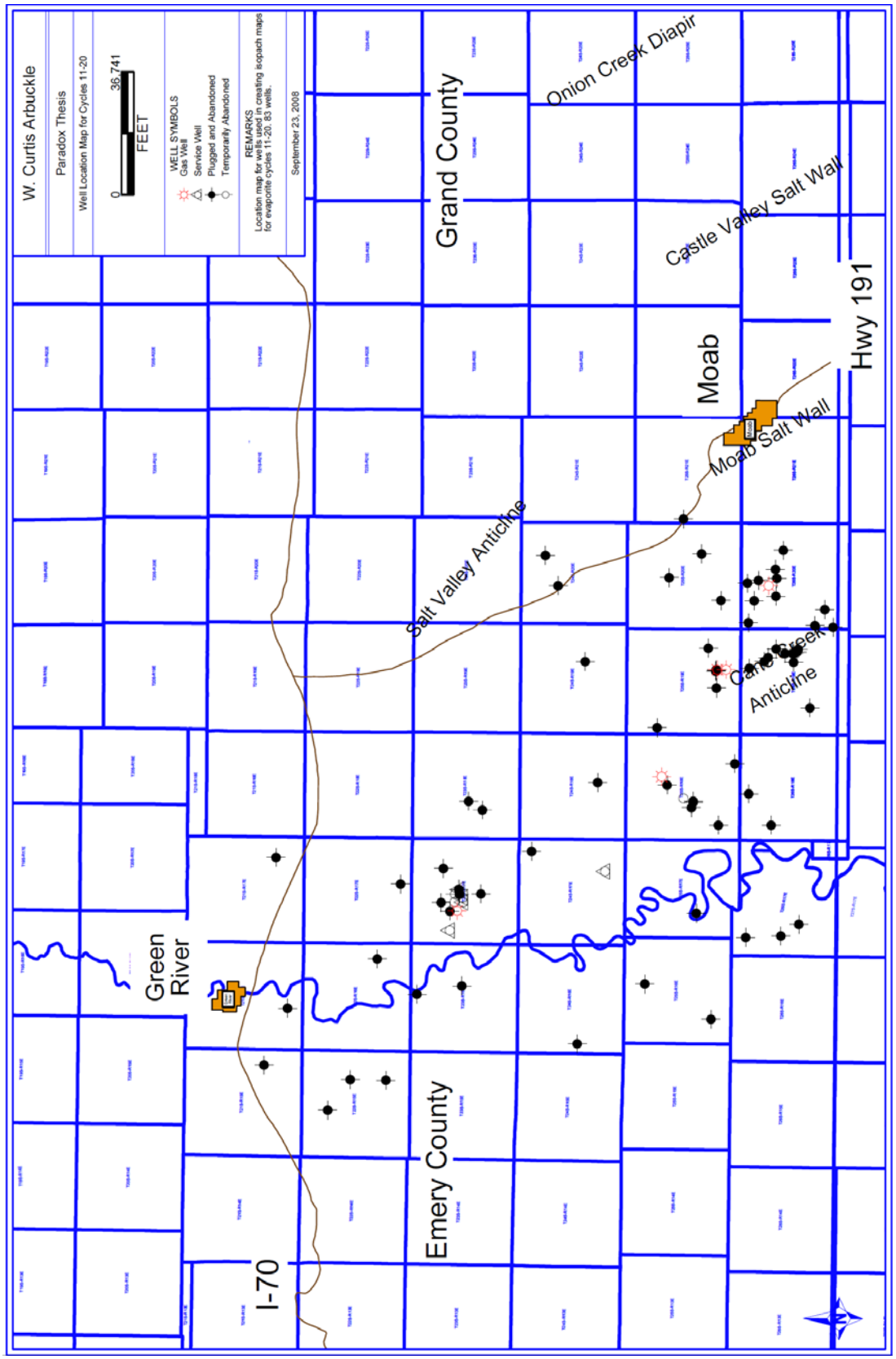

Figure B.2: Map showing the location of the wells used to create evaporite cycle maps 11-20.

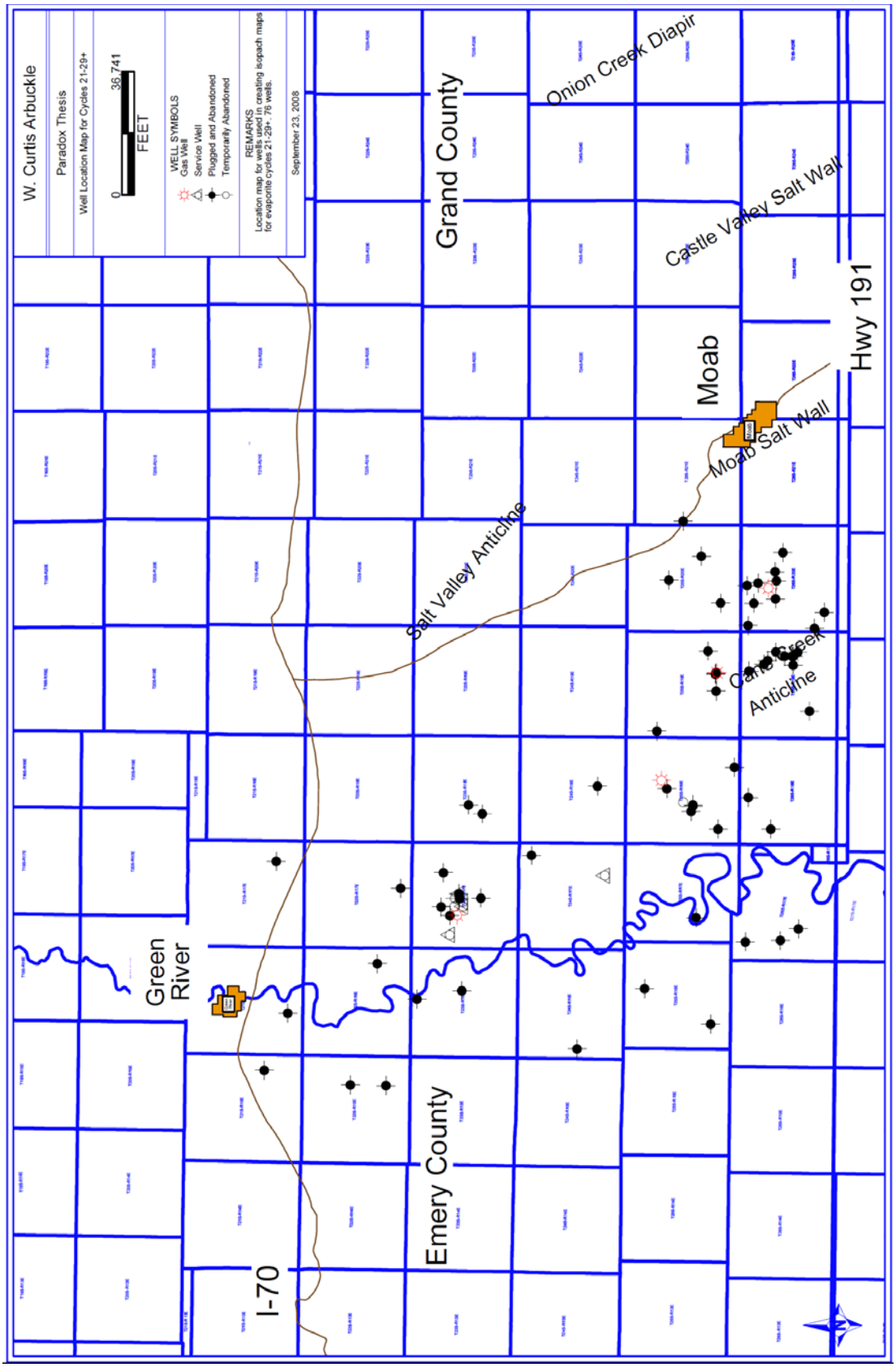

Figure B.3: Map showing the location of the wells used to create evaporite cycle maps 21-29+.

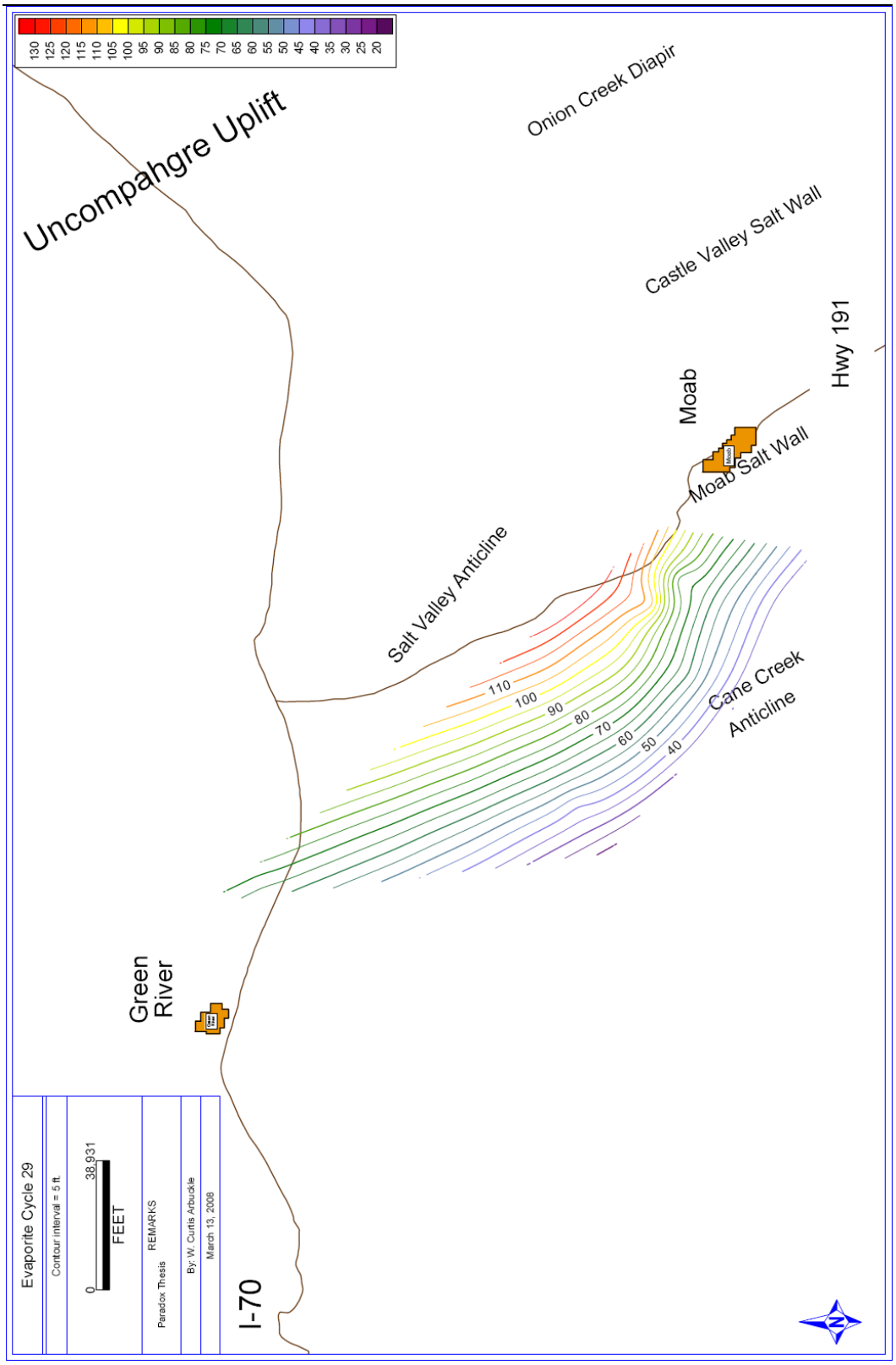

Figure B.4: Isopach map of evaporite cycle 29 within the Paradox Formation. See text for analysis. Contour interval = 5 feet (1.52 m).

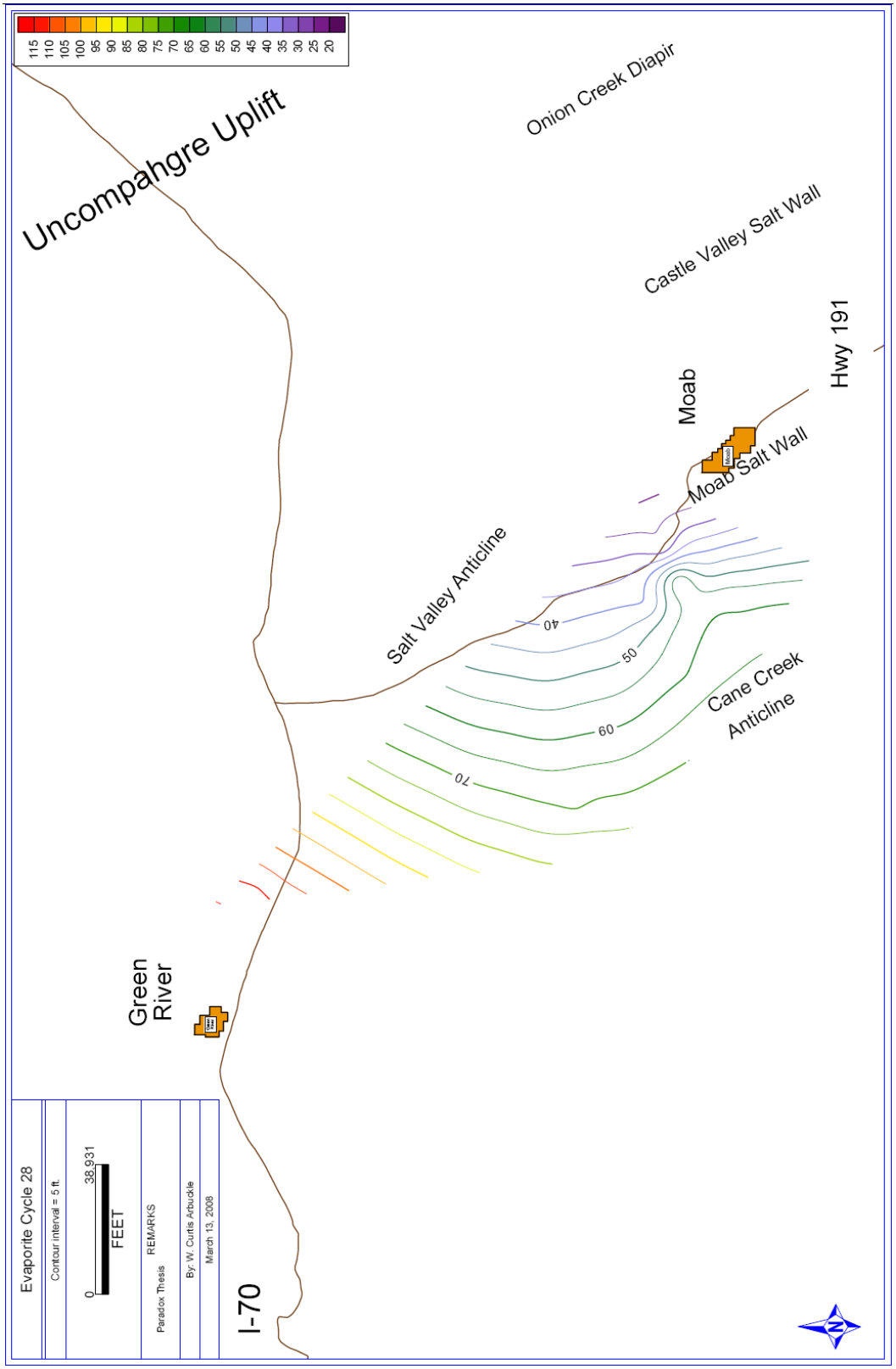

Figure B.5: Isopach map of evaporite cycle 28 within the Paradox Formation. See text for analysis. Contour interval = 5 feet (1.52 m).

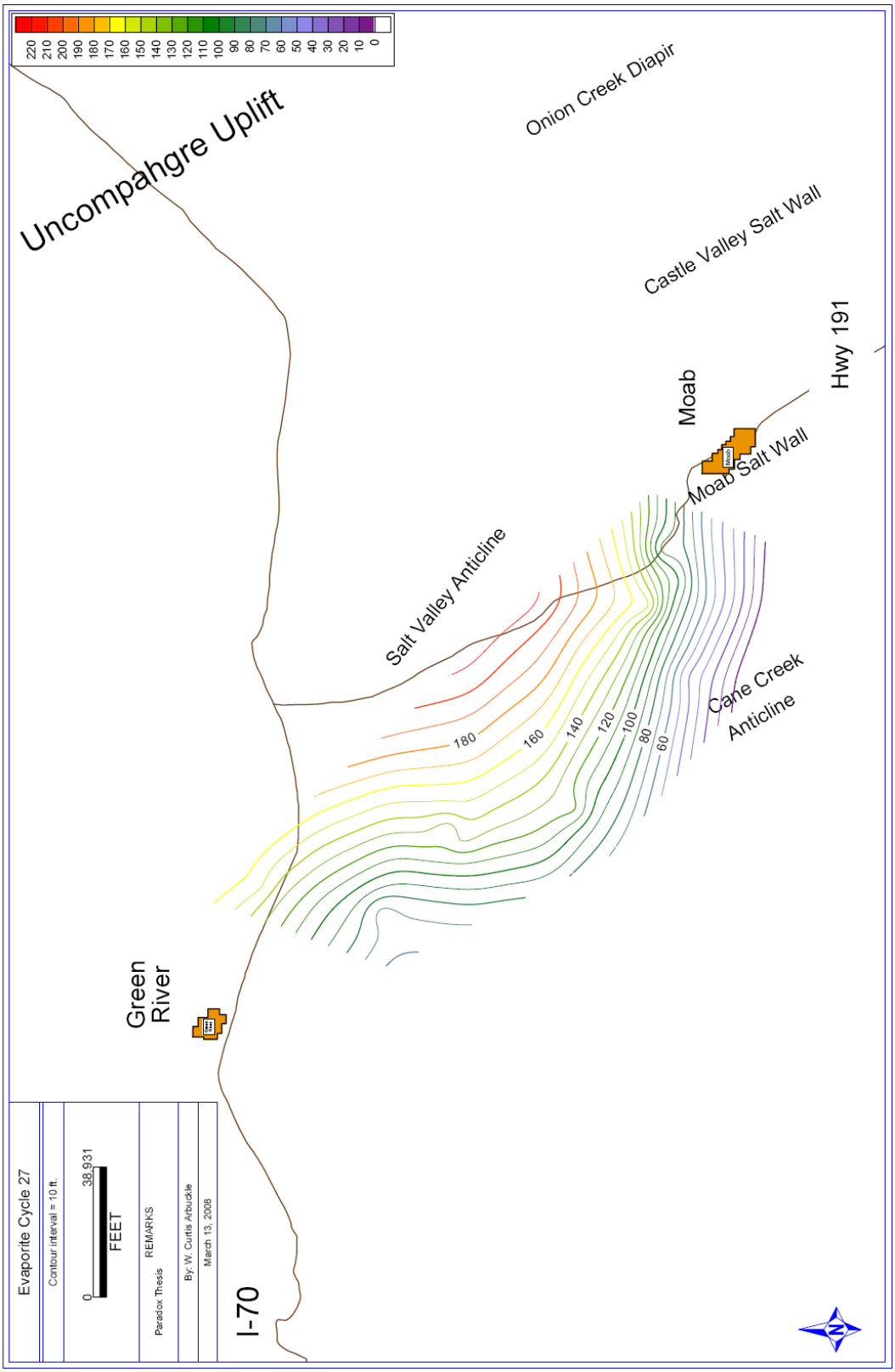

Figure B.6: Isopach map of evaporite cycle 27 within the Paradox Formation. See text for analysis. Contour interval = 10 feet (3.05 m).

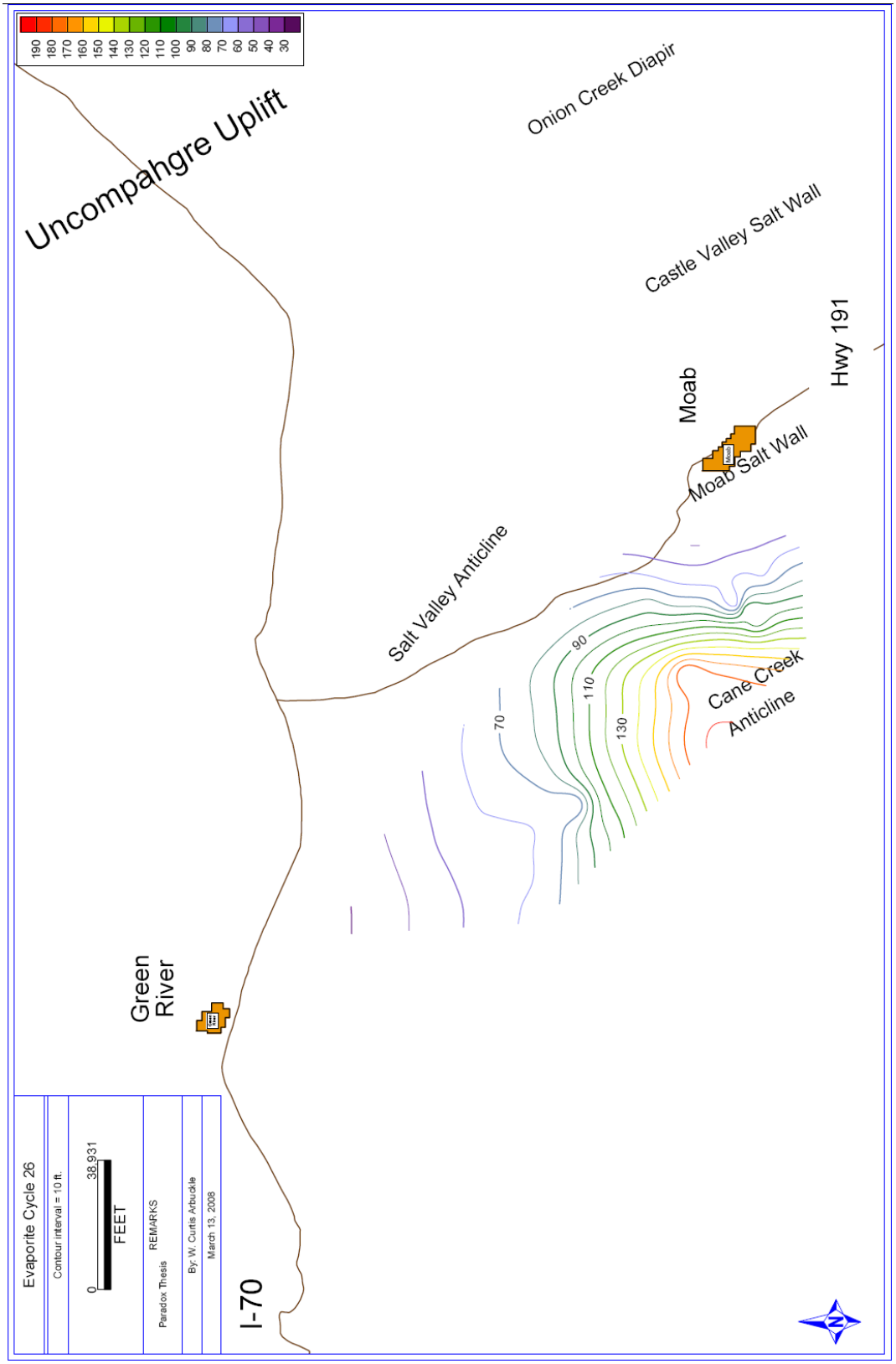

Figure B.7: Isopach map of evaporite cycle 26 within the Paradox Formation. See text for analysis. Contour interval = 10 feet (3.05 m).

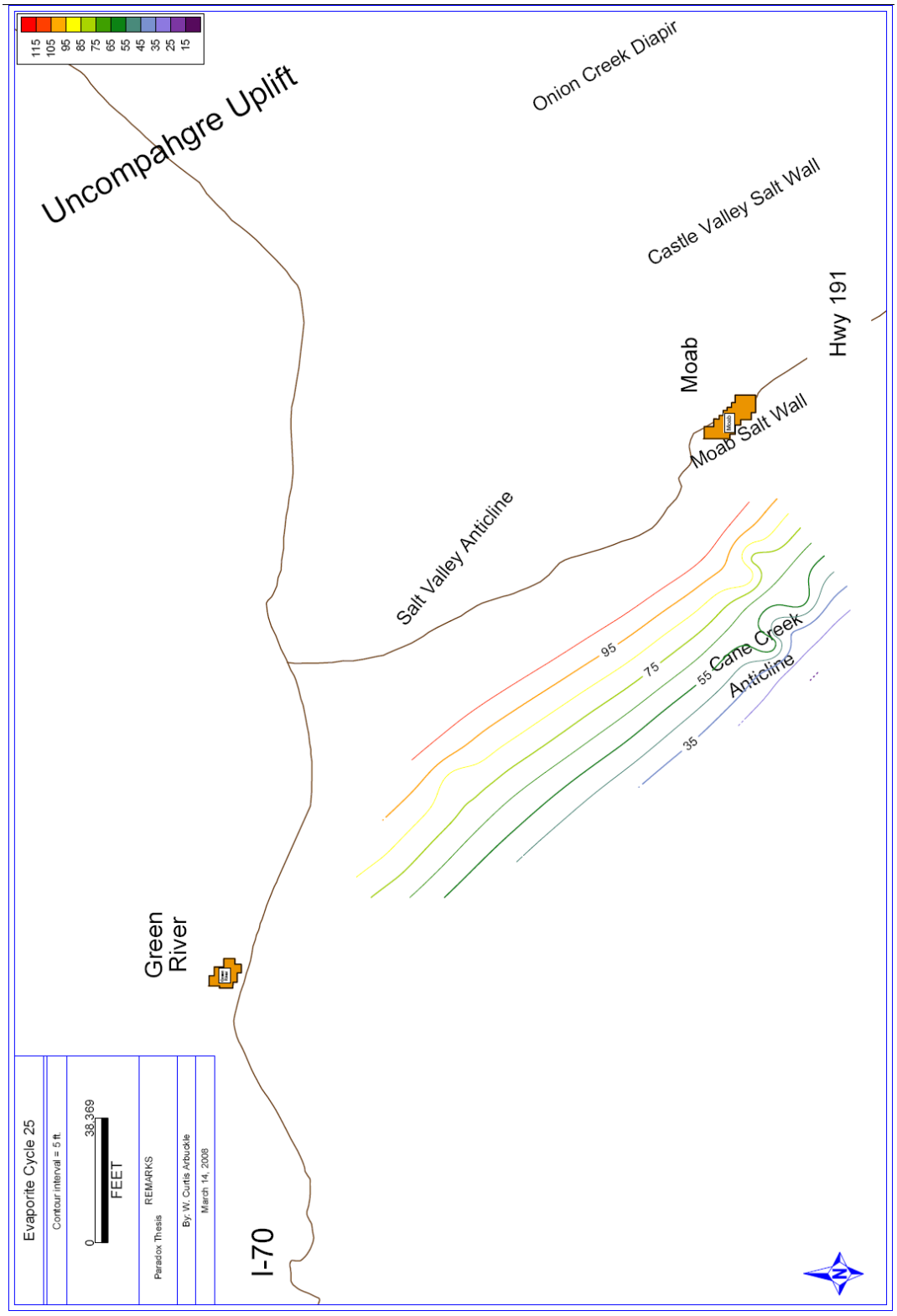

Figure B.8: Isopach map of evaporite cycle 25 within the Paradox Formation. See text for analysis. Contour interval = 5 feet (1.52 m).

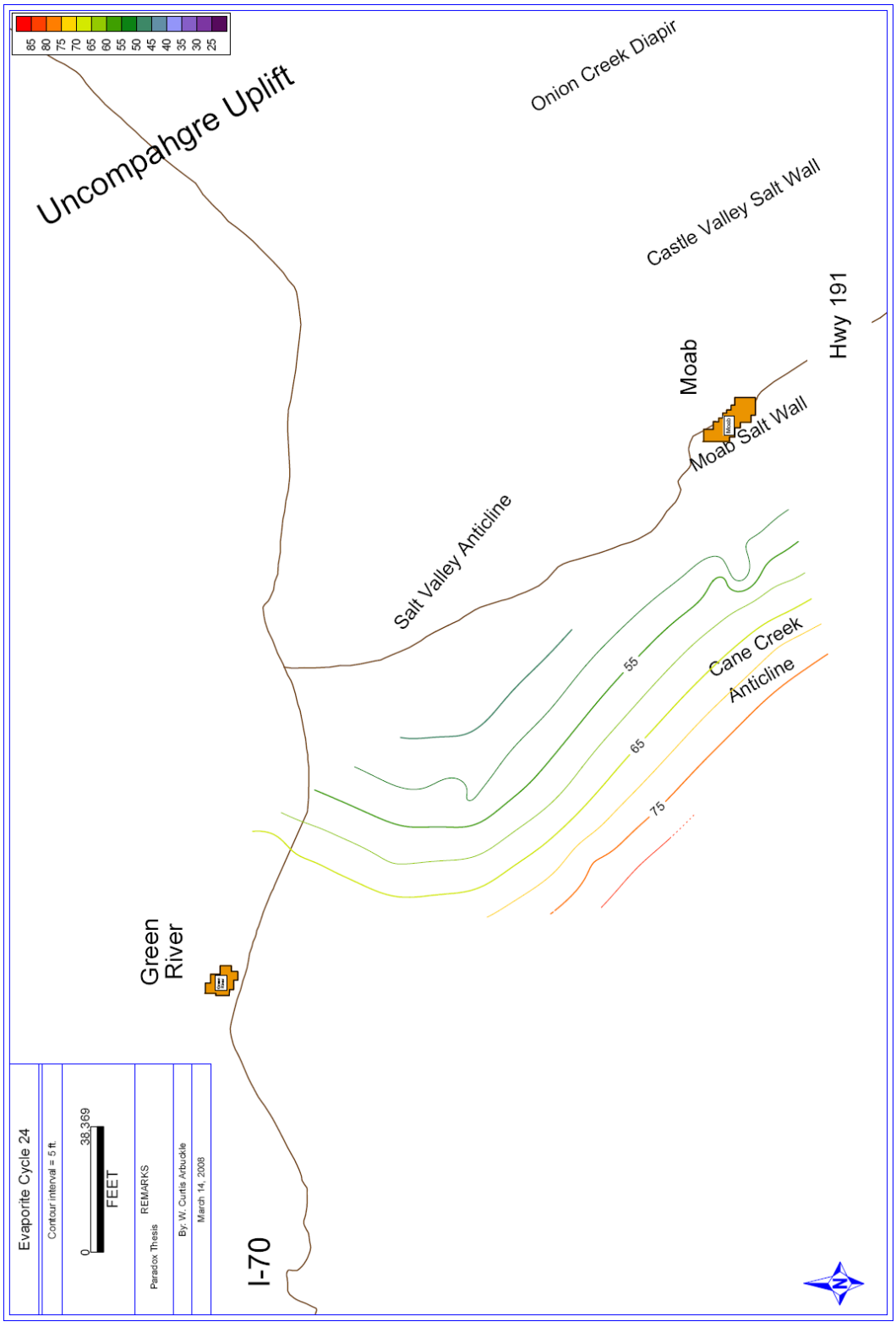

Figure B.9: Isopach map of evaporite cycle 24 within the Paradox Formation. See text for analysis. Contour interval = 5 feet (1.52 m).

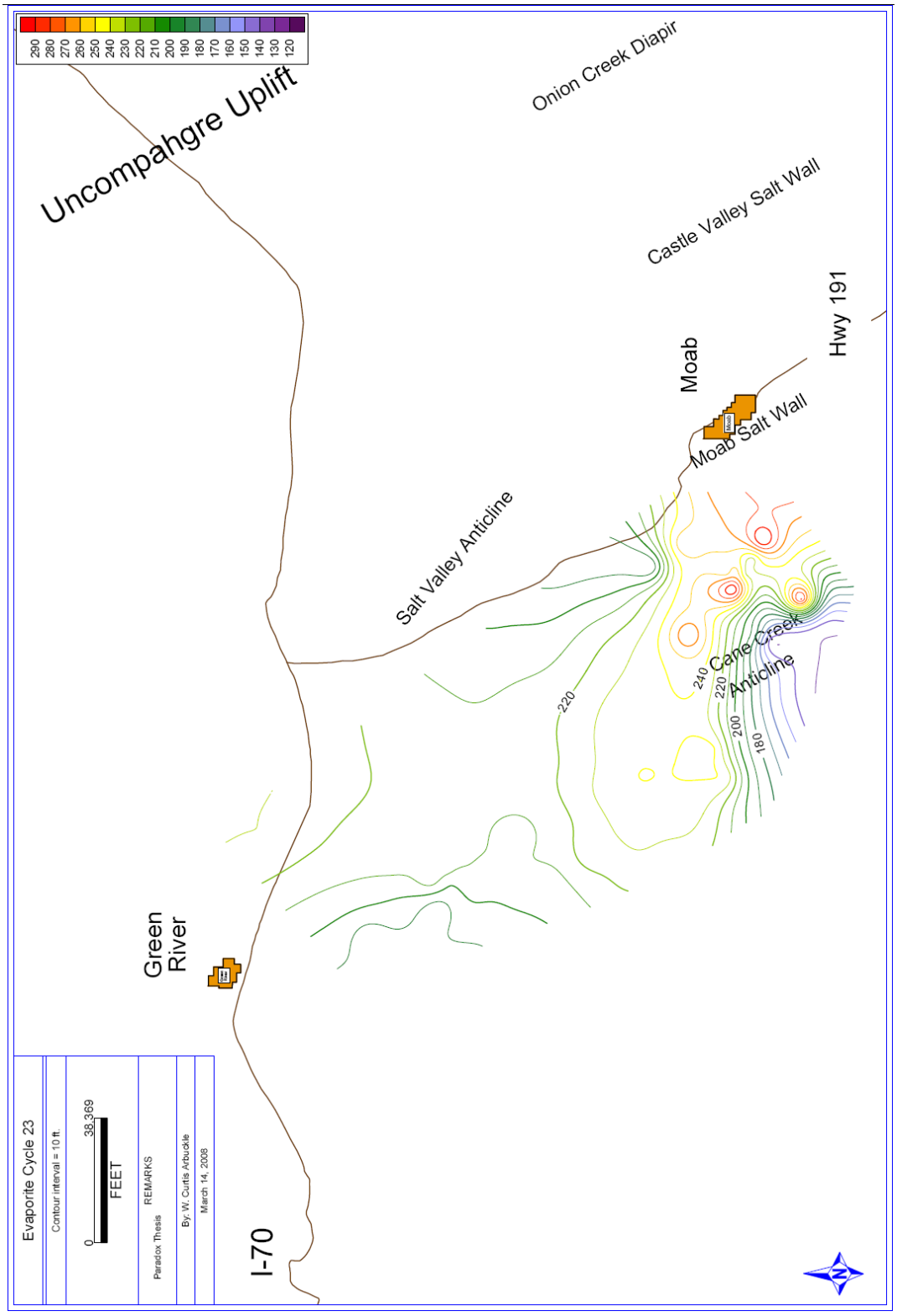

Figure B.10: Isopach map of evaporite cycle 23 within the Paradox Formation. See text for analysis. Contour interval = 10 feet (3.05 m).

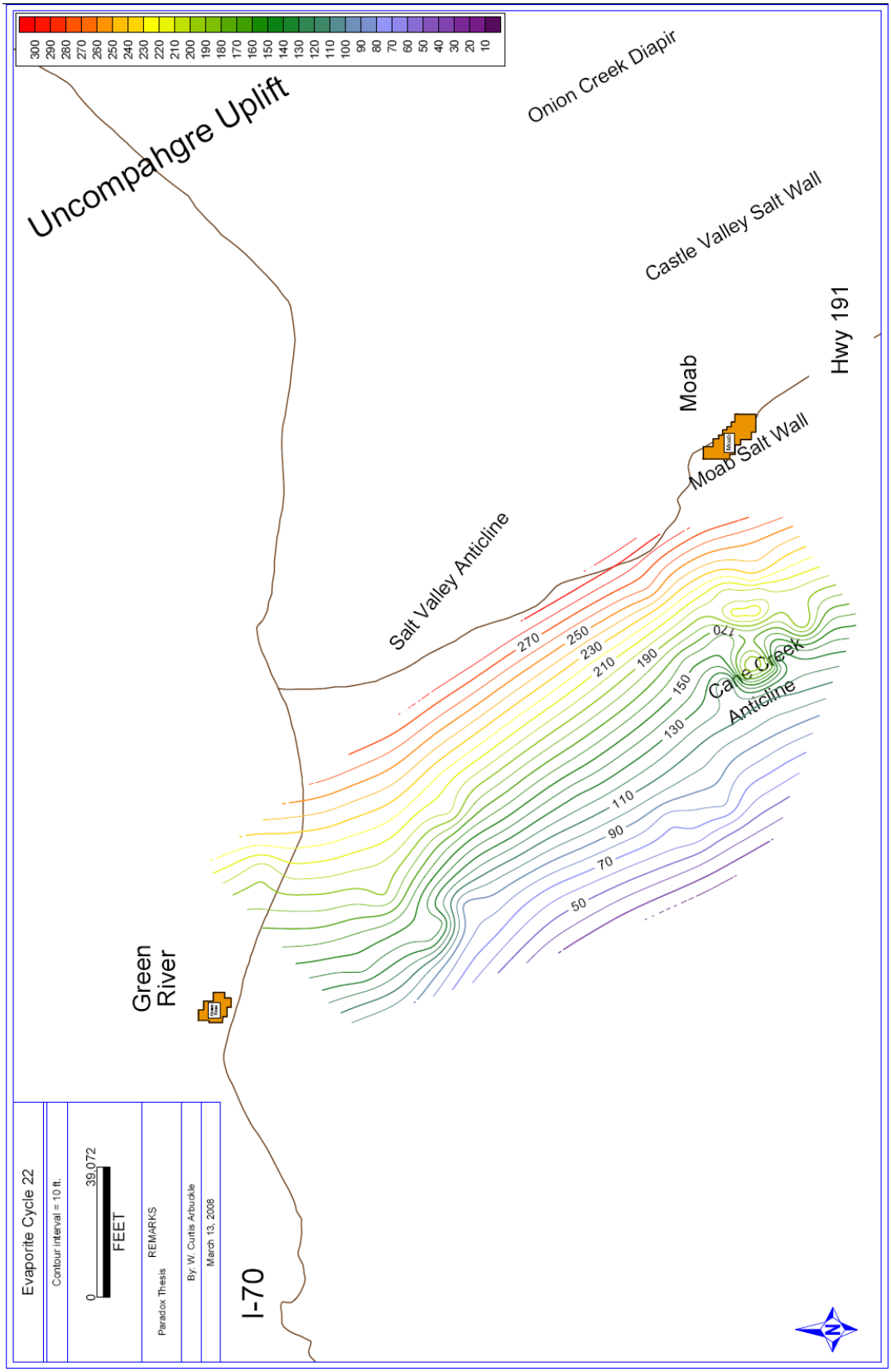

Figure B.11: Isopach map of evaporite cycle 22 within the Paradox Formation. See text for analysis. Contour interval = 10 feet (3.05 m).

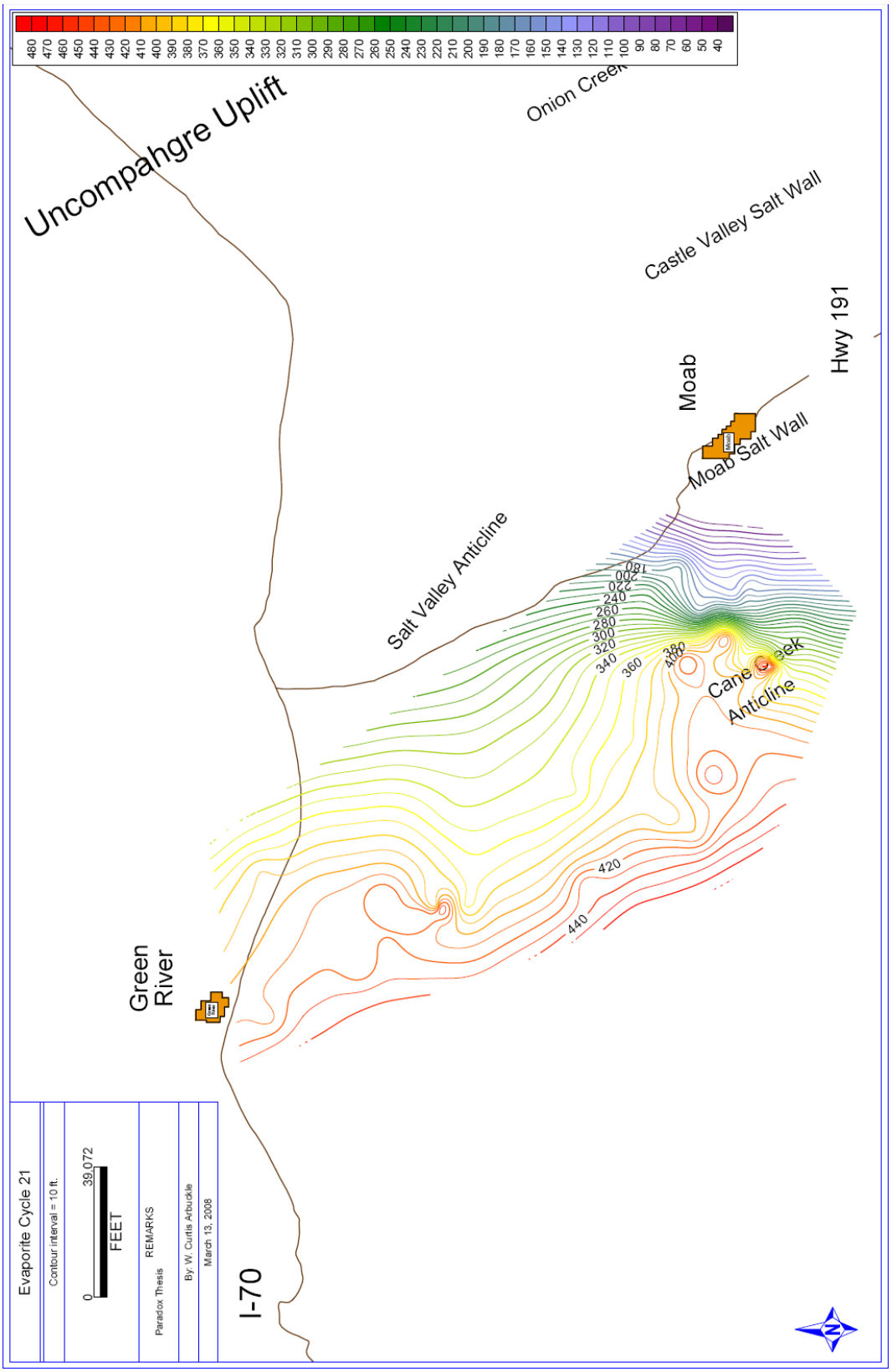

Figure B.12: Isopach map of evaporite cycle 21 within the Paradox Formation. See text for analysis. Contour interval = 10 feet (3.05 m).

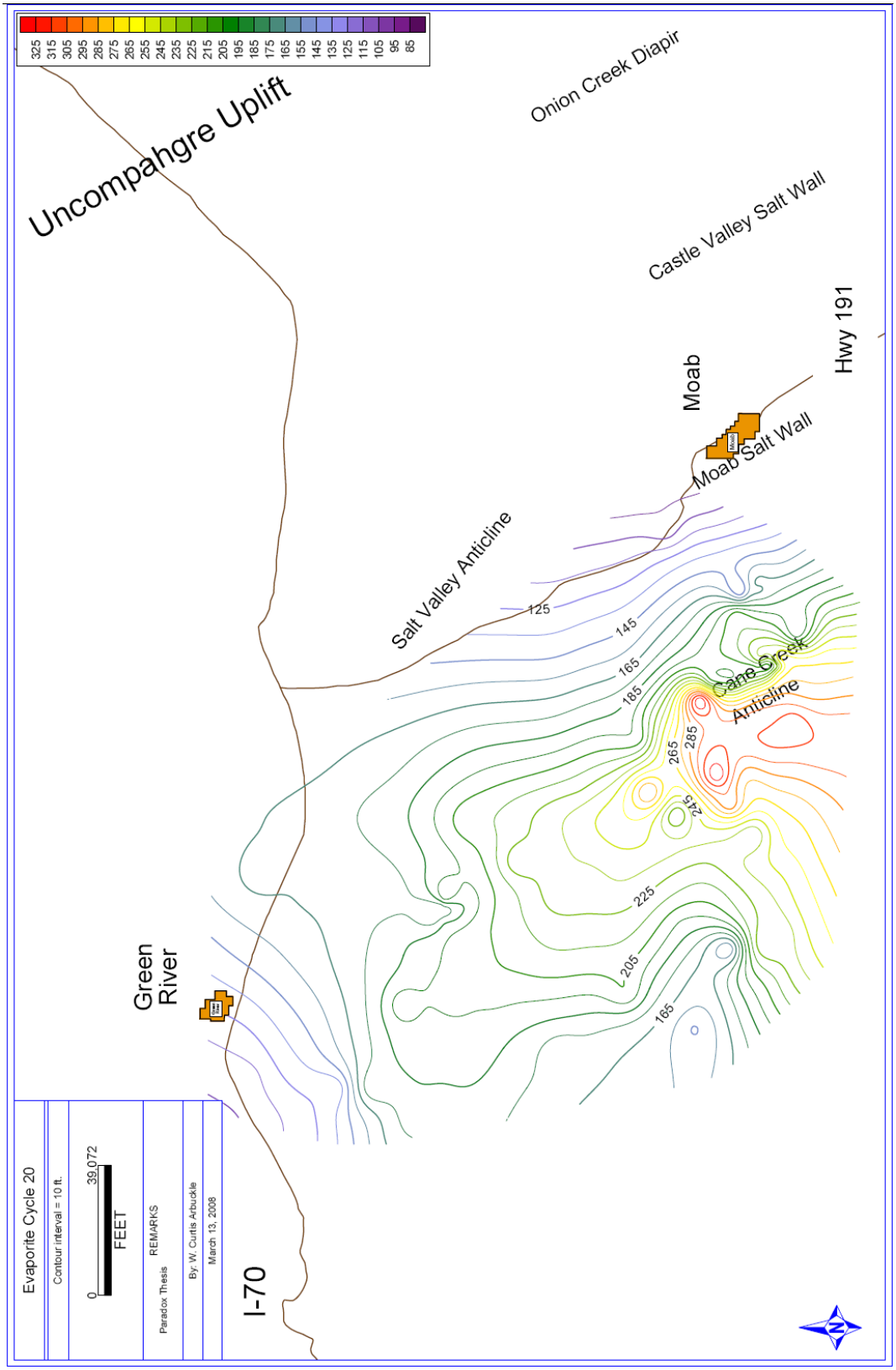

Figure B.13: Isopach map of evaporite cycle 20 within the Paradox Formation. See text for analysis. Contour interval = 10 feet (3.05 m).

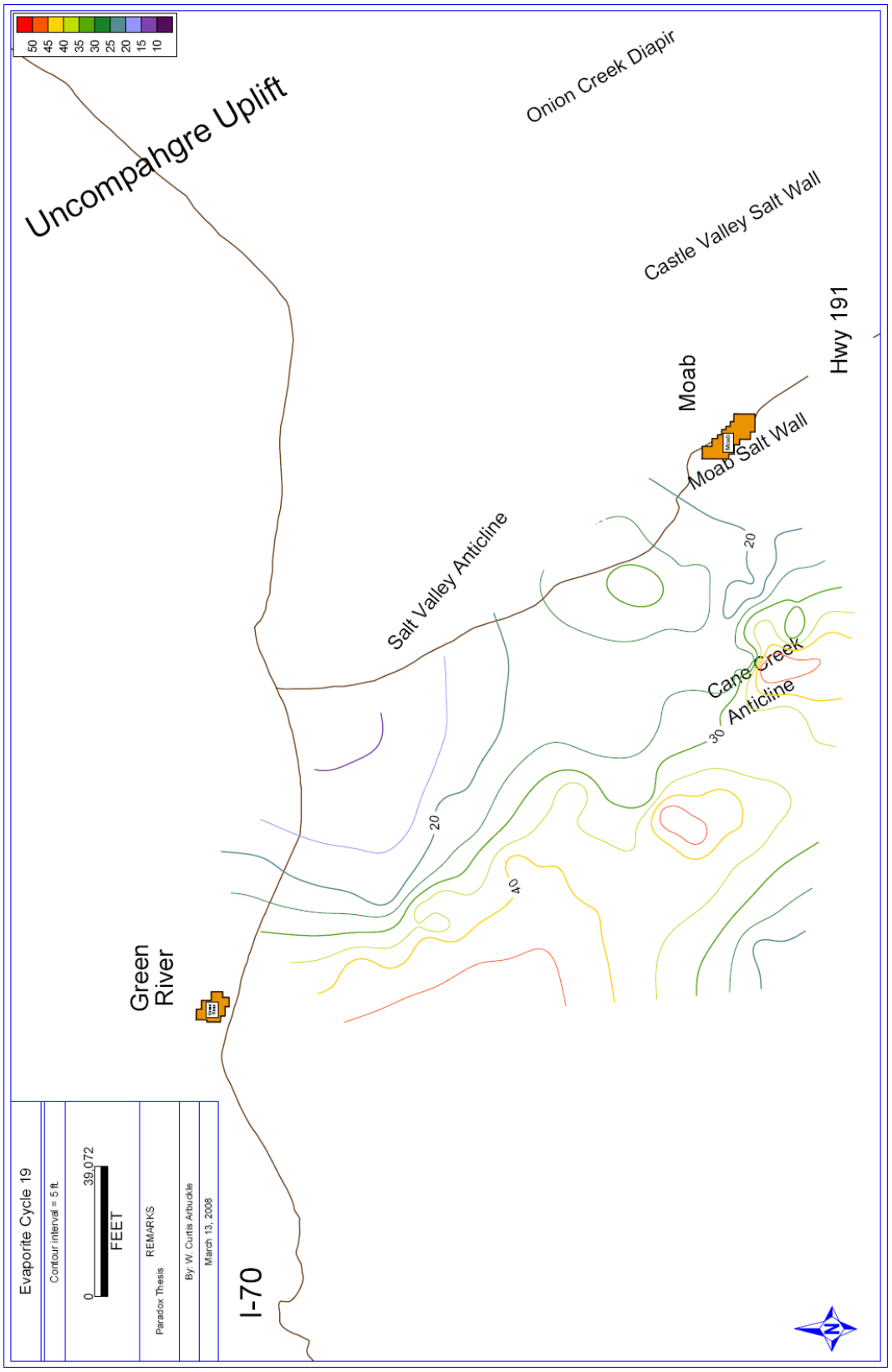

Figure B.14: Isopach map of evaporite cycle 19 within the Paradox Formation. See text for analysis. Contour interval = 5 feet (1.52 m).

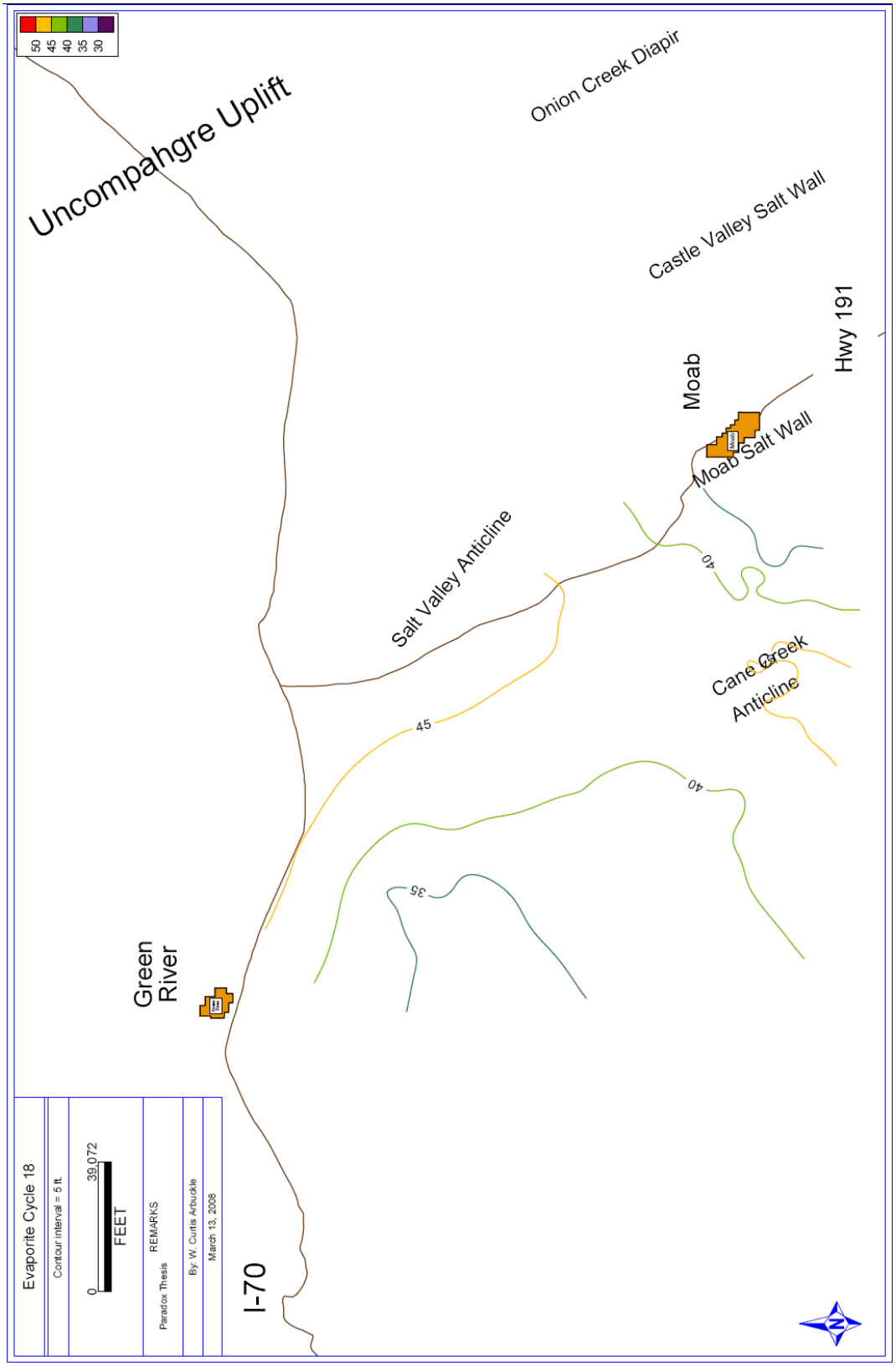

Figure B.15: Isopach map of evaporite cycle 18 within the Paradox Formation. See text for analysis. Contour interval = 5 feet (1.52 m).

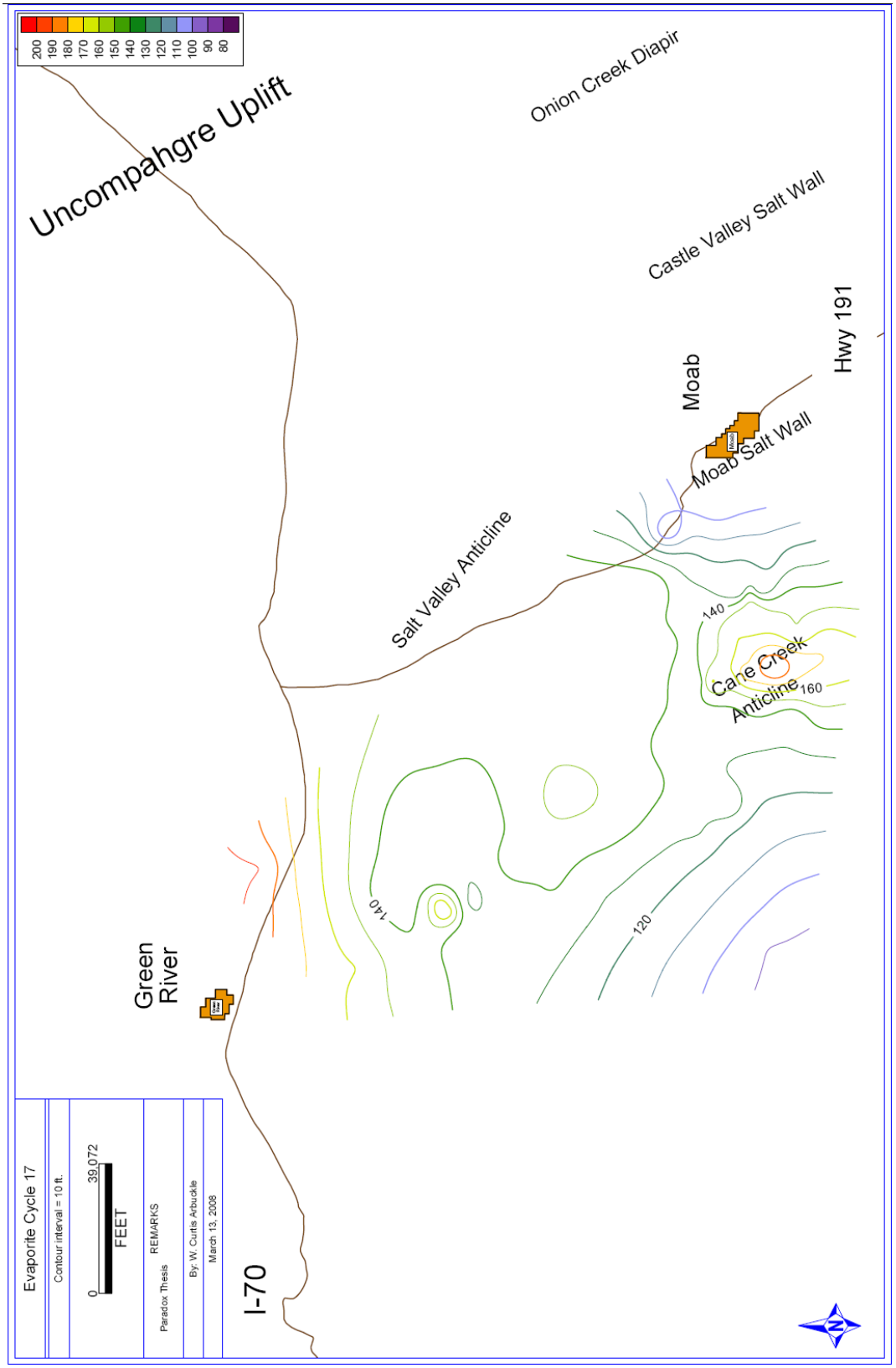

Figure B.16: Isopach map of evaporite cycle 17 within the Paradox Formation. See text for analysis. Contour interval = 10 feet (3.05 m).

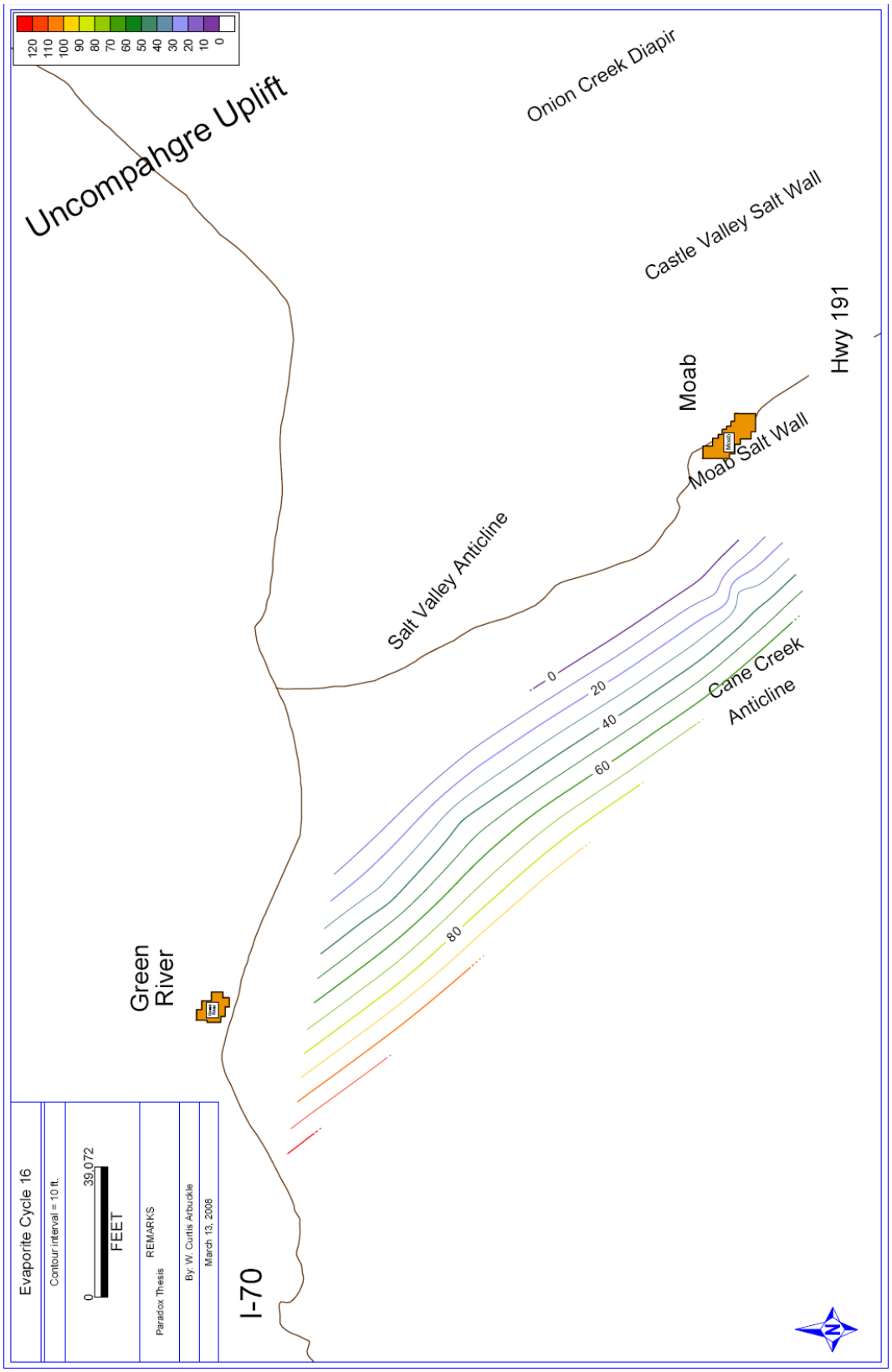

Figure B.17: Isopach map of evaporite cycle 16 within the Paradox Formation. See text for analysis. Contour interval = 10 feet (3.05 m).

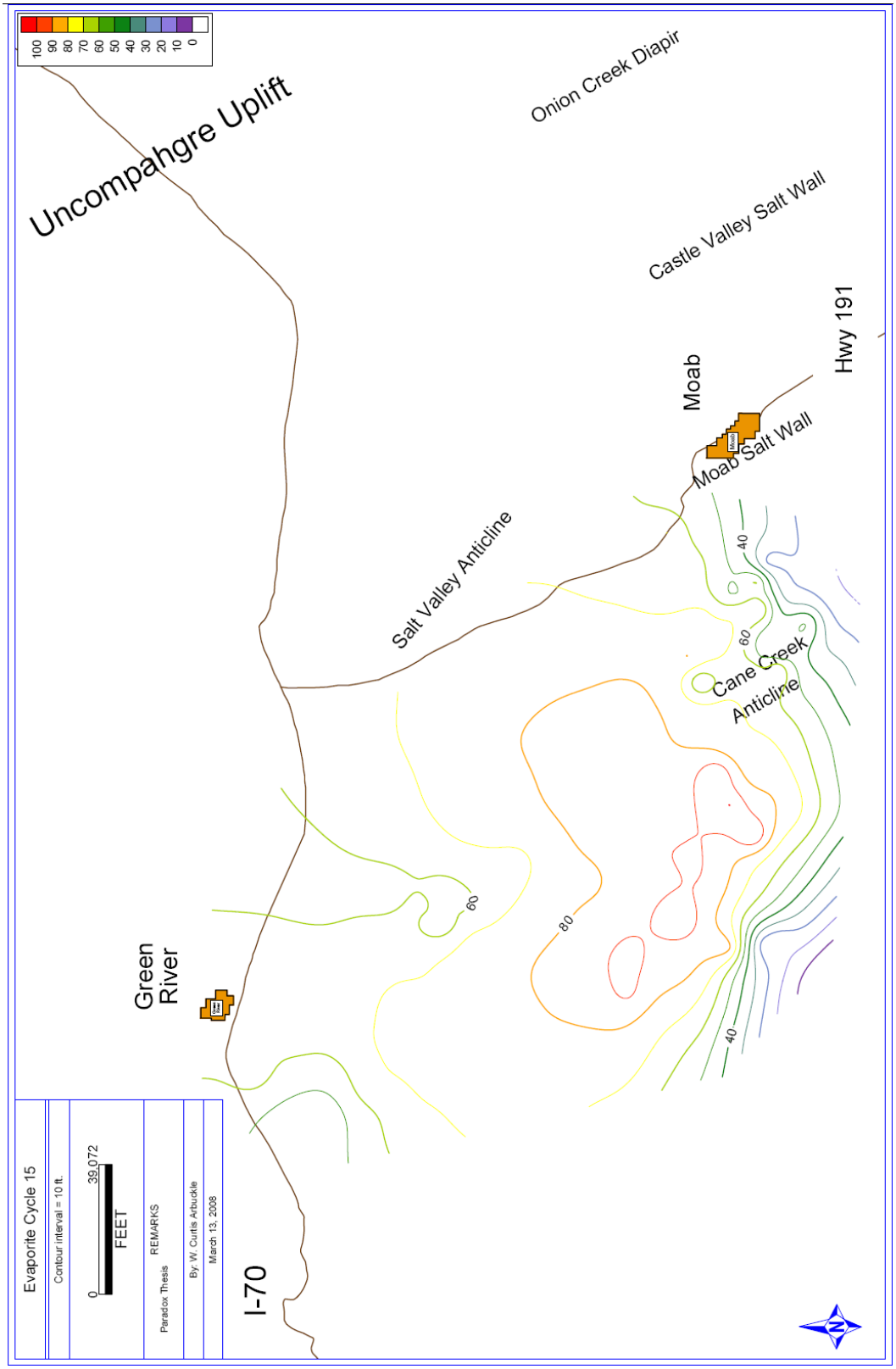

Figure B.18: Isopach map of evaporite cycle 15 within the Paradox Formation. See text for analysis. Contour interval = 10 feet (3.05 m).

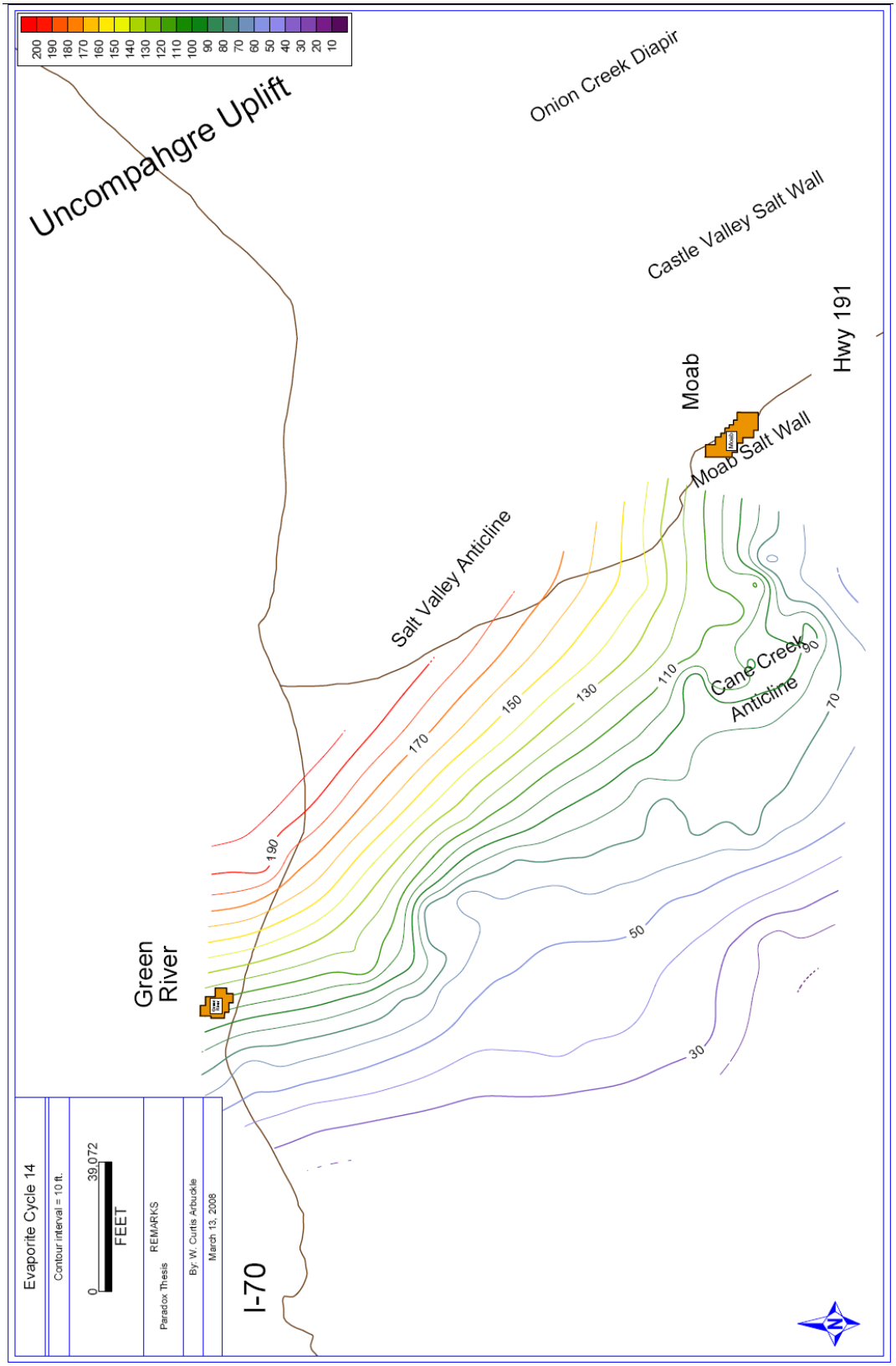

Figure B.19: Isopach map of evaporite cycle 14 within the Paradox Formation. See text for analysis. Contour interval = 10 feet (3.05 m).

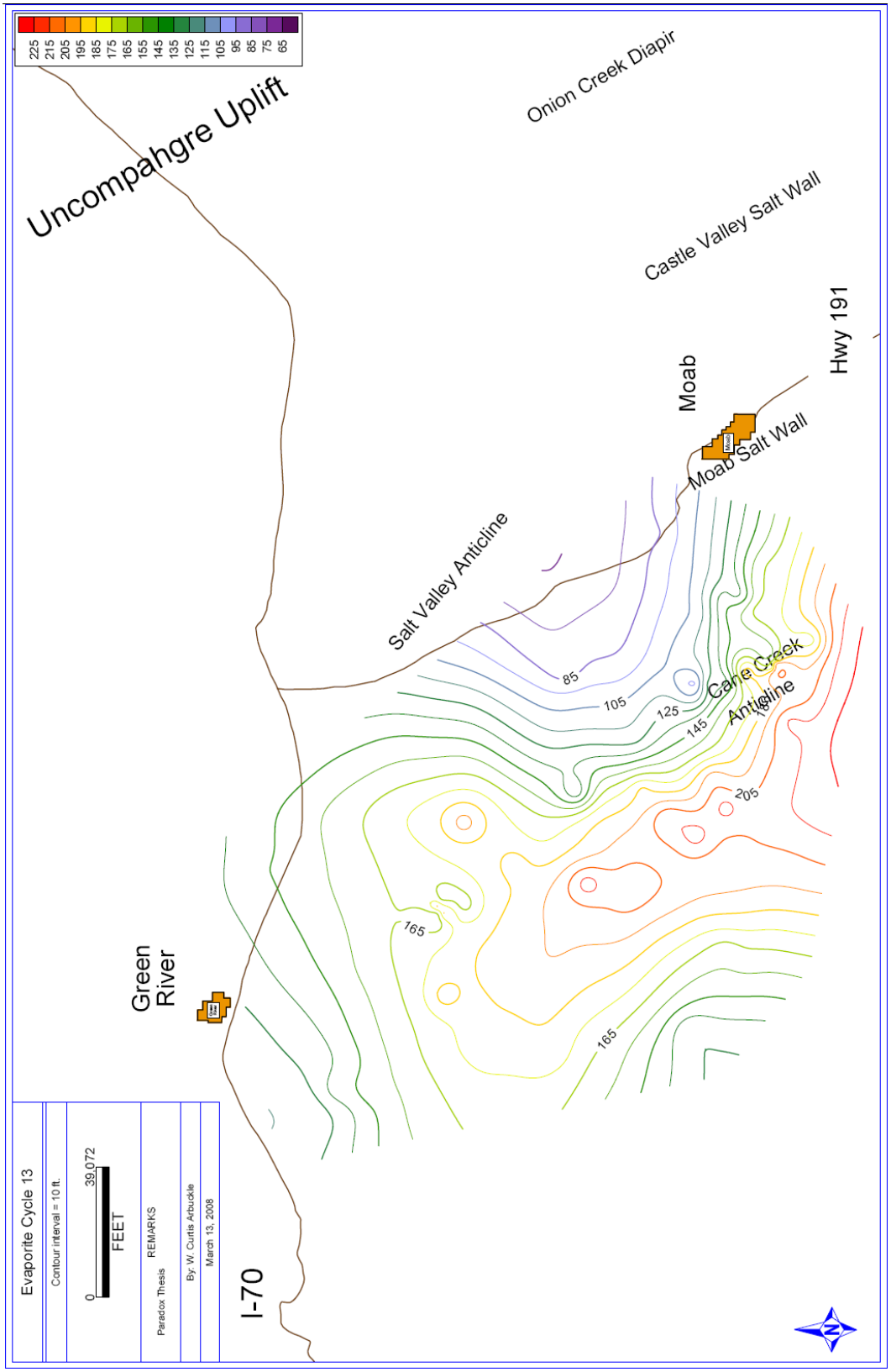

Figure B.20: Isopach map of evaporite cycle 13 within the Paradox Formation. See text for analysis. Contour interval = 10 feet (3.05 m).

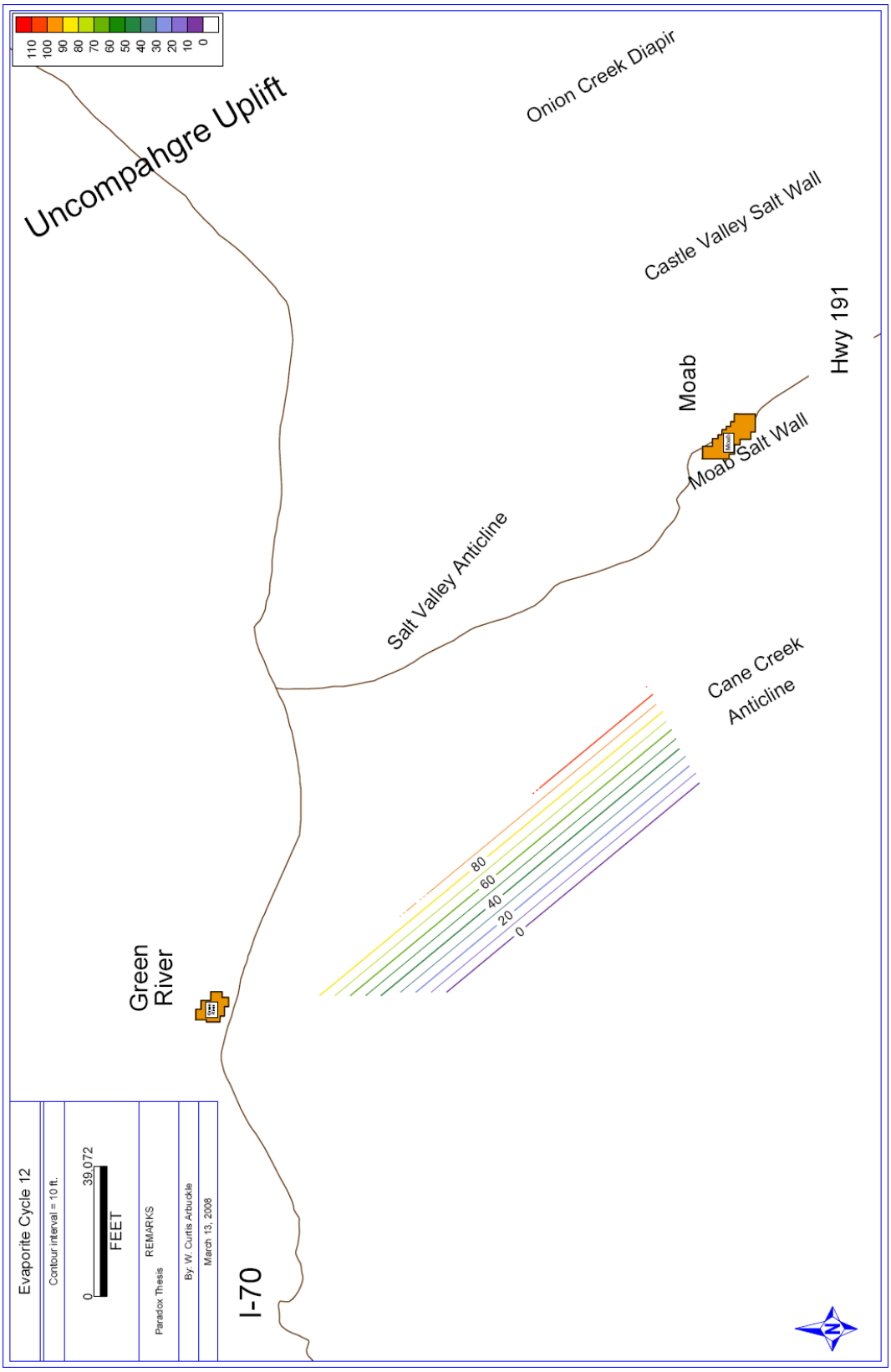

Figure B.21: Isopach map of evaporite cycle 12 within the Paradox Formation. See text for analysis. Contour interval = 10 feet (3.05 m).

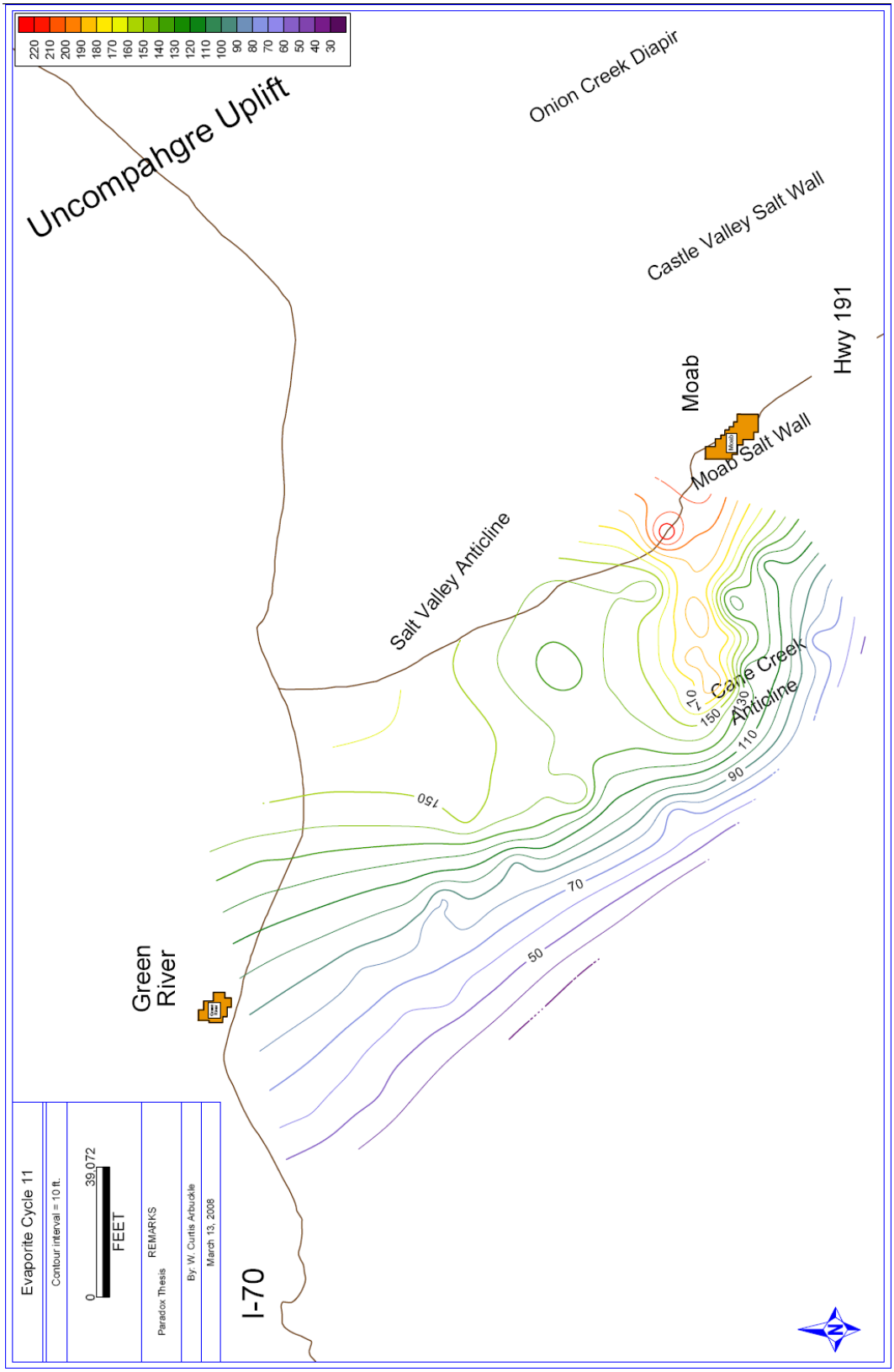

Figure B.22: Isopach map of evaporite cycle 11 within the Paradox Formation. See text for analysis. Contour interval = 10 feet (3.05 m).

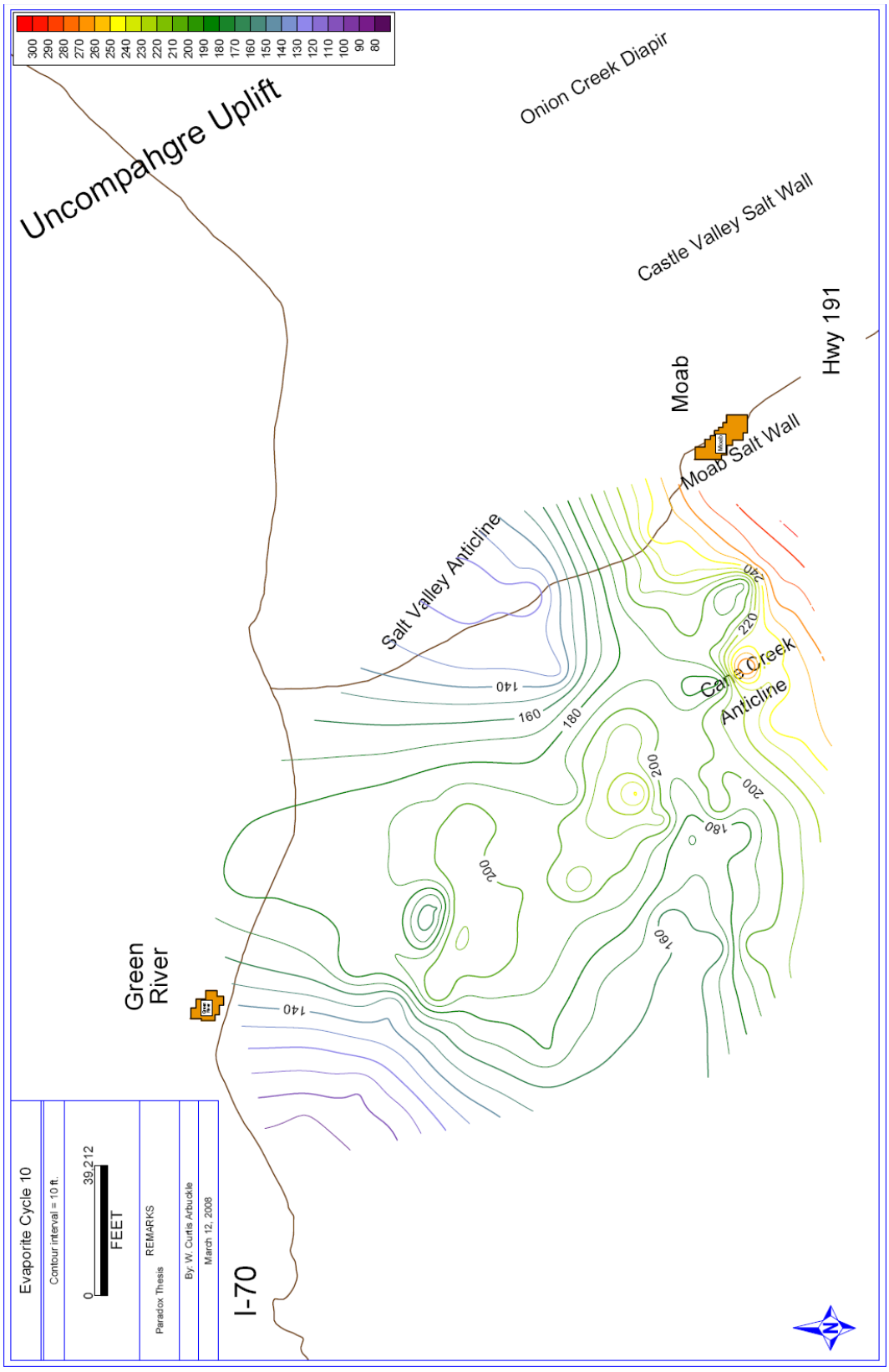

Figure B.23: Isopach map of evaporite cycle 10 within the Paradox Formation. See text for analysis. Contour interval = 10 feet (3.05 m).

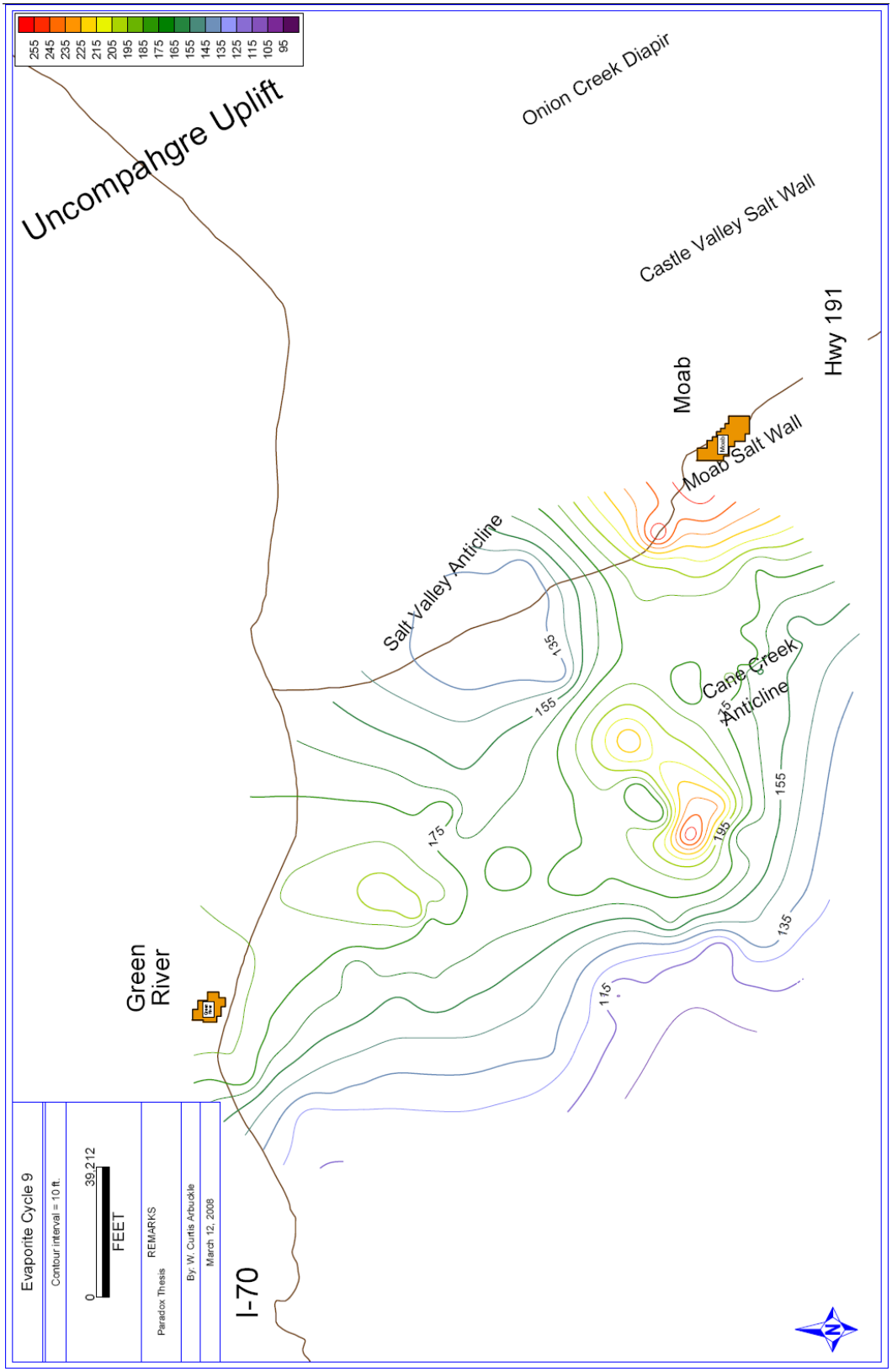

Figure B.24: Isopach map of evaporite cycle 9 within the Paradox Formation. See text for analysis. Contour interval = 10 feet (3.05 m).

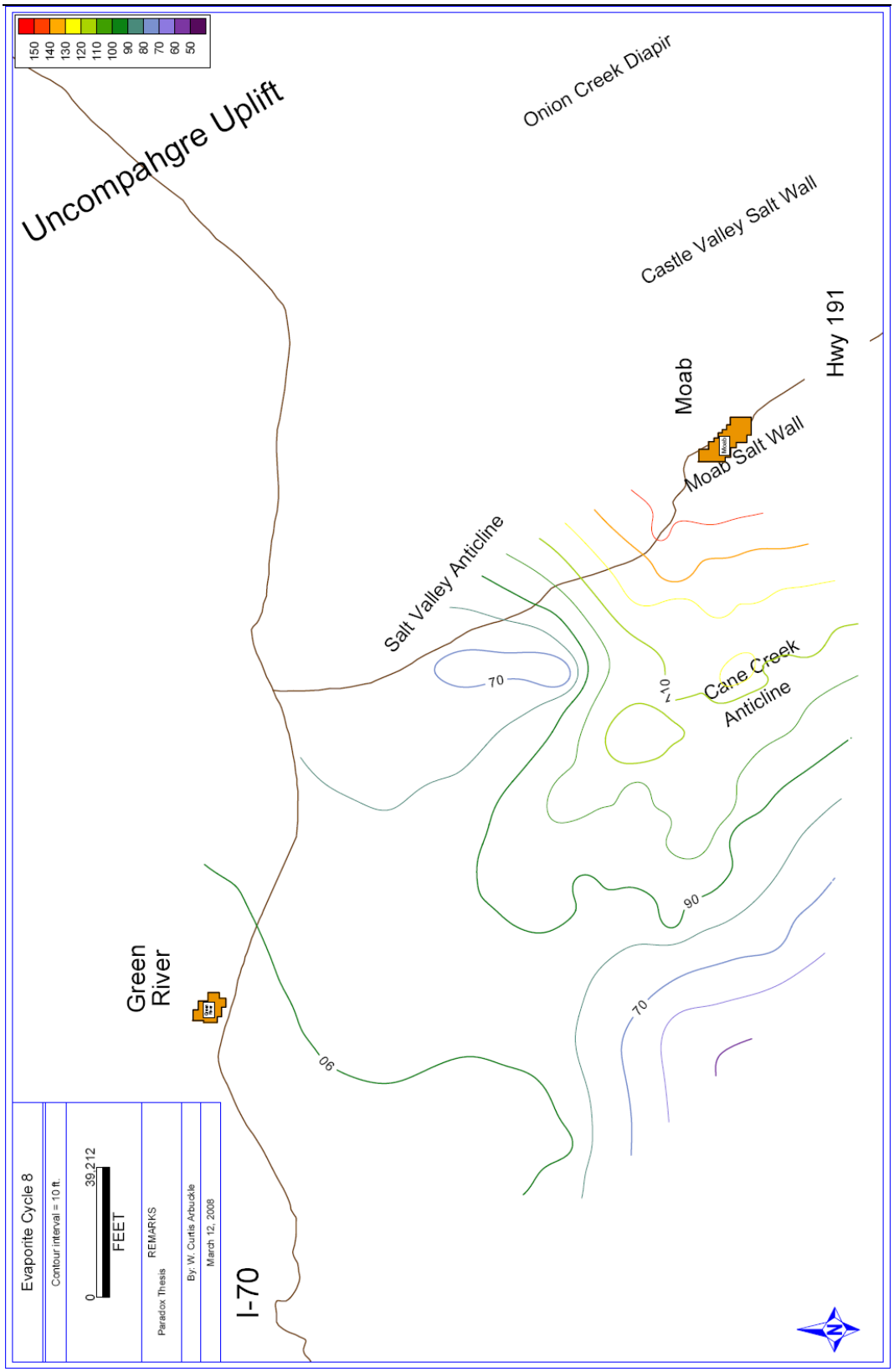

Figure B.25: Isopach map of evaporite cycle 8 within the Paradox Formation. See text for analysis. Contour interval = 10 feet (3.05 m).

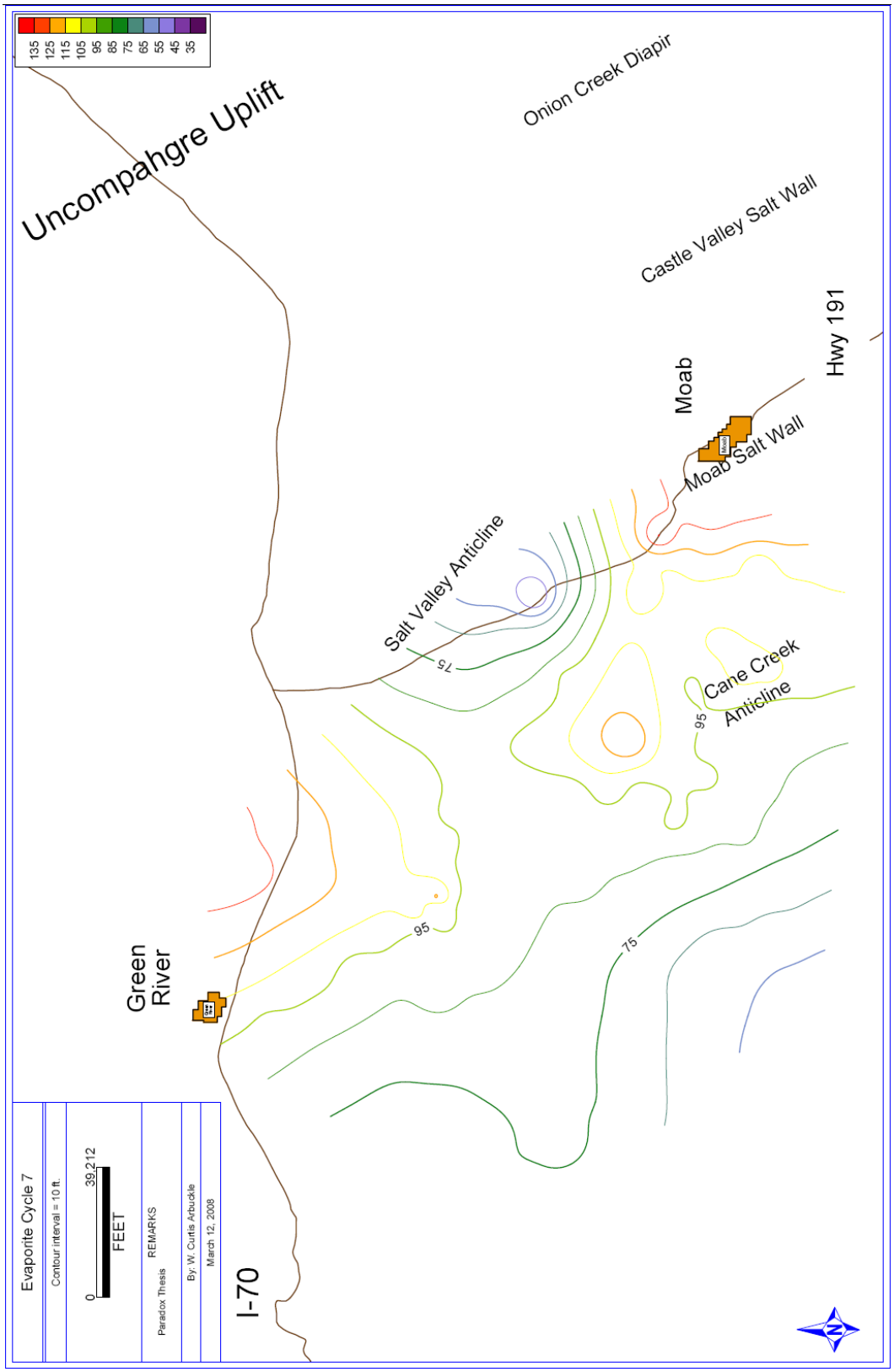

Figure B.26: Isopach map of evaporite cycle 7 within the Paradox Formation. See text for analysis. Contour interval = 10 feet (3.05 m).

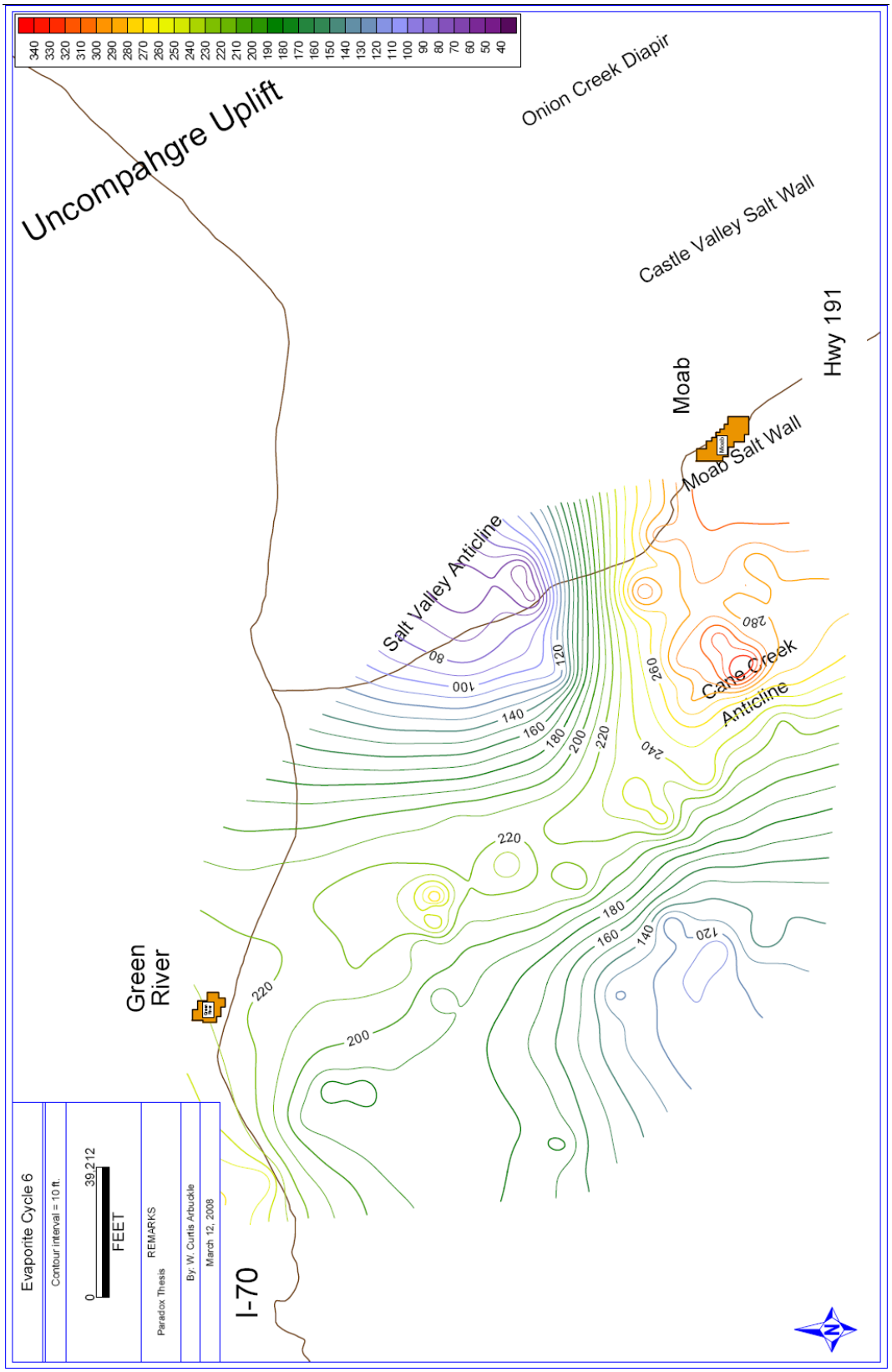

Figure B.27: Isopach map of evaporite cycle 6 within the Paradox Formation. See text for analysis. Contour interval = 10 feet (3.05 m).

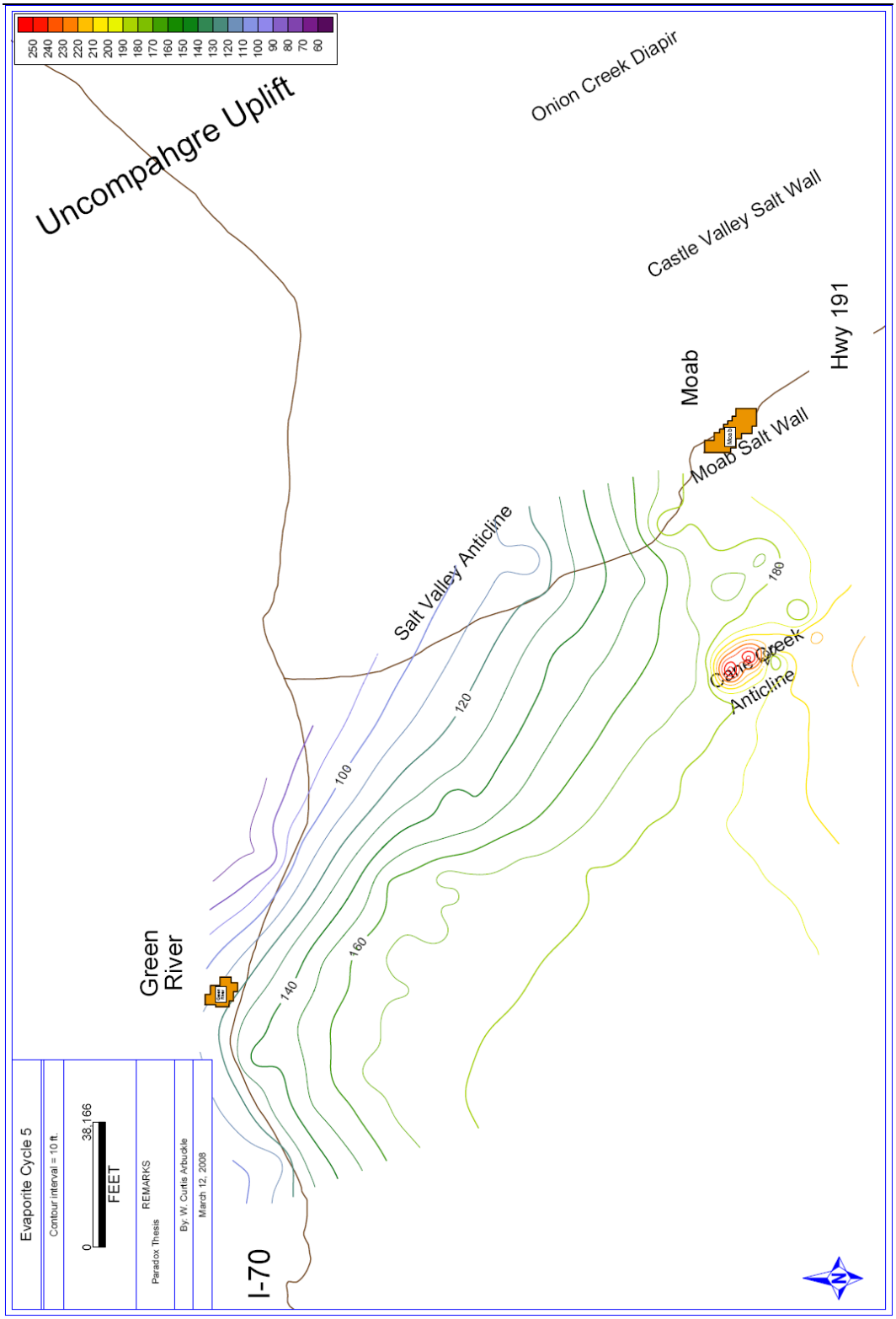

Figure B.28: Isopach map of evaporite cycle 5 within the Paradox Formation. See text for analysis. Contour interval = 10 feet (3.05 m).

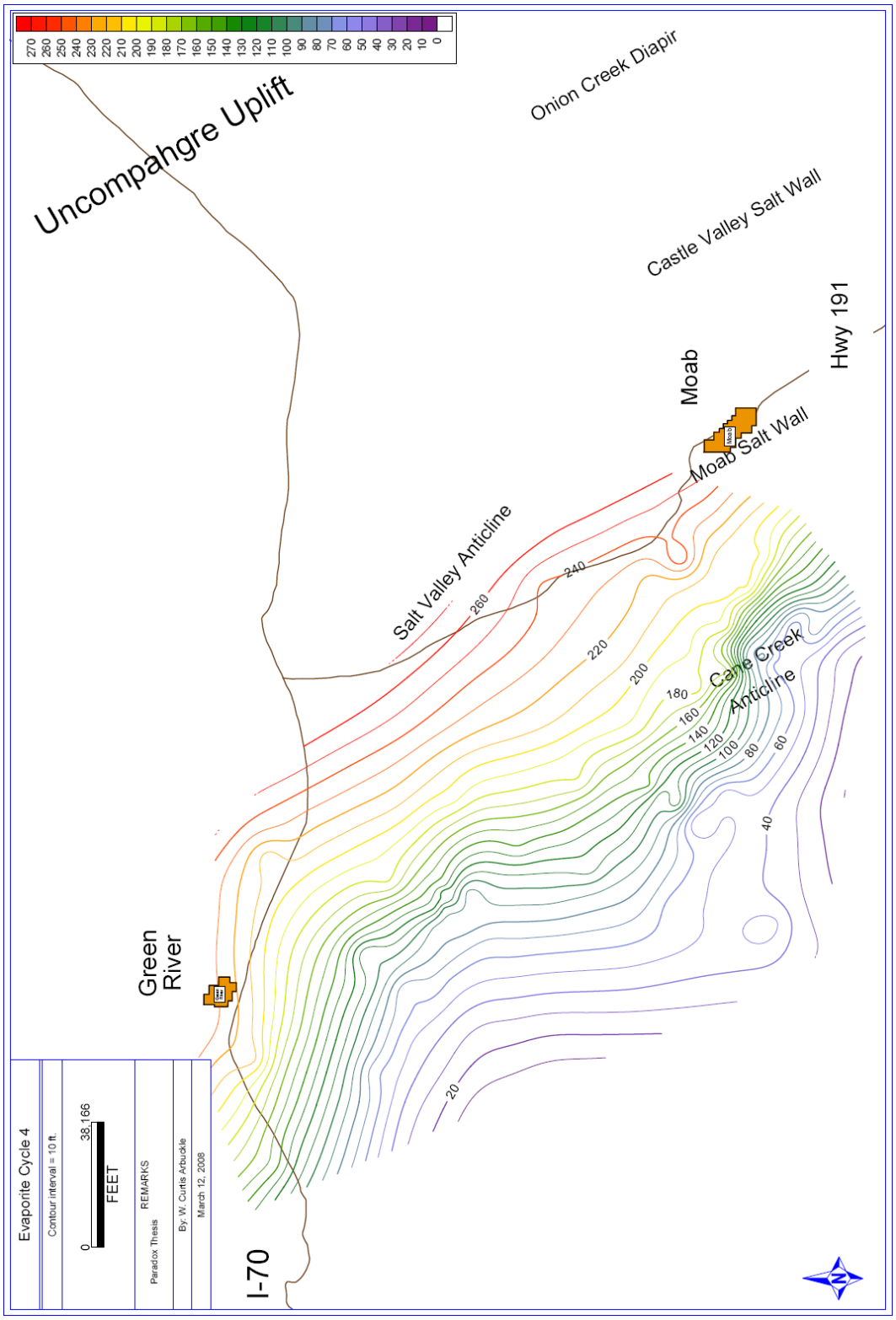

Figure B.29: Isopach map of evaporite cycle 4 within the Paradox Formation. See text for analysis. Contour interval = 10 feet (3.05 m).

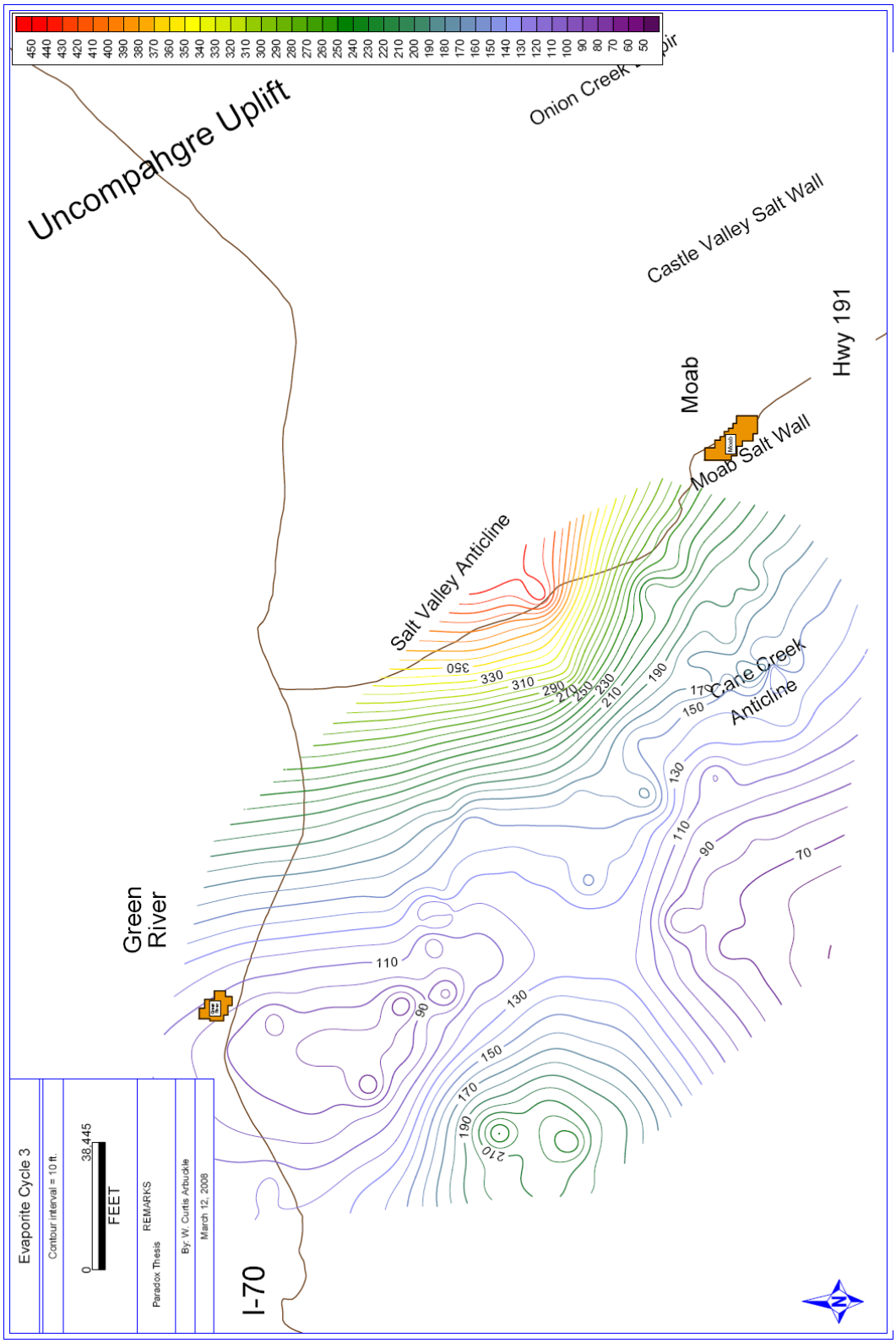

Figure B.30: Isopach map of evaporite cycle 3 within the Paradox Formation. See text for analysis. Contour interval = 10 feet (3.05 m).

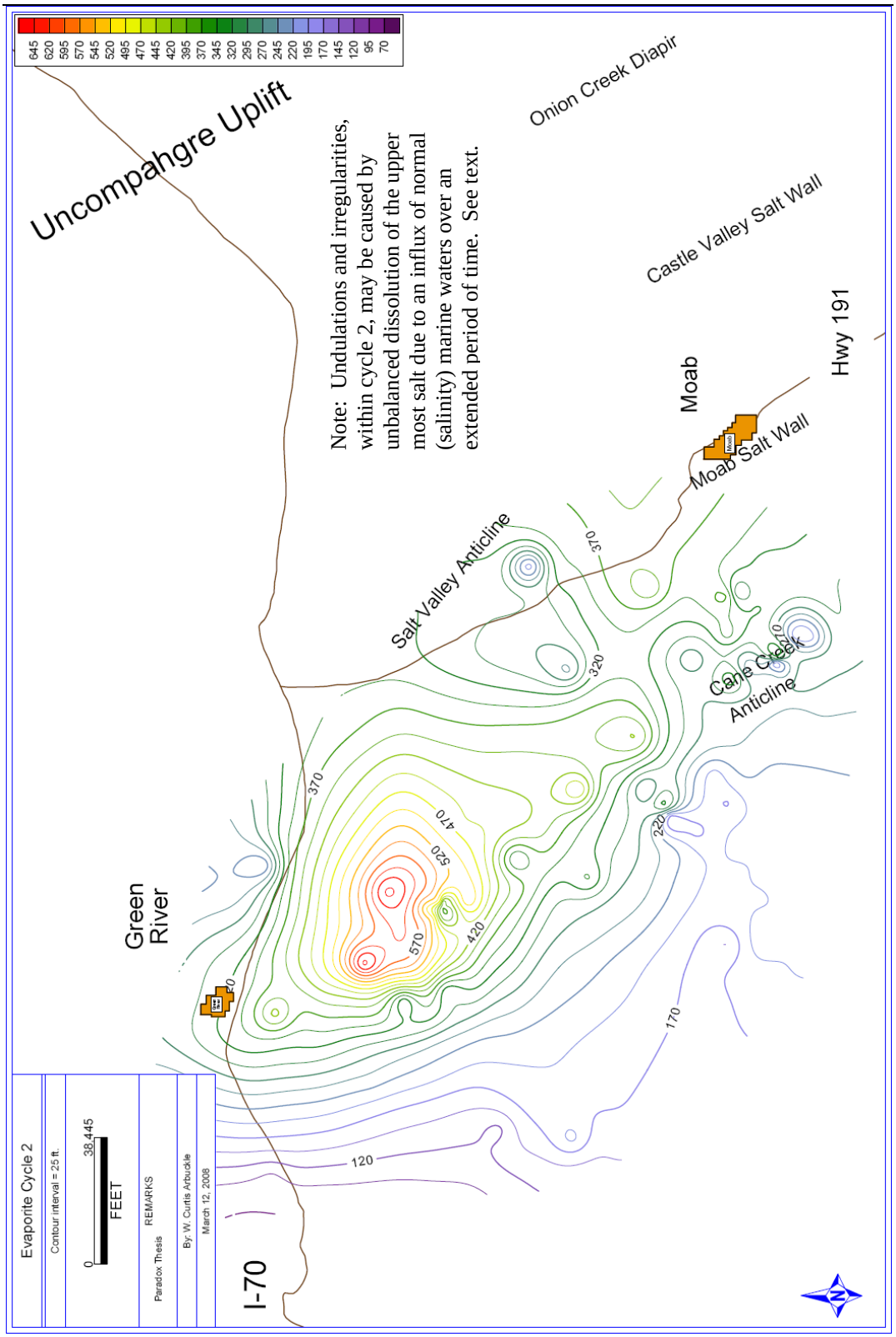

Figure B.31: Isopach map of evaporite cycle 2 within the Paradox Formation. See text for analysis. Contour interval = 25 feet (7.62 m).

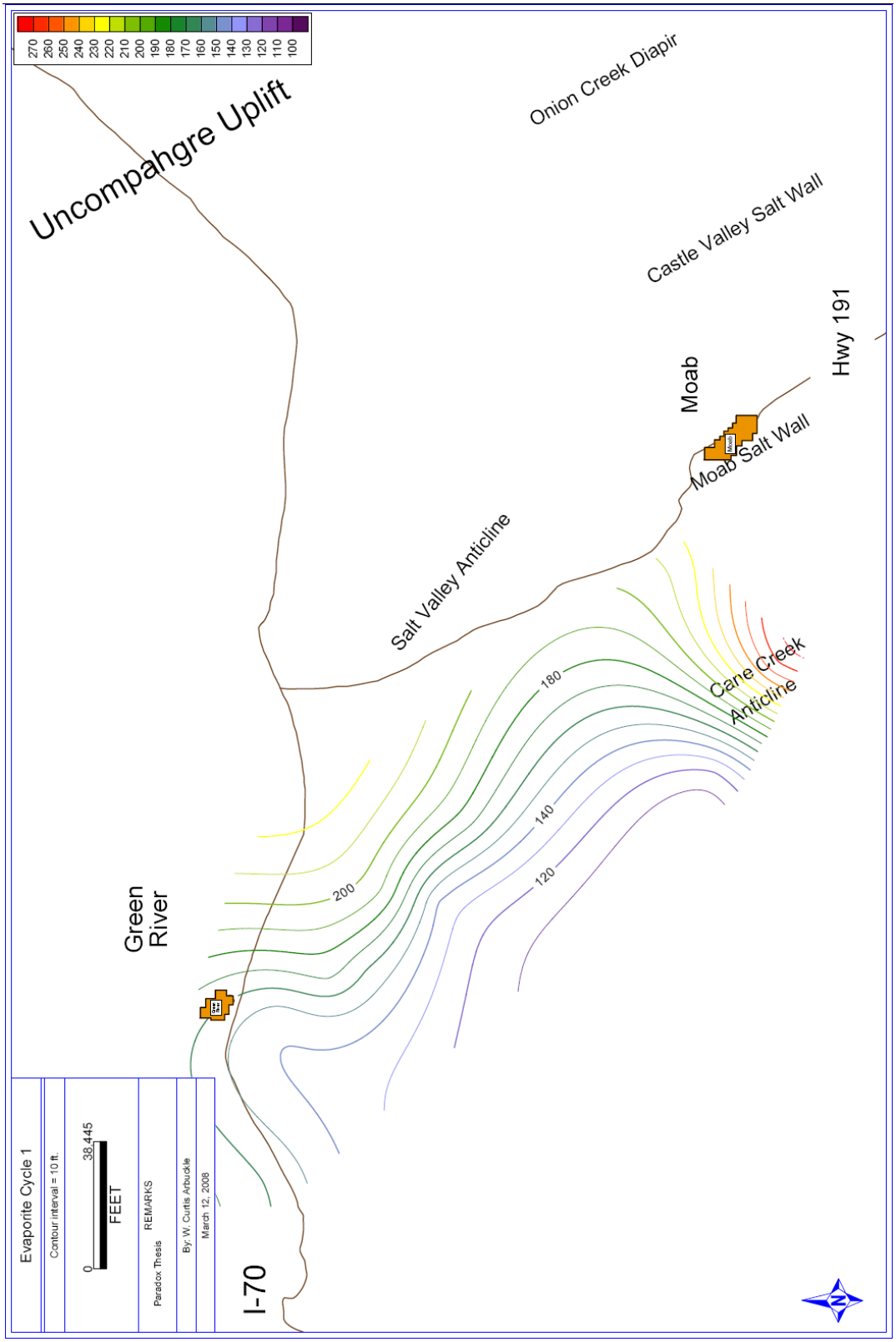

Figure B.32: Isopach map of evaporite cycle 1 within the Paradox Formation. See text for analysis. Contour interval = 10 feet (3.05 m).

APPENDIX C

WELLS USED FOR THICKNESS AND AGE CALCULATIONS

No.	API #	Well Name	Lithology Thicknesses (feet)					
			Anhydrite (total)	Silt/Dolo (T)	Black Shale	Silt/Dolo (R)	Halite	Total
1	4301511182	GRAND FAULT UNIT 14	249	387.1	136	428.9	1,196	2,397
2	4301530079	GEYSER DOME 1-14	251	210.35	87	220.65	1,211	1,980
3	4301930124	MT FUEL-SKYLINE GEYS	275	324.78	184	251.22	2,693	3,728
4	4301930282	SALT WASH NORTH 1	238	311.8	140	255.2	2,381	3,326
5	4301930688	FEDERAL 1-26	281	283.8	155	246.2	2,354	3,320
6	4301930050	BIG ROCK FED 1	273	392.4	176	208.6	2,910	3,960
7	4301930910	MOAB FED 16-9	334	198.45	214	192.55	2,691	3,630
8	4301530145	POOL UNIT 1	264	147.3	68	145.7	1,210	1,835
9	4301931190	COORS USA 1-10LC	426	267.85	162	227.15	3,876	4,959
10	4301910767	LITTLE VALLEY-FED 1	360	189.15	259	136.85	2,286	3,231

Table C.1: A table showing the thicknesses (in feet) of anhydrite, silty dolomite (T = transgressive), black shale, silty dolomite (R = regressive) and halite for 10 wells used in age estimation for the Paradox Formation.

Cycle 2

No.	API #	Operator	Well Name	Age (years)	
				(max.)	(min.)
1	4301511182	SUPERIOR OIL COMPANY	GRAND FAULT UNIT 14	96,894	85,524
2	4301530079	MEGADON ENTERPRISES	GEYSER DOME 1-14	109,340	99,017
3	4301930124	MOUNTAIN FUEL SUPPLY	MT FUEL-SKYLINE GEYS	112,254	104,076
4	4301930282	RESERVE OIL & GAS	SALT WASH NORTH 1	99,798	91,769
5	4301930688	MEGADON ENTERPRISES	FEDERAL 1-26	124,620	119,334
6	4301930050	GENERAL CRUDE OIL CO	BIG ROCK FED 1	92,974	85,344
7	4301930910	CHANDLER & ASSOCIATE	MOAB FED 16-9	102,303	93,177
8	4301530145	DAVIS OIL COMPANY	POOL UNIT 1	98,551	96,706
9	4301931190	COORS ENERGY	COORS USA 1-10LC	102,303	93,177
10	4301910767	MURPHY CONSTRUCTION	LITTLE VALLEY-FED 1	91,980	79,712

Table C.2: A table displaying evaporite cycle 2 age estimations for 10 wells within the northern Paradox Basin. Ages were calculated using sedimentation rates listed in Table 7.3 and thicknesses tallied from well logs.

Cycle 3

No.	API #	Operator	Well Name	Age (years)	
				(max.)	(min.)
1	4301511182	SUPERIOR OIL COMPANY	GRAND FAULT UNIT 14	N/A	N/A
2	4301530079	MEGADON ENTERPRISES	GEYSER DOME 1-14	N/A	N/A
3	4301930124	MOUNTAIN FUEL SUPPLY	MT FUEL-SKYLINE GEYS	85,426	76,200
4	4301930282	RESERVE OIL & GAS	SALT WASH NORTH 1	84,714	78,929
5	4301930688	MEGADON ENTERPRISES	FEDERAL 1-26	88,372	79,495
6	4301930050	GENERAL CRUDE OIL CO	BIG ROCK FED 1	75,527	64,058
7	4301930910	CHANDLER & ASSOCIATE	MOAB FED 16-9	83,483	70,367
8	4301530145	DAVIS OIL COMPANY	POOL UNIT 1	53,979	50,837
9	4301931190	COORS ENERGY	COORS USA 1-10LC	83,483	70,367
10	4301910767	MURPHY CONSTRUCTION	LITTLE VALLEY-FED 1	79,588	66,373

Table C.3: A table displaying evaporite cycle 3 age estimations for 10 wells within the northern Paradox Basin. Ages were calculated using sedimentation rates listed in Table 7.3 and thicknesses tallied from well logs. N/A = insufficient data needed for calculation.

Cycle 5

No.	API #	Operator	Well Name	Age (years)	
				(max.)	(min.)
1	4301511182	SUPERIOR OIL COMPANY	GRAND FAULT UNIT 14	99,516	94,629
2	4301530079	MEGADON ENTERPRISES	GEYSER DOME 1-14	88,314	81,282
3	4301930124	MOUNTAIN FUEL SUPPLY	MT FUEL-SKYLINE GEYS	86,751	78,174
4	4301930282	RESERVE OIL & GAS	SALT WASH NORTH 1	102,677	99,386
5	4301930688	MEGADON ENTERPRISES	FEDERAL 1-26	79,250	72,368
6	4301930050	GENERAL CRUDE OIL CO	BIG ROCK FED 1	73,751	63,478
7	4301930910	CHANDLER & ASSOCIATE	MOAB FED 16-9	64,359	55,382
8	4301530145	DAVIS OIL COMPANY	POOL UNIT 1	61,500	53,570
9	4301931190	COORS ENERGY	COORS USA 1-10LC	65,227	56,500
10	4301910767	MURPHY CONSTRUCTION	LITTLE VALLEY-FED 1	53,442	42,621

Table C.4: A table displaying evaporite cycle 5 age estimations for 10 wells within the northern Paradox Basin. Ages were calculated using sedimentation rates listed in Table 7.3 and thicknesses tallied from well logs.

Cycle 9

No.	API #	Operator	Well Name	Age (years)	
				(max.)	(min.)
1	4301511182	SUPERIOR OIL COMPANY	GRAND FAULT UNIT 14	83,994	81,002
2	4301530079	MEGADON ENTERPRISES	GEYSER DOME 1-14	54,820	52,177
3	4301930124	MOUNTAIN FUEL SUPPLY	MT FUEL-SKYLINE GEYS	56,781	53,989
4	4301930282	RESERVE OIL & GAS	SALT WASH NORTH 1	72,305	68,615
5	4301930688	MEGADON ENTERPRISES	FEDERAL 1-26	65,101	61,660
6	4301930050	GENERAL CRUDE OIL CO	BIG ROCK FED 1	44,912	42,667
7	4301930910	CHANDLER & ASSOCIATE	MOAB FED 16-9	34,028	28,991
8	4301530145	DAVIS OIL COMPANY	POOL UNIT 1	58,200	55,408
9	4301931190	COORS ENERGY	COORS USA 1-10LC	38,800	33,115
10	4301910767	MURPHY CONSTRUCTION	LITTLE VALLEY-FED 1	32,395	29,752

Table C.5: A table displaying evaporite cycle 9 age estimations for 10 wells within the northern Paradox Basin. Ages were calculated using sedimentation rates listed in Table 7.3 and thicknesses tallied from well logs.

Cycle 10

No.	API #	Operator	Well Name	Age (years)	
				(max.)	(min.)
1	4301511182	SUPERIOR OIL COMPANY	GRAND FAULT UNIT 14	N/A	N/A
2	4301530079	MEGADON ENTERPRISES	GEYSER DOME 1-14	N/A	N/A
3	4301930124	MOUNTAIN FUEL SUPPLY	MT FUEL-SKYLINE GEYS	54,284	50,594
4	4301930282	RESERVE OIL & GAS	SALT WASH NORTH 1	49,865	45,925
5	4301930688	MEGADON ENTERPRISES	FEDERAL 1-26	N/A	N/A
6	4301930050	GENERAL CRUDE OIL CO	BIG ROCK FED 1	43,141	40,648
7	4301930910	CHANDLER & ASSOCIATE	MOAB FED 16-9	32,762	29,471
8	4301530145	DAVIS OIL COMPANY	POOL UNIT 1	N/A	N/A
9	4301931190	COORS ENERGY	COORS USA 1-10LC	39,789	36,198
10	4301910767	MURPHY CONSTRUCTION	LITTLE VALLEY-FED 1	44,029	41,635

Table C.6: A table displaying evaporite cycle 10 age estimations for 10 wells within the northern Paradox Basin. Ages were calculated using sedimentation rates listed in Table 7.3 and thicknesses tallied from well logs. N/A = insufficient data needed for calculation.